STUDIA UNIVERSITATIS
BABEŞ-BOLYAI

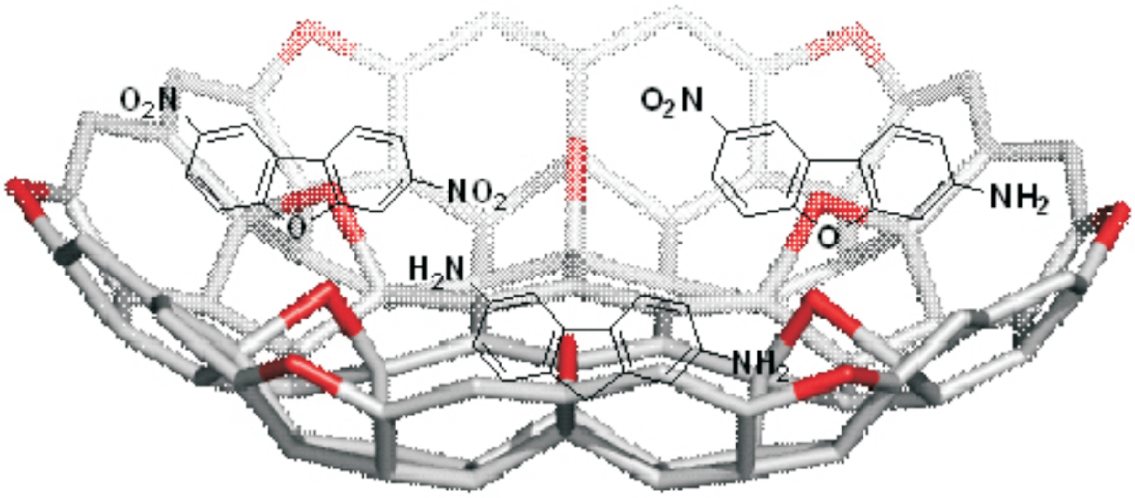

CHEMIA

4/2009
tom II

ANUL LIV **2009**

S T U D I A

UNIVERSITATIS BABEŞ-BOLYAI

CHEMIA

4

tom II

Desktop Editing Office: 51ST B.P. Hasdeu Street, Cluj-Napoca, Romania, Phone + 40 264-405352

CUPRINS – CONTENT – SOMMAIRE – INHALT

Studia Universitatis Babes-Bolyai Chemia has been selected for coverage in Thomson Reuters products and custom information services. Beginning with V. 53 (1) 2008, this publication is indexed and abstracted in the following:

- Science Citation Index Expanded (also known as SciSearch®)
- Chemistry Citation Index®
- Journal Citation Reports/Science Edition

STUDIA UNIVERSITATIS BABEŞ-BOLYAI, CHEMIA, LIV, 4, 2009

CORSU NETWORK - A NEW GRAPHENE DESIGN

MIRCEA V. DIUDEA[a] AND ALEKSANDAR ILIĆ[b]

ABSTRACT. A new graphene pattern, called CorSu, was designed and the energy of some small fragments of the lattice, functionalized by groups containing oxygen, carbon, nitrogen and phosphorus, was evaluated at the level of semiempirical method PM3. The topology of the network is described in terms of Omega counting polynomial. Close formulas for calculating the polynomial and the Cluj-Ilmenau index derived from this polynomial are given.

Keywords: Counting polynomial, lattice, CI index.

INTRODUCTION

Nano-era can be the name of the last twenty years, period when several new carbon allotropes have been discovered and studied for applications in nano-technology, in view of reducing the dimensions of devices and increasing their performance, al a lower cost of energy and money. Among the carbons structures, fullerenes (zero-dimensional), nanotubes (one dimensional), graphene (two dimensional) and spongy carbon (three dimensional) represent the novelty [1,2]. The attention of scientists was also focused to inorganic compounds, a realm where almost any metal atom can form clusters, tubules or crystal networks, very ordered structures at the nano-level. Recent articles in crystallography promoted the idea of topological description and classification of crystal structures [3-8]. They present data on real, but also hypothetical lattices, designed by computer.

The present study deals with a hypothetical graphene patterned by coronene- and sumanene-like units, described in terms of Omega counting polynomial and evaluated as energy by the PM3 method.

OMEGA POLYNOMIAL

Let $G(V,E)$ be a connected graph, with the vertex set $V(G)$ and edge set $E(G)$. Two edges $e = uv$ and $f = xy$ of G are called *codistant e co f* if they obey the following relation [9]:

[a] *Faculty of Chemistry and Chemical Engineering, "Babes-Bolyai" University, 400028 Cluj, Romania, diudea@gmail.com*

[b] *Faculty of Sciences and Mathematics, University of Niš, Višegradska 33, 18000 Niš, Serbia, aleksandari@gmail.com*

$$d(v,x) = d(v,y) + 1 = d(u,x) + 1 = d(u,y) \quad (1)$$

Relation *co* is reflexive, that is, *e co e* holds for any edge *e* of *G*; it is also symmetric, if *e co f* then *f co e*. In general, relation *co* is not transitive; an example showing this fact is the complete bipartite graph $K_{2,n}$. If "*co*" is also transitive, thus an equivalence relation, then *G* is called a *co-graph* and the set of edges $C(e) := \{f \in E(G);\ f\ co\ e\}$ is called an *orthogonal cut oc* of *G*, *E*(*G*) being the union of disjoint orthogonal cuts:

$$E(G) = C_1 \cup C_2 \cup ... \cup C_k,\ C_i \cap C_j = \varnothing, i \neq j\ .$$

Klavžar [10] has shown that relation *co* is a theta Djoković-Winkler relation [11,12].

We say that edges *e* and *f* of a plane graph *G* are in relation *opposite, e op f,* if they are opposite edges of an inner face of *G*. Note that the relation *co* is defined in the whole graph while *op* is defined only in faces. Using the relation *op* we can partition the edge set of *G* into *opposite* edge *strips, ops.* An *ops* is a quasi-orthogonal cut *qoc*, since *ops* is not transitive.

Let *G* be a connected graph and S_1, S_2, ..., S_k be the *ops* strips of *G*. Then the *ops* strips form a partition of *E(G)*. The length of *ops* is taken as maximum. It depends on the size of the maximum fold face/ring F_{max}/R_{max} considered, so that any result on Omega polynomial will have this specification.

Denote by *m*(*G*,*s*) the number of *ops* of length *s* and define the Omega polynomial as [13-15]:

$$\Omega(G,x) = \sum_s m(G,s) \cdot x^s \quad (2)$$

Its first derivative (in *x*=1) equals the number of edges in the graph:

$$\Omega'(G,1) = \sum_s m(G,s) \cdot s = e = |E(G)| \quad (3)$$

On Omega polynomial, the Cluj-Ilmenau [9] index, *CI*=*CI*(*G*), was defined:

$$CI(G) = \{[\Omega'(G,1)]^2 - [\Omega'(G,1) + \Omega''(G,1)]\} \quad (4)$$

Within this paper, the main results refer to F_{max}(6). If rings instead of faces are considered, the polynomial is different. The inclusion of hexagons lying "under" the bridge brings complications in the number and length of *ops*, particularly at the maximum length.

Data were calculated by an original program called Nano Studio [16], developed at the TOPO Group Cluj.

LATTICE BUILDING

The lattice was built on the graphene sheet, of (6,3) tessellation, by decorating it with coronene-like flowers, having sumanene units as petals. The pattern, called CorSu, can be described as: [6:(6:(5,6)3)6], with vertices/atoms of degree 3 (sp^2) and 4 (sp^3), as shown in Figure 1.

This idea came out from the TOPO Group Cluj older studies on aromaticity, in which circulene/flower units were proposed as extensions of the Clar theory of aromaticity. Notice, the coronene and sumanene are molecules synthesized in the labs. It was also supported by the synthesis of several bowl-shaped molecules, inspired from the architecture of fullerenes and, more recently, by the direct synthesis of fullerenes starting from open precursors. The design of various domains on the graphene sheet is nowadays a challenge study and practice.

The pentagonal rings, possibly entering as local bridges over the graphite sheet by reactions like oxidation, amination, or carbene action, will force the geometry of graphene to a bowl-shaped one (Figure 1, the right hand column). The overall positive curvature depends on the bond length of the atoms involved in the bridges, it being as bowl-shaped as the atom covalent radius is smaller (see Table 1). The lattice appears as alternating positive (sumanene) and negative (coronene) curved domains.

MAIN RESULTS

The graphene lattice patterned by CorSu repeat units was designed in the idea of coronene [17] circulene [6:6_6] whose petals were replaced by sumanene [18,19] units, two molecules appearing as domains in fullerenes. Data in Table 1, computed at the PM3 level of theory, show the fragments of the lattice, functionalized by groups containing oxygen, carbon, nitrogen and phosphorus, as relatively stable ones, both as the total energy per atom and HOMO-LUMO geap. The bond lengths are quite reasonable, slightly elongated than the normal values. In comparison, the total energy per atom (in kcal/mol) for C_{60} is -2722.45, while the gap is around 6.59 eV. The bridges defining the pentagonal rings of the sumanene units, will force the planar graphene to adopt a bowl-shaped form and the sp^2 carbon atom is supposed to shift to the sp^3 hybridization. In the whole, the lattices appears as a waved surface, with margins eventually positively curved (Figure 1) or in sent to hyperbolic geometry.

Table 1. Energy and structural data for two fragments of the hypothetical lattice CorSu

	Structure	C_X (A)	TE/HeavyN (Kcal/mol)	HOMO-LUMO Gap (eV)
	CorSu_96 _X			
1	O	1.52	-3271.32	5.950
2	C (CH2)	1.64	-2925.55	6.655
3	N (NH)	1.61	-3007.54	6.740
4	P (PH)	2.06	-2889.53	6.057
	CorSu_198 _X			
5	O	1.52	-3289.57	8.776
6	C (CH2)	1.62	-2889.05	8.603
7	N (NH)	1.58	-2967.23	8.143
8	P (PH)	2.05	-2853.45	6.590

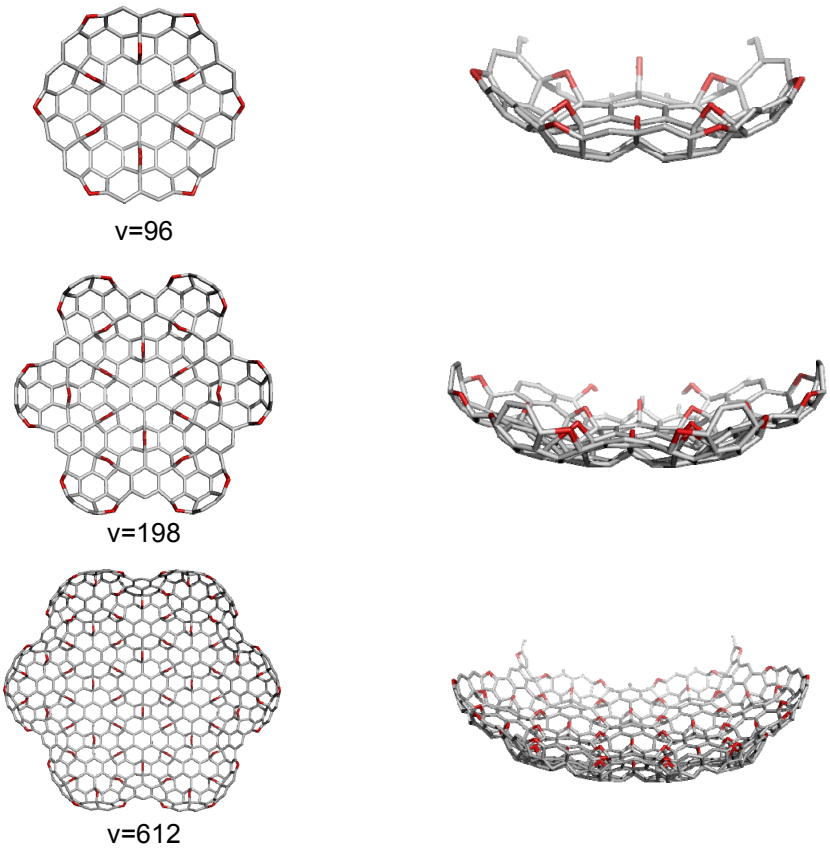

Figure 1. Hexagonal domains in the CorSu graphene sheet: top view (left hand column) and side view (right hand column).

This is the first description of a completely new (hypothetically, yet) lattice, of which functionalization we believe to be soon performed. Of course, the route to such structures is not suggested, remaining as a challenge.

The topology of the lattice is described here in terms of Omega polynomial. Table 2 gives examples for hexagonal (complete) domains.

Table 2. Omega polynomials of hexagonal domains $CorSu_{h,k}$

k	Omega	CI	Atoms	Bonds
0	$24x + 12x^2 + 24x^3 + 3x^6$	18648	96	138
1	$144x + 36x^2 + 156x^3 + 39x^6$	839628	612	918
2	$372x + 60x^2 + 396x^3 + 129x^6$	6013296	1614	2454
3	$708x + 84x^2 + 744x^3 + 273x^6$	22506948	3102	4746
4	$1152x + 108x^2 + 1200x^3 + 471x^6$	60717096	5076	7794

The Omega polynomial for the CorSu lattice of hexagonal domains of $CorSu_{h,k}$ type is:

$$\Omega(CorSu_{h,k}, x) = a_k x + b_k x^2 + c_k x^3 + d_k x^6 .$$

For the starting values, we have $a_0 = 24, b_0 = 12, c_0 = 24, d_0 = 3$. Based on the composition rule, we can deduce the following recurrent formulas:

$$a_{k+1} = a_k + 120 + 108k$$
$$b_{k+1} = b_k + 24$$
$$c_{k+1} = c_k + 132 + 108k$$
$$d_{k+1} = d_k + 36 + 54k$$

After solving these recurrent relations, we get:

$$\Omega(CorSu_{h,k}, x) = (24 + 66k + 54k^2)x + (12 + 24k)x^2 + (24 + 78k + 54k^2)x^3 + (3 + 9k + 27k^2)x^6$$

The number of atoms in the lattice is:

$$v = 96 + 273k + 243k^2 ,$$

while the number of bonds, following (3):

$$e = 138 + 402k + 378k^2 .$$

CI index follows from (4), and is given by the following formula:

$$CI(CorSu_{h,k}) = 18648 + 109764k + 264420\,k^2 + 303912k^3 + 142884k^4$$

Parallelogram domains were also considered; data are given in Table 3.

Table 3. Omega polynomials of parallelogram domains p(a,b)

a	b	Omega	CI	Atoms	Bonds
1	1	$24x + 12x^2 + 24x^3 + 3x^6$	18648	96	138
1	2	$46x + 20x^2 + 50x^3 + 6x^6$	73192	187	272
1	3	$68x + 28x^2 + 76x^3 + 9x^6$	163648	278	406
1	4	$90x + 36x^2 + 102x^3 + 12x^6$	290016	369	540
1	5	$112x + 44x^2 + 128x^3 + 15x^6$	452296	460	674
2	2	$86x + 28x^2 + 94x^3 + 18x^6$	281332	359	532
2	3	$126x + 36x^2 + 138x^3 + 30x^6$	624672	531	792
2	4	$166x + 44x^2 + 182x^3 + 42x^6$	1103212	703	1052
2	5	$206x + 52x^2 + 226x^3 + 54x^6$	1716952	875	1312
3	3	$184x + 44x^2 + 200x^3 + 51x^6$	1383688	784	1178
3	4	$242x + 52x^2 + 262x^3 + 72x^6$	2440696	1037	1564
3	5	$300x + 60x^2 + 324x^3 + 93x^6$	3795696	1290	1950
4	4	$318x + 60x^2 + 342x^3 + 102x^6$	4302468	1371	2076
4	5	$394x + 68x^2 + 422x^3 + 132x^6$	6688528	1705	2588
5	5	$488x + 76x^2 + 520x^3 + 171x^6$	10395448	2120	3226

Let $v(a,b)$ be the number of atoms in the parallelogram domain. We have the following symmetric recurrent formulas

$$v(a,b) = v(a,b-1) + (10+81a)$$
$$v(a,b) = v(a-1,b) + (10+81b)$$

After solving this second degree recurrent relation, using the starting value $v(1,1) = 96$, it follows:

$$v(a,b) = 81ab + 10a + 10b - 5.$$

Similarly, we can calculate the number of bonds and CI index

$$e(a,b) = 126ab + 8a + 8b - 4$$
$$CI(a,b) = (126ab + 8a + 8b - 4)^2 - 108 + 108(a+b) - 504ab.$$

In case of parallelogram p(a,b) domains, the Omega polynomial equals:

$$\Omega(CorSu_{p(a,b)}, x) = (-2 + 4a + 4b + 18ab)x + (-4 + 8a + 8b)x^2 + (-10 + 8a + 8b + 18ab)x^3 + (6 - 6a - 6b + 9ab)x^6$$

CONCLUSIONS

A new graphene lattice, patterned by CorSu units, was functionalized by groups containing oxygen, carbon, nitrogen and phosphorus, and its stability evaluated at the level of semiempirical method PM3. The small fragments, taken into consideration, showed relatively good stability, as compared with the data for the well-known C_{60}. The topology of the network is described in terms of Omega counting polynomial. Close formulas for calculating the polynomial and the Cluj-Ilmenau index derived from this polynomial were given.

ACKNOWLEDGMENTS

The work was supported in part by the ID_506 Romanian GRANT 2009, and the Research grant 144007 of the Serbian Ministry of Science.

REFERENCES

1. M.V. Diudea, Ed., “Nanostructures, novel architecture”, NOVA, **2005**.
2. M.V. Diudea and Cs. L. Nagy, “Periodic Nanostructures”, Springer, **2007**.
3. L. Carlucci, G. Ciani and D. Proserpio, *Coord. Chem. Rev.*, **2003**, *246*, 247.
4. L. Carlucci, G. Ciani and D. Proserpio, *Cryst. Eng. Comm.*, **2003**, *5*, 269.

5. V.A. Blatov, L. Carlucci, G. Ciani and D. Proserpio, *Cryst. Eng. Comm*., **2004**, *6*, 377.
6. I.A. Baburin, V.A. Blatov, L. Carlucci, G. Ciani and D. Proserpio, *J. Solid State Chem.*, **2005**, *178*, 2452.
7. O. Delgado-Friedrichs and M. O'Keeffe, *J. Solid State Chem*., **2005**, *178*, 2480.
8. V.A. Blatov, O. Delgado-Friedrichs, M. O'Keeffe, and D. Proserpio, *Acta Cryst.,* **2007**, *A63*, 418.
9. P.E. John, A.E. Vizitiu, S. Cigher, M.V. Diudea, *MATCH Commun. Math. Comput. Chem.*, **2007**, *57*, 479.
10. S. Klavžar, *MATCH Commun. Math. Comput. Chem.,* **2008**, *59*, 217.
11. D.Ž. Djoković, *J. Combin. Theory Ser. B*, **1973**, *14*, 263.
12. P.M. Winkler*, Discrete Appl. Math.,* **1984**, *8*, 209.
13. M.V. Diudea, *Carpath. J. Math.,* **2006**, *22*, 43.
14. M.V. Diudea, S. Cigher, P.E. John, *MATCH Commun. Math. Comput. Chem.*, **2008**, *60*, 237.
15. M.V. Diudea, S. Cigher, A.E. Vizitiu, M.S. Florescu, P.E. John, *J. Math. Chem.*, **2009**, *45*, 316.
16. Cs. L. Nagy, M.V. Diudea, *Nano Studio software*, Babes-Bolyai Univ., **2009**.
17. K. Yamamoto, *Pure Appl. Chem.,* **1993**, *65*, 157.
18. H. Sakurai, T. Daiko, T. Hirao, *Science,* **2003**, *301*,1878.
19. H. Sakurai, T. Daiko, H. Sakane, T. Amaya, T. Hirao, *J. Am. Chem. Soc.*, **2005**, *127*, 11580.

STUDIA UNIVERSITATIS BABEŞ-BOLYAI, CHEMIA, LIV, 4, 2009

DETERMINATION OF STEROID HORMONES IN SOMES RIVER WATER BY SOLID PHASE MICROEXTRACTION AND GAS CHROMATOGRAPHY - MASS SPECTROMETRY

LACRIMIOARA SENILA[a], MIRELA MICLEAN[a], CECILIA ROMAN[a], CORNELIA MAJDIK[b], GYULA ZÁRAY[c]

ABSTRACT. In this study, the occurrence of steroid hormones in Somes River was evaluated. The water samples were collected downstream of municipal sewage treatment plant of Cluj-Napoca, Romania. The used method was based on solid-phase microextraction (SPME), on-fiber silylation and, final, analysis by gas chromatography–mass spectrometry (GC-MS). The target compounds were estrone and beta-estradiol and were detected in wastewater effluent and river water. The values of target compounds in water samples were in the range of 0.010–0.080 µg/l.

Keywords: steroid hormones, SPME, MSTFA, GC-MS

INTRODUCTION

Humans and animals produce hormones, constantly excreted into the environment. The steroids of major concern are estrone and β-estradiol, since they exert their physiological effects at lower concentrations than other steroids [1, 2]. Estrone and β-estradiol cause reproductive disorders and abnormal development in wildlife and reduced fertility in human males, problems that may be caused by so-called endocrine disrupting chemicals (EDCs) released anthropogenically into the environment [3, 4].

Natural steroids, like estrone and β-estradiol are released into the aquatic environment through discharges from sewage treatment [5, 6, 7].

The purpose of this paper is to determine two natural steroid hormones in Somes River water samples using a sensitive and rapid technique. The method employs the solid-phase microextraction (SPME) by direct immersion in aqueous samples, with on-fiber silylation to separate the target compounds from the samples, followed by simultaneous determinations of the silylated

[a] *INCDO-INOE 2000, Research Institute for Analytical Instrumentation, Donath 67, 400293, Cluj-Napoca, Romania; E-mail: icia@icia.ro*

[b] *"Babes-Bolyai" University, Faculty of Chemistry and Chemical Engineering, Arany Ianos 11, 400028, Cluj-Napoca, Romania*

[c] *Institute of Chemistry, Department of Analytical Chemistry, L. Eötvös University, Budapest, Hungary*

derivatives by GC–MS. N-Methyl-N-(trimethylsilyl) trifluoroacetamide (MSTFA) was used as derivatization reagent to enhance selectivity and sensitivity [8, 9]. The chemical structures of estrone and β-estradiol are shown in Figure 1.

Due to the very low concentration (ng/l) of estrogenic compounds in the aqueous environment, sensitive and reliable methods are required for their determination [10, 11].

The most used analytical technique for estrogen detection and quantification is gas chromatography coupled to mass spectrometry (GC–MS), tandem mass spectrometry (GC–MS–MS), liquid chromatography coupled to mass spectrometry (LC–MS) and tandem mass spectrometry (LC–MS–MS). The drawback of GC-MS technique is the use of derivatization step prior to chromatographic analysis. The target compounds need to be derivatised to produce less polar compounds [12, 13].

Until this study, we did not find any information about hormones levels in Somes River water obtained using SPME-GC/MS method.

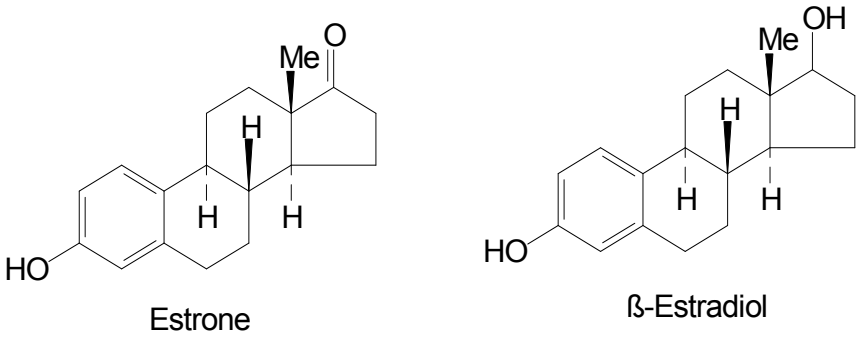

Figure 1. Structures of the steroid hormones

EXPERIMENTAL SECTION

Study area and sampling

The water samples were collected downstream of municipal sewage treatment plant, which collect and filter the urban residues of Cluj-Napoca, a city with approximate 400000 inhabitants. The geographic coordinates of sampling points are shown in Table 1.

Table 1. Geographic coordinates of sampling points

Sampling point	Latitude, N	Longitude, E
1	46°47'29,03"	23°41'7,53"
2	46°47'37,03"	23°43'10,60"
3	46°48'54,65"	23°44'56,61"

The study area comprising the three sampling points along the Somes River, downstream of sewage water treatment plant of Cluj-Napoca city is shown in Figure 2.

The samples collected in sampling point 1 point contained effluent sewage water after filtration, and the samples collected in sampling points 2 and 3 contained river water, downstream the treatment plant, approximately 3.5 km and 10 km, respectively.

Water samples were collected in triplicate, in August 2009 and were collected in pre-cleaned amber-glass bottles. Samples were stored at 4°C until filtration and extraction.

Filtered sewage water was filtered again in the laboratory through a 1µm glass fibre filter (Whatman, Mainstone, UK) prior to extraction.

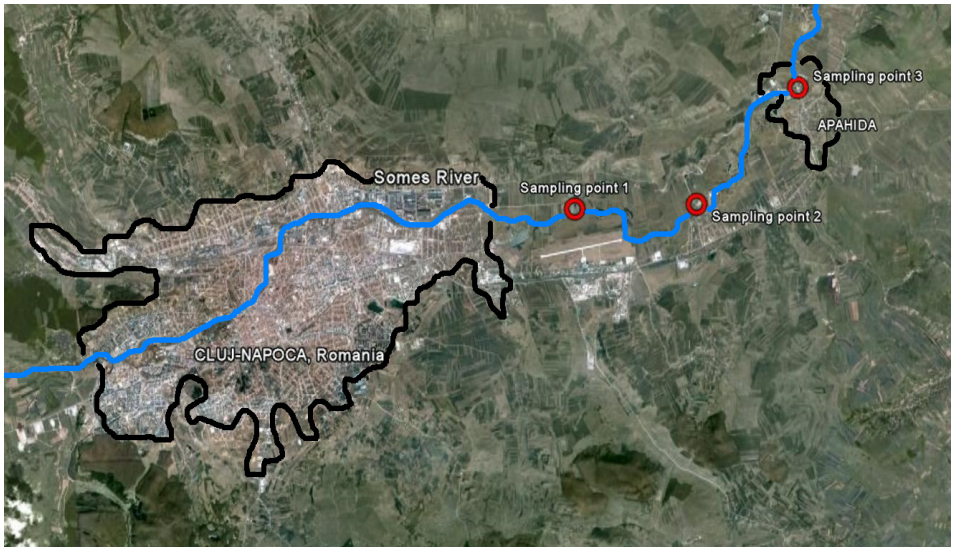

Figure 2. Study area (source Google Earth)

Chemicals

Methanol HPLC-grade was purchased from Merck (Darmstadt, Germany). Steroid hormones: estrone (99 %) and ß-estradiol (98 %) were supplied by Sigma–Aldrich. Sodium chloride (NaCl, 99%) and hydrochloric acid (HCl, 37%) were obtained from Merck (Darmstadt, Germany). The derivatization agents N-Methyl-N-(trimethylsilyl) trifluoro acetamide (MSTFA) were purchased from Sigma–Aldrich.

Sodium chloride was used to decrease the solubility of organic compounds in water. A concentration level of 100 g/l NaCl was selected, according to other studies [8].

Hydrochloric acid was used to adjust the pH of the sample at value 5, in order to increase the extraction efficiency of the analytes [8].

Stock standard solutions of estrone and β-estradiol (1 mg/ml) were prepared in methanol and stored at −18 °C in dark. Working solutions were prepared by appropriate dilution of the stock standard solutions with ultrapure water and were stored at 4 °C in dark. Ultrapure water was obtained from a Milli-Q system (Millipore, Bedford, MA, USA).

Instrumentation

A gas chromatograph 6890N (Agilent Technologies) coupled with a mass spectrometer 5973N MSD (Agilent Technologies) and a capillary column HP-5 MS (30 m×0.25 mm×0.25 μm) were used to analyze the steroid hormones.

For the SPME extraction a manual fiber holder Supelco Inc. (Bellefonte, PA, USA) with an 85 μm polyacrylate (PA) fiber Supelco Inc. (Bellefonte, PA, USA) were used. After every analysis the fiber was conditioned in the GC inlet for 2 h at 300 °C [8].

Direct SPME extraction and headspace derivatization

Solid phase microextraction (SPME) is a unique sample preparation technique that requires no solvents or complicated apparatus. It can concentrate volatile and nonvolatile compounds (in liquids or gaseous samples), for subsequent analysis by GC or HPLC. Because analytes are concentrated on the fiber, and are rapidly delivered to the column, minimum detection limits are improved and resolution is maintained [11].

A volume of 18 ml sample, 1.8 g NaCl and a magnetic stirring bar for sample homogenization were put in a 20 ml sampler vial sealed with septa. The needle of the manual fiber holder pierced the septa, the PA fiber was released into the water sample and the extraction was performed at 120 min, and the temperature at 45 °C [8, 9].

After SPME, the analytes were derivatized using the headspace derivatization technique, by exposing the fiber to the vapor of 100 μl MSTFA, in a sampler vial sealed with a septum, for 60 min at 25 °C [8, 9].

GC-MS analysis

For quantitative determination, the MS system was operated in SIM mode. The injector was equipped with a 4 mm-I.D. glass liner. The carrier gas was helium at constant flow rate of 1.0 $mLmin^{-1}$. The GC column temperature program is shown in Table 2.

Table 2. GC column temperature program

Step	Ramp, °C/min	Temperature, °C	Holding time, min
1		90	2
2	30	180	0
3	10	240	0
4	3	270	0
5	15	300	2

The identification of steroid hormones was based on the standard mass spectra of the MS spectral library.

RESULTS AND DISCUSSION

The SIM chromatograms of the steroid hormones after silylated derivatization are shown in Figures 3-4. The ions monitored for each compound are listed in Table 3. Both target compounds in this work contained hydroxyl-group (Figure 1).

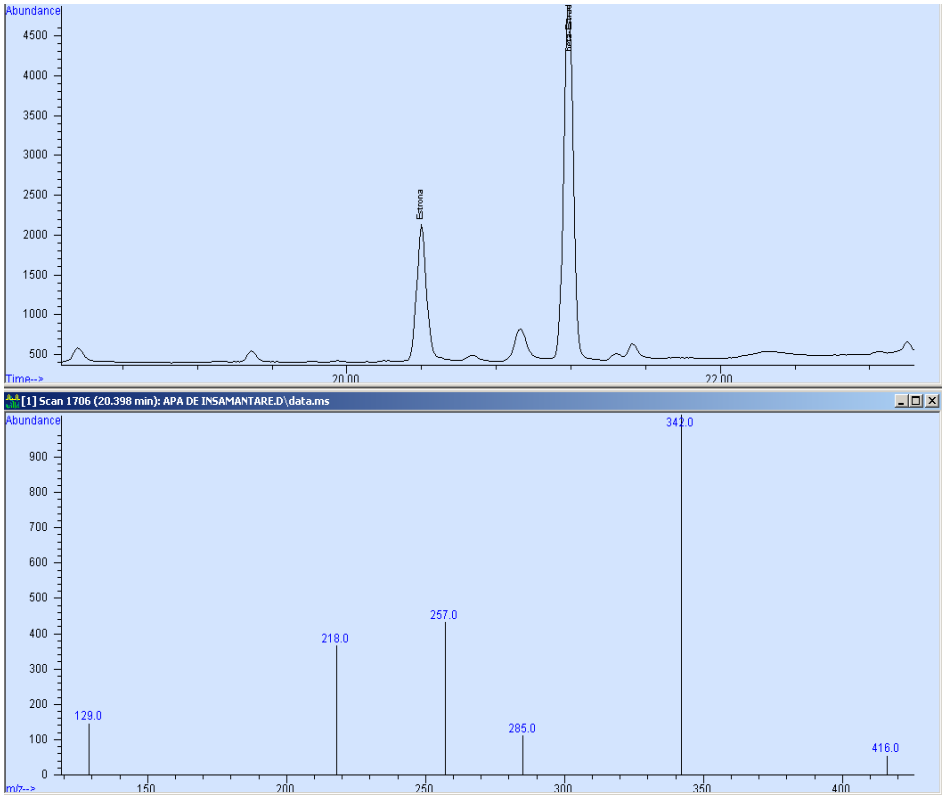

Figure 3. The SIM chromatogram of target compounds from waste water effluent (and the ions for the quantitative and qualitative analysis of silylation derivatives of estrone)

Estrone contained one hydroxyl group, the mono-TMSi derivatives were formed, and ß-estradiol contained two hydroxyl groups, the bis- TMSi derivatives were formed. The mono derivates for estrone were evidenced by the presence of *m/z* 342, 218 and 257, respectively. For ß-estradiol containing bis-hydroxi groups, the molecular ion at *m/z* 416 was show in the mass of derivative for ß-estradiol, indicating silylation of both hydroxyl groups. The ions monitored for estrone and ß-estradiol are listed in Table 3.

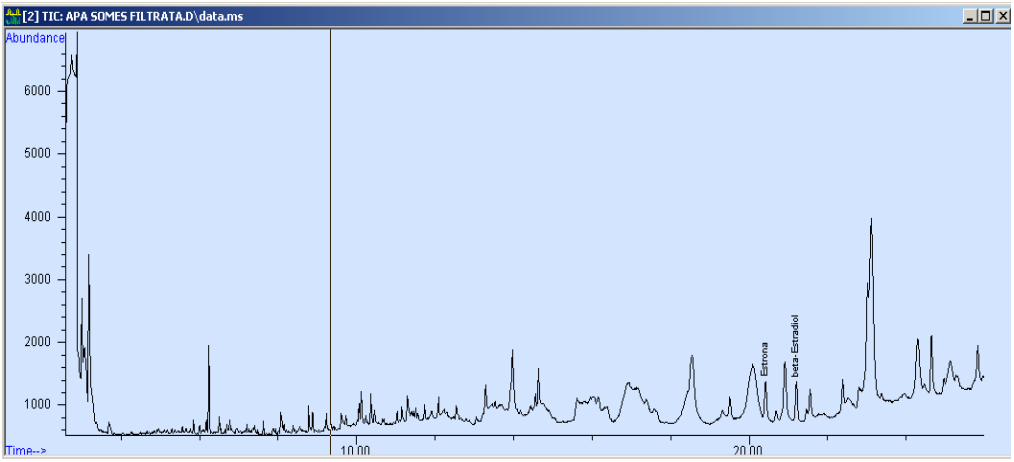

Figure 4. The SIM chromatogram of target compounds from river water (sampling point 2)

Table 3. Ions for the quantitative and qualitative analysis of silylation derivatives of target compounds

Compounds	Molecular mass	Ret. time (min)	Quantitative ions	Qualitative ions
Estrone	270	20.550	342	218, 257
ß-estradiol	272	21.368	416	129, 285

The relative standard deviations (RSD) for the target compounds were 10.2 and 11.5% for estrone and ß-estradiol, respectively, showing good reproducibility for the analytes. The RDSs were calculated for 6 replicates of a water sample. The limit of detection (DL), defined as the concentration that corresponds to three times the standard deviation of blanks, was measured by integrating blank peak area for each compound in 10 independent analyses with ultrapure water as blank [8]. The obtained DL for estrone and ß-estradiol were 0.013 and 0.008, respectively.

Highest concentrations of both estrogens were found in sampling point 1, the concentrations decreased after waste water treatment plant, along the Somes River. The obtained concentrations are shown in Table 4.

Table 4 The concentrations of estrogenic compounds in river water obtained by SPME GC-MS

Sampling point	Concentration estrone, μg/l	Concentration ß-estradiol, μg/l
1	0.056	0.080
2	0.032	0.040
3	0.020	< DL

The optimizations of reactions conditions (temperature, pH, derivatization time, extraction time) were selected according to other studies [8, 9].

Beta-estradiol was not detected in sampling point 3, suggesting that the concentration of this estrogen compound decreased due to the dilution effect.

The concentrations of this hormones obtained in the present study were higher than those obtained by Yang et al. (2006) in water samples collected from a pond in Sanjiao district (China), where the concentrations for estrone and ß-estradiol were 0.18 and 0.10 μg/l, respectively [8].

Extraction of estrogens from Somes River by SPME with on-fiber silylation with MSTFA is a simple and fast analytical method, environmental friendly and capable to analyze small sample volume.

CONCLUSIONS

Exposure of aquatic organisms to steroid hormones is an important concern due to the possible harmful effect. Discharges of municipal sewage in Somes River at Cluj-Napoca are the primary sources of estrogenic steroids. In this study, the analysis of estrogenic steroids in treated sewage, after dilution in Somes River was investigated. The results indicated the presence of natural estrogens, estrone and β-estradiol in water samples. The concentrations of both estrogens decreased along the Somes River, downstream from waste water treatment plant.

ACKNOWLEDGEMENTS

This work was supported by the Bilateral Project Romanian-Hungarian No. 19/2009, CONTALIM (ANCS Program).

REFERENCES

1. L.S. Shore, M. Shemesh, *Pure Applied Chemistry,* **2003**, *75 (11–12),* 1859–1871.
2. J.Q. Jiang, Q. Yin, J.L. Zhou, P. Pearce, *Chemosphere*, **2005**, *61(4*), 544-550.
3. M.S. Colucci, H. Bork, E. Topp, *Journal of Environmental Quality*, **2001**, *30*, 2070-2076.
4. A.N. Neale, B.I. Escher, A.I. Schäfer, *Science of the Total Environment*, **2009**, *407,* 1167-1173.
5. Z. Zhang, H. Duan, L. Zhang, X.Chen, Wei Liu, G. Chen, *Talanta*, **2009**, *78*, 1083-1089.
6. S. Zorita, P. Hallgren, L. Mathiasson, *Journal of Chromatography A*, **2008**, *1192*, 1-8.

7. C. Chia-Yang, W. Tzu-Yao, W. Gen-Shuh, C. Hui-Wen, L. Ying-Hsuan, L. Guang-Wen, *Science of the Total Environment,* **2007***, 378,* 352-365.
8. L. Yang, T. Luan, C. Lan, *Journal of Chromatography A*, **2006**, *1104*, 23–32.
9. L. Yang, C. Lan, H. Liu, J. Dong, T. Luan, *Analytical and Bioanalytical Chemistry,* **2006**, *386*, 391-397.
10. H. Noppe, B.L. Bizec, K. Verheyden, H.F. Brabander, *Analytica Chimica Acta*, **2008**, *611*, 1-16.
11. H.S.N. Lee, M.T. Sng, C. Basheer, H.K. Lee, *Journal of Chromatography A,* **2007***, 1148,* 8-15.
12. R. Liu, J.L. Zhou, A. Wilding, *Journal of Chromatography A,* **2004***, 1022,* 179-189.
13. http://www.sigmaaldrich.com/analytical-chromatography/.html

STUDIA UNIVERSITATIS BABEŞ-BOLYAI, CHEMIA, LIV, 4, 2009

CHANGES IN FATTY ACIDS COMPOSITION OF ANIMAL FATS DURING STORAGE

FLAVIA POP[a]

ABSTRACT. In this article the fatty acids composition for 2 types of animal fats (pork fat and beef tallow), following the variation of saturated and unsaturated fatty acids proportion during freezing storage was studied. Determination of chemical composition of animal fats is important in establishing organoleptic and physico-chemical parameters, the variation of them in time, nature and proportion of fatty acids conferring specific characteristics to them. For pork fat was determined the following chemical composition: saturated fatty acids (SFA) 48.32%, monounsaturated fatty acids (MUFA) 36.78% and polyunsaturated fatty acids (PUFA) 14.89%. After 4 months of storage under freezing there was a change in fatty acids proportion, saturated fatty acid content increased slightly to 48.83%, due to installation of hydrolysis leading to release of fatty acids from triglycerides, monounsaturated fatty acids content decreased to 35.99%, and polyunsaturated fatty acids content increased to 15.18%. In the case of beef tallow there was an increasing in saturated and monounsaturated fatty acids content and a decreasing in polyunsaturated fatty acids content.

Keywords: fatty acids, animal fats, storage

INTRODUCTION

In chemical terms fats are glycerol esters with fatty acids. Theoretically there is the possibility that one group of alcoholic glycerine is esterificated with a fatty acid molecule (monoglyceride), or two alcoholic groups are esterificated with two fatty acids molecules (diglyceride). In nature we meet only triglycerides. There are opinions that fats are made from simple triglycerides such as tripalmitin, tristearin, triolein, etc. But it turned out that in most of cases, fats are glycerin esters with 2 or 3 different fatty acids [1, 5]:

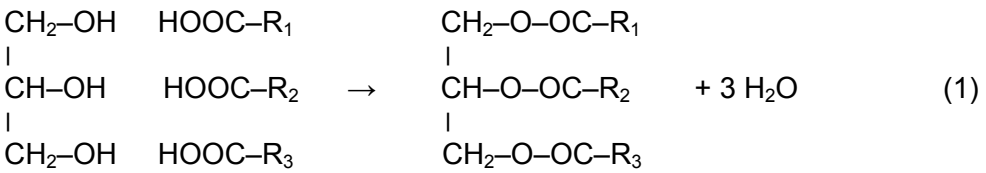

[a] *North University, Department of Chemistry-Biology, 76 Victoriei str., 430122, Baia Mare, Romania, flavia_maries@yahooo.com*

Fatty acids represent the variable structure of lipids, the characteristics of the fats being conferred by the nature and proportion of fatty acids that enters into their composition [11].

Major fatty acids from animal fats composition are those who have a number of 4 to 18 carbon atoms in the molecule, namely [5, 7]:

Butyric acid	$CH_3–(CH_2)_2–COOH$
Caproic acid	$CH_3–(CH_2)_4–COOH$
Caprylic acid	$CH_3–(CH_2)_6–COOH$
Caprynic acid	$CH_3–(CH_2)_8–COOH$
Lauric acid	$CH_3–(CH_2)_{10}–COOH$
Miristic acid	$CH_3–(CH_2)_{12}–COOH$
Palmitic acid	$CH_3–(CH_2)_{14}–COOH$
Stearic acid	$CH_3–(CH_2)_{16}–COOH$

The main unsaturated fatty acids in animal fats are oleic and linoleic acid. Oleic acid has 18 carbon atoms and one double link located between C9 and C10: $CH_3–(CH_2)_7–CH=CH–(CH_2)_7–COOH$. Linoleic acid has 18 carbon atoms, but two double links located between C9 and C10, C12 and C13: $CH_3–(CH_2)_4–CH=CH–CH_2–CH=CH–(CH_2)_7–COOH$ [28].

Animal fats has nutritional-biological and sensory value through: the provision of essential fatty acids for human body (linoleic, linolenic and arachidonic acids); concentrated sources of energy (cca.9 kcal/g, proteins and carbohydrates providing approx. 4 kcal/g); medium for transport/storage of liposoluble vitamins (A, D, E, K); formation of phospholipids with essential role in proper functionation of membranes; precursors of prostaglandins, essential hormones for the body; texture formers; structure formers in certain products (fillings for bakery products and confectionery); lipids confer softness (a slight bite and mastication), smaller the dry and granular feeling of food consumption (due to the lubrication effect and the liquid part of the fat); flavor providers (with positive or negative effect on the overall flavor of the product) and medium for hydrophobic flavour compounds [2, 3].

RESULTS AND DISCUSSION

The content of SFA in pork fat was higher (48.32%) than MUFA (36.78%) and PUFA (14.89%), the major fatty acids present in pork fat were palmitic, stearic, oleic and linoleic acids. Oleic acid was determined in the largest proportion (33.51%), these results are in agreement with previous studies on this type of fat [4, 6].

Figure 1 illustrates sample chromatogram for pork fat in witch fatty acids are registered in the form of peaks separated from each other by increasing the length chain, and at the same length chain by increasing of unsaturated degree.

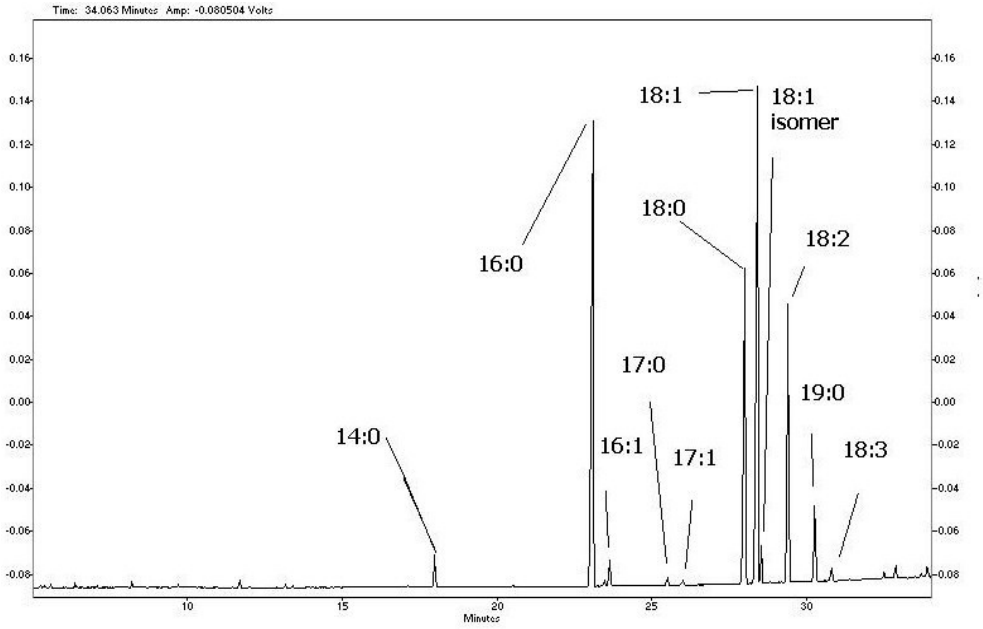

Figure 1. Chromatogram for fresh pork fat

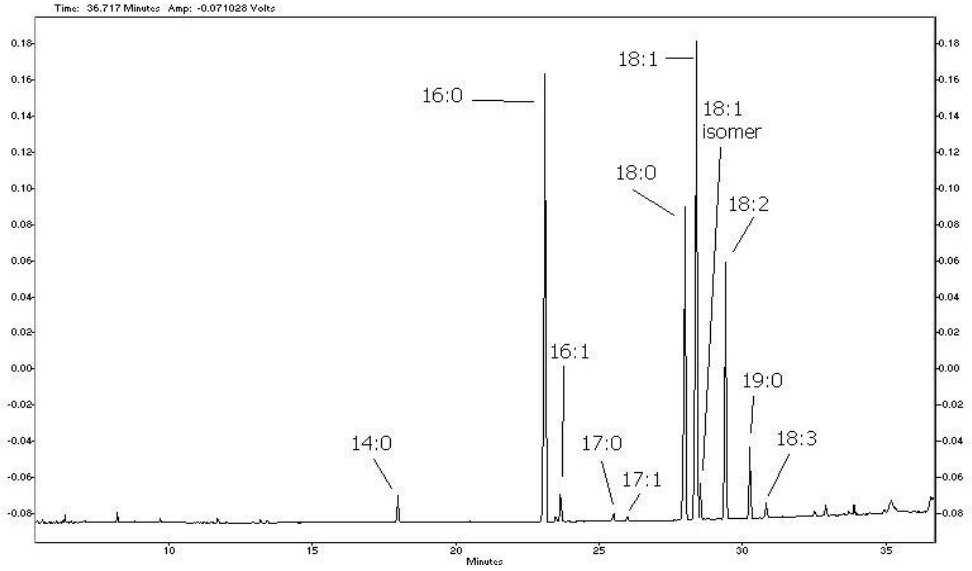

Figure 2. Chromatogram for pork fat at 4 months freezing

In pork fat sample to 4 months freezing there were some differences from the fresh sample: miristic acid content decreased to 1.29%, palmitic acid increased to 27.15%, palmitoleic acid increased to 1.35%, margaric acid decreased to 0.35%, *cis*-10-heptadecanoic acid remained constant, stearic acid increased to 20.03%, oleic acid decreased to 32.66%, vaccenic acid remained constant, linoleic acid increased to 14.41% and alfalinoleic acid increased to 0.76%. In general, the SFA content increased to 48.83%, the MUFA content decreased to 35.99% and the PUFA content increased to 15.18% (fig.2). The increas of saturated and polyunsaturated fatty acids content is due to the installation of hydrolysis leading to the release of acids from glycerides structure, which translates through the increas of titrable acidity.

The content of SFA in beef tallow was higher (57.13%) than MUFA (34.47%) and PUFA (8.4%), the major fatty acids present were palmitic, stearic and oleic acids [8, 10, 12]. Oleic acid was determined in the largest proportion (30.14%).

Figure 3 illustrates sample chromatogram for beef tallow in witch fatty acids are registered in the form of peaks separated from each other by increasing the length chain, and at the same length chain by increasing of unsaturated degree.

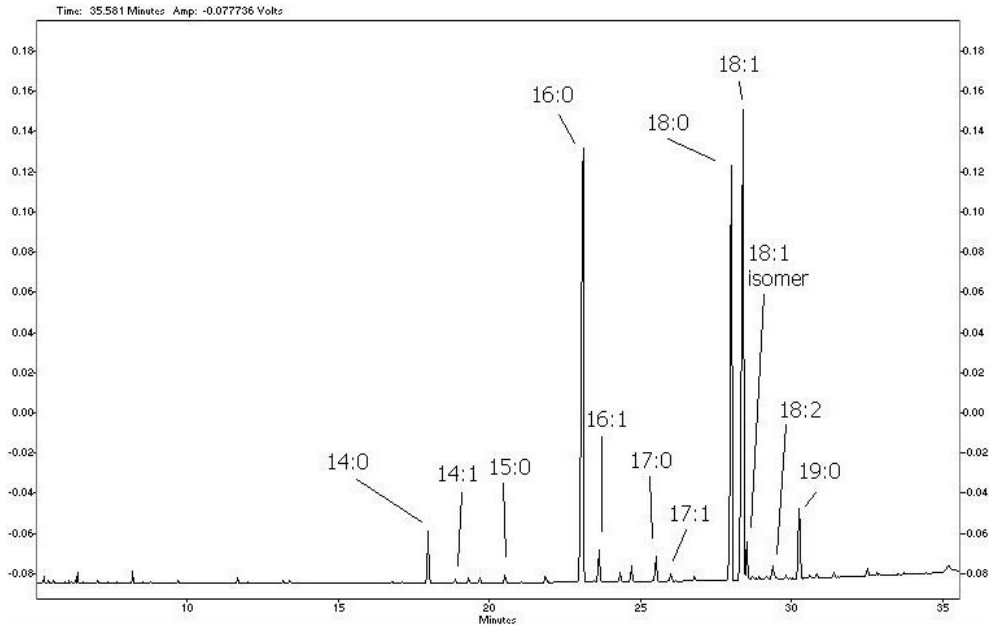

Figure 3. Chromatogram for fresh beef tallow

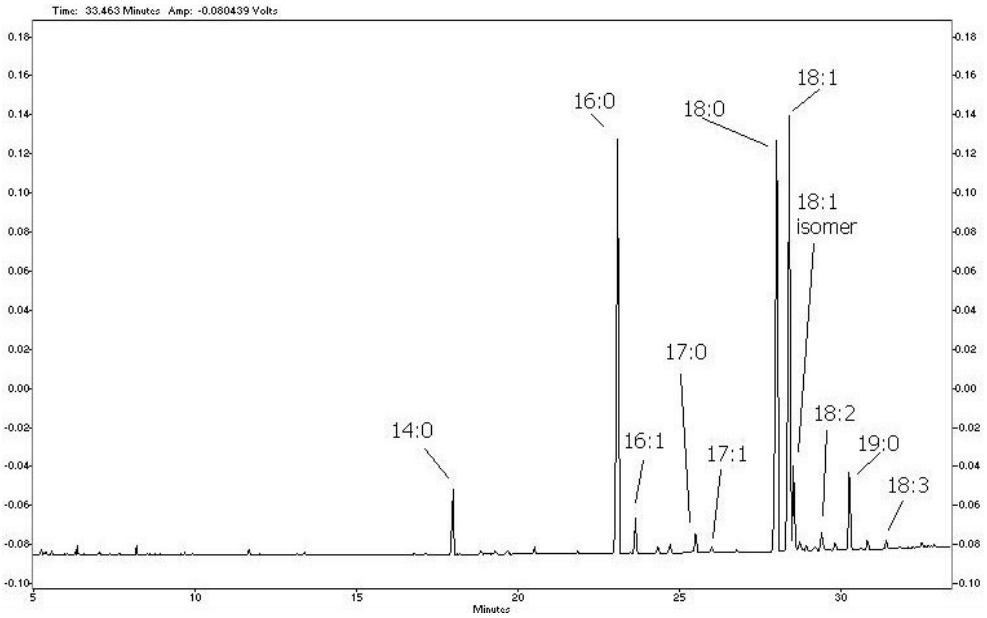

Figure 4. Chromatogram for beef tallow at 4 months freezing

In beef tallow sample at 4 months freezing there were some differences from the fresh sample: miristic acid content increased to 3%, pentaedecanoic and miristoleic acid were not detected, palmitic acid increased to 27.03%, palmitoleic acid increased to 1.77%, margaric acid decreased to 1.19%, *cis*-10-heptadecanoic acid decreased to 0.35%, stearic acid increased to 30.09%, oleic acid decreased to 30.09%, vaccenic acid increased to 4.64% and linoleic acid decreased to 1.32%. In general, the content of SFA increased to 61.3%, the MUFA content to 36.86% and the content of PUFA decreased to 1.84% (fig.4). In the case of beef tallow at 4 months congelation, monounsaturated fatty acids recorded an increase and polyunsaturated fatty acids a decrease, for pork fat at 4 months freezing we found the opposite.

Pork fat presents a highest proportion of mono and polyunsaturated fatty acids, than beef tallow, having aspect of alifios and homogeneous mass, beef tallow is presented as a compact and dense mass, fine granulated, with hard consistence, brittle to break or jam due to the higher content of saturated fatty acids [9, 11, 13].

CONCLUSIONS

Determination of chemical composition of animal fats is important in establishing organoleptic and physico-chemical parameters, the variation of them in time, being an indicator of their stability compared to alterative processes.

Beef tallow presented the lowest content of PUFA (8.4%), which are the most susceptible to autooxidation, it can be kept for a long period of time under refrigeration and freezing. Of studied fats, the most susceptible to altering is pork fat because its high content of PUFA (14.89%).

Chemical composition of fats influence their consistency, pork fat having aspect of alifios and homogeneous mass, beef tallow is presented as a compact and dense mass, fine granulated, with hard consistence, brittle to break or jam, with a higher value for melting point and a lower value for refractive and iodine index.

EXPERIMENTAL SECTION

Samples

Pork fat was obtained by melting of fresh bacon and lard pork and beef tallow was obtained by raw tallow melting, collected from "Baltata Romaneasca" race, female, age of 8 years, which were determined the chemical composition in fresh state and after 4 months of storage under freezing (-15 ...- 18^{o}C).

Physicochemical examination

Fatty acid composition was determined using gas chromatography (GC) Shimadzu GC-17 A coupled with flame ionisation detector FID. Gas chromatography column is Alltech AT-Wax, 0.25 mm I.D., 0.25 μm thick stationary phase (polyethylene), used helium as carrier gas at a pressure of 147 kPa, temperature of the injector and detector was set to 260^{o}C, the oven programm was the following: 70^{o}C for 2 min., then the temperature was raised up to 150^{o}C with a gradient of 10^{o}C/min., a level of 3 min. and the temperature was raised up to 235^{o}C with a gradient of 4^{o}C/min.

The method consists in transforming of fatty acids in methyl esters in the sample under analysis, followed by separation of components on a chromatography column, their identification by comparison with standard chromatograms and quantitative determination of fatty acids. Esterificated analyzed sample is introduced in column chromatography. By chromatography separation the sample chromatogram is obtained in which fatty acids are recorded in the form of peaks separated from each other by increasing the length chain, and at the same length chain by increasing of unsaturated degree. By comparing the distances of each peak from analyzed sample chromatogram with peaks distances from standard chromatograms, we identify each fatty acid present in the analyzed sample [14, 15, 16].

REFERENCES

1. C. Banu et al., *Tratat de chimia alimentelor*, Ed. Agir, Bucureşti, **2002**
2. C. Banu et al., *Alimentația şi sănătatea*, Editura Macarie, Târgovişte*,* **2001**
3. C. Banu, N. Preda, S. Vasu, *Produsele alimentare şi inocuitatea lor*, Editura Tehnică, Bucureşti, **1982**
4. J. Cháves, A. Castellote, M. Martin, R. Chifré, C. López-Sabater, *Food Chem.,* **2008**, *113*, 484
5. D. Ciobanu, R. Ciobanu, *Chimia produselor alimentare*, Ed. Tehnică-INFO, Chişinău, **2001**
6. A. Flåtten, A. Bryhni, A. Kohler, B. Egelandsdal, T. Isaksson, *Meat Sci.,* **2005**, *69,* no.3, 433
7. M. Leonte, T. Florea, *Tratat de chimia alimentelor*, I, Ed. Pax-Aura Mundi, Galaţi, **1998**
8. P. Manglano, M.J. Lagarda, M.D. Silvestre, C. Vidal, G. Clemente, R. Farre, *Eur. J. of Lipid Sci. and Tech*., **2005**, *107*, no.11, 815
9. S. Naz, R. Siddiqi, H. Sheikh, S. Asad Sayeed, *Food Res. Int*., **2005**, *38*, 127
10. E. Olsen, E.O. Rukke, A. Flátten, T. Isaksson, *Meat Sci*., **2007**, *76*, no.4, 628
11. N. Popescu, S. Meica, *Bazele controlului sanitar veterinar al produselor de origine animală*, Ed. Diacon Coresi, Bucureşti, **1995**
12. O. Samet-Bali, M.A. Ayadi, H. Attia, *Food Sci. and Tech*., **2008**, *30*, 7
13. V. Vito, F. Ferioli, Y. Riciputi, G. Iafelice, E. Marconi, M.F. Caboni, *Food Chem.*, **2008**, *78*, 384
14. ***Standard român SR ISO 661, **1998**
15. ***Standard român SR EN 14082, **2003**
16. ***International Standard ISO 3976, **2006**

STUDIA UNIVERSITATIS BABEŞ-BOLYAI, CHEMIA, LIV, 4, 2009

THE EFFECT OF ELECTROMAGNETIC FIELDS ON BAKER'S YEAST POPULATION DYNAMICS, BIOCATALYTIC ACTIVITY AND SELECTIVITY

DALIA SANDU[a], IOSIF LINGVAY[b], SZABOLCS LÁNYI[c], DAN DORU MICU[d], CLAUDIA LAURENTA POPESCU[e], JÜRGEN BREM[a], LÁSZLÓ CSABA BENCZE[a], CSABA PAIZS[*a]

ABSTRACT. The influence of ultralow frequency in the range of 23.8 -35.7 mT electromagnetic field on growth dynamics of *Saccharomyces cerevisiae* cells and the activity and selectivity for the cellular bioreduction of the prochiral 1-(benzofuran-2-yl)ethanone has been evaluated. The interaction of cell populations with the electromagnetic field reduced their growth rate, their activity and selectivity. The effects directly depends on the intensity of the applied field.

Keywords: Saccharomyces cerevisiae, electromagnetic field, cell growth dynamics, activity, selectivity, bioreduction, biocatalysis

INTRODUCTION

Electromagnetic fields with low frequencies (50-60 Hz) and low intensity are associated with the production, transmission and use of electricity. They interfere with the frequency of many biological processes involving changes in the electrical charges movements of the biomolecules. Furthermore, nowadays, due to the antropic activities, a large spectrum of electromagnetic fields, differing in their frequency are present in the biosphere as presented in Table 1 [1]. Communication, remote controls are the most common such applications.

Being a part of our environment, these fields were considered among potential interference factors that can modify the behavior of organism. That explains the great number of studies on this topic, dedicated to cells [2], tissues,

[a] *Babeş-Bolyai University, Faculty of Chemistry and Chemical Engineering, Str. Kogălniceanu, Nr. 1, RO-400084 Cluj-Napoca,Romania, paizs@chem.ubbcluj.ro*
[b] *National Institute of Research and Development in Electrical Engineering, Bucharest, Sector 3, Splaiul Unirii Nr. 313.*
[c] *Sapientia University, Faculty of Technical and Social Siences Piața Libertății, Nr. 1, Miercurea Ciuc, RO-530104,*
[d] *Technical University of Cluj Napoca, Faculty of Electrical Engineering, Constantin Daicoviciu Nr 15, Cluj-Napoca, RO-400020*
[e] *Politehinca University of Bucharest, Faculty of Electrical Engineering, Splaiul Independentei Nr. 313, Sector 6, RO- 060042*

whole living organisms [3]. Also the cell dynamics, the ion transport or gene transcription and expression [4] were consistent study objects. The effects of magnetic fields are numerous and apparently contradictory, depending on their static or alternative nature, intensity and frequency, by influencing the production of certain metabolites [5] they can stimulate or inhibit the cell growth [6- 7].

Electromagnetic fields influence DNA structure even at extremely low frequency. Based on the reported effects, the International Agency for Research on Cancer (IARC) has classified the extremely low-frequency (ELF) electromagnetic fields (EMF) as "possible carcinogenic" [8].

Saccharomyces cerevisiae is a validated experimental model, being one of the most intensively studied eukaryotic organisms in molecular and cell biology [9]. Our interest was focused on the investigation of possible action of the electromagnetic field on the catalytic parameters (activity and selectivity) and growth dynamic of *Saccharomyces cerevisiae*.

Table 1. Clasification of electromagnetic fields according to the frequency and use [1]

Frequency zone	**Frequency**	**Wavelength in the air**	**Use**
Extremely low	0-300 Hz	>1000 km	Many biological processes, electricity transport
Low, middle, high	30 kHz-30 MHz	10 km -10 m	Amateur radio, remote controls
Very, ultrahigh	30-300 MHz	10-1 m	Radio/TV
Superhigh	300 Mhz- 30 GHz	1 m-10 cm	Satellite communication
Extremely high	30-300 GHz	10-1 cm	RADAR
Infrared	300 GHz- 300 THz	1 cm-100 mm	
Visible light	429-750 THz	700-400 nm	Light

RESULTS AND DISCUSSION

Literature data showed that in the range of extremely low frequencies associated to commercial electric power at low values of amplitude (0.2-12 mT), a slight stimulation of cell growth [10] and also dehydrogenase activity [11] may occur. We investigated the influence of a 50 Hz magnetic field, generated in a toroidal coil, on *Saccharomyces cerevisiae* cellular proliferation. The activity and selectivity of yeast dehydrogenases in the reduction reaction of a substrate was tested in both the presence and the absence of the electromagnetic field.

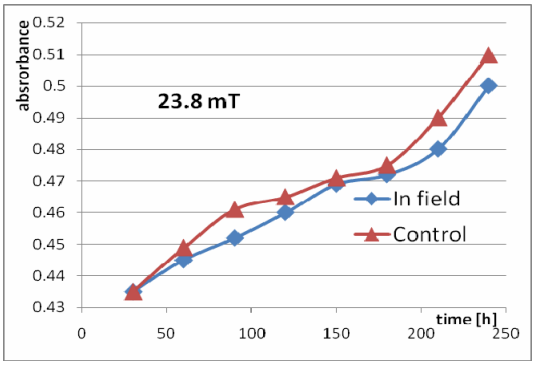

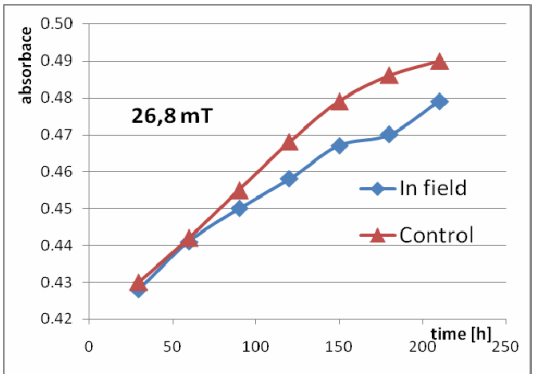

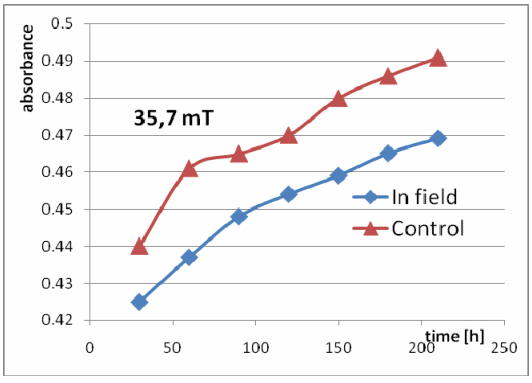

Figure 1. Comparative cell population dynamics in a magnetic field

a) The effect of the electromagnetic field on Saccharomyces cerevisiae growth dynamics

The cellular growth rate was slowed at all tested intensities of the electromagnetic field with the frequency of 50 Hz. As shown in Figure 1, the growth curves of the exposed yeast populations had lower values than the curves of the control populations.

In all cases the growth was positive, but the electromagnetic field showed a slight inhibitory effect.

The slowing of the cell growth was proportional with the intensity of the field.

b) The effect of the electromagnetic field on enzyme activity and selectivity

Biocatalyst-assisted conversion of the substrate is an estimate of the biocatalytic activity of the cells.

Parallel determinations in presence of the electromagnetic field at 26.8 and 35.7 mT and in unexposed cultures showed that in the range of these intensities the field reduced the catalytic activity (Figure 2) and selectivity of yeast dehydrogenases (Table 2).

The selectivity of the biocatalytic reaction was estimated by measuring the enantiomeric excess of the bioreduction product using as substrate 2-acetyl-benzofuran (Figure 3).

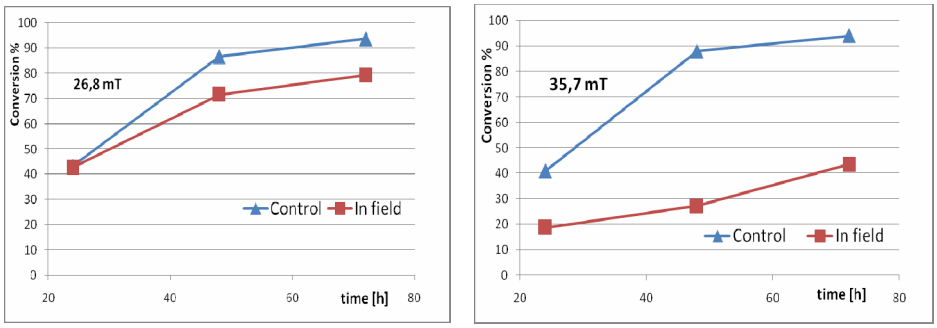

Figure 2. Influence of electromagnetic field on the conversion of the bioreduction of 2-acetylbenzofuran

As for enzymatic activity, determinations showed that samples exposed to the electromagnetic field, in the range of 26.8 and 35.7 mT intensity, lead to enantiomeric excesses of the product under the values found for the unexposed samples.

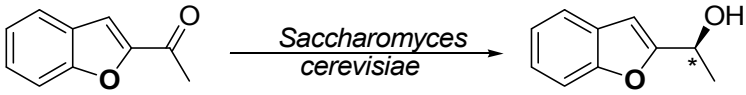

1-(benzofuran-2-yl)ethanone (*S*)-1-(benzofuran-2-yl)ethanol

Figure 3. Cellular reduction of 2-acetyl-benzofuran

Table 2. Enantiomeric excesses of the reaction product obtained with exposed and unexposed cells

Enantiomeric excesses (ee%)	**1.8 A**			**2.4 A**		
	24h	48h	72h	24h	48h	72h
Control sample	72%	73%	75.4%	66%	71%	77%
Exposed sample	67%	72%	74%	38%	44%	45%

CONCLUSIONS

The electromagnetic field generated by an alternative current of 50 Hz, applied at intensities in the range of 23.8-35.7 mT on *Saccharomyces cerevisiae* suspensions produced significant alterations in the growth dynamics of the cell populations. The catalytic activity and the selectivity in the reduction of the investigated prochiral 1-(benzofuran-2-yl)ethanone were impaired.

The results obtained in parallel experiments, with samples unexposed and exposed to the electromagnetic field, are in aggreement with the literature data and demonstrate the lowering of the growth dynamics.

Our original experiments on the biocatalytic activity and selectivity showed that the interference of the electromagnetic field with the biochemical process resulted the decrease of the substrate transformation rate and also reduced the discrimination capability of the enzymatic equipment for the two enantiotope faces of the substrate.

EXPERIMENTAL SECTION

The electromagnetic field was generated in a toroidal coil powered by an autotransformer at three values of the AC power: 1.6 A, 1.8 A and 2.4 A, which produced in the coil axis magnetic inductions of 23.8, 26.8 and 35.7 mT, respectively.

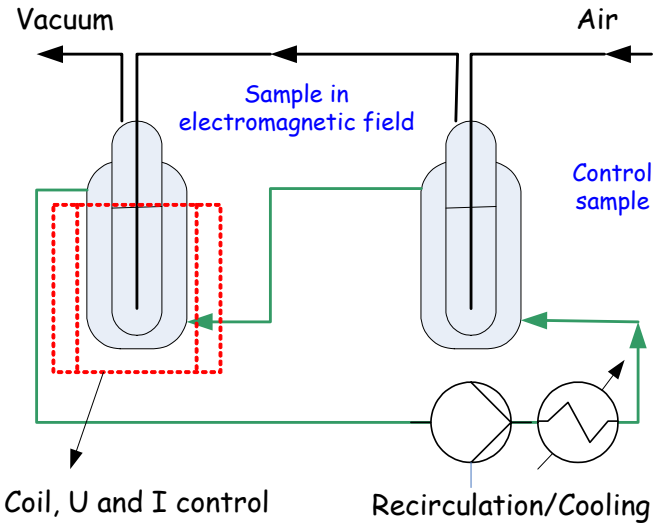

Figure 4. Experimental design for studying the effect of the electromagnetic field on certain functional parameters in *Saccharomyces cerevisiae*

A glass vial (bioreactor) provided with a cooling jacket and an air bubbler was introduced in the axis of the coil. An identical inexposed vial was used as control reactor. Both vials were termostated at 25 ^{o}C. The yeast suspensions were agitated with the same rate by air bubbling using an arrayed assembly as shown in Figure 4. Two experiments were performed, one at three different intensity values of the field and the second at two values of field intensity. In the first experiment it was investigated the influence of the intensity of the field upon the cell population growth and in the second one the effect of the field upon the stereoselectivity and the reaction rate for the cellular bioreduction of 2-acetyl-benzofuran was monitored. In all experiments commercially available baker's yeast was used.

For the growth experiment first a calibration curve was draw on, using the correlation between absorbance at 600 nm, and cellular concentration (gl^{-1}). The absorbance was measured using an UV-VIS Perkin-Elmer, type Lambda 1 spectrophotometer.

A suspension with the initial concentration of 0.500 gl^{-1} yeast and 2.5 gl^{-1} sugar was introduced in the two bioreactors. Samples were taken every 30 min. from both bioreactors, for a period of 240 min.

In the selectivity experiment, the investigated reaction was the enantiotope selective reduction of 2-acetyl-benzofuran (1-(benzofuran-2-yl)ethanone). The synthesis and the reduction of acetyl-benzofuran was synthesized according to literature data in the literature and was performed as earlier described by us [12].

The non-fermentative system was used in these experiments which provide a superior selectivity, but a prolonged reaction time in comparison with the fermenting system.

The solution of 2-acetyl-benzofuran (50 mg) in absolute ethanol (5 ml) was added into each bioreactor containing a suspension of 20 g yeast in 100 ml distilled water. Samples (1 ml) taken perodically (24h) from both exposed and unexposed bioreactor to appreciate the difference in biocatalyst selectivity due to the action of the electromagnetic field were extracted with ethyl acetate (3ml). The organic layer was dried over anhydrous sodium sulphate and the solvent was eliminated by rotary evaporation. The crude solide was redissolved in hexane (0.5 ml) and the solution was subjected for chromatographic analysis using an Agilent 1200 HPLC. Using a Chiracel OJ-H analytical column and a mixture of hexane:isopropanol 90:10 (v/v) as eluent previously tested succesfully for the enantiomeric separation of the racemic 1-(benzofuran-2-yl) ethanol, the enantiomeric excess of (*S*)-1-(benzofuran-2-yl) ethanol produced in both bioreactors were measured.

The conversion of the substrate was calculated from using the area of the alcohol and prochiral ketone chromatograpic signals corrected with the *ratio* of the specific molar absorbance of the compounds.

ACKNOWLEDGMENTS

The financial support from the Romanian Ministry of Education and Research (No. **X2C37/2006**, within the PN2 Program) is gratefully acknowledged.

REFERENCES

1. R. Funk, T. Monsees, N. Özkucur. *Progress in Histochemistry and Cytochemistry,* **2009**, *43*: 87.
2. S. Kwee, P. Raskmark. *Bioelectrochemistry and Bioenergetics,* **1995**, *36*: 109.
3. R. Beraldi, I. Sciamanna, R. Mangiacasale, R. Lorenzini, C. Spadafora. *Mutation Research/Genetic Toxicology and Environmental Mutagenesis,* **2003**, *538*: 163.

4. J.L. Phillips, N.P. Singh, H. Lai. *Pathophysiology,* **2009**, *16*: 79.
5. D.C. Alvarez, V.H. Pérez, O.R. Justo, R.M. Alegre. *Process Biochemistry,* **2006**, *41*: 1967.
6. L. Potenza, L. Ubaldi, R. De Sanctis, R. De Bellis, L. Cucchiarini, M. Dachŕ. *Mutation Research/Genetic Toxicology and Environmental Mutagenesis,* **2004**, *561*: 53.
7. W. Triampo, G. Doungchawee, D. Triampo, J. Wong-Ekkabut, I.M. Tang. *Journal of Bioscience and Bioengineering,* **2004**, *98*: 182.
8. M. Ruiz-Gómez, M.-M. M. *Electromagn Biol Med,* **2009**, *28*: 201.
9. J. Novák, L. Strasák, L. Fojt, I. Slaninová, V. Vetterl. *Bioelectrochemistry,* **2007**, *70*: 115.
10. M. Mehedintu, H. Berg. *Bioelectrochemistry and Bioenergetics,* **1997**, *43*: 67.
11. L. Zhang, H. Berg. *Journal of Electroanalytical Chemistry,* **1992**, *343*: 341.
12. C. Paizs, M. Tosa, C. Majdik, P. Moldovan, L. Novák, P. Kolonits, A. Marcovici, F.-D. Irimie, L. Poppe. *Tetrahedron: Asymmetry,* **2003**, *14*: 1495.

STUDIA UNIVERSITATIS BABEŞ-BOLYAI, CHEMIA, LIV, 4, 2009

SYNTHESIS OF ESTER DERIVATIVES OF CALIX[N]ARENE

ALINA SAPONAR[a], ELISABETH-JEANNE POPOVICI[a], RODICA GRECU[a], IOAN SILAGHI-DUMITRESCU[b], NICOLAE POPOVICI[a]

ABSTRACT. The synthesis of *p-tert*-butyl calix[n]arene derivatives with two and four, as well as, four and six (ethoxycarbonyl)methoxy groups at the lower rim is reported. The selective alkylation of the parent calix[n]arenes is performed in organic solvents, with ethyl bromoacetate in the presence of potassium carbonate or sodium hydride as a base. UV-Vis, FTIR, ^{1}H-NMR investigations confirmed the formation of the ester derivatives of calix[n]arene with variable number of ester groups at the narrow rim.

Keywords: Calix[n]arene, selective O-alkylation, ethyl bromoacetate

INTRODUCTION

A dedicated class of [1n] metacyclophanes generally designed as calixarene are nowadays receiving an increasing attention in the field of supramolecular chemistry because of their simple synthesis, easy modification (functionalisation) and unique properties [1, 2]. It is well known that calixarene derivatives containing oxygen donor groups, acid, ester or keto, linked at the phenolic oxygen at the narrow rim, exhibit excellent properties as neutral receptors for metallic ions [3-16]. Many recent works have been focussed on the utilisation of calixarene derivatives as prospective ionophores for ion selective electrodes, optical sensors or colorimetric reagents for use in the determination of clinically important species [17].

Our earlier findings on the synthesis of calix[n]arene for sequestration of rare earth and precious ions revealed that derivatives having three 2-butenyl (crotyl) groups at the narrow rim show good extraction ability for europium and palladium ions [18]. Good results we also obtained with organo-phosphorus and/or crotyl functionalised calix[6]arene [19,20].

Aiming to develop new ionophores or cation extraction reagents based on calixarene derivatives, a variable number of oxygen donor groups e.g. ester groups was grafted on the parent *p-tert*-butyl calix[6,8]arenes.

[a] *Raluca Ripan Institute for Research in Chemistry, Babes Bolyai University, 400294, Cluj-Napoca, Romania, salina@chem.ubbcluj.ro*

[b] *Faculty of Chemistry and Chemical Engineering, Babes-Bolyai University, 40084, Cluj-Napoca, Romania.*

Due to the presence of the *p*-electrons of the ester groups, these derivatives are of practical interest for rare earth and precious metal sequestration.

Herein we present our study referring to the synthesis and characterization of new derivatives of *p-tert*-butyl calix[6]arene and *p-tert*-butyl calix[8]arene with two and four, as well as, four and six (ethoxycarbonyl)methoxy groups. We previously reported the synthesis of some other ester derivatives [25-27] in this class of compounds.

RESULTS AND DISCUSSION

The chemistry we followed is shown in scheme 1 (depicted).

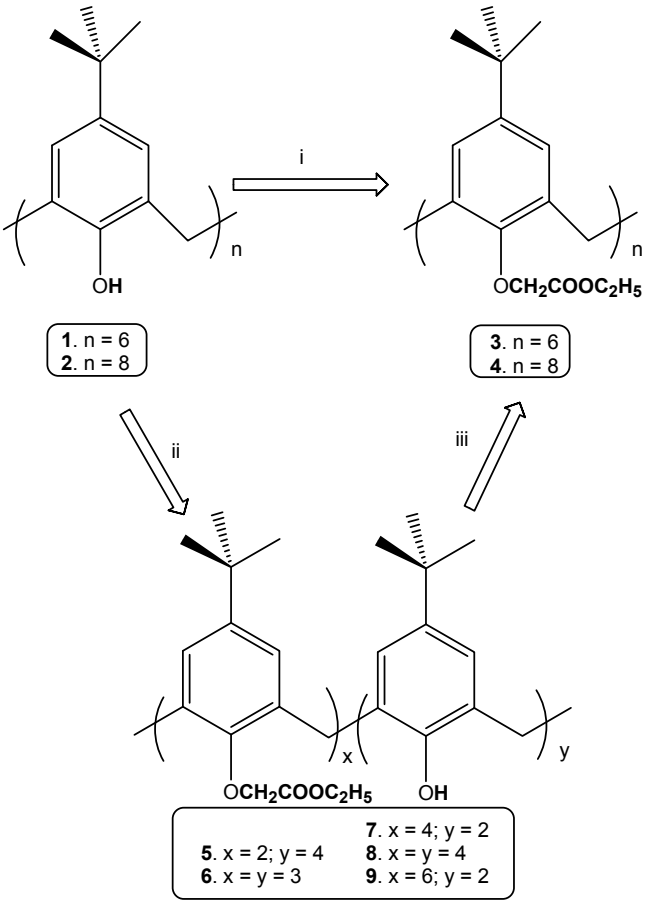

Scheme 1

Thus, the parent calix[n]arenes were O-alkylated with ethyl bromoacetate in alkaline conditions in order to prepare derivatives with two-to-eight [(ethoxycarbonyl)methoxy] groups grafted at the narrow rim.

Reaction of *p-tert*-butyl calix[n]arene (**1-2**) in the presence of K_2CO_3 or NaH as a base, with the required amount of ethyl bromoacetate in organic solvents or mixture of them, yielded calix[n]arene ester derivatives with two (**5**), three (**6**), tetra (**7,8**), hexa (**3,9**) and octa (**4**) ester groups respectively.

UV-Vis, FTIR and ^{1}H-NMR investigations confirmed the formation of the desired O-functionalised calix[n]arene.

^{1}H-NMR spectra

The ^{1}H-NMR spectra of calixarene contain several broad bands which are characteristic for the conformational flexibility of calix[6]- and calix[8]arene derivatives. Indeed, the ^{1}H-NMR spectra showed the expected differences between the chemical shifts of the parent calixarene and their derivatives. The position of the singlet belonging to the phenolic OH groups varies with the ring size of the calixarene. Thus the chemical shifts of OH groups appeared at 10.55 ppm for compound **1**, and 9.86 ppm for compound **2**, whereas calixarene derivatives **5** and **7-9** showed the chemical shifts at: 7.11 (**5**), 7.11 (**7**), 7.10 (**8**) and 7.06 (**9**) ppm.

Table 1 collects the relevant ^{1}H-NMR data of calixarene derivatives.

Table 1. Selected ^{1}H-NMR data of compounds **5,7-9** in comparison with the parent calixarenes **1, 2**

	$C(CH_3)_3$	$O\text{-}CH_2\text{-}CH_3$	$O\text{-}CH_2\text{-}CH_3$	$ArCH_2Ar$	$O\text{-}CH_2\text{-}CO$	ArH	ArOH
1	1.27,s	-	-	3.78,bs	-	7.16,s	10.55,s
2	1.26,s	-	-	3.53,d; 4.39,d	-	7.17,s	9.86,s
5	0.87,s; 1.19,s	1.24,t	4.06-4.20,m	3.48,bs	4.49,s	6.99,s; 7.04,s	7.11,s
7	1.15,s; 1.20,s	1.17,t	4.06 – 4.12,m		4.47,s	6.84,s; 6.90,s	7.11,s
8	0.93s; 1.04,s	1.02,t	3.64 – 4.07,m			6.83,s; 6.87,s	7.10,s
9	1.02,s; 1.18,s	0.94,t	3.93 – 4.37,m		4.61,s	6.83,s; 6.86,s	7.06, s

FTIR spectra

FTIR spectra of the parent calixarene showed the stretching vibration of the phenol group at 3149 (**1**) and 3244 (**2**) cm^{-1}, respectively, in agreement with literature data [2]. By functionalisation at the narrow rim, the strong circular hydrogen bonding was supressed and derivatives **5-9** show the OH vibrations to be shifted at 3423 (**5**), 3448 (**7**), 3448 (**8**) 3438 (**9**) cm^{-1}, close to the OH stretching in isolated phenolic OH.

The stretching vibration arising from carbonyl group were observed as two strong bands at 1762, 1740 (**5**), 1759, 1735 (**7**), 1759, 1730 (**8**), and 1760, 1738 (**9**) cm^{-1}, respectively. The presence of two $\nu_{C=O}$ bands in the IR spectra suggests that two different carbonyl groups exist in these calixarene under different environments [28].

A relevant example is shown in Figure 1.

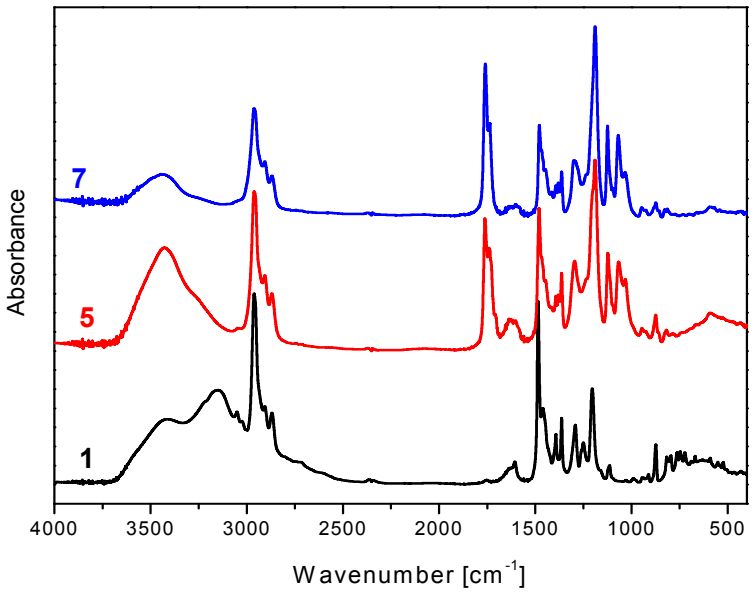

Figure 1. FTIR spectra of compounds **1** (parent calix[6]arene), **5** (diester derivative) and **7** (tetraester derivative)

UV-VIS spectra

The functionalisation of parent calixarene **1, 2** induced significant changes in the UV-Vis absorption spectra allowing pertinent analysis of the resulting ester derivatives (Figure 2). absorption maxima at about 280 and 288 nm in the UV region. The

According to literature [2], such cyclic oligomers have a pair of absorption ratio of these two maxima is a function of the ring size.

The starting calixarene revealed the specific absorption bands at 280, 288 (**1**), and 283, 291 (**2**) nm, respectively. In parallel with the increase of the number of phenolic rings, the shift of the maxima toward longer wavelengths as well as the rise of the band ratios were noticed.

The specific UV absorptions of our O-functionalised calixarene appeared at 278, 286 (sh) (**5**), 273, 279 (**7**), 273, 278, 289 (sh) (**8**) and 270, 278 (**9**). For comparison, the complete O-alkylation of calix[8]arenes (**4**) is also presented, showing the specific absorption bands at 271 and 279 nm, respectively.

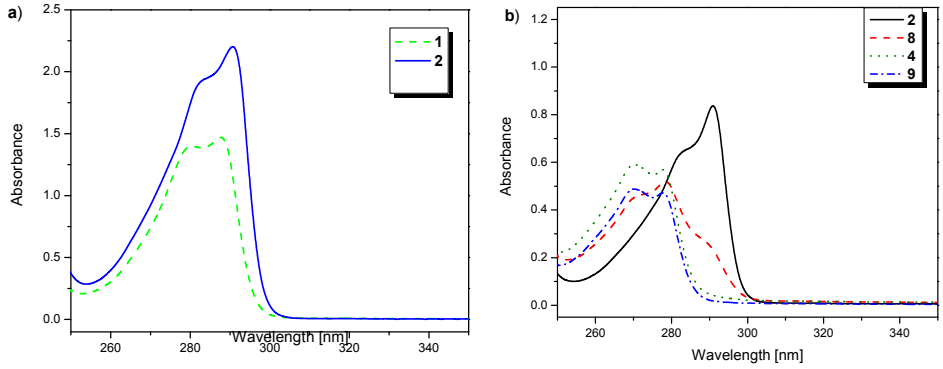

Figure 2. UV-vis absorption spectra of *p-tert*-butyl calix[n]arene and their derivatives ($CHCl_3$ solution;$1x10^{-4}$M): a) **1** (calix[6]arenes), **2** (calix[8]arenes); b) **4** (octaester derivative), **8**(tetraester derivative), **9** (hexaester derivative) and **2**(calix[8]arenes; $0.322x10^{-4}$M).

One note that the ester functionalisation brings about a new absorption band at shorter wavelength that increases in intensity with the number of grafted ester groups. The decrease of the absorption energy with the increasing of number of phenolic rings is also evident.

The ester calix[n]arene derivatives were tested as extracting reagent for precious metal and rare earth ions. Extraction was performed at pH= 2-3, from $1x10^{-3}$ M aqueous solution of $PdCl_2/Eu(NO_3)_3$, using $1x10^{-3}$ M solution of calixarene in $CHCl_3$. Relative high ability for the sequestration of divalent palladium was found, especially, for half substituted calix[6]arene or calix[8]arene. For instance, the extraction yield was ~53% for compound **6** and ~35% for compound **3**. The extraction capability for trivalent europium ions was low for all the ester calix[n]arene derivatives.

CONCLUSIONS

Calix[n]arene [n=6,8] derivatives comprising bi-, tetra-, hexa- and octa (ethoxycarbonyl)methoxy groups were obtained by O-alkylation of calix[n]arene with variable amounts of ethyl bromoacetate. Their structure was confirmed by spectroscopic investigations (UV-Vis, FTIR, ^{1}H-NMR).

Ester calix[n]arene derivatives with variable number of oxygen donor groups e.g. ester linked at the narrow rim, showed ability for the extraction of precious metal ions e.g. palladium from aqueous medium.

EXPERIMENTAL SECTION

All reactions were performed under nitrogen atmosphere using oven-dried glassware. Reagents were purchased from commercial suppliers and were used without further purification. All solvents were dried over standard

drying agents and distilled prior to use. Reactions were monitored by TLC on Kiselgell 60 F_{254} plates with detection by UV or Iodine.

Melting points were determined with POINT METER KSP II apparatus in a sealed capillary and are uncorrected values. ^{1}H-NMR spectra were recorded on VARIAN GEMINI 300 S (300 MHz) spectrometer. Deuterated chloroform was used as solvent and TMS as references. IR spectra were recorded on FTIR (JASCO) 610 and UV-Vis spectra on UNICAM UV 4 spectrometers. Elemental analysis (E.A.) was performed with a Vario EL analyser.

The starting calixarenes **1** and **2** were synthesised according to literature [21-23].

Reaction of *p-tert*-butyl calix[n]arene **1** or **2** with the required amount of ethyl bromoacetate was performed in the presence of K_2CO_3 or NaH as a base, using THF/DMF or acetone as solvent (Scheme 1). *p-tert-* butyl calix[n]arene derivatives containing two (**5**), three (**6**), tetra (**7, 8**), hexa (**3, 9**) and octa (**4**) ester groups were isolated and recrystallised from dichloromethane-ethanol mixture. The synthesis of compounds **3** and **4** [24] and **6** [25] was carried out according to literature.

The preparation yield was 81%(**3**), 61%(**4**), 62%(**5**), 38%(**6**), 72%(**7**), 71%(**8**) and 49%(**9**).

The main characteristics of the new synthesised calixarenes derivatives are presented bellow. For the 1H chemical shifts, see Table 1.

5,11,17,23,29,35-hexa-*tert*-butyl-bis[(ethoxycarbonyl)methoxy]-tetrahydroxy-calix[6]arene (5)
M.p.=221°C
M.W. calcd. for $C_{74}H_{96}O_{10}$=1144
E.A: Calcd: C=77.59; H=8.45 ; *Found:* C=77.90; H=8.21
UV-Vis: [$CHCl_3$; λ_{max} (nm)/ε($M^{-1}cm^{-1}$)]=278/6373; 286/5000
FTIR: ($\nu_{max.}$, KBr, cm^{-1}): $\nu_{C=O}$=1740, 1762; ν_{OH}=3423

5,11,17,23,29,35-hexa-*tert*-butyl-tetrakis[(ethoxycarbonyl)methoxy]-dihydroxy-calix[6]arene (7)
M.p.=261°C
M.W. calcd. for $C_{82}H_{108}O_{14}$=1316
E.A.: Calcd: C=74.74; H=8.26 ; *Found:* C=74.90; H=8.21
UV-Vis: [$CHCl_3$; λ_{max} (nm)/ε($M^{-1}cm^{-1}$)]=273/5880; 279/5697
FTIR: ($\nu_{max.}$, KBr, cm^{-1}): $\nu_{C=O}$=1759, 1735; ν_{OH}=3448

5,11,17,23,29,35,41,47-octa-*tert*-butyl -tetrakis-((ethoxycarbonyl)methoxy)- tetrahydroxy-calix[8]arene (8)
M.p.=195°C
M.W. calcd. for: $C_{104}H_{136}O_{16}$=1640
E.A.: Calcd: C=76.06; H=8.35; *Found:* C=74.90; H=8.21
UV-Vis: [$CHCl_3$; λ_{max} (nm)/ε($M^{-1}cm^{-1}$)]=273/4680; 278/5210;289(sh)/2670
FTIR: ($\nu_{max.}$, KBr, cm^{-1}): $\nu_{C=O}$=1759, 1730; ν_{OH}=3448

5,11,17,23,29,35,41,47-octa- *tert*-**butyl -hexakis-((ethoxycarbonyl)methoxy)- dihydroxy-calix[8]arene (9)**
M.p.=216°C
M.W. calcd for: $C_{112}H_{148}O_{20}$=1812
E.A. Calcd: C=74.14; H=8,22; *Found:* C=74.60; H=8.45
UV-Vis: [$CHCl_3$; λ_{max} (nm)/ε($M^{-1}cm^{-1}$)]=270/4900; 278/4760
FTIR: ($\nu_{max.}$, KBr, cm^{-1}): $\nu_{C=O}$=1760, 1738; ν_{OH}=3438

ACKNOWLEDGEMENTS

The financial support of the Romanian Ministry of Education and Innovation under the project PNII-71-062 is gratefully appreciated.

REFERENCES

1. Z. Asfari, V. Bohmer, J. Harrowfield, J. Vicens, “Calixarenes 2001”, Kluwer, Dordrecht, **2001**.
2. C.D. Gutsche, “Calixarene revisited”, J.F. Stoddart Ed., J.F. Royal Society of Chemistry, London, **1998**.
3. A. Arduini, G. Giorgi, A. Pochini, A. Secchi, F. Ugozzoli, *Tetrahedron*, **2001**, *57*, 2411.
4. N.J. Wolf, E.M. Georgiev, A.T. Yordanov, B.R. Whittlesey, H.F. Koch, D.M. Roundhill, *Polyhedron*, **2002**, *21*, 763.
5. M. Bochenska, R. Banach, A. Zielinska, V.C. Kravtsov, *J. Incl. Phenom. Makromol. Chem*, **2001**, *39*, 219.
6. H. Halouani, I. Dumazet-Bonnamour, C. Duchamp, C. Bavoux, N. Ehlinger, M. Perrin, R. Lamartine, *Eur.J. Org. Chem.*, **2002**, 4202.
7. A. Casnati, L. Baldini, N. Pelizzi, K. Rissanen, F. Ugozzoli, R. Ungaro, *J. Chem. Soc. Dalton Tr.*, **2000**, 3411.
8. A. Casnati, S. Barboso, H. Rouqueette, M. J. Schwing-Weill, F. Arnaud-Neu, J.F. Dozol, R. Ungaro, *J. Am. Chem. Soc.*, **2001**, *123*, 12182.
9. A. Moser, G.P.A. Yap, C. Detllier, *J. Chem. Soc. Dalton Tr.*, **2002**, 428.
10. P.D. Beer, M.G.B. Drew, M.I. Ogden, *J. Chem. Soc. Dalton Tr.*,**1997**, *11*, 1489.
11. P.D. Beer, M.G.B. Drew, P.B. Leeson, M.I. Ogden, *Inorg. Chim. Acta*, **1996**, *246*, 133.
12. P.D. Beer, M.G.B. Drew, M.Kan, P.B. Leeson, M.I. Ogden, G. Williams, *Inorg. Chim. Acta*, **1996**, *35*, 2202.
13. P.D. Beer, M.G.B. Drew, A. Grieve, M.I. Ogden, *J. Chem. Soc. Dalton Tr.*, **1995**, 3455.

14. P.D. Beer, M.G.B. Drew, P.B. Leeson, M.I.Ogden, *J. Chem. Soc. Dalton Tr.*, **1995**, 1273.
15. F. Arnaud-Neu, G. Barrett, D. Corry, S. Cremin, G. Ferguson, J.F. Gallagher, S.J. Harris, M.A. McKervey, M.J. Schwing-Weil, *J. Chem. Soc. Perkin Tr. 2*, **1997**, 575.
16. M.I. Ogden, B.W. Skelton, A.H. White, *J. Chem. Soc. Dalton Tr.*, **2001**, 3073.
17. B.T.T. Lan, K. Toth, *Analytical Sciences*, **1998**, *14*, 191.
18. T. Ursales, I. Silaghi-Dumitrescu, R. Ciocan, N. Palibroda, N. Popovici, E.J. Popovici, *Rev. Roum. Chim.*, **2004**, *49*, 741.
19. T. Ursales, I. Silaghi-Dumitrescu, E.J. Popovici, A. Ursales, N. Popovici, *J. Optoelectron. Adv. Mater.*, **2004**, *6(1)*, 307.
20. T. Ursales, I. Silaghi-Dumitrescu, E.J. Popovici, A. Ursales, N. Popovici, *Studia Universitatis Babes-Bolyai, Physica*, **2003**, XLVII(*2)*, 370.
21. C.D. Gutsche, M. Iqbal, *Org. Synthesis*, **1989**, *68*, 234.
22. C.D. Gutsche, B. Dhawan, M. Leonis, D. Stewart, *Org. Synthesis*, **1989**, *68,* 238.
23. J.H. Munch, C.D. Gutsche, *Org. Synthesis*, **1989**, *68*, 243.
24. G. McMahon, R. Wall, K. Nolan, D. Diamond, *Talanta*, **2002**, *57*, 1119.
25. N. Popovici, E.J. Popovici, M. Ladar, R. Grecu, *Studia Universitatis Babes-Bolyai, Physica*, **2005**, *L(4b)*, 650.
26. A. Saponar, I. Silaghi-Dumitrescu, E.J. Popovici, N. Popovici, *Studia Universitatis Babes-Bolyai, Chimia*, **2007**, *LII(4)*, 67.
27. A. Saponar, I. Silaghi-Dumitrescu, E.J. Popovici, N. Popovici, *Rev. Chim.*, **2007**, *58(5)*, 481.
28. P. Leyton, C. Domingo, S. Sanchez-Cortes, M. Campos-Valette, J.V. Garcia-Ramos, *Langmuir,* **2005**, *21(25)*, 11814.

MORE DETAILS CONCERNING THE USE OF THE THOMSON RADIAL FREQUENCIES $\omega_{Th,s}$, $\omega_{Th,p}$ (OF THE SERIES, RESPECTIVE PARALLEL, CIRCUITS, CONSIDERED INSTEAD OF THE WARBURG PSEUDO CAPACITANCE C_W), AS CRITERIA OF CLASSIFYING THE DRUGS

NICOLAE BONCIOCAT[a] AND ADINA COTARTA[a]

ABSTRACT. In a very recent communication we have shown that the EIS method may be used for classifying the drugs. More precisely it has been shown that to explain the phase difference between the current and the tension it is necessary to use instead of the Warburg pseudo-capacitance $C_W(\omega_1)$, two physically quantities, namely: a pseudo-inductance $L_W(\omega_1)$ and a pseudo-capacitance $C_W(\omega_1)$, which may be arranged in series or in parallel. Consequently, two criteria of classifying the drugs have resulted: for the series arrangement the Thomson radial frequency $\omega_{Th,s} = [L_s(\omega_1)C_s(\omega_1)]^{-1/2}$, respective for the parallel arrangement, the Thomson radial frequency $\omega_{Th,p} = [L_p(\omega_1)C_p(\omega_1)]^{-1/2}$. As for ω_1 it represents the lowest radial frequency used in getting the Nyquist plots(e.g., 1.256 s^{-1}) and has a very important physical meaning: it represents the resonance Thomson radial frequency of both series or parallel circuits, and expresses the highest efficiency that a drug may have, irrespective of the fact that it belongs to the class characterized by the criterion $\omega_{Th,s}(\omega_1)$ or by the criterion $\omega_{Th,p}(\omega_1)$. At the resonance Thomson radial frequency, ω_1 the electric energy of the drug, transforms in its magnetic energy and back in its electric energy and this oscillation between electric and magnetic energies occur permanently with a maximum amplitude. This explains why at the resonance radial Thomson frequency $\omega_{Th,s} = \omega_{Th,p} = \omega_1$ the efficiency of drug is maximum.

Keywords: multielectrode, Thomson radial frequencies, drugs classification

INTRODUCTION

In a series of papers, Bonciocat et al., have shown that the faradaic current density of an electrode redox reaction occuring with combined limitations of charge transfer and nonstationary, linear, semiinfinite diffusion is the solution

[a] *University Politehnica of Bucharest, Department of Applied Physical Chemistry and Electrochemistry, Computer Aided Electrochemistry Laboratory UPB-LEAC, Bucharest, Romania, PO BOX 12-112, e-mail: adina@cael.pub.ro*

of an integral equation of Volterra type[1-6]. By solving this integral equation, new methods of direct and cyclic voltammetry have been developed [7-15]. The above mentioned equation has led to a new approach to the Electrochemical Impedance Spectroscopy (EIS) when only the charge transfer and diffusion limitations are present. Very recently has been shown that the E I S method may have important applications in drug research[16-19].

In this paper, one analysis more deeply the physical meaning of this *resonance* Thomson radial frequency, and how it is related to the *normal* Thomson radial frequencies $\omega_{Th,s}$, respective $\omega_{Th,p}$. Two formulae have resulted, expressing the quantities $\omega_1^2 / \omega_{Th,s}^2$, respective $\omega_{Th,p}^2 / \left(\omega_{Th,p}^2 - \omega_1^2\right)$, in terms of the contributions that a drug may have upon the processes occurring at the electrode/ solution interface. Thus, it may introduce new electrode reactions, or it may change the *Warburg diffusion resistance*, if the drug adsorbs at the electrode/ solution interface, and, in this way, the surface of the electrode changes from A to ${}_iA^*$, or ${}_iA^{**}$. Of course, the drug may introduce new ionic species in the RRD solution, but, because the concentrations of these species are very small in comparison with those of $[Fe(CN_6)]^{3-}$, $[Fe(CN_6)]^{4-}$ the effect of these new ionic species may be neglected. Consequently, taking into account only the two effects that a drug may have, i.e., the change of both, charge transfer and Warburg diffusion resistances, Bonciocat and Adina Cotarta have proposed the following expressions for the two quotients $\omega_1^2 / [\omega_{Th,s}^2]_0$, respective : $[\omega_{Th,p}^2]_0 / [\omega_{Th,p}^2]_0 - \omega_1^2$:

$$J^* = \frac{\omega_1^2}{\left[\omega_{Th,s}\right]_0^2} = \frac{\left(A_{ct}\right)_{RRD} - \left({}_iA_{ct}^*\right)_{(ME)_{Di}^*}}{\left[R_W(\omega_1)\right]_{RRD} \cdot \frac{A}{\left({}_iA^*\right)}} \qquad (1*)$$

respective:

$$J^{**} = \frac{\left[\omega_{Th,p}\right]_0^2}{\left[\omega_{Th,p}\right]_0^2 - \omega_1^2} = \frac{\left(A_{ct}\right)_{RRD} - \left({}_iA_{ct}^{**}\right)_{(ME)_{Di}^{**}}}{\left[R_W(\omega_1)\right]_{RRD} \cdot \frac{A}{\left({}_iA^{**}\right)}} \qquad (1**)$$

where the Thomson radial frequencies $[\omega_{Th,s}]_0$ and $[\omega_{Th,p}]_0$ have the meanings:

$$\left[\omega_{Th,s}\right]_0 = \left\{\omega_{Th,s}\left[\alpha_D^*(\omega_1)\right]\right\}_{\eta(0)=0} = \frac{\omega_1}{\sqrt{1-\alpha_D^*(\omega_1)}}$$

$$\left[\omega_{Th,p}\right]_0 = \left\{\omega_{Th,p}\left[\alpha_D^{**}(\omega_1)\right]\right\}_{\eta(0)=0} = \omega_1\sqrt{1-\alpha_D^{**}(\omega_1)} \qquad (2*)$$

and:

$$0 \le \alpha_D^{*}(\omega_1) \le 1; \qquad 0 \le \alpha_D^{**}(\omega_1) \le 1 \qquad (3*)$$

In this paper one shows that J^* and J^{**} represent two criteria very useful for a better and more correct classification of the drugs which belong to the classes (I^*), respective (I^{**}).

THEORETICAL SECTION

Introduction

The quotients (1^*) and (1^{**}) permit to consider the following situations:

A) $D_i \in$ (I), i.e., has no effect. Then:

$$\frac{\omega_1^2}{\left[\omega_{Th,s}\right]_0^2} = \frac{\left[\omega_{Th,p}\right]_0^2}{\left[\omega_{Th,p}\right]_0^2 - \omega_1^2} = 0 \qquad (4*)=(4**)$$

which means:

either $\left[\omega_{Th,s}\right]_0 = \left\{\omega_{Th,s}[\alpha_{D_i}^{*}(\omega_1)=1]\right\}_{\eta(0)=0} = \infty$

or $\left[\omega_{Th,p}\right]_0 = \left\{\omega_{Th,p}[\alpha_D^{**}(\omega_1)=1]\right\}_0 = 0 \qquad (5*)=(5**)$

B) $D_i \in$ (I^*) and has effect if:

$$J^* = \frac{\omega_1}{\left[\omega_{Th,s}\right]_0} = \frac{\omega_1}{\left\{\omega_{Th,s}\left[1 \rangle \alpha_D^{*}(\omega_1) \rangle 0\right]\right\}_0}$$ = finite and positive value less than 1, and:

$D_i \in$ (I*) has a maximum effect if:

$$J^* = \frac{\omega_1}{[\omega_{Th,s}]} = \frac{\omega_1}{\left\{\omega_{Th,s}\left[\alpha_D^{*}(\omega_1)=0\right]\right\}_0} = 1 \qquad (6*)$$

C) $D_i \in$ (I^{**}) and has effect if:

$$J^{**} = \frac{\left[\omega_{Th,p}\right]_0^2}{\left[\omega_{Th,p}\right]_0^2 - \omega_1^2} = \frac{\left\{\omega_{Th,p}[1 \rangle \alpha_D^{**}(\omega_1) \rangle 0]\right\}_0^2}{\left\{\omega_{Th,p}[1 \rangle \alpha_D^{**}(\omega_1) \rangle 0\right\}_0^2 - \omega_1^2}$$ =finite and negative value $(7*)$

and

$D_i \in (I^{**})$ has a maximum effect, if :

$$J^{**} = \frac{\left[\omega_{Th,p}\right]_0^2}{\left[\omega_{Th,p}\right]_0^2 - \omega_1^2} = \frac{\left\{\omega_{Th,p}\left[\alpha_D^{**}(\omega_1) = 0\right]\right\}_0^2}{\left\{\omega_{Th,p}\left[\alpha_D^{**}(\omega_1) = 0\right]\right\}_0^2 - \omega_1^2} \rightarrow - \infty \qquad (8^{**})$$

Therefore, from (5*) and (6*), respective (7*) and (8**), it follows:

$$0 \leq J^{*} \leq 1 \qquad (9*)$$

respective:

$$-\infty \leq J^{**} \leq 0 \qquad (9**)$$

Anti -oxidizer and Pro -oxidizer drugs

The inequalities (9∗) and (9∗∗) show that the pair (J^* , J^{**}) satisfies the necessary conditions for being a pair of criteria of classifying the drugs, because the values of J^* are greater than zero, while those of J^{**} are less than *zero.* The class of drugs characterized by the criterion J^{**} will be a sub-class of the class (I^{**}), while the class of drugs characterized by the criterion J^*, will be a sub-class of the class (I^*).

We shall write these two subclasses by $\left(J_{A.O}^{**}\right)$, respective $\left(J_{P.O}^{*}\right)$, because, as we shall see further, in these sub-classes enter the *anti-oxidant* drugs (i.e., A.O-drugs), respective the *pro-oxidant* drugs (i.e., P.O-drugs). Thus, $(J_{A.O}^{**}) \subset (I^{**})$, while $(J_{P.O}^{**}) \subset (I^{*})$.

The most important conclusion concerning the Theoretical Section:

- A drug $D_i \in (I^*)$ is characterized by the radial Thomson frequency $\omega_{Th,s}[\alpha_{D_i}^{*}(\omega_1) = 0]$ and has a maximum effect if his radial Thomson frequency is equal to the *resonance* Thomson frequency

$$res\ \omega_{Th,s}\ [\alpha_{D_i}^{*}(\omega_1) = 0] = \omega_1\ ;$$

- A drug $D_i \in (I^{**})$ is characterized by the radial Thomson frequency $\omega_{Th,p}\,[\alpha_{D_i}^{*}(\omega_1) = 0]$ and has a maximum effect if his radial Thomson frequency ω is equal to *the resonance* Thomson frequency

$$\text{res}\ \omega_{Th,p}\ [\alpha_{D_i}^{**}(\omega_1) = 0] = \omega_1.$$

- An A.O- drug is characterized by the criterion $J^{**}_{A.O}$, and has a maximum effect, if his $J^{**}_{A.O}$ criterion has the value - ∞.

- An P.O –drug is characterized by the criterion $J^{*}_{P.O}$, and has a maximum effect, if his $J^{*}_{P.O}$ criterion has the value 1.

EXPERIMENTAL

In the paper hold at Journees d'Electrochimie 2009, Sinaia (6-10 Jouillet), Roumanie, we have investigated 6 drugs and 2 mixtures of drugs, namely:

B (Sweedish Bitter), Am (Achillea Millefolium), Cf_1 and Cf_2 (Calendula floss), Uh_1 and Uh_2 (Urticae herba), M_1 = Uh + Am, M_2 = B + Am + Cf + Uh[1].

By using eqs.(37') and (37'') [1], where $Re^{**}(\omega_1)$, $Re^{**}(\omega_2)$ represent the abscissa of the first two points of the Nyquist plots(i.e., corresponding to ω_1=1.256s^{-1} and ω_2=1.582s^{-1}) recorded for the drugs and mixtures of drugs investigated, while $Re(\omega_1)$, $Re(\omega_2)$ represent the abscissa of the first two points of the Nyquist plots, recorded for the RRD-dielectrode, it was possible to get the values of the quantities a^{**} and b^{**}[1]. Because the values thus obtained have proved to obey all the inequality $a^{**} \langle b^{**}$, it results that all drugs and mixtures of drugs investigated belong to the class (I^{**}), i.e., in their electrical schemes, the Warburg pseudo-capacitance $C_W(\omega)$ must be replaced by a parallel circuit of a pseudo-inductance $L_W(\omega)$, in parallel with a pseudo-capacitance $C_W(\omega)$. Once the values a^{**} and b^{**} known, the radial Thomson frequency $\left\{\omega_{Th,p}[\alpha^{**}_D(\omega_1)=0]\right\}_0 = [\omega_{Th,p}]_0$, have resulted by means of eq.(37) [1].

In Table 1 is shown, in *details,* the procedure by which have been obtained the values of a^{**} , b^{**} and $[\omega_{Th,p}]_0$ in the case of the drug B.

$$a^{**} = 1.122\,[\mathrm{Re}(\omega_2) - \mathrm{Re}^{**}(\omega_2)]; \qquad b^{**} = \mathrm{Re}(\omega_1) - \mathrm{Re}^{**}(\omega_1)$$

(37') and (37'')[1]

$$\left[\omega_{Th,p}\right]_0 = \left\{\frac{-a^{**}+b^{**}}{1.121\left[\mathrm{Re}^{**}(\omega_1) - \mathrm{Re}^{**}(\omega_2)\right] - a^{**}+b^{**}}\right\}^{1/2} \cdot \omega_1$$

(37)[1]

Further, the procedure exemplified in Table 1, has been used for obtaining the values $[\omega_{Th,p}]_0$, corresponding to all drugs and mixtures of drugs investigated. The results are given in Table 2, where for sake of simplicity, are given the multielectrods containing the respective drugs or mixtures of drugs, and the mean values of $[\omega_{Th,p}]_0$ obtained from 4 experimental values.

Table 1. Example of obtaining the values a^{**} and b^{**} (by means of eqs.(37') and (37")) and of the values of $[\omega_{Th,p}]_0$ (by means of eq.(37))[1]

We mention that $[\omega_{Th,p}]_0$ is the mean value of the 4 values $\left\{\omega_{Th,p}[\alpha_D^{**}(\omega_1)=0]\right\}_0$ obtained by applying eq.(37)[1].

Dielectrode RRD V= 300mL	Re(ω_1) (Ω)	Re(ω_2) (Ω)	
	319 329 318 320	291 291 289 290	

Multi electrode	$\mathrm{Re}^{**}(\omega_1)$ (Ω)	$\mathrm{Re}^{**}(\omega_2)$ (Ω)	a^{**} (Ω)	b^{**} (Ω)	$\left\{\omega_{Th,p}[\alpha_D^{**}(\omega_1)=0]\right\}_0$ (s^{-1})
$(ME)_B$ V=300mL V=20mL	10447 10936 11688 12721	9944 10409 11125 12266	-10830 -10761 -12158 -13370	-10128 -10614 -11370 -12401	0.935 0.561 0.936 0.994

Table 2. The Thomson radial frequencies $[\omega_{Th,p}]_0 = \left\{\omega_{Th,p}[\alpha_D^{**}(\omega_1)=0]\right\}_0$ estimated by using eq.(37)[1]

Multielectrode	$[\omega_{Th,p}]_0$ Mean values	Multielectrode	$[\omega_{Th,p}]_0$ Mean values
$(ME)_B$ V= 300mL v= 20mL	0.857	$(ME)_{Uh}$ V= 300mL v= 20mL	0.949
$(ME)_{Am}$ V= 300mL v= 30mL	0.823	$(ME)_{Uh2}$ V= 300mL v= 30mL	1.002

Multielectrode	$[\omega_{Th,p}]_0$ Mean values	Multielectrode	$[\omega_{Th,p}]_0$ Mean values
$(ME)_{Cf_1}$ V= 300mL v= 20mL	1.067	$(ME)_{Uh+Am}$ V= 300mL v=20mL+20mL	0.898
$(ME)_{Cf_2}$ V= 300mL v= 30mL	0.874	$(ME)_{B+Am+Cf+Uh}$ V= 300mL v=(10+10+10+10)mL	0.954

Because all drugs and mixtures of drugs investigated have proved to belong to the class (I**), it is important to decide if they are AO-drugs, i.e., if they belong to the sub-class $J^{**}_{A.O} \subset \left(I^{**}\right)$.

Therefore it is necessary to estimate the values of the criterion:

$$J^{**} = \frac{[\omega_{Th,p}]_0^2}{[\omega_{Th,p}]_0^2 - \omega_1^2}$$

for these 6 drugs and 2 mixtures of drugs.

The corresponding values are given in Table 3.

As one sees in Table 3, all the values of the criterion J** are negative, and belong to the interval (9**). Consequently, *the most important conclusions of the Experimental Section are:*

- All the drugs and mixtures of drugs investigated, belong to the sub-class ($J^{**}_{A.O} \subset \left(I^{**}\right)$), i.e., are A.O-drugs.
- The drug Cf_1 has the maximum effect, because $J^{**}_{Cf_1}$ = -2.586, i.e., has the most negative value. This means that this drug acts by changing both, the charge transfer resistance and the Warburg diffusion resistance, i.e., this drug *adsorbs significantly* at the electrode/solution interface. This adsorption process explains also why, by increasing the concentration of the drug, i.e., by passing from Cf_1 to Cf_2 the value of $\left|J^{**}_{Cf}\right|$ decreases from +2.586 to +0.939 because the quotient A/ $_i A^{**}$ increases (see eq.(1**)).
- In the case of the drug Uh, by increasing its concentration, the value of $\left|J^{**}_{Uh}\right|$ increases too, from 1.331 to 1.749. This may be explained by the fact that the drug Uh acts *firstly by changing the charge transfer resistance*, which, of course, *increases* if the concentration of drug *increases.*

Table 3. The values of the criterion $J^{**} = [\omega_{Th,p}]_0^2 / \left\{[\omega_{Th,p}]_0^2 - \omega_1^2\right\}$ for the investigated drugs and mixtures of drugs

Drugs and mixtures of drugs	$[\omega_{Th,p}]_0^2$ (s^{-2})	ω_1^2 (s^{-2})	J^{**}
B	0.901	1.578	-1.331
Am	0.677	1.578	-0.751
Cf_1	1.138	1.578	-2.586
Cf_2	0.764	1.578	-0.939
Uh_1	0.901	1.578	-1.331
Uh_2	1.004	1.578	-1.749
Uh+Am	0.806	1.578	-1.044
B+Am+Cf+Uh	0.910	1.578	-0.247

This two effects (i.e., changing of the charge transfer resistance and of the Warburg diffusion resistance may compensate each other, and this may explain why the values $\left|J^{**}\right|$ corresponding to the two mixtures of drugs investigated are not far away from the values $\left|J^{**}\right|$ corresponding to their individual components.

It remains to explain how an A.O-drug acts. Let's start by remembering the reactions of the RRD-dielectrode. They are:

$$\frac{1}{4}O_2 + H^+ + e \rightarrow \frac{1}{2}H_2O \text{ cathodic reaction}$$

$$[Fe(CN)_6]^{4-} \rightarrow [Fe(CN)_6]^{3-} + e \text{ anodic reaction}$$

The electrons resulted by the oxydation of $[Fe(CN)_6]^{4-}$ are consumed by the reduction of the physically dissolved oxygen and H^+-ions (i.e., $\frac{1}{4}O_2 + H^+$) to $\frac{1}{2}H_2O$.

Therefore, $\frac{1}{4}O_2 + H^+$ acts as an *oxidizer* of $[Fe(CN)_6]^{4-}$. It thus results that an A.O- drug **reduces** the oxidating effect of $\frac{1}{4}O_2 + H^+$, *by consuming a part, or all electrons resulted by the oxidation* of $[Fe(CN)_6]^{4-}$ to $[Fe(CN)_6]^{3-}$.

This consuming of electrons may take place, either by a *chemical* reaction in solution, e.g.,

$$(A.O-D)_{\mathrm{Re}d}+\frac{1}{4}O_2+H^+\rightarrow(A.O-D)_{Ox}+\frac{1}{2}H_2o$$

when the A.O-drug (see A.O-D) passes from its reduce form, to its oxidize form, when at the electrode / solution interface, occur three electrode reactions, e.g.,

$$\frac{1}{4}O_2+H^+ + e\rightarrow\frac{1}{2}H_2O$$
$$[Fe(CN)_6]^{4-}\rightarrow[Fe(CN)_6]^{3-}+e$$
$$[A.O-D]_{\mathrm{Re}d}\rightarrow[A.O-D]_{Ox}+e$$

In both ways of action, the important effect of the A.O - D is the reduction of the intensity of the *important oxydation reaction.*

If this important *oxidation* is a biological reaction, responsible for a very dangerous illness, the A.O-drugs may have *very important therapeutic applications*, in fighting against this dangerous illness.

As for the P.O-drugs, there are two ways in which they may act.

A first possibility is to act chemically, i.e., by a reaction in solution, e.g.,

$$(A.O-D)_{Ox}+\frac{1}{2}H_2O\rightarrow(A.O-D)_{\mathrm{Re}d}+\frac{1}{4}O_2+H^+$$

increasing the concentration of the $\frac{1}{4}O_2+H^+$ and in this way *increasing* the intensity of the oxidation reaction:

$$[Fe(CN)_6]^{4-}\rightarrow[Fe(CN)_6]^{3-}+e$$

or electro-chemically when at the electrode / solution interface, occur the reactions:

$$\frac{1}{4}O_2+H^+ + e\rightarrow\frac{1}{2}H_2O$$
$$[Fe(CN)_6]^{4-}\rightarrow[Fe(CN)_6]^{3-}+e$$
$$[P.O-D]_{\mathrm{Re}d}\rightarrow[P.O-D]_{Ox}+e$$

when, a part of the electrons necessary to the first cathodic reaction come from the de-electronation (i.e., oxydation) of the P.O-D- drug.

In both ways of action, the important effect of a P.O.-drug is the *increase* of the intensity of the important oxydation reaction.

CONCLUSIONS

Because the efficiency of an A.O-drug increases if the value of $\left| J^{**} \right|$ increases, it results the following sequence concerning the efficiencies of the 6 drugs and 2 mixtures of drugs (all A.O-drugs) investigated:

$$\left| J^{**}_{Am} \right| \langle \left| J^{**}_{B} \right| \langle \left| J^{*\cdot *}_{C\, f_2} \right| \langle \left| J^{**}_{Uh+Am} \right| \langle \left| J^{**}_{Uh_1} \right| \langle \left| J^{**}_{B+Am+Cf+Uh} \right| \langle \left| J^{**}_{Uh_2} \right| \langle \left| J^{**}_{Cf_1} \right|$$

Finally, it is very important to underline that, presently, are known many oxidation reactions, occurring in biological systems, about which one supposes that are at the origin of many illnesses, and for this reason, the development of experimental methods for estimating the therapeutic efficiencies of the A.O.-drugs represents the most important aim of the future researchers in the domain of biological and pharmaceutical sciences.

From this point of view, one may conclude that the two EIS methods presented at Journees d'Electrochimie 2009 and RICCCE 2009, have the necessary conditions for playing a very important role for a *scientific classification of drugs*, produced by the *chemical industry*, or taken from the **God pharmacy** [i.e., by an *adequate transforming of the medicinal plants*].

Unfortunately, such an action necessitates about 4-5 years, and a team of researchers in which must enter: electrochemists, biochemists, physicist and specialists in medicinal plants. Although such an action implies so many difficulties, it must be done, because the results that will be obtained, will justify the efforts, and what it is much more important, will decide the directions in which the future developments of the medical sciences in Romania must be made. This also explains the importance of the criteria $[\omega_{Th,s}]$, $[\omega_{Th,p}]_0$, respective $J^{*}_{P.O}$, $J^{**}_{A.O}$, for the future development of drug-sciences not only in Romania, but also in the world.

REFERENCES

1. N. Bonciocat, A. Cotarta, *Journees d'Electrochimie 6-10 Jouillet 2009, Sinaia, Romania,* Communication Orale 3-O-13, *Studia Universitatis Babes-Bolyai*, *Seria Chemia*, **2009**, in press
2. Adina Cotarta, Ph.D Thesis, Chemical Research Institute, Bucharest, **1992**
3. N. Bonciocat, *Electrokhimiya*, **1993**, *29*, 97.
4. N. Bonciocat, *Electrochimie si Aplicatii*, Dacia Europa - Nova, Timisoara, **1996**, chapter 5, 262.
5. N. Bonciocat and A. Cotarta, *Revue Roumaine de Chimie*, **1998**, *43*, 925.

6. N. Bonciocat, "*Alternativa Fredholm in Electrochimie*", Editura Mediamira, Cluj-Napoca, **2005**, chapter 2.
7. N. Bonciocat, *Electrochimie si Aplicatii*, Dacia Europa-Nova, Timisoara, **1996**, chapter 6, 268-277; 283.
8. I.O. Marian, E. Papadopol, S. Borca and N. Bonciocat*, Studia Universitatis Babes-Bolyai, Cluj Napoca, Ser. Chemia*, **1998**, *43*, 91.
9. N. Bonciocat, Scientific Bulletin Chemistry, Series Politechnica University Timisoara, **1998**, *43 (57*), 5.
10. N. Bonciocat, "*Alternativa Fredholm in Electrochimie*", Editura Mediamira, Cluj-Napoca, vol.I, **2005**, chapter 5.
11. N. Bonciocat, E. Papadopol, S. Borca and I.O. Marian, *Revue Roumaine de Chimie*, **2000**, *45*, 981.
12. I.O. Marian, R. Sandulescu and N. Bonciocat, *Journal of Pharmaceutical and Biomedical Anal*ysis, **2000**, *23*, 227.
13. I.O. Marian, N. Bonciocat, R. Sandulescu and C. Filip, *Journal of Pharmaceutical and Biomedical Anal*ysis, **2001**, *24*, 1175.
14. N. Bonciocat, A. Cotarta, J. Bouteillon and J.C. Poignet, *Journal of High Temperature Material Processes*, **2002**, *6*, 283.
15. N. Bonciocat, I.O. Marian, R. Sandulescu, C. Filip and S. Lotrean, *Journal of Pharmaceutical and Biomedical Analysis*, **2003**, *32*, 1093.
16. N. Bonciocat and A. Cotarta, Annals of West University of Timisoara, Series Chemistry, **2006**, *15*(2), 137.
17. N. Bonciocat and A. Cotarta, *Scientific Bulletin Chemistry Series Politehnica University Timisoara*, **2007***, 52*(66), 1-2, 90.
18. N. Bonciocat, *Studia Universitatis Babes-Bolyai, Cluj Napoca, Seria Chemia, LIII*, 1, **2008**, 31.
19. N. Bonciocat, A. Cotarta, *Scientific Bulletin Chemistry Series Politehnica University Timisoara,* **2009**, in press.

HYPERVALENT TETRA- AND TRIORGANOLEAD(IV) COMPOUNDS CONTAINING 2-(R_2NCH_2)C_6H_4 GROUPS (R = Me, Et)

ADINA CRISTEA[a], ANCA SILVESTRU[a], CRISTIAN SILVESTRU[a]

ABSTRACT. Reaction of [2-(R_2NCH_2)C_6H_4]Li with R'_3PbCl or Ph_2PbCl_2, in 1:1 molar ratio, gave the new organolead(IV) compounds [2-(R_2NCH_2)C_6H_4]R'_3Pb [R = Me, R' = Me (**1**), Ph (**2**); R = Et, R' = Ph (**3**)] and [2-(Me_2NCH_2)C_6H_4]Ph_2PbCl (**4**). Treatment of [2-(R_2NCH_2)C_6H_4]Ph_3Pb with iodine resulted in isolation of [2-(R_2NCH_2)C_6H_4]Ph_2PbI [R = Me (**5**), Et (**6**)]. The iodide **5** was also obtained by halogen exchange reaction between **4** and KI. The compounds were characterized in solution by ^1H and ^{13}C NMR. The molecular structure of **2** and **4** was established by single-crystal X-ray diffraction. In both cases the nitrogen atom from the pendant Me_2NCH_2 arm is coordinated intramolecularly to the lead atom [Pb-N 3.051(9) Å in **2** and 2.635(8) Å in **4**, respectively] leading to distorted trigonal bipyramidal geometry around the metal atom and thus to hypervalent 10-*Pb*-5 species. Compounds **2** and **4** crystallize as 1:1 mixtures of *R*- and *S*-isomers (planar chirality induced by the non-planar PbC_3N chelate ring).

Keywords: organoleadIV) compounds, hypervalent, solution NMR studies, single-crystal X-ray diffraction

INTRODUCTION

Aromatic ligands with pendant arm containing nitrogen as donor atom, such as 2-(Me_2NCH_2)C_6H_4 or related organic compounds have been largely used in organotin chemistry in last years [1-17]. By contrast, such ligands were only sparingly used in organolead chemistry. Only one lead(II) compound, [2-(Me_2NCH_2)C_6H_4]$_2$Pb [18], and few organoled(IV) derivatives, *i.e.* [2-(Me_2NCH_2)C_6H_4]$_4$Pb [18], [2-(Me_2NCH_2)C_6H_4](4-MeC_6H_4)$_2$PbI [19] and [2-(Me_2NCH_2)C_6H_4](4-MeC_6H_4)(4-$MeOC_6H_4$)PbI [19,20], were described in early works and the structure of the latter chiral compound was established by single-crystal X-ray diffraction. Some related derivatives, *i.e.* [CpFe{C_5H_3(CH_2NMe_2)-2}]$_2$Pb [21] and [CpFe{C_5H_3(CH_2NMe_2)-2}]$_2$PbM(CO)$_5$ (M = Cr, Mo, W) [22], were also recently described.

We report here on the synthesis and solution behavior of new tetraorganolead(IV) compounds, [2-(R_2NCH_2)C_6H_4]R'_3Pb [R = Me, R' = Me (**1**), Ph (**2**); R = Et, R' = Ph (**3**)], and triorganolead(IV) halides, [2-(Me_2NCH_2)C_6H_4]Ph_2PbCl (**4**), [2-(R_2NCH_2)C_6H_4]Ph_2PbI [R = Me (**5**), Et (**6**)], as well as the molecular structure of **2** and **4**.

[a] *Babeş-Bolyai University, Faculty of Chemistry and Chemical Engineering, Arany Janos 11, 400028 Cluj-Napoca, Romania; E-mail: cristi@chem.ubbcluj.ro*

RESULTS AND DISCUSSION

The new tetraorganolead(IV) compounds **1**-**3** were obtained by reacting R'_3PbCl with $[2\text{-}(R_2NCH_2)C_6H_4]Li$ in 1:1 molar ratio, in hexane, at at –78 °C, while reaction of Ph_2PbCl_2 with $[2\text{-}(Me_2NCH_2)C_6H_4]Li$ in 1:1 molar ratio, in same conditions, resulted in isolation of the chloride **4** (Scheme 1).

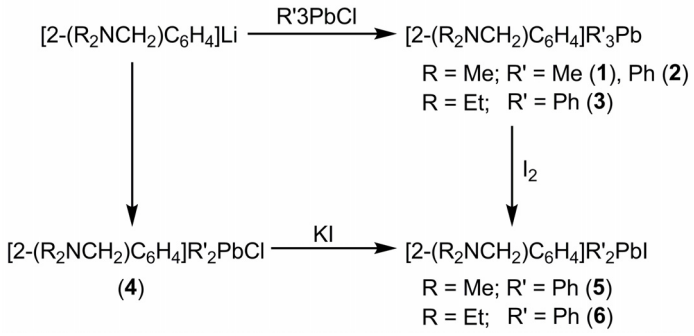

Scheme 1

Treatment of $[2\text{-}(R_2NCH_2)C_6H_4]Ph_3Pb$ with iodine, in CH_2Cl_2, at room temperature, resulted in selective cleavage of one phenyl group and isolation of the iodides $[2\text{-}(R_2NCH_2)C_6H_4]Ph_2PbI$ [R = Me (**5**), Et (**6**)]. This suggests that the presence of the CH_2NR_2 pendant arm on the aromatic ring stabilizes the Pb-C bond established by the $[2\text{-}(Me_2NCH_2)C_6H_4]$ group with respect to that which involves the phenyl moiety, probably through the intramolecular N→Pb interaction. The same iodide **5** was obtained by halogen exchange when the chloride **4** was treated with excess of KI, in CH_2Cl_2/water.

The new organolead(IV) compounds were isolated in rather good yields (50-90%) as colorless (**1**-**4**) or yellowish (**5**, **6**) crystalline solids. They are air-stable compounds, soluble in common organic solvents. The compounds were investigated by NMR spectroscopy (^1H, ^{13}C, 2D) in solution and for compounds **2** and **4** the molecular structures were established by single-crystal X-ray diffraction.

The NMR spectra for the compounds **1**-**6** were recorded in $CDCl_3$, at room temperature. The assignment of the ^1H and ^{13}C chemical shifts was made according to the numbering schemes shown in Scheme 2, based on 2D experiments and the lead-carbon coupling constants.

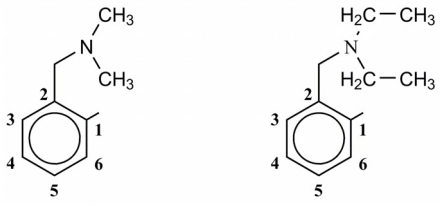

Scheme 2

The NMR (^{1}H, ^{13}C) spectra of compounds **1**, **2**, **4** and **5** are very similar with respect to the [2-(Me_2NCH_2)C_6H_4] group attached to the lead atom, showing the expected resonances in the alkyl and the aryl regions. All four compounds show in the alkyl region singlet resonances for NMe_2 and CH_2 protons of the pendant arm, respectively, with the latter surrounded by lead satellites. The ^{1}H NMR spectrum of the mixed alkyl-aryllead(IV) derivative **1** exhibits in the alkyl region an additional singlet resonance for the protons of the methyl groups bonded to lead. The aromatic region is much better resolved for compound **1**, with four multiplet resonances (that for the H_3 proton is partially overlapped by the resonance of residual $CHCl_3$). For the mixed tetraaryllead(IV) compound **3** the aromatic region is more complicated due to overlapping of the resonances for the protons of the C_6H_4 group and those corresponding to the phenyl groups, respectively. The main influence of the halogen atom attached to lead in the chloride **4** and the iodide **5** is the downfield shift of the resonance for the proton H_6 with respect to the other *ortho* protons from the phenyl groups bonded to lead. For compounds **3** and **6**, containing the [2-(Et_2NCH_2)C_6H_4] group attached to lead, in addition to a broad signal for the benzylic CH_2 protons, one triplet and one quartet resonance were observed for the ethyl groups in the aliphatic region of the ^{1}H NMR spectra. The aromatic region exhibits a rather complex pattern due to partial overlapping of the resonance signals.

According to the ^{1}H NMR data, the ^{13}C NMR spectra of compounds **2**-**5** contain, in addition of six resonances for the different aromatic carbons of the [2-(R_2NCH_2)C_6H_4] group, a single set of four resonances for the phenyl groups, indicating their equivalence in solution. Most of these singlet resonances are surrounded by lead satellites due to lead-carbon coupling. The unambiguous assignment of the ^{13}C resonance signals for these organolead(IV) compounds was based on the 2D correlation spectra and carbon-lead coupling constants, respectively.

The NMR data suggest that in solution these compounds might have similar structures as found in solid state for **2** and the chloride **4**, *i.e.* a trigonal bipyramidal coordination geometry around the lead atom due to the intramolecular N→Pb coordination (assuming a fast conformational change in solution for the nonplanar, five-membered PbC_3N chelate ring, which gives averaged ^{1}H NMR signals). Alternatively, a tetrahedral geometry around the lead atom can also be considered, a behavior which will assume the lack of intramolecular coordination in solution. Unfortunately, the ^{207}Pb NMR spectra, which might provide further information on the coordination degree of the lead atom, could not be yet recorded.

Single-crystals suitable for X-ray diffraction studies were obtained by slow diffusion from a mixture of CH_2Cl_2 and hexane (1/4, v/v) for compounds [2-(Me_2NCH_2)C_6H_4]Ph_3Pb (**2**) and [2-(Me_2NCH_2)C_6H_4]Ph_2PbCl (**4**).

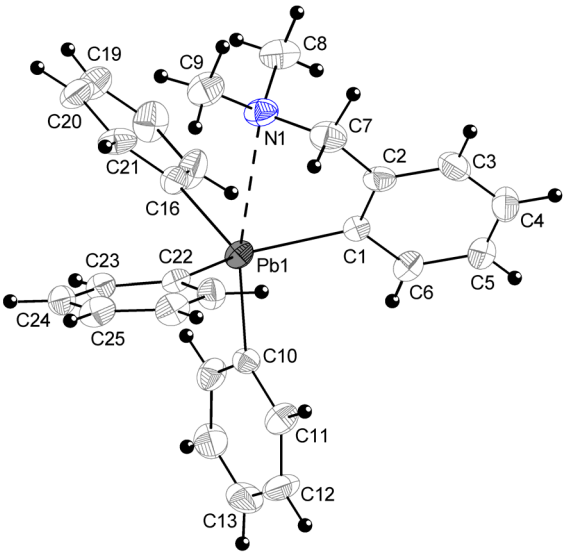

Figure 1. ORTEP representation at 30% probability and atom numbering scheme for R_N-**2** isomer.

The crystal of **2** consists of discrete monomers separated by normal van der Waals distances, while compound **4** has two independent, very similar, molecules (**4a** and **4b**) in the unit cell and therefore the subsequent discussion will refer only to molecule **4a**. The ORTEP diagrams of the molecular structures of **2** and **4a**, with the atom numbering scheme, are shown in Figures 1 and 2. Selected interatomic distances and angles are listed in Tables 1 and 2.

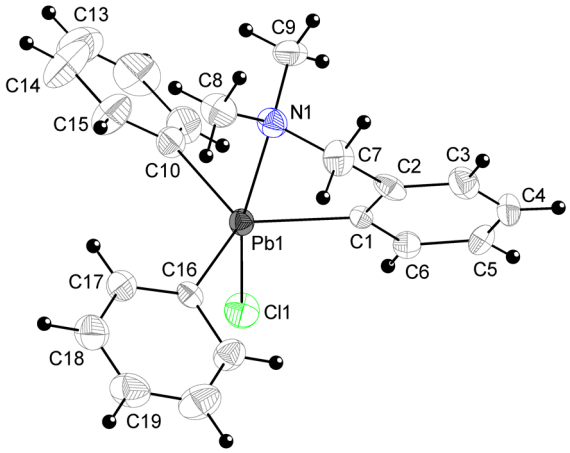

Figure 2. ORTEP representation at 30% probability and atom numbering scheme for R_N-**4a** isomer.

Table 1. Interatomic bond distances (Å) and angles (°) for compound **2**.

Pb(1)-C(1)	2.223(8)	Pb(1)-C(16)	2.222(8)
Pb(1)-C(10)	2.253(8)	Pb(1)-C(22)	2.207(8)
Pb(1)-N(1)	3.051(9)		
N(1)-C(7)	1.475(12)	N(1)-C(9)	1.453(11)
N(1)-C(8)	1.440(12)		
C(1)-Pb(1)-C(10)	102.2(3)	C(10)-Pb(1)-C(16)	105.7(3)
C(1)-Pb(1)-C(16)	118.6(3)	C(10)-Pb(1)-C(22)	104.9(3)
C(1)-Pb(1)-C(22)	114.2(3)	C(16)-Pb(1)-C(22)	109.6(3)
N(1)-Pb(1)-C(10)	169.1(3)		
N(1)-Pb(1)-C(1)	66.8(3)	N(1)-Pb(1)-C(22)	80.8(3)
N(1)-Pb(1)-C(16)	80.6(3)		
C(7)-N(1)-C(8)	109.0(8)	Pb(1)-N(1)-C(7)	94.8(6)
C(7)-N(1)-C(9)	111.0(8)	Pb(1)-N(1)-C(8)	110.3(6)
C(8)-N(1)-C(9)	111.3(8)	Pb(1)-N(1)-C(9)	119.2(7)

Table 2. Interatomic bond distances (Å) and angles (°) for compound **4**.

4a		**4b**	
Pb(1)-C(1)	2.202(8)	Pb(2)-C(22)	2.205(9)
Pb(1)-C(10)	2.191(10)	Pb(2)-C(31)	2.197(9)
Pb(1)-C(16)	2.190(9)	Pb(2)-C(37)	2.198(9)
Pb(1)-Cl(1)	2.597(3)	Pb(2)-Cl(2)	2.616(2)
Pb(1)-N(1)	2.636(8)	Pb(2)-N(2)	2.646(9)
N(1)-C(7)	1.489(13)	N(2)-C(28)	1.478(15)
N(1)-C(8)	1.481(13)	N(2)-C(29)	1.458(14)
N(1)-C(9)	1.462(13)	N(2)-C(30)	1.452(14)
Cl(1)-Pb(1)-N(1)	166.11(19)	Cl(2)-Pb(2)-N(2)	167.2(2)
Cl(1)-Pb(1)-C(1)	94.9(2)	Cl(2)-Pb(1)-C(22)	93.3(3)
Cl(1)-Pb(1)-C(10)	93.4(3)	Cl(2)-Pb(1)-C(31)	99.1(2)
Cl(1)-Pb(1)-C(16)	98.5(2)	Cl(2)-Pb(1)-C(37)	93.9(3)
N(1)-Pb(1)-C(1)	72.9(3)	N(2)-Pb(1)-C(22)	74.2(3)
N(1)-Pb(1)-C(10)	89.0(3)	N(2)-Pb(1)-C(31)	89.0(3)
N(1)-Pb(1)-C(16)	92.6(3)	N(2)-Pb(1)-C(37)	91.3(3)
C(1)-Pb(1)-C(10)	126.7(4)	C(22)-Pb(1)-C(31)	117.0(3)
C(1)-Pb(1)-C(16)	113.7(3)	C(22)-Pb(1)-C(37)	124.3(3)
C(10)-Pb(1)-C(16)	116.8(4)	C(31)-Pb(1)-C(37)	116.1(4)
C(7)-N(1)-C(8)	108.8(9)	C(28)-N(1)-C(29)	109.6(10)
C(7)-N(1)-C(9)	111.2(9)	C(28)-N(1)-C(30)	108.3(10)
C(8)-N(1)-C(9)	110.0(9)	C(29)-N(1)-C(30)	111.0(10)
Pb(1)-N(1)-C(7)	98.0(6)	Pb(2)-N(1)-C(28)	97.7(6)
Pb(1)-N(1)-C(8)	118.4(6)	Pb(2)-N(1)-C(29)	111.8(7)
Pb(1)-N(1)-C(9)	109.8(7)	Pb(2)-N(1)-C(30)	117.4(8)

The molecule of **2** contains an intramolecular N→Pb interaction [Pb(1)-N(1) 3.051(9) Å] placed *trans* to the carbon atom of a phenyl group attached to lead. The strength of this interaction is enough strong to be taken into account [c.f. the sum of the van der Waals radii, Σr_{vdW}(Pb,N) 3.54 Å] [23]. The overall geometry at the lead atom is distorted trigonal bipyramidal, with the axial positions occupied by the nitrogen and the carbon atom [N(1)-Pb(1)-C(10) 169.1(3)°], while the carbon atoms of the other two phenyl groups and that of the pendant arm aryl ligand are in the equatorial positions. The distortion of the coordination geometry is due to the small bite of the *C,N*-ligand [N(1)-Pb(1)-C(1) 66.8(3)°]. The C_3PbN chelate ring is not planar, the nitrogen atom being out of the plane defined by the remaining C_3Pb unit. This results in coordination isomers, *i.e.* planar chirality, with C(1)-C(6) aromatic ring and the N(1) atom as chiral plane and pilot atom, respectively [24]. As result compound **2** crystallizes as a 1:1 mixture of R_N and S_N isomers.

In the molecule of the chloride **4a** a much stronger intramolecular N→Pb interaction is established in the *trans* to the chlorine atom and the overall molecular structure is very similar to that reported for the related tin compound, [2-$(Me_2NCH_2)C_6H_4$]Ph_2SnCl [4]. The lead-nitrogen interatomic distance [Pb(1)-N(1) 2.636(8) Å] is of similar magnitude as observed in the related chiral iodide, [2-$(Me_2NCH_2)C_6H_4$](4-MeC_6H_4)(4-$MeOC_6H_4$)PbI [2.686(8) Å] [20], pointing out the lack of significant influence of the electronegativity of the atom placed in the *trans* position relative to nitrogen in the N→Pb-X fragment.

The axial positions in the resulted distorted trigonal bipyramidal geometry achieved around the metal centre are occupied by nitrogen and chlorine atoms [Cl(1)-Pb(1)-N(1) 166.11(19)°], while the aromatic carbon atoms are in the equatorial positions.

The *trans* effect is reflected in the length of the Pb-Cl bond, considerably shorter in **4a** [Pb(1)-Cl(1) 2.597(3) Å] than in the polymeric Ph_3PbCl [2.7059(7) Å] [25]. This is consistent with the stronger *trans* influence of the more electronegative chlorine atom in the Cl→Pb-Cl bridge in Ph_3PbCl than in the N→Pb-Cl system.

As in the case of **2**, the C_3PbN chelate ring in the molecule of **4** is not planar, resulting in planar chirality. The crystal of the chloride **4** consists of a 1:1 mixture of R_N-**4a** / S_N-**4a** and R_N-**4b** / S_N-**4b** isomers, separated by normal van der Waals distances between heavy atoms. However, a closer check of the crystal structure revealed that weak intermolecular Cl···H interactions are established between neighboring molecules. This results in helicoidal chain polymers formed by alternating R_N-**4a** / R_N-**4b** and S_N-**4a** / S_N-**4b** isomers (Figure 3), respectively, supported by $Cl(1)\cdots H(30A)_{methyl}$ (2.95 Å) and $Cl(2)\cdots H(13b)_{phenyl}$ (2.87 Å) interactions [c.f. Σr_{vdW}(Cl,H) ca. 3.01 Å] [23]. No inter-chain contacts are present between parallel polymeric chains developed along the *b* axis.

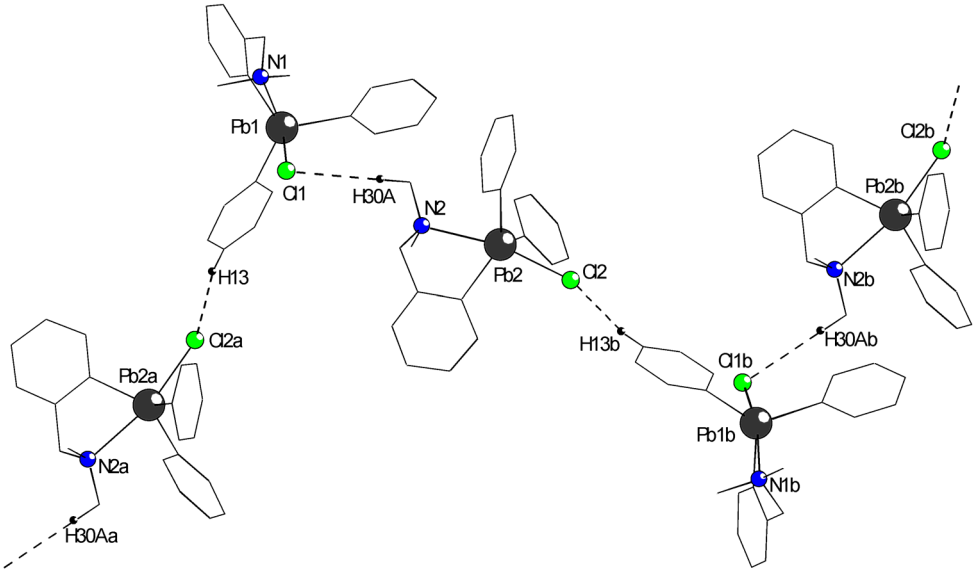

Figure 3. View of a chain polymer based on Cl···H contacts between S_N-**4a** and S_N-**4b** isomers in the crystal of **4** (only hydrogens involved in intermolecular interactions are shown) [symmetry equivalent atoms: Pb2a (1.5 – *x*, 0.5 + *y*, 0.5 – *z*); Pb1 (–0.5 + *x*, 0.5 – *y*, –0.5 + *z*); Pb1b (2 – *x*, –*y*, 1 – *z*) and Pb2b (1.5 – *x*, –0.5 + *y*, 0.5 – *z*)].

CONCLUSIONS

Six new hypervalent organolead(IV) compounds of the type $[2\text{-}(R_2NCH_2)C_6H_4]R'_3Pb$ (R = Me, R' = Me, Ph; R = Et, R' = Ph) and $[2\text{-}(R_2NCH_2)C_6H_4]Ph_2PbX$ (R = Me, X = Cl, I; R = Et, X = I) were obtained. All compounds were characterized in solution using multinuclear and 2D NMR spectroscopy. For both type of compounds single-crystal X-ray diffraction studies provide evidence for an intramolecular N→Pb interaction, resulting in distorted trigonal bipyramidal geometry around the lead atom (hypervalent 10-*Pb*-5 species). It was also found that cleavage of a phenyl group under treatment with iodine is preferred *versus* cleavage of the pendant arm aryl ligand, probably due to the intramolecular N→Pb interaction. All compounds crystallize as 1:1 mixtures of R_N- and S_N isomers (planar chirality induced by the non-planar PbC_3N chelate ring).

EXPERIMENTAL SECTION

All compounds were prepared under an inert atmosphere of argon (Linde, 99.999%) using Schlenk techniques. Solvents were dried and freshly distilled under argon prior to use. Ph_3PbCl, Me_3PbCl and Ph_2PbCl_2 were

commercially available. The other starting materials were prepared accordingly to literature methods: [2-(Me_2NCH_2)C_6H_4]Li [26] and [2-(Et_2NCH_2)C_6H_4]Li [27]. The ^{1}H, ^{13}C and 2D NMR spectra were recorded at room temperature, in dried $CDCl_3$, on Bruker Avance 300 instrument. The chemical shifts are reported in ppm relative to the residual peak of the solvent (ref. $CHCl_3$: ^{1}H 7.26, ^{13}C 77.0 ppm). The NMR spectra were processed using the *MestReC* and *MestReNova* software [28].

*Preparation of [2-(Me_2NCH_2)C_6H_4]Me_3Pb (**1**)*

A suspension of [2-(Me_2NCH_2)C_6H_4]Li (0.72 g, 5.1 mmol) in hexane (30 ml) was added dropwise, under stirring, to a solution of Me_3PbCl (1.49 g, 5.1 mmol) in hexane (50 ml), cooled (–78 °C). After the organolithium suspension was added, the reaction mixture was stirred for 1 h at –78 °C, and then left over night to reach the room temperature. The reaction mixture was filtered in open atmosphere and the solvent was removed in vacuum from the clear filtrate. The white solid residue was recrystallized from hexane to give the title compound as colorless crystals. Yield: 1.3 g (65%), m.p. 234 °C. ^{1}H NMR (300 MHz, 20 °C): δ 1.60s (9H, Pb-CH_3, $^2J_{PbH}$ 82.6 Hz), 2.33s (6H, N-CH_3), 3.64s (2H, -CH_2-N, $^4J_{PbH}$ 16.1 Hz), 7.25m (1H, H_3, partially overlapped by $CDCl_3$ resonance), 7.32ddd (1H, H_4, $^3J_{HH}$ 7.3, $^4J_{HH}$ 1.3 Hz), 7.42ddd (1H, H_5, $^3J_{HH}$ 7.3, $^4J_{HH}$ 1.4 Hz), 8.31dd (1H, H_6, $^3J_{HH}$ 7.4, $^4J_{HH}$ 0.9, $^3J_{PbH}$ 115.5 Hz). ^{13}C NMR (75.4 MHz, 20 °C): δ 16.28s (Pb-CH$_3$), 45.39s (N-CH$_3$), 65.78s (-CH$_2$-N), 128.16s (C_3), 129.00s (C_4), 129.24s (C_5), 137.78s (C_6), 142.28s (C_2), 156.67s (C_1).

*Preparation of [2-(Me_2NCH_2)C_6H_4]Ph_3Pb (**2**)*

A suspension of [2-(Me_2NCH_2)C_6H_4]Li (0.69 g, 4.9 mmol) in hexane (30 ml) was added dropwise, under stirring, to a cooled (–78 °C) solution of Ph_3PbCl (1.9 g, 4.9 mmol) in hexane (50 ml). After the organolithium suspension was added, the reaction mixture was stirred for 1 h at –78 °C, and then left over night to reach the room temperature. The reaction mixture was filtered and the solvent was removed in vacuum from the clear filtrate. The white solid residue was recrystallized from hexane to give the title compound as colorless crystals. Yield: 1.1 g (47%), m.p. 245 °C. ^{1}H NMR (300 MHz, 20 °C): δ 1.76s (6H, N-CH_3), 3.35s (2H, -CH_2-N, $^4J_{PbH}$ 9.0 Hz), 7.39m (12H, $H_{3\text{-}5}$ + C_6H_5-*meta+para*), 7.69m (7H, H_6 + C_6H_5-*ortho*, $^3J_{PbH}$ 78.7 Hz). ^{13}C NMR (75.4 MHz, 20 °C): δ 44.96s (N-CH$_3$), 66.07s (-CH$_2$-N, $^3J_{PbC}$ 31.5 Hz), 127.78s (C_5, $^3J_{PbC}$ 92.9 Hz), 127.88s (C_6H_5-*para*, $^4J_{PbC}$ 18.2 Hz), 128.35s (C_4, $^4J_{PbC}$ 19.7 Hz), 129.05s (C_6H_5-*meta*, $^3J_{PbC}$ 78.1 Hz), 130.22s (C_3, $^3J_{PbC}$ 75.6 Hz), 137.38s (C_6H_5-*ortho*, $^2J_{PbC}$ 65.3 Hz), 138.51s (C_6, $^2J_{PbC}$ 78.1 Hz), 145.98s (C_2, $^2J_{PbC}$ 51.6 Hz), 151.59s (C_1, $^1J_{PbC}$ 579.8 Hz), 153.40s (C_6H_5-*ipso*, $^1J_{PbC}$ 484.8 Hz).

*Preparation of [2-(Et_2NCH_2)C_6H_4]Ph_3Pb (**3**)*

A solution of Ph_3PbCl (2.52 g, 6.5 mmol) in hexane (20 ml) was added during 1 h to a stirred suspension of [2-(Et_2NCH_2)C_6H_4]Li (1.1 g, 6.65 mmol) in hexane (50 ml), kept at –78 °C. The reaction mixture was stirred at this temperature for 1 h and then over night to reach the room temperature. The reaction mixture was filtered under argon and the solvent was removed in vacuum from the clear filtrate. The white solid residue was recrystallized from hexane to give the title compound as colorless crystals. Yield: 2.0 g (58%), m.p. 223 °C. ^{1}H NMR (300 MHz, 20 °C): δ 0.68t (6H, N-CH_2-C*H*$_3$, $^3J_{HH}$ 7.1 Hz), 2.20q (4H, N-C*H*$_2$-CH_3, $^3J_{HH}$ 7.1 Hz), 3.50s (2H, -C*H*$_2$-N, $^4J_{PbH}$ 10.6 Hz), 7.33m (12H, *H*$_{3\text{-}5}$ + C_6*H*$_5$-*meta+para*), 7.63m (7H, *H*$_6$ + C_6*H*$_5$-*ortho*, $^3J_{PbH}$ 79.4 Hz). ^{13}C NMR (75.4 MHz, 20 °C): δ 9.84s (N-CH_2-*C*H_3), 44.80s (N-*C*H_2-CH_3), 60.85s (-*C*H_2-N, $^3J_{PbC}$ 41.1 Hz), 127.53s (*C*$_5$, $^3J_{PbC}$ 90.2 Hz), 128.11s (*C*$_6$H$_5$-*para*, $^4J_{PbC}$ 18.4 Hz), 128.53s (*C*$_4$, $^4J_{PbC}$ 19.4 Hz), 129.19s (*C*$_6$H$_5$-*meta*, $^3J_{PbC}$ 78.4 Hz), 129.89s (*C*$_3$, $^3J_{PbC}$ 72.0 Hz), 137.49s (*C*$_6$H$_5$-*ortho*, $^2J_{PbC}$ 65.9 Hz), 138.19s (*C*$_6$, $^2J_{PbC}$ 77.5 Hz), 146.90s (*C*$_2$, $^2J_{PbC}$ 54.0 Hz), 151.02s (*C*$_1$, $^1J_{PbC}$ 542.0 Hz), 152.32s (*C*$_6$H$_5$-*ipso*, $^1J_{PbC}$ 472.2 Hz).

*Preparation of [2-(Me_2NCH_2)C_6H_4]Ph_2PbCl (**4**)*

A suspension of [2-(Me_2NCH_2)C_6H_4]Li (0.69 g, 3.8 mmol) in hexane (30 ml) was added dropwise, under stirring, to a cooled (–78 °C) solution of Ph_2PbCl_2 (1.62 g, 3.77 mmol) in hexane (50 ml). After the organolithium suspension was added, the reaction mixture was stirred for 1 h at –78 °C, and then left over night to reach the room temperature. The reaction mixture was filtered and the solvent was removed in vacuum from the clear filtrate. The white solid residue was recrystallized from hexane to give the title compound as colorless crystals. Yield: 1.33 g (66%), m.p. 225 °C. ^{1}H NMR (300 MHz, 20 °C): δ 2.02s (6H, N-C*H*$_3$), 3.57s (2H, -C*H*$_2$-N, $^4J_{PbH}$ 16.4 Hz), 7.44m (9H, *H*$_{3\text{-}5}$ + C_6*H*$_5$-*meta+para*), 7.77 d (4H, C_6*H*$_5$-*ortho*, $^3J_{HH}$ 7.8, $^3J_{PbH}$ 111.6 Hz), 8.60d (1H, *H*$_6$, $^3J_{HH}$ 7.4, $^3J_{PbH}$ 130.7 Hz). ^{13}C NMR (75.4 MHz, 20 °C): δ 45.72s (N-*C*H_3), 65.32s (-*C*H_2-N, $^3J_{PbC}$ 38.5 Hz), 128.96s (*C*$_3$, $^3J_{PbC}$ 44.5 Hz), 129.47s (*C*$_6$H$_5$-*para*, $^4J_{PbC}$ 24.1 Hz), 129.57s (*C*$_4$, $^4J_{PbC}$ 24.8 Hz), 130.06s (*C*$_6$H$_5$-*meta*, $^3J_{PbC}$ 110.6 Hz), 136.01s (*C*$_6$H$_5$-*ortho*, $^2J_{PbC}$ 87.3 Hz), 138.51s (*C*$_6$, $^2J_{PbC}$ 70.7 Hz), 142.66s (*C*$_2$, $^2J_{PbC}$ 68.4 Hz), 154.45s (*C*$_1$, $^1J_{PbC}$ 826.6 Hz), 157.92s (*C*$_6$H$_5$-*ipso*, $^1J_{PbC}$ 726.3 Hz) (the resonance for *C*$_5$ carbon is overlapped by the resonance for the *C*$_6$H$_5$-*para* carbon).

*Preparation of [2-(Me_2NCH_2)C_6H_4]Ph_2PbI (**5**)*

Method A. The chloride **4** (0.2 g, 0.45 mmol) was suspended in CH_2Cl_2 (20 ml) and solvent was added until the solid compound was completely solved. An aqueous solution of KI (0.375 g, 2.26 mmol, 500% excess) was then added and the obtained mixture was stirred for 3 h at room temperature. The organic

layer was separated from the water layer and the latter was washed with CH_2Cl_2 (2 x 5 ml). The organic solution was dried over anhydrous Na_2SO_4. The solvent was removed in vacuum and the remaining yellow material was recrystallized from a CH_2Cl_2/hexane mixture to give the title compound. Yield: 0.22 g (91%).

Method B. Compound **2** (0.2 g, 0.4 mmol) was suspended in CH_2Cl_2 (20 ml) and solvent was added until the solid compound was completely solved. A solution of iodine (0.1 g, 0.4 mmol) in CH_2Cl_2 was added and the mixture was stirred for 2 h at room temperature. The solvent was removed under vacuum and the remaining yellow solid was recrystallized from a CH_2Cl_2/hexane mixture to give the title compound. Yield: 0.15 g (68%), m.p. 236 °C. ^{1}H NMR (300 MHz, 20 °C): δ 1.95s (6H, N-CH_3), 3.54s (2H, -CH_2-N, $^4J_{PbH}$ 15.0 Hz), 7.42m (9H, $H_{3\text{-}5}$ + C_6H_5-*meta+para*), 7.77dd (4H, C_6H_5-*ortho*, $^3J_{HH}$ 7.9, $^4J_{HH}$ 1.2, $^3J_{PbH}$ 111.6 Hz), 8.66dd (1H, H_6, $^3J_{HH}$ 7.4, $^4J_{HH}$ 1.0, $^3J_{PbH}$ 134.4 Hz). ^{13}C NMR (75.4 MHz, 20 °C): δ 45.72s (N-CH_3), 65.18s (-CH_2-N, $^3J_{PbC}$ 33.3 Hz), 128.86s (C_3), 129.29s (C_6H_5-*para*), 129.55s (C_4), 129.61s (C_5), 129.96s (C_6H_5-*meta*, $^3J_{PbC}$ 108.7 Hz), 135.88s (C_6H_5-*ortho*, $^2J_{PbC}$ 84.3 Hz), 140.67s (C_6, $^2J_{PbC}$ 74.0 Hz), 142.61s (C_2), 150.51s (C_1), 157.21s (C_6H_5-*ipso*).

*Preparation of [2-(Et_2NCH_2)C_6H_4]Ph_2PbI (**6**)*

Compound **3** (0.25 g, 0.4 mmol) was suspended in CH_2Cl_2 (20 ml) and solvent was added until the solid compound was completely solved. A solution of iodine (0.1 g, 0.4 mmol) in CH_2Cl_2 was added and the mixture was stirred for 2 h at room temperature. The solvent was removed under vacuum and the remaining yellow solid was recrystallized from a CH_2Cl_2/hexane mixture to give the title compound. Yield: 0.18 g (67%), m.p. 223 °C. ^{1}H NMR (300 MHz, 20 °C): δ 0.69t (6H, N-CH_2-CH_3, $^3J_{HH}$ 7.1 Hz), 2.30q (4H, N-CH_2-CH_3, $^3J_{HH}$ 7.1 Hz), 3.63s (2H, -CH_2-N, $^4J_{PbH}$ 12.8 Hz), 7.44m (9H, $H_{3\text{-}5}$ + C_6H_5-*meta+para*), 7.78d (4H, C_6H_5-*ortho*, $^3J_{HH}$ 7.4, $^3J_{PbH}$ 110.7 Hz), 8.66d (1H, H_6, $^3J_{HH}$ 7.4, $^3J_{PbH}$ 129.9 Hz).

X-ray Crystallographic Study

Data were collected with a SMART APEX diffractometer (*National Center for X-Ray Diffractometry*, "Babes-Boyai" University, Cluj-Napoca, Romania) at 297 K, using a graphite monochromator to produce a wavelength (Mo-$K\alpha$) of 0.71073 Å. The crystal structure measurement and refinement data for compounds **2** and **4** are given in Table 3. Absorption correction was applied for **2** (semi-empirical from equivalents). The structure was solved by direct methods (full-matrix least-squares on F^2). All non hydrogen atoms were refined with anisotropic thermal parameters. For structure solving and refinement a software package SHELX-97 was used [29]. The drawings were created with the Diamond program [30].

Table 3. Crystallographic data for compounds **2** and **4**.

	2	**4**
chemical formula	$C_{27}H_{27}NPb$	$C_{21}H_{22}ClNPb$
crystal habit	colorless block	colorless block
crystal size [mm]	0.30 x 0.20 x 0.15	0.20 x 0.19 x 0.18
crystal system	monoclinic	monoclinic
space group	*P2(1)/c*	*P2(1)/n*
a [Å]	9.5351(12)	9.3153(5)
b [Å]	27.172(3)	24.2365(13)
c [Å]	10.1510(12)	17.8184(10)
α [deg]	90	90
β [deg]	117.036(2)	97.286(1)
γ [deg]	90	90
U [Å^3]	2342.6(5)	3990.4(4)
Z	4	8
D_c [g cm^{-3}]	1.624	1.768
M	572.69	531.04
F(000)	1112	2032
θ range [deg]	1.50 – 25.00	1.43 – 25.00
μ(Mo Kα) [mm^{-1}]	7.214	8.591
no. of reflections collected	16748	28670
no. of independent reflections	4114 (R_{int} = 0.0534)	7016 (R_{int} = 0.0463)
R_1 [$I > 2\sigma(I)$]	0.0490	0.0567
wR_2	0.0955	0.1048
no. of parameters	264	437
no. of restraints	0	0
GOF on F^2	1.133	1.292
largest difference electron density [e Å^{-3}]	0.987, –2.018	1.768, –1.675

CCDC-750465 (**2**) and -750466 (**4**) contains the supplementary crystallographic data for this paper. These data can be obtained free of charge at www.ccdc.cam.ac.uk/conts/retrieving.html [or from the Cambridge Crystallographic Data Centre, 12, Union Road, Cambridge CB2 1EZ, UK; fax: (internat.) +44-1223/336-033; E-mail: deposit@ccdc.cam.ac.uk].

ACKNOWLEDGEMENTS

We thank the Ministry of Education and Research of Romania (CNCSIS, Research Project No. 709/2007 and TD-342/2007) for financial support. We also thank the NATIONAL CENTER FOR X-RAY DIFFRACTION (”Babes-Bolyai” University, Cluj-Napoca, Romania) for the support in the solid state structure determinations.

REFERENCES

1. J. T. B. H. Jastrzebski, G. van Koten, Adv. Organomet. Chem., **1993**, *35*, 241.
2. R. Jambor, L. Dostál, in *The Chemistry of Pincer Compounds* [D. Morales-Morales, C. Jensen (Eds.)], Elsevier, Amsterdam, **2007**, pp. 357.
3. J. T. B. H. Jastrzebski, D. M. Grove, J. Boersma, G. van Koten, J. M. Ernsting, *Magn. Reson. Chem.*, **1991**, *29*, S25.
4. R. Varga, Schürmann, C. Silvestru, *J. Organomet. Chem.*, **2001**, *623*, 161.
5. J P. Novák, Z. Padělková, L. Kolářová, I. Císařová, A. Růžička, J. Holeček, *Appl. Organomet. Chem.*, **2005**, *19*, 1101.
6. P. Novák, J. Brus, I. Císařová, A. Růžička, J. Holeček, *J. Fluorine Chem.*, **2005**, *126*, 1531.
7. R. A. Varga, C. Silvestru, C. Deleanu, *Appl. Organomet. Chem.*, **2005**, *19*, 153.
8. R. A. Varga, A. Rotar, M. Schürmann, K. Jurkschat, C. Silvestru, *Eur. J. Inorg. Chem.*, **2006**, 1475.
9. R. A. Varga, C. Silvestru, *Acta Crystallogr. Sect. E*, **2006**, *62*, m1964.
10. P. Novák, Z. Padělková, I. Císařová, L. Kolářová, A. Růžička, J. Holeček, *Appl. Organomet. Chem.*, **2006**, *20*, 226.
11. R. A. Varga, C. Silvestru, *Acta Crystallogr. Sect. C*, **2007**, *63*, m48.
12. A. Rotar, R. A. Varga, C. Silvestru, *Acta Crystallogr. Sect. C*, **2007**, *63*, m355.
13. R. A. Varga, C. Silvestru, *Acta Crystallogr. Sect. C*, **2007**, *63*, m2789.
14. Z. Padělková, T. Weidlich, L. Kolářová, A. Eisner, I. Císařová, T. A. Zevaco, A. Růžička, *J. Organomet. Chem.*, **2007**, *692*, 5633.
15. R. A. Varga, K. Jurkschat, C. Silvestru, *Eur. J. Inorg. Chem.*, **2008**, 708.
16. A. Rotar, R. A. Varga, C. Silvestru, *Acta Crystallogr. Sect. E*, **2008**, *64*, m45.
17. A. Rotar, R. A. Varga, K. Jurkschat, C. Silvestru, *J. Organomet. Chem.*, **2009**, *694*, 1385.
18. P. P. De Wit, H. O. Van der Kooi, J. Wolters, *J.Organomet.Chem.,* **1981**, *216***,** C9.
19. H. O. van der Kooi, J. Wolters, A. van der Gen, *Rec. Trav. Chim. Pays Bas*, **1979**, *98*, 353.
20. H. O. van der Kooi, W. H. den Brinker, A. J. de Kok, *Acta Crystallogr.*, **1985**, *C41*, 869.
21. N. Seidel, K. Jacob, A. A. H. van der Zeijden, H. Menge, K. Merzweiler, C. Wagner, *Organometallics*, **2000**, *19*, 1438.
22. N. Seidel, K. Jacob, A. K. Fischer, *Organometallics*, **2001**, *20*, 578.
23. J. Emsley, *Die Elemente*, Walter de Gruyter: Berlin, **1994**.
24. J. Rigauy, S. P. Klesney (Eds.), *Nomenclature of Organic Chemistry – The Blue Book*, Pergamon Press, Oxford, **1979**.
25. H. Preut, F. Huber, *Z. Anorg. Allg. Chem.*, **1977**, *435*, 234.

26. A. Meller, H. Hoppe, W. Meringgele, A. Haase, M. Noltemeyer, *Organometallics*, **1998**, *17*, 123.
27. I. C. M. Wehman-Ooyevaar, I. F. Luitwieler, K. Vatter, D. M. Grove, W. J. J. Smeets, E. Horn, L. A. Spek, G. van Koten, *Inorg. Chim. Acta*, **1996**, *252*, 55.
28. MestReC and MestReNova, Mestrelab Research S.L., A Coruña 15706, Santiago de Compostela.
29. G. M. Sheldrick, *Acta Crystallogr., Sect. A* **2008**, *64*, 112.
30. *DIAMOND – Visual Crystal Structure Information System*, Crystal Impact, Postfach 1251, 53002 Bonn, Germany, **2001**.

STUDIA UNIVERSITATIS BABEŞ-BOLYAI, CHEMIA, LIV, 4, 2009

SYNTHESIS OF A DIMERIC G-2 MELAMINE DENDRIMER. FIRST USE OF A MASKED PIPERIDONE MOTIF IN DENDRITIC CHEMISTRY

FLAVIA POPA[a,b], OANA MOLDOVAN[a], MARIA IUSCO[a], PEDRO LAMEIRAS[c], CARMEN BATIU[a], YVAN RAMONDENCB[b] AND MIRCEA DARABANTU*[a]

ABSTRACT. Using iterative aminations of cyanuric chloride, we account the concise synthesis of a dimeric melamine based G-2 dendrimer having 1,4-dioxa-8-azaspiro[4.5]decane (piperidone ethyleneketal) in tandem with 2-amino-2-hydroxymethylbutanol *("ethylserinol"*) as peripheral groups piperazine and 4,4'-bispiperidine as internal and central linker, respectively.

Keywords: amination, dendrimers, iterative synthesis, 4-piperidone, 4,4'-bispiperidine, serinols.

INTRODUCTION

We have recently reported the strong and resourceful nucleophilicity of piperidone or of its ethyleneketal with respect to selective amination of cyanuric chloride [1, 2a]. From our previous contributions in the field of iterative synthesis directed to melamine dendritic structures based on *C*-substituted 2-aminopropane-1,3-diols (*"serinols"*) [2], we also learned that, until now, only *l*-2-amino-1-arylpropane-1,3-diols (enantiomeric *"phenylserinols"*) are suitable starting materials in the above convergent approaches[*]. Indeed, commercial C-2-substituted-2-aminopropane-1,3-diols [*"methylserinol"*, *"ethylserinol"* and 2-amino-2-(hydroxymethyl)propan-1,3-diol, known as TRIS] provided, up to G-0 dendrons, unstable as difficult to purify intermediates [3].

Therefore, we consider, as an alternative challenging attempt, the use of a C-2-substituted serinol, for example 2-amino-2-(hydroxymethyl)-butanol (*"ethylserinol"*) in tandem with 1,4-dioxa-8-azaspiro[4.5]decane (piperidone ethyleneketal) as peripheral groups in a target dimeric G-2 melamine dendrimer synthesis (Scheme 1).

[a] *"Babes-Bolyai" University, Department of Organic Chemistry, 11 Arany Jànos st., 400 028 Cluj-Napoca, ROMANIA, (darab@chem.ubbcluj.ro)*
[b] *Université et INSA de Rouen, IRCOF – LCOFH, UMR 6014 CNRS COBRA, BP 08, 76131 Mont Saint-Aignan Cedex, FRANCE*
[c] *Université de Reims Champagne-Ardenne, ICMR - LIS, UMR 6229, BP 1039, 51687 Reims Cedex 2, FRANCE*

[*] For continuous discussion in this communication, nomenclature, definitions and concepts according to Tomalia (Ref. [3a]) and Vögtle *et al.* (Ref. [3b]) were used throughout.

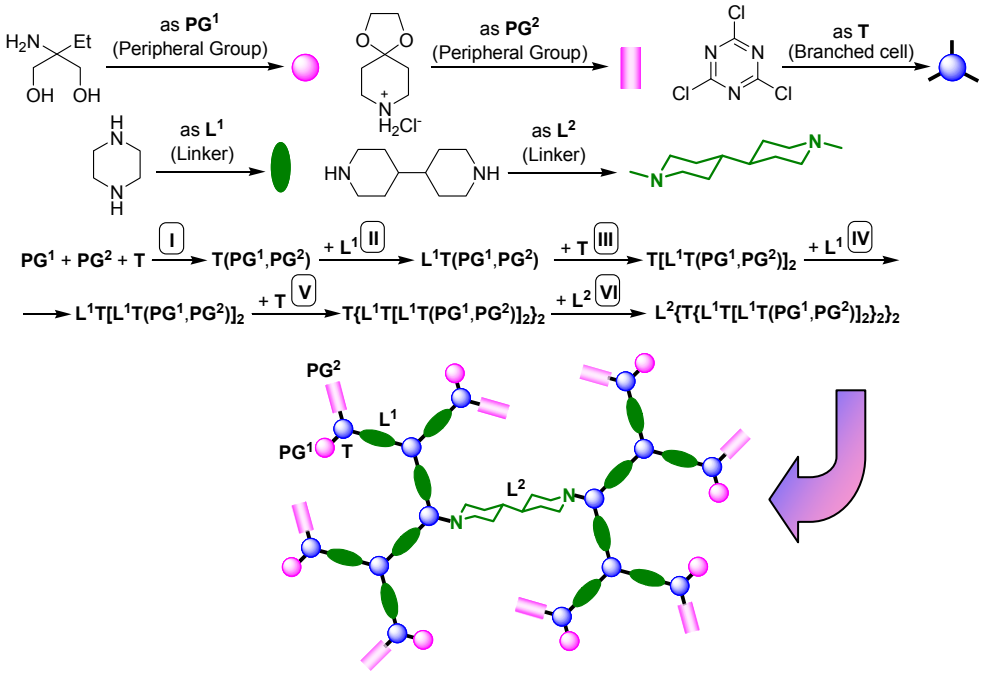

Scheme 1

As shown in Scheme 1, our strategy was convergent, consisting of six linear steps, **I – VI**, as ten selective aminations of cyanuric chloride with the depicted amino nucleophiles. We note the use of 4,4'-bispiperidine (**L^2**), ethylserinol (**PG^1**) and piperidone ethyleneketal (**PG^2**) as central linker and peripheral groups respectively, not reported previously. Along with C-2-substituted serinols, only TRIS (2-amino-2-hydroxymethylpropan-1,3-diol) is known, since 1985 [4a], to be a key element in dendritic chemistry, playing all roles, core, branched cell and peripheral group [4]. Concerning linker **L^1**, piperazine, it is nowadays a widely employed structural motif in dendrimer synthesis connecting cores [5a-d], generations [5e-h] or both [5i-l].

RESULTS AND DISCUSSION

1. Synthesis

We commenced our study (Scheme 2) with the anchorage of peripheral groups on *s*-triazine. Ethylserinol **1**, the less reactive nucleophile, was firstly reacted with cyanuric chloride providing dichloroamino-*s*-triazine **2a** in quantitative yield (TLC monitoring)*. For this reason, **2a** was not isolated but treated with the subsequent nucleophile, piperidone ethylene ketal hydrochloride whose

* We previously discussed the synthesis and structure of **2a**, see Ref. [2a].

free base, generated *in situ*, was, as expected, much more reactive in 10% aq. THF [1]. Indeed, the very mild shown conditions were found step by step, in order to avoid, as much as possible, the complete replacement of chlorine in **2a** by two dioxaazaspiranic units (compound **2c**). We note the optimised yield of **2b**, 58%, to be also mandatory to the purity of commercial **1** (about 80%).

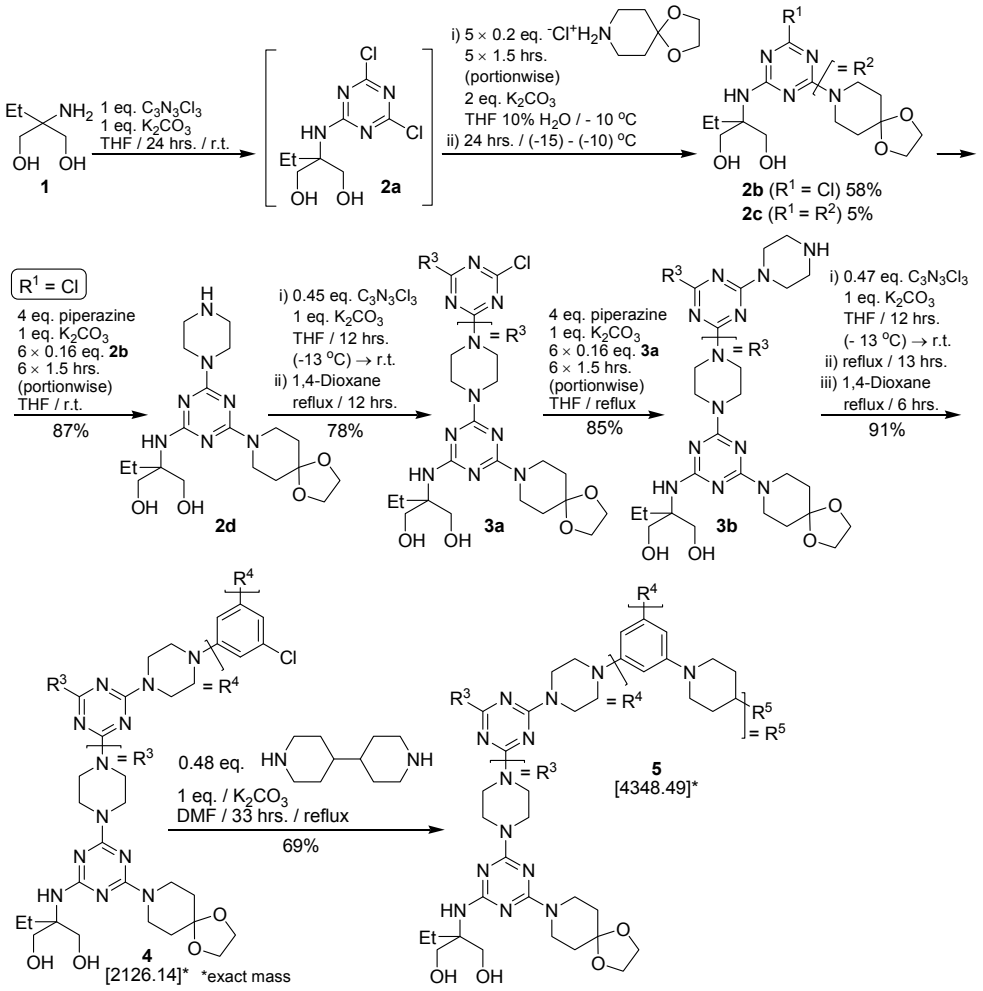

Scheme 2

Reaction of chlorodiamino-*s*-triazine **2b** with excess of piperazine afforded amine **2d** with good yield, following our already established protocol [2a, 2c, 6]. Purification of **2d** by column chromatography on partially deactivated silica gel (eluent *i*-PrOH: aq. NH_3 25% 9:1 v/v) ensured the analytical purity of this intermediate.

With **2d** in our hands, we reiterated the double amination of cyanuric chloride and accessed the G-1 dendron **3a** by operating on a large scale of temperature, from -13 to 102 ^{o}C. That is, only in these conditions we were confident that the contaminating possible side reactions, such as *O*- instead *NH*-anchorage of **2d** on *s*-triazine, were completely eliminated.

Next, selective amination of **3a** by piperazine was realised similarly as for **2b**, the refluxing solvent being however required in agreement with the stronger solvation of **3a** *vs*. **2b** in THF. Although isolated by column chromatography on partially deactivated silica gel, in order to reach analytical purity, the G-1 aminodendron **3b** needed a supplementary routine recrystallisation.

At this stage, the triple anchorage of **3b** on *s*-triazine skeleton upon treatment with 0.3 eq. of cyanuric chloride failed, presumably because of the already manifested starburst effect [7]. Thus, only the chloro-*s*-triazine G-2 dendron **4** could be isolated with small conversion (about 10%) from a complex polymeric reaction mixture (attempt not depicted in Scheme 1).

Therefore, we had to change the final strategy by using 0.47 eq. of cyanuric chloride against **3b**. In a very clean reaction, we were delighted to obtain the G-2 dendron **4** with an excellent yield in very comparable conditions to those in the case of G-1 analogue **3a**. Finally we coupled two G-2 dendrons **4** through a 4,4'-bispiperidine central linker, seen as a larger divalent central spacer than the trivalent *s*-triazine. Both dendritic structures **4** and **5** were isolated and purified by simple crystallisations.

2. Preliminary structural assignments

Besides synthetic and applied interest [5], dendritic melamines have received increased structural attention in the last period [8], [9].

Starting from the pioneering works of Katritzky, Ghiviriga [8a-c] *et al*. [8d-g] focused on restricted rotations about the C(*s*-triazine)-N(exocyclic) partial double bonds, the current concepts with respect to this expected hindered mobility comprise a more concise terminology. Thus, the above connections are seen by us as (pro)diastereomerism axis [2a, 2b] promoting, in some cases, chirality [2a] or, if dendritically exacerbated, an entire "dendrimeric choreography" [9].

For the present communication, we will limit our discussion to the first isolated intermediate, chlorodiamino-*s*-triazine **2b** and the target dendrimer **5**.

At room temperature, NMR spectra of compound **2b** revealed its frozen rotamerism about C(*s*-triazine)-N(exocyclic) partial double bonds, C-4-N-8' (axis of prodiastereomerism[**]) and C-6-N(serinol) (axis of diastereomerism) as two blocked rotational diastereomers, **2b**-*syn* (minor) and **2b**-*anti* (major) (Figure 1). We discriminated the *anti vs. syn* rotamers by taken into account the strong dipole moment induced by the remainder chlorine substituent at C-2 [2a, 2b, 4c, 9]

[**] C-4-N-8' is also an axis of chirality, see ref. [2a] (to be discussed in the full paper).

creating a more deshielding influence of the protons NH in the **2b**-*anti* environment. *Mutatis-mutandis* the resonance of hydroxyl protons in rotamer **2b**-*anti* was located upfield with respect to **2b**-*syn*.

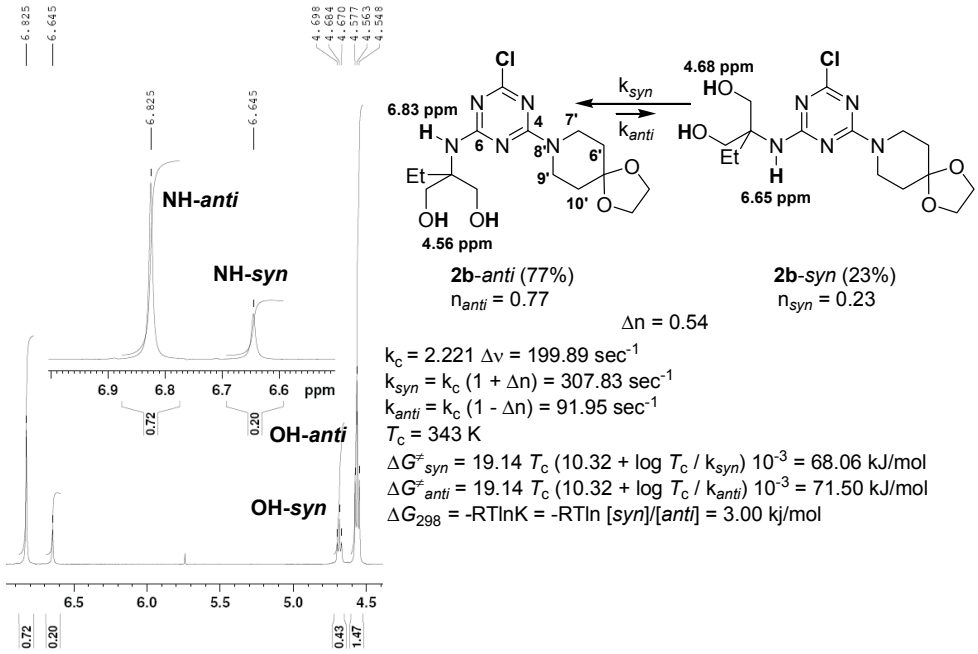

Figure 1. Detailed ^{1}H NMR spectrum (400 MHz, [D_6]DMSO, 293 K) of frozen rotamers of compound **2b**

Evidently, the ^{13}C NMR spectrum exhibited two sets of δ values for almost all positions of the **2b**(*anti* + *syn*) rotameric mixture. For example, although rotamerism about the axis of prodiastereomerism C-4-N-8' was not clearly observed in the ^{1}H NMR spectrum, on 100 MHz time scale, piperidine carbons C-7' *vs.* C-9' and C-6' *vs.* C-10' in the major as detectable **2b**-*anti* rotamer were diastereotopic, Δδ = 0.23 and 0.29 ppm respectively.

By rising the temperature up to 343 K, compound **2b** reached, at 353 K, the fast exchange status between unequally populated sites as freely rotating structure [10a]. Taking into account Eliel's *et al*. recommended precautions [10b], calculation based on Eyring equations [10a] applied for unequally two terms populated systems [10c] provided plausible data of the rotational barriers about the bond C-6-N(serinol) as Enthalpies of Activation $\Delta G^{\neq}$ [2a, 8]. Indeed, the $\Delta G_{298} = \Delta G^{\neq}_{anti} - \Delta G^{\neq}_{syn}$ value was 3.43 kJ/mol *vs.* 3.00 kJ/mol issued from classical two terms equilibrium relationship (Figure 1).

The ΔG *anti vs. syn* at 343 K and up could be not determined since, upon heating, NH protons changed their character, from an “amide” (6.83 - – 6.65 ppm, “rigid” protons) to an “amine” one (6.41 ppm, “mobile” protons).

All these complex rotational phenomena disappeared in the case of the much less π-deficient melamine **2c** which, at room temperature, already displayed a slow exchange status between unequal populated sites.

The mass spectrum of the dendrimer **5** fully confirmed the designed structure (Figure 2).

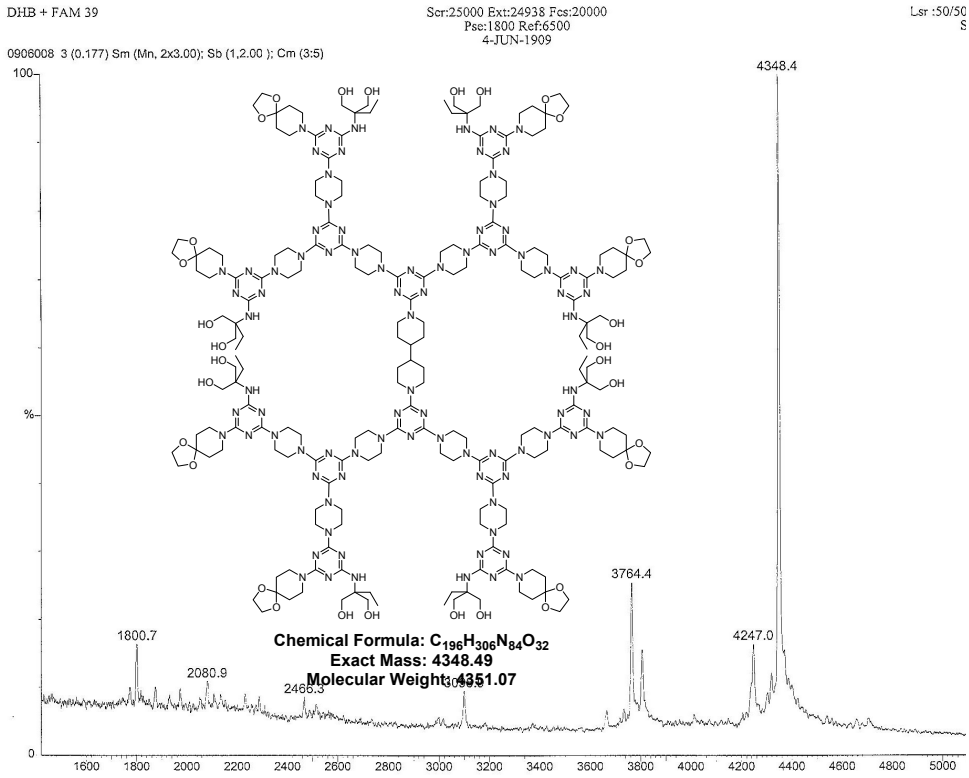

Figure 2. Mass Spectrum of compound **5** (Linear MALDI+ in 2,5-dihydroxybenzoic acid)

The ^{1}H NMR spectrum of **5** (Figure 3) recorded at 353 K indicated for this macromolecule a complex appearance. From rotational point of view, the six membered saturated heterocyclic rings were still in a slow exchange status between unequal populated sites, at least with respect to the ten piperidine peripheral and central units (see the broad signal assigned to the 42 protons at 1.61 ppm). In contrast, the geminal anisochrony of the sixteen peripheral hydroxymethylene groups is clearly visible in the region 3.5 – 3.7 ppm.

In ^{13}QC NMR spectrum, (Figure 4) from 196 carbon atoms, 194 were assignable. Only the two C-4, -4' carbons of the central 4,4'-bispiperidine linker remained obscured.

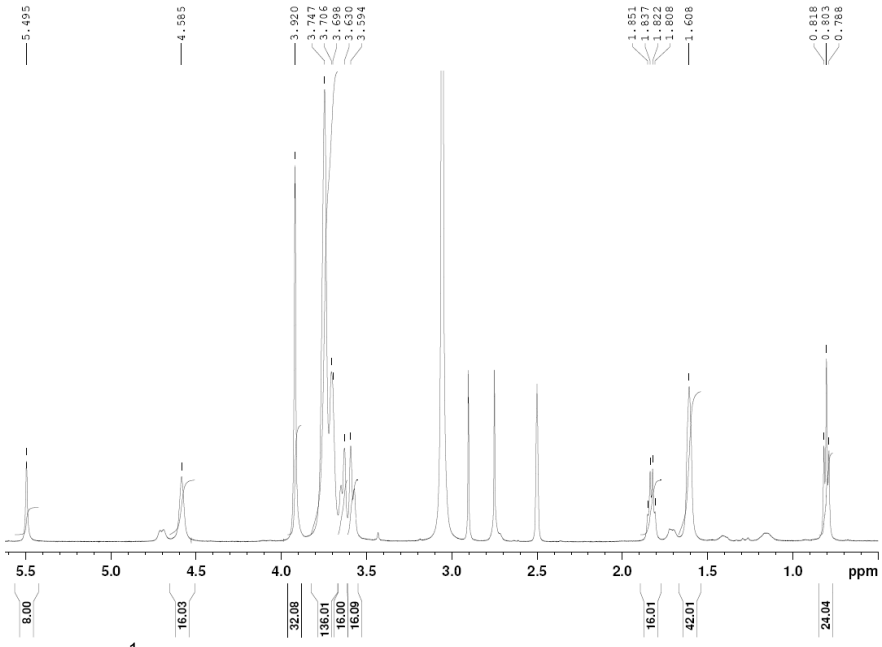

Figure 3. ^{1}H NMR spectrum of compound **5** (500 MHz, [D_6]DMSO, 353 K)

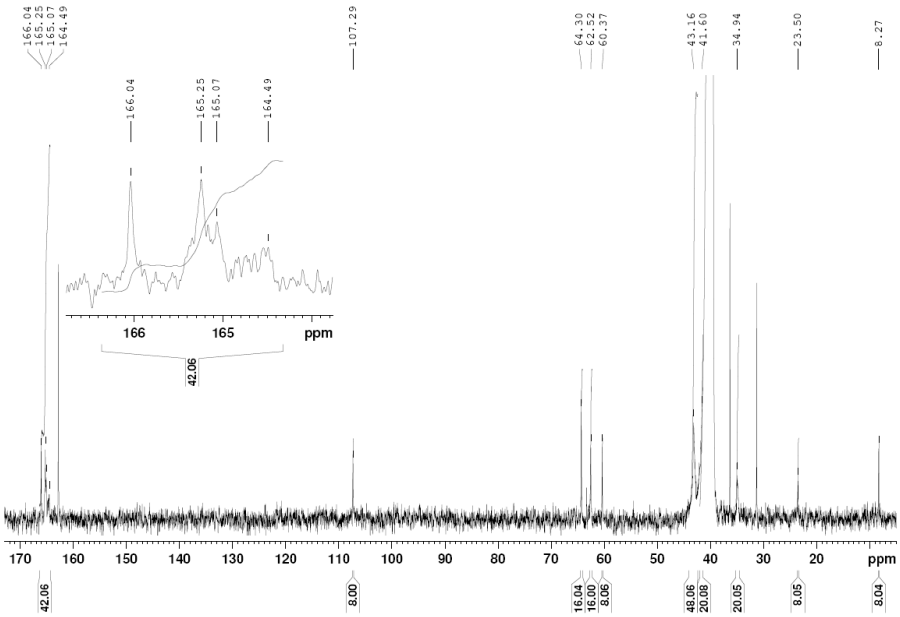

Figure 4. ^{13}QC NMR spectrum of compound **5** (125 MHz, [D_6]DMSO, 298 K)

The signal located at 41.6 ppm (20 carbon atoms) accounts for sixteen piperidine methylenes of the eight spiranic peripheral groups and four piperidine methylenes of the central 4,4'-bispiperidine linker. They are placed at the α-positions with respect to the heterocyclic nitrogens. Accordingly, the signal located at 34.9 ppm discloses the other 20 carbon atoms of the peripheral and central piperidine methylenes located at the β-positions *vs.* azaatom.

Both ^{1}H and ^{13}C NMR spectra also evidenced the presence of DMF, the reaction solvent (Scheme 2), despite of very careful final manipulation of the product. For the moment, we are unable to distinguish between problems of drying the compound or encapsulating phenomena.

CONCLUSIONS

We realised the concise synthesis of the first dimeric G-2 melamine dendrimer comprising, in tandem, eight C-2-substituted serinolic motifs and eight masked piperidone units as peripheral groups. The overall yield was optimised at 19%. More developments *vs.* inherent restrictions of this convergent strategy will be published in due course.

EXPERIMENTAL SECTION

General. Conventional NMR spectra were recorded on a Bruker® AM 300 instrument operating at 300 and 75 MHz for ^{1}H and ^{13}C nuclei respectively. Bruker® AV400 and DMX500 instruments, operating at 400 (500) and 100 (125) MHz for ^{1}H and ^{13}C nuclei respectively, were used for DNMR and QC experiments. All NMR spectra were measured in anhydrous commercially available deuteriated solvents. No $SiMe_4$ was added; chemical shifts were measured against the solvent peak. TLC was performed by using aluminium sheets with silica gel 60 F_{254} (Merck®); flash column chromatography was conducted on Silica gel Si 60 (40–63 μm, Merck®). Microanalyses were performed on a Carlo Erba® CHNOS 1160 apparatus. Mass spectra (MS) were recorded on Bruker® Esquire Instrument.

*Preparation of compound **2b***

2-Amino-2-hydroxymethylbutanol (*"ethylserinol"*) [1.67 g 80%, Aldrich® (Cat. No. 38, 168-3) 1.34 g 100%, 11.2 mmol] and potassium carbonate (> 99%, 1.55 g 100%, 11.2 mmol, S.C.CRISTAL R CHIM SRL) were suspended with stirring in anh. THF (80 mL) then cooled at 0 °C. At this temperature, cyanuric chloride (> 99%, 2.07 g 100%, 11.2 mmol, Merck®, Cat. No. S4249515 526) as anh. THF (20 mL) solution was rapidly injected and the resulted suspension was let to reach room temperature and stirred for additional 24 hrs. At this stage, TLC monitoring (eluent toluene: isopropanol 2: 1 v/v, visualisation in UV 254 nm) indicated the presence of a single compound. Water (10 mL) and potassium

carbonate (3.10 g, 22.4 mmol) were added and the resulted suspension was cooled at (-10) – (-15) ^{o}C. At this temperature, fine powdered 1,4-dioxa-8-azaspiro[4.5]decane (2.01 g, 11.2 mmol) was added portionwise as 5 equal portions each 90 min. The reaction mixture was stirred at -10 ^{o}C for additional 24 hrs. then let to reach room temperature. The suspension was filtered off and minerals were well washed with anh. THF. The organic filtrate was taken and treated under vigorous stirring, with chloroform (150 mL) and water (75 mL). After separation, the organic layer was washed with water to neutrality (× 25 mL) then the combined aqueous layer was extracted with chloroform (2 × 40 mL). The combined organic layer was dried over sodium sulphate, filtered off and evaporated under reduced pressure to provide the crude material (4.10 g). This was separated by column chromatography (eluent toluene: isopropanol 4:1 v/v) to yield 2.41 g compound **2b** and 0.263 g compound **2c** as side product.

2-Chloro-4-(1,4-dioxa-8-azaspiro[4.5]decan-8-ylamino)-4-[1-hydroxy-2- (hydroxymethyl)but-2-ylamino]-s-triazine ***2b***; white crystalline powder; yield 58%; m.p. = 147.4-152.7 ^{o}C; Anal. calcd. for $C_{15}H_{24}ClN_5O_4$: C, 48.19; H, 6.47; N, 18.73%; found: C, 48.44; H, 6.16; N, 18.66%. R_f (80% toluene/isopropanol) = 0.65. ^{1}H NMR (400 MHz, 293 K, [D$_6$]DMSO) 0.73 ppm (3 H, m, CH_2CH_3, *anti* + *syn*), 1.62 ppm (4 H, m, H-6', -10'-ax., -eq., spirane, *anti* + *syn*), 1.71 (2 H, q, ^{3}J = 7.4 Hz, CH_2CH_3, *anti* + *syn*), 3.46 ppm (2 H, dd, ^{2}J = 10.8 Hz, ^{3}J = 6.0 Hz, CH_2OH, *anti* + *syn*), 3.65 ppm (2 H, dd, ^{2}J = 10.8 Hz, ^{3}J = 6.0 Hz, CH_2OH, *anti* + *syn*), 3.72 ppm (4 H, t, ^{3}J = 5.4 Hz, H-7', -9'-ax., -eq., spirane, *anti* + *syn*), 3.91 ppm (4 H, s, H-2', -3', spirane, *anti* + *syn*), 4.56 ppm (1.47 H, dd as t , ^{3}J = 5.8 Hz, CH_2OH, *anti*), 4.68 ppm (0.43 H, dd as t , ^{3}J = 5.6 Hz, CH_2OH, *syn*), 6.65 ppm (0.20 H, bs, NH, *syn*), 6.83 (0.72 H, bs, NH, *anti*). ^{1}H NMR (400 MHz, 353 K, [D$_6$]DMSO) 0.79 ppm (3 H, t, ^{3}J = 7.4 Hz, CH_2CH_3), 1.66 ppm (2 H, dt, ^{3}J = 5.8, 3.8 Hz, H-6', -10'-ax., -eq., spirane), 1.65 ppm (2 H, dt, ^{3}J = 5.6, 4.0 Hz, H-6', - 10'-ax, -eq., spirane), 1.79 (2 H, q, ^{3}J = 7.4 Hz, CH_2CH_3), 3.57 ppm (2 H, dd, ^{2}J = 11.0 Hz, ^{3}J = 5.4 Hz, CH_2OH), 3.68 ppm (2 H, dd, ^{2}J = 10.8 Hz, ^{3}J = 5.6 Hz, CH_2OH), 3.765 ppm (2 H, dt, ^{3}J = 7.0, 5.0 Hz, H-7', -9'-ax., -eq., spirane), 3.760 ppm (2 H, dt, ^{3}J = 5.6, 4.0 Hz, H-7', -9'-ax., -eq., spirane), 3.93 ppm (4 H, s, H-2', -3', spirane), 4.40 ppm (2 H, bs, CH_2OH), 6.41 ppm (1 H, bs, NH). ^{13}C NMR (100 MHz, 293 K, [D$_6$]DMSO, ppm) 7.9 (1 C, CH_2CH_3, *anti*), 8.1 (1 C, CH_2CH_3, *syn*), 22.4 (1 C, CH_2CH_3, *anti*), 23.0 (1 C, CH_2CH_3, *syn*), 34.9, 34.8, 34.6 (4 C, C-6', -10', spirane, *anti* + *syn*), 42.1, 41.9, 41.4 (4 C, C-7', -9', spirane, *anti* + *syn*), 61.5, 60.8 (4 C, CH_2OH, *anti* + *syn*), 61.4 (2 C, Cq, serinol, *anti* + *syn*), 64.4 (4 C, C-2', -3', spirane, *anti* + *syn*), 106.9 (2 C, C-5', spirane, *anti* + *syn*), 163.6 (1 C, C-4, *s*-triazine, *syn*), 164.2 (1 C, C-4, *s*-triazine, *anti*), 165.1 (1 C, C-6, *s*-triazine, *anti*), 165.8 (1 C, C-4, *syn*), 168.4 (1 C, C-2, *s*-triazine, *anti*), 168.6 (1 C, C-2, *s*-triazine, *syn*).

2,4-Bis(1,4-dioxa-8-azaspiro[4.5]decan-8-ylamino)-6-[1-hydroxy-2-(hydroxy methyl)but-2-ylamino]-s-triazine ***2c***; yellowish crystalline powder; yield 5 %; m.p. = 143.1 – 146.8 ^{o}C; Anal. calcd. for $C_{22}H_{36}N_6O_6$: C, 54.99; H, 7.55; N,

17.49%; found: C, 55.22; H, 7.88; N, 17.55%. R_f (80% toluene/isopropanol) = 0.60 ^{1}H NMR (400 MHz, 298 K, [D$_6$]DMSO) 0.73 ppm (3 H, t, ^3J = 7.4 Hz, CH_2CH_3), 1.57 ppm (8 H, t, ^3J = 5.2 Hz, H-6', -6", -10', -10"-ax., -eq., spirane), 1.77 (2 H, q, ^3J = 7.4 Hz, CH_2CH_3), 3.50 ppm (2 H, dd, ^2J = 10.6 Hz, ^3J = 5.4 Hz, CH_2OH), 3.58 ppm (2 H, dd, ^2J = 10.6 Hz, ^3J = 5.8 Hz, CH_2OH), 3.71 ppm (8 H, t, ^3J = 5.6 Hz, H-7', -7", -9', -9"-ax., -eq., spirane), 3.90 ppm (8 H, s, H-2', -2", -3', -3" spirane), 4.73 ppm (2 H, dd as t , ^3J = 5.8 Hz, CH_2OH), 5.60 ppm (1 H, bs, NH). ^{1}H NMR (400 MHz, 353 K, [D$_6$]DMSO) 0.79 ppm (3 H, t, ^3J = 7.6 Hz, CH_2CH_3), 1.60 ppm (8 H, t, ^3J = 5.6 Hz, H-6', -6", -10', -10"-ax., -eq., spirane), 1.81 (2 H, q, ^3J = 7.4 Hz, CH_2CH_3), 3.57 ppm (2 H, d, ^2J = 10.8 Hz, CH_2OH), 3.63 ppm (2 H, dd, ^2J = 10.4 Hz, CH_2OH), 3.73 ppm (8 H, t, ^3J = 5.8 Hz, H-7', -7", -9', -9"-ax., -eq., spirane), 3.92 ppm (8 H, s, H-2', -2", -3', -3" spirane), 4.56 ppm (2 H, bs, CH_2OH), 5.47 ppm (1 H, bs, NH). ^{13}C NMR (100 MHz, 298 K, [D$_6$]DMSO, ppm) 8.2 (1 C, CH_2CH_3), 23.5 (1 C, CH_2CH_3), 34.8 (4 C, C-6', -6", -10', -10"), 41.5, 41.0 (4 C, C-7', -7", -9', -9", spirane), 60.3 (2 C, Cq, serinol), 62.6 (2 C, CH_2OH), 64.2 (4 C, C-2', -2", -3', -3", spirane), 107.3 (2 C, C-5', -5", spirane), 164.7 (1 C, C-2, -4, *s*-triazine), 166.1 (1 C, C-6, *s*-triazine).

Preparation of compound ***5***

Perfectly dried G-2 dendron **4** (analytically weighted 0.515 g, 0.242 mmol), freshly prepared and perfectly dried 4,4'-bispiperidine (analytically weighted 0.0194 g, 0.115 mmol), potassium carbonate (analytically weighted 0.035 g, 0.253 mmol) and freshly distilled dimethylformamide (DMF) (25 mL) were mixed together and the resulting suspension was heated at 100 ^{o}C (CARE! Avoid refluxing DMF to prevent the solvent decomposition!) for 35 hrs. (TLC monitoring, eluent chloroform: ethanol 3:1 v/v, visualisation in UV 254 nm). DMF was distilled under reduced pressure and the solid residue was taken with distilled water (10 mL), stirred at room temperature for 30 min. then filtered off. The crude product was well washed with distilled water (× 5 mL) to neutrality then dried at 70 ^{o}C to constant weight. The crude product was dissolved in distilled DMF (2 mL), then crystallised by adding anh. diethyl ether (6 mL). The resulted suspension was cooled at – 20 ^{o}C for 24 hrs., filtered off and well washed with anh. diethyl ether. After drying at 70 ^{o}C to constant weight, 0.345 g (0.079 mmol) compound **5** were obtained.

4,4'-{4,6-Bis{4-{4,6-bis{4-{4-(1,4-dioxa-8-azaspiro[4.5]decan-8-ylamino)-6-[1-hydroxy-2-(hydroxymethyl)but-2-ylamino]-s-triazin-2-yl}-piperazin-1-yl}-s-triazin-2-yl}-piperazin-1-yl}-s-triazin-2-yl}-bispiperidine **5**; white amorphous powder; yield 69 %; m.p. = 260 - 261 ^{o}C. R_f (75% chloroform/ethanol) = 0.75. ^{1}H NMR (500 MHz, 298 K, [D$_6$]DMSO) 0.75 ppm (24 H, bs, CH_2CH_3), 1.58, 1.79 ppm (58 H, 2 × bs as: 16 H, CH_2CH_3; 32 H, H-6, -10-ax., -eq., spirane; 10 H, H-3, -5, -3', -5'-ax., -eq., H-4, -4', 4,4'-bispiperidine), 3.91 – 3.52 ppm (200 H, bm, as: 96 H, piperazine; 32 H, H-7, -9-ax., -eq., spirane; 32 H, H-2, -3, spirane; 32 H, CH_2OH; 8 H, H-2, -6, -2', -6'-ax., -eq., 4,4'-bispiperidine),

4.76 ppm (16 H, bs, CH_2OH), 5.63 ppm (8 H, bs, NH); ^{1}H NMR (500 MHz, 353 K, [D_6]DMSO) 0.80 ppm (24 H, t, ^3J = 7.5 Hz, CH_2CH_3), 1.61 ppm (42 H, bs, as: 32 H, bs, H-6, -10-ax., -eq., spirane; 10 H, H-3, -5, -3', -5'-ax., eq., H-4, -4', 4,4'-bispiperidine), 1.85 (16 H, q, ^3J = 7.2 Hz, CH_2CH_3), 3.59 ppm (16 H, d, ^2J = 10.5 Hz, CH_2OH), 3.63 ppm (16 H, d, ^2J = 10.0 Hz, CH_2OH), 3.75 – 3.59 ppm (136 H, bm, as: 96 H, piperazine; 32 H, H-7, -9-ax., -eq., spirane; 8 H, H-2, -6, -2', -6'-ax., -eq., 4,4'-bispiperidine), 3.92 (32 H, s, H-2, -3, spirane), 4.59 (16 H, bs, CH_2OH), 5.50 (8 H, bs, NH). ^{13}QC NMR (125 MHz, 298 K, [D_6]DMSO, ppm) 8.3 (8 C, CH_2CH_3), 23.5 (8 C, CH_2CH_3), 34.9 (20 C as 16 C, C-6, -10, spirane; 4 C, C-3, -3', -5, -5', 4,4'-bispiperidine), 41.6 (20 C as 16 C, C-7, -9, spirane; 4 C, C-2, -6, -2', -6', 4,4'-bispiperidine), 60.4 (8 C, Cq, serinol), 62.5 (16 C, CH_2OH), 64.3 (16 C, C-2, -3, spirane), 107.3 (8 C, C-5, spirane), 164.5, 165.1, 165.3, 166.0 (42 C, *s*-triazine). MS (Linear MALDI+ in 2,5-dihydroxybenzoic acid): 4348.4 (100%) [M^+].

ACKNOWLEDGMENTS

Financial support from Grant provided by the *National Council of Scientific Research* C.N.C.S.I.S. (1482) is gratefully acknowledged. F. P. also thanks C.N.C.S.I.S. for the Doctoral Fellowship.

REFERENCES

1. F. Popa, I. Simioanca, M. Pintea, M. Fazekas, L. Gratecap, C. Berghian, C. Batiu, M. Darabantu, *Studia Universitatis Babes-Bolyai, Chemia*, **2008**, LIII, *4*, 5.
2. a) M. Pintea, M. Fazekas, P. Lameiras, I. Cadis, C. Berghian, I. Silaghi-Dumitrescu, F. Popa, C. Bele, N. Plé, M. Darabantu, *Tetrahedron,* **2008**, *64*, 8851; b) M. Fazekas, M. Pintea, P. Lameiras, A. Lesur, C. Berghian, I. Silaghi-Dumitrescu, N. Plé, M. Darabantu, *Eur. J. Org. Chem.*, **2008**, 2473; c) M. Darabantu, M. Pintea, M. Fazekas, P. Lameiras, C. Berghian, I. Delhom, I. Silaghi-Dumitrescu, N. Plé, A. Turck, *Letters in Organic Chemistry*, **2006**, *3*, 905.
3. a) D. A. Tomalia, *Aldrichimica Acta,* **2004***, 37,* 39; b) F. Vögtle, G. Richard, N. Werner, *Dendrimer Chemistry (Concepts, Syntheses, Properties, Applications)*, WILEY-VCH Verlag Gmbh & Co. KGaA, **2009**, pp. 7-22, 25.
4. a) G. R. Newkome, Z. –Q. Yao, G. R. Baker, V. K. Gupta, *J. Org. Chem.*, **1985**, *50*, 2003; b) G. R. Newkome, X. Lin, C. D. Weis, *Tetrahedron Asymmetry*, **1991**, *10*, 957; c) B. A. Hernandez, V. Chang, I. Villanueva, M. D. Heagy, *J. Org. Chem.*, **1999**, *64*, 6905; d) M. Plevoets, F. Vögtle, L. De Cola, V. Balzani, *New. J. Chem.*, **1999**, *23*, 63; e) J. Issberner, F. Vögtle, L. De Cola, V. Balzani, *Chem. Eur. J.*, **1997**, *3*, 706; f) G. R. Newkome, E. He, C. N. Moorefield, *Chem. Rev.*, **1999**, *99*, 1689; g) S. Mattei, P. Seiler, F. Diederich, V. Gramlich, *Helv. Chim. Acta*, **1995**, *78*, 1904; h) S. Mattei, P. Wallimann, B. Kenda, W. Amrein, F. Diederich, *Helv. Chim. Acta*, **1997**, *80*, 2391;

i) P. Wallimann, P. Seiler, F. Diederich, *Helv. Chim. Acta*, **1996**, *79*, 779; j) C.M. Cardona, R. E. Gawley, *J. Org. Chem.*, **2002**, *67*, 1411; k) G. R. Newcome, X. Lin, *Macomolecules*, **1991**, *24*, 1443; k) A. Dupraz, P. Guy, C. Dupuy, *Tetrahedron Lett.*, **1996**, *37*, 1237; l) I. Bury, B. Heinrich, C. Bourgogne, D. Guillon, B. Donnio, *Chem. Eur. J.*, **2006**, *12*, 8396.

5. a) W. Zhang, D. T. Nowlan, L. M. Thomson, M. W. Lackowski, E. E. Simanek, *J. Am. Chem. Soc.*, **2001**, *123*, 8914; b) M. B. Steffensen, E. E. Simanek, *Angew. Chem. Int. Ed.*, **2004**, *43*, 5178; c) J. Lim, E. E. Simanek, *Molecular Pharmaceutics*, **2005**, *2*, 273; d) G. R. Newcome, J. Gross, C. N. Moorefield, B. D. Woosley, *Chem. Commun.*, **1997**, 515; e) A. P. Umali, E. E. Simanek, *Org. Lett.*, **2003**, *5*, 1245; f) H. T. Chen, M. F. Neerman, A. R. Parrish, E. E. Simanek, *J. Am. Chem. Soc.*, **2004**, *126*, 10044; g) L. –L. Lai, L. –Y. Wang, C. -H. Lee, C. Y. Lin, K. –L. Cheng, *Org. Lett.*, **2006**, *8*, 1541; h) E. J. Acosta, S. O. Gonzalez, E. E. Simanek, *J. Polym. Sci. Part A.*, **2005**, *43*, 168; i) W. Zhang, S. O. Gonzalez, E. E. Simanek, *Macromolecules*, **2002**, *35*, 9015; j) E. Hollink, E. E. Simanek, *Org. Lett.*, **2006**, *8*, 2293; k) M. F. Neerman, W. Zhang, A. R. Parrish, E. E. Simanek, *Int. J. Pharm.*, **2004**, *281*, 129; l) L. –L. Lai, C. –H. Lee, L. –Y. Wang, K. L. Cheng, H. –F. Hsu, *J. Org. Chem.,* **2008**, *73*, 485.
6. Z. Antal, C. Batiu, M. Darabantu, *Studia Universitatis Babes-Bolyai, Chemia*, **2008**, LIII, *4*, 51.
7. a) P. –G. de Gennes, H. Hervet, *J. Phys. Lett. Fr.*, **1983**, *44*, L351; b) D. A. Tomalia, A. Naylor, W. A. Goddard III, *Angew. Chem.*, **1990**, *102*, 119; c) D. A. Tomalia, A. Naylor, W. A. Goddard III, *Angew. Chem. Int. Ed.*, **1990**, *29*, 138.
8. a) A. R. Katritzky, I. Ghiviriga, D. C. Oniciu, A. Barkock, *J. Chem. Soc. Perkin Trans. 2*, **1995**, 785; b) A. R. Katritzky, I. Ghiviriga, P. G. Steel, D. C. Oniciu, *J. Chem. Soc. Perkin Trans. 2*, **1996**, 443; c) I. Ghiviriga, D. C. Oniciu, *Chem. Commun*., **2002**, *22*, 2718; d) M. Amm, N. Platzer, J. Guilhem, J. P. Bouchet, J. P. Volland, *Magn. Reson. Chem*., **1998**, *36*, 587; e) M. Amm, N. Platzer, J. P. Bouchet, J. P. Volland, *Magn. Reson. Chem*., **2001**, *39*, 77; f) H. E. Birkett, R. K. Harris, P. Hodgkinson, K. Carr, M. H. Charlton, J. C. Cherryman, A. M. Chippendale, R. P. Glover, *Magn. Reson. Chem.*, **2000**, *38*, 504; g) H. E. Birkett, J. C. Cherryman, A. M. Chippendale, J. O. S. Evans, R. K. Harris, M. James, I. J. King, G. Mc. Pherson, *Magn. Reson. Chem*., **2003**, *41,* 324.
9. X. K. Moreno, E. E. Simanek, *Macromolecules* **2008**, *41*, 4108.
10. a) H. Friebolin, *Basic One- and Two Dimensional NMR Spectroscopy*; VCH Verlagsgesellschaft /VCH: Weinheim/New York **1991**; p.93, 263; b) E. L. Eliel, H. S. Wilen, *Stereochemistry of the Organic Compounds*; John Wiley & Sons, Inc. **1994**; pp 221–239, 488–507, 678, 788, 1210; c) H. Shanan-Atidi, K. H. Bar-Eli, *J. Phys. Chem.*, **1970**,*74*, 961.

STUDIA UNIVERSITATIS BABEŞ-BOLYAI, CHEMIA, LIV, 4, 2009

STUDY ON THE INHIBITION OF BRIGGS-RAUSCHER OSCILLATING REACTION

LÉNÁRD-ISTVÁN CSEPEI[a,b], CSABA BOLLA[a]

ABSTRACT: We present the results concerning our exploratory study on the effect of four compounds (ascorbic acid, tartaric acid, pyrogallol and salicylic acid) on the Briggs-Rauscher oscillating reaction. In case of ascorbic acid, tartaric acid and pyrogallol, a linear increase of the inhibition time with the concentration of these substances was observed. We also paid attention on the changes of color and redox potential of the reacting mixture in the moment of addition of the above mentioned compounds. The observations showed that ascorbic acid and tartaric acid manifest an inhibitory effect through their strong reducing properties. Pyrogallol acts like other polyphenolic antioxidants studied before. Salicylic acid, unlike all of the phenolic and polyphenolic compounds described before, did not stop instantly the oscillations.

Keywords: Briggs-Rauscher oscillating reaction, inhibitory effect, ascorbic acid, tartaric acid, pyrogallol, salicylic acid

INTRODUCTION

The Briggs-Rauscher (BR) reaction is one of the most spectacular oscillating reactions, which is a hybrid of the well-known Belousov-Zhabotinskii and the Bray-Liebhafsky reactions. The net chemical transformation of the BR reaction is the oxidation and iodination of malonic acid by hydrogen-peroxide and iodate ion, catalyzed by manganous ion in acidic media [1]. The concentration of intermediates (I_2, I^-, HOI, HIO_2, IO_2•, HOO•, etc.) presents more than one extreme point (i.e.: maximum and minimum) in time. The first mechanistic investigations were carried out by Cooke [2], Noyes and Furrow [3-5], De Kepper and Epstein [6], respectively. As a result of these studies, 30 elementary steps have been identified. Two almost identical skeleton mechanisms were proposed, which described qualitatively well the nonlinear behavior of the reacting system in a batch reactor [5] and in a continuous-flow stirred tank reactor (CSTR) [6]. However there was a discrepancy between the experimental

[a] *Universitatea Babeş-Bolyai, Facultatea de Chimie şi Inginerie Chimică, Str. Kogălniceanu, Nr. 1, RO-400084 Cluj-Napoca, Romania, csbolla@chem.ubbcluj.ro*

[b] *Fritz Haber Institute der Max Planck Gesellschaft, Faradayweg 4-6, 14195 Berlin, Deutschland, cslenard@gmail.com*

and the simulated quantitative features (period time, concentration ranges for different intermediates and the cross-shaped phase diagram) of the reaction [5, 6]. Furrow has recognized that the hydroperoxyl radical mediates the autocatalytic HIO_2 production and plays an important role in the reaction [7]. The modification of the skeleton mechanism by inclusion of the elementary steps involving IO_2• and HOO• improved the predicting ability of the model [7, 8].

Cervellati *et al*. reported that the addition of mono- and polyphenolic compounds to the active mixture causes a temporary but instant cessation of oscillations [9, 10]. The time elapsed between the cessation and the subsequent regeneration of the oscillatory regime was denominated as inhibition time. A linear correlation was found between the concentration and the inhibition time for every phenolic substance added in the BR-mixture. The inhibitory effect was accounted for a fast reaction involving the phenolic compound and HOO• radical. Since polyphenols are known to be effective free radical scavengers, they reduce drastically the concentration of HOO• in the BR-mixture. As soon as the antioxidant is totally consumed, the HOO• concentration rises up to the critical range, where the oscillations reappear. The side-reaction between the phenolic compounds and the oxidative species of the BR mixture was also taken into account [10, 11]. For quantitative modeling of the inhibitory effect, the modified skeleton model [8] was complemented with the steps involving the antioxidant [11]. Based on these results it was possible to develop a new analytical method for determination of the antioxidant activity of free radical scavengers.

In contrast with the other antioxidant assays (Trolox Equivalent Antioxidant Capacity /TEAC/, Total Radical Trapping Parameter /TRAP/, Ferric Ion Reducing Antioxidant Parameter /FRAP/, and Oxygen Radical Absorbance Capacity /ORAC/), in the method proposed by Cervellati *et al*. the antioxidants react with HOO• radical [12]. This radical is a reactive oxygen metabolite produced in the human body, to which oxidative stress, cell damage, aging, cancer and other diseases are associated [13, 14]. Therefore the method validated by Cervellati *et al*. gives more reliable data with respect to the reactivity of the antioxidants with reactive oxygen species (ROS).

Furrow *et al*. found that the better known antioxidant, ascorbic acid acts different than the polyphenols. Being a strong reducing agent, the ascorbic acid is oxidized instantly by the reactive oxy-iodide species when is added to the BR-mixture, while iodide ion is produced. An inhibitory effect of iodide ion on the BR-reaction was observed. The qualitative mechanistic interpretation of inhibitory effect of iodide ion was also given [15]. Since the ascorbic acid added to the BR-mixture does not react with HOO• radical, it was concluded that the BR-method is not suitable to determine the antioxidant activity of ascorbic acid.

RESULTS AND DISCUSSION

The effect of ascorbic acid on the BR-reaction

Foremost we tried to reproduce the experiments made by Furrow *et al*. [15]. When we added ascorbic acid solution, the color of the oscillating BR-mixture changed suddenly to brown. At the same time the redox potential rise (ΔE) instantly and then decreased gradually during the inhibition time (Fig.1). When starch was also present in the BR mixture, a sudden deep blue coloration was noticed after addition of the ascorbic acid solution. The blue color faded out gradually during the inhibition period. Nor the appearance of the brown color, neither the redox potential rise was noticed by Furrow *et al.* in the moment of ascorbic acid solution to the BR-mixture.

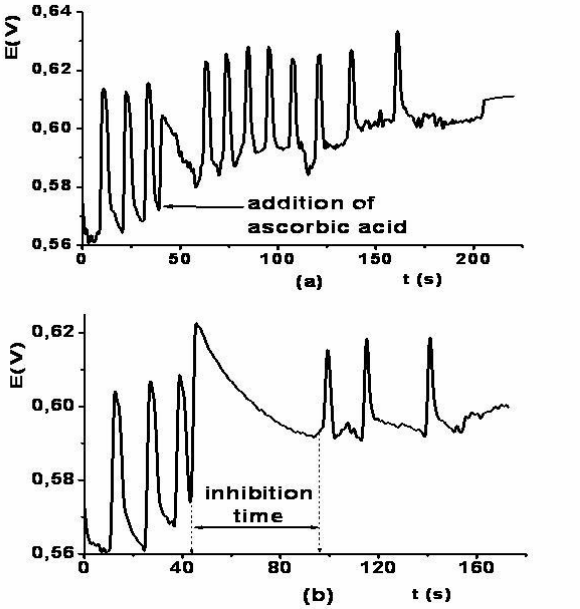

Figure 1. Effect of 3,36 mM (a) and 7,70 mM (b) ascorbic acid on the BR-reaction.

Our observation suggests that there is a rapid and significant I_3^- production when ascorbic acid is added to the BR-mixture. We attribute the sudden change of the redox potential to the fast and coupled redox reaction steps involving ascorbic acid and the oxidizing iodide species (IO_3^-, HOI, HIO_2 and I_2) of the BR-mixture. However the reaction has been monitored using a bright platinum electrode, which is reversible for every redox couple existing in the solution, the measured potential is a mixed potential (i.e. every redox system contributes to the measured potential). Therefore it is not possible to assign directly the potential change to any change of concentration of the species.

The reproducibility of the inhibition time was good. The inhibition time and the magnitude of the redox potential change (∆E) varies linearly with the ascorbic acid concentration within the 3,36−9,97 mM interval (Figure 2.).

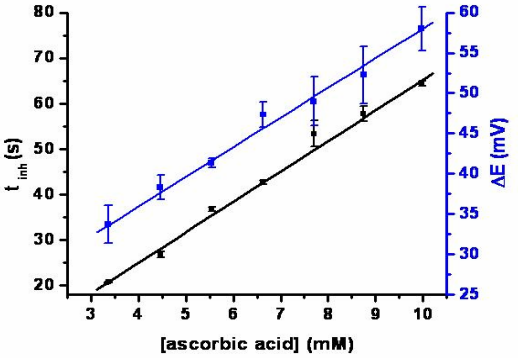

Figure 2. Plot of the inhibition time and the redox potential change against the concentration of ascorbic acid.

$$t_{inh} = (6,7\pm0,1)\cdot[ASC] - (1,8\pm0,5) \quad R^2=0,9985 \quad (1)$$
$$\Delta E = (3,7\pm0,3)\cdot[ASC] - (21,2\pm1,5) \quad R^2=0,9770 \quad (2)$$

If the ascorbic acid concentration was higher than 9,97 mM, the oscillations did not restart after a long time (more than 350 s), however the color of the mixture remained brown or blue (depending on the absence or presence of starch in the initial BR-mixture).

The features of restarted oscillations (amplitude, period) were different of those observed in the non-inhibited reactions. The amplitude of the restarted oscillations were smaller, the period length was longer and steadily increased in the successive periods. These latter observations are in accordance with those reported by Furrow *et al.* [15].

The effect of tartaric acid on the BR-reaction

Since Cervellati *et al*. has shown that the hydroxyl groups are responsible for the antioxidant effect of mono- and polyphenols [9-11], we tried to find out whether a compound containing aliphatic hydroxyl group can inhibit the BR-reaction. Also the ascorbic acid contains two aliphatic hydroxyl groups, which are not affected by the oxidation. However it would be difficult to figure out whether these hydroxyl groups have any inhibitory effect [15]. Thus, we choose tartaric acid, a simple, bi-functional compound to our study. On the other hand this compound can be found in white wines as *trans*-caffeoyl-tartaric acid. Most of the antioxidant activity of the Riesling white wine was accounted for this ester and hydroxy-cinnamic acid derivatives [16]. However in the human stomach the *trans*-caffeoil-tartaric acid is hydrolysed by the gastric juice to caffeic acid and tartaric acid. The antioxidant activity

of caffeic acid is already known from the literature [10], but there is no information about the tartaric acid. Tartaric acid contains, like ascorbic acid, two aliphatic hydroxyl groups, and it is a reducing agent at the same time.

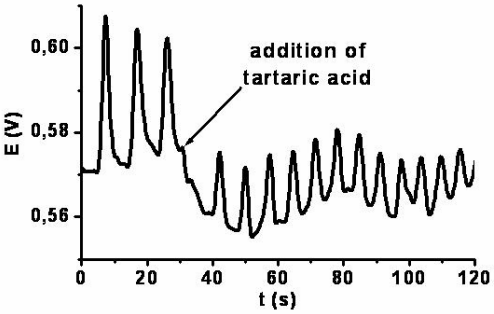

Figure 3. The effect of 10,2 mM tartaric acid on the BR-reaction.

We observed a drop of redox potential (∆E) in the moment of addition of tartaric acid, while the mixture remains colorless. The rapid change of redox potential suggests that a fast redox reaction involving tartaric acid and oxy-iodine species occurred. However compared to the experiments carried out with ascorbic acid, the main difference is that I_3^- was not observed. The more likely is that I^-, HOI or HIO_2 colorless oxy-iodine species were formed. If the concentration of these compounds exceeds a certain limit, they also perturb the oscillatory regime for a while [4, 5, 6, 15].

The inhibition time increased linearly with the concentration of the tartaric acid only within the range of 9,1-17,1 mM (Eq.3). At concentrations larger than 17,1 mM the oscillations did not restart at all.

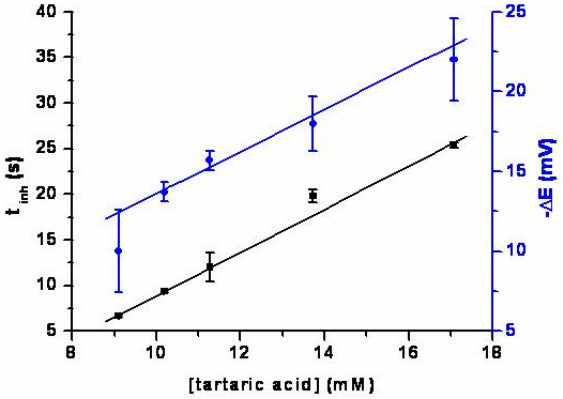

Figure 4. Plot of the inhibition time and the redox potential change against the concentration of tartaric acid.

t_{inh} = (2,4±0,1)·[tartaric acid] − (14,8±0,7) R^2=0,9972 (3)

−∆E = (1,3±0,3)·[tartaric acid] − (0,4±2,5) R^2=0,9180 (4)

The effect of pyrogallol on the BR-reaction

The third compound we studied was pyrogallol. This polyphenol can be prepared by decarboxylation of gallic acid, a naturally occurring organic acid which has an antioxidant activity. Addition of this pyrogallol to the oscillating mixture caused brown coloration and an inhibition time. No significant redox potential change has been noticed in the moment of addition of pyrogallol solution to the mixture, or during the inhibition period. The brown color faded out gradually during the inhibiton period. When starch was also present in the initial BR-mixture, no blue coloration was noted after addition of pyrogallol and/or during the inhibition period. Similarly to other polyphenolic compounds, pyrogallol appeared to be an effective inhibitor of the BR-reaction: it caused an inhibition time of 133,5 s at a concentration of 33 μM. The periods of the oscillations after the inhibition time were the same as those of non-inhibited reaction.

The pyrogallol is also a very strong reducing agent. Therefore the strong oxidants present in the BR reaction oxidized it instantly. However in this case the appearance of the brown color cannot be assigned to I_3^- production because of the following facts: pyrogallol was added to (i) acidic iodate, and (ii) acidic iodate and hydrogen peroxide mixture. In both cases a brown coloration has been observed.

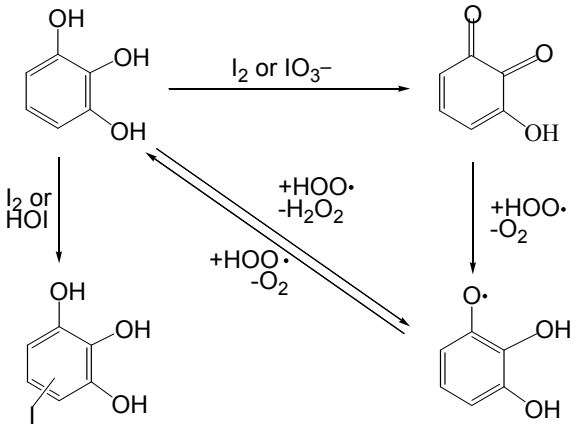

Scheme 1

This coloration did not disappear when tiosulphate solution has been added to the mixture, suggesting that the colored product was not I_3^-, the more likely an oxidized form of pyrogallol. On the other hand based on the stoechiometry, the production of I_3^- in large quantities can be excluded (i.e. the pyrogallol was added to the BR-mixture in the concentration range of several 10 μM which upon oxidation by the oxy-iodine species does not produce such large quantity of I_3^- which would cause a visible and durable coloration).

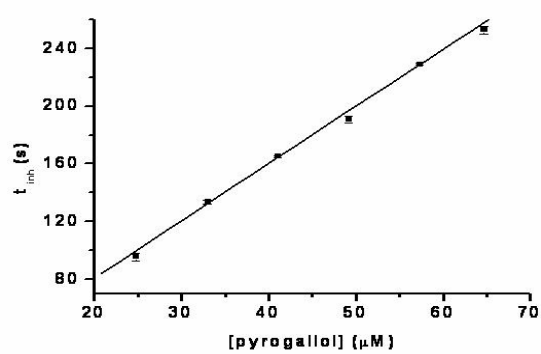

Figure 5. Plot of the inhibition time against the concentration of pyrogallol.

When pyrogallol is oxidized, the aromatic electronic structure is braked up. The product is an unsaturated cyclic di-oxo-compound with a planar structure. The hydroxyl groups in the 1 and 3 positions can not be oxidized, because after the breaking up of the aromatic ring it is not possible to reach a stable electronic structure, hence *meta*-quinones does not exist. Based on the same consideration, the simultaneous oxidation of each hydroxyl group is also impossible [11].

$$t_{inh} = (3{,}96\pm0{,}07)\cdot[\text{pyrogallol}] + (1{,}7\pm3{,}9) \quad R^2=0{,}9986 \quad (5)$$

Cervellati *et al.* pointed out that the quinone derivatives also have antioxidant activity [11]. The inhibitory effect of quinone derivatives is very complicated, and it is not yet fully unraveled. Based on thermodynamic considerations, the HOO· can reduce the quinone derivatives back to polyphenolic compounds. The inhibition time depends on the relative rates of the possible consecutive-parallel steps shown in Scheme 1.

The effect of salicylic acid on the BR-reaction

It was shown that monophenolic compounds (i.e.: 3-(4-hydroxy-3-metoxyphenyl)-prop-2-enoic acid and 4-hydroxy-3-metoxy-benzeneacetic acid) are as efficient inhibitors of the BR reaction as polyphenols [10]. We tried to inhibit the BR reaction with salicylic acid a very simple, naturally occurring monophenolic compound. In the few ten-fold μM concentration range this compound has no effect on the reaction. When we added in the BR mixture in the mM concentration range, we observed that the oscillations were not stopped at all, even at higher concentration they were not stopped immediately. However the amplitudes were progressively reduced in the successive periods. The period length was not affected by the presence of salicylic acid in concentrations lower than 6,18 mM. At 6,18 and 6,94 mM salicylic acid concentration the amplitude reduction and period lengthening was significant. At the last concentration the oscillations were completely stopped for 120 seconds, but only after a damping period of 140 seconds (Figure 6 and Table 1).

The shape of oscillations was modified in the presence of salicylic acid. The uninhibited oscillations have typically four segments [17]: a slightly decreasing segment when the iodine intermediate is consumed relatively slowly by the organic substrate and iodide ion is produced. Then a fast increase in redox potential happens because of the rapid radical steps which consume iodide ions. The slowly decreasing segment corresponds to the slow radical steps that produce iodide ions. During the fast decreasing step, iodine is produced and the color of the mixture changes into brown and then the cycle repeats. However after addition of salicylic acid the oscillations have only two segments: an increasing and a decreasing one. It is also notable that after the addition of salicylic acid the mixture remained transparent until the end of the reaction even in presence of starch, and the potential range of the oscillations decreased slightly from 745-765 to 720-740 mV.

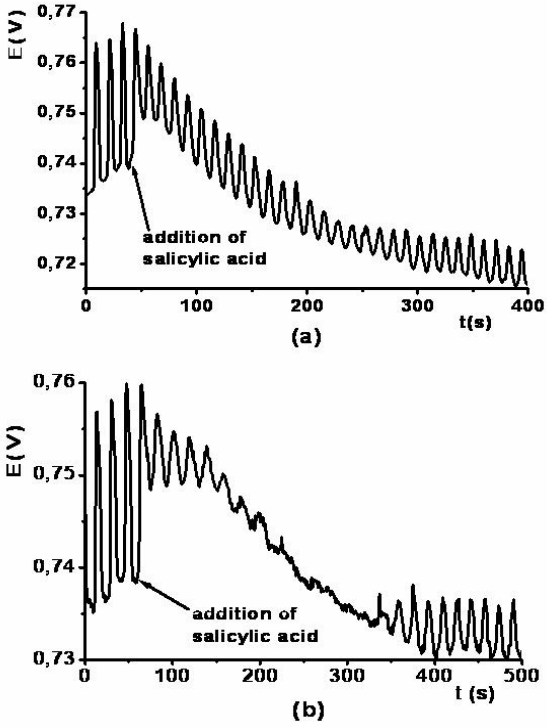

Figure 6. Effect of 5,41 mM (a) and 6,94 mM (b) salicylic acid on the BR reaction.

The unusual effect of salicylic acid constitutes a subject of further studies. By our knowledge, in the literature there is no description of this kind of damping effect of an added substance upon the BR reaction.

We found two descriptions about “spontaneous” oscillation damping phenomena (i.e. without adding a substance in the mixture) in the literature: Wittmann *et al*. used in the Belousov-Zhabotinsky reaction instead of malonic acid an oxalic acid - acetone mixture as organic substrate. They observed that after the first regular periods, the amplitudes of the following oscillations were progressively reduced. In some cases the oscillations were completely damped, and after some time they reappeared. The shape and period length of oscillations observed before and after the oscillation break were different [18].

Table 1. The effect of salicylic acid concentration on the amplitudes and the periods of the oscillations. (a) The salicylic acid solution was added after the minimum of the 3rd oscillation. (b) Completely stopped oscillations for 120 s.

Conc.	4,65 mM		5,41 mM		6,18 mM		6,94 mM	
N	Amp (mV)	p (s)	Amp (mV)	p (s)	Amp (mV)	p (s)	Amp (mV)	p (s)
1	30	13,8	29	12,8	30	13,4	27	14,6
2	31	12,6	28	11,6	31	13,4	26	14,8
3	34	13,2	30	12,2	28	15,4	28	14,8
4 [(a)]	23	13,0	18	11,6	16	17,0	11	17,8
5	17	13,0	14	11,6	11	16,4	8	19,2
6	17	13,8	14	12,0	10	18,4	6	17,6
7	18	14,0	14	12,2	11	19,2	5	20,2
8	19	13,8	14	12,2	9	17,4	5	19,8
9	19	14,0	14	12,0	10	18,4	4	19,4
10	18	13,8	14	12,6	9	17,8	3	20,2
11	20	13,8	13	12,4	11	17,8	3	12,4
12	18	13,8	12	11,6	11	18,4	0 [(b)]	120 [(b)]
13	19	14,0	12	12,6	10	17,8	2	11,8
14	18	14,2	11	12,6	12	17,4	4	15,8
15	18	14,2	9	12,2	10	18,4	7	16,8
16	17	14,6	10	12,4	9	18,4	5	17,6
17	17	13,8	8	12,4	10	17,8	6	16,4
18	14	14,8	7	12,8	7	17,4	6	16,4
19	14	14,2	5	13,8	8	18,4	5	15,6
20	14	14,6	5	11,6	7	18,0	7	15,6

Szabó studied the effect of iodate ion concentration upon the BR reaction. In BR mixtures containing 20 mM, 17,5 mM, and 15 mM iodate ion respectively; he observed a break after the first large amplitude oscillation. At 1,25 mM iodate ion concentration the damping of oscillations occurred only after the 6th period. In this case the duration of oscillation break was 50 seconds [19]. In any cases the amplitudes, the period lengths and the shape of oscillations before and after the break were different.

However it is very important to emphasize that the oscillation breaks observed by Wittmann *et al.* and Szabó should be not considered as inhibition time, because these were not caused by an added substance.

CONCLUSIONS

Among the numerous methods developed to determine the antioxidant activity, the method based on the Briggs-Rauscher oscillating reaction has a unique advantageous feature: the antioxidant reacts with hydroperoxyl radical. This radical is a reactive oxygen species which is also produced by the human body during the metabolism. Therefore the hydroperoxyl radical can be considered to be a biologically more relevant substrate, than the various organic substrates of the other methods. However the BR-method has also its own limitations due to the fact that there are strong oxidizing agents which can oxidize the antioxidant added to the mixture. Furrow *et al.* has shown that ascorbic acid is readily oxidized by these oxidizing agents, while iodide ion is produced which causes a break in the oscillations.

Our aim was to reproduce the effect of ascorbic acid on the BR-reaction and to explore the applicability of this method in case of three other compounds: tartaric acid, pyrogallol and salicylic acid. We have shown that in case of the first three compounds there is a linear relationship between the concentration and the inhibition time. One would be tempted to calculate the relative antioxidant activities based on the inhibition times, but we have shown that all these compounds act differently on the reaction; therefore such a comparison is useless. The fourth compound had the most surprising behavior: we observed a damping effect on the oscillations.

EXPERIMENTAL SECTION

Three stock solutions have been prepared with the following composition:

(A). 1,84 M H_2O_2 (Merck, p.a),
(B). 0,27 M KIO_3 (AnalytiCals, p.a), 0,1 M H_2SO_4 (Riedel de Haen, p.a)
(C). 0,2 M $CH_2(COOH)_2$ (Reachim, p.a), 0,026 M $MnSO_4$ (Reactivul, p.a).

These solutions were thermostated to 25±0,1ºC . A volume of 10,0 of A, 5,0 ml of B and 5,0 ml of C stock solution has been mixed in a double-walled glass reactor, which was thermostated to 25±0,1ºC. The composition of a reactive system was: $[CH_2(COOH)_2]_0=5\cdot10^{-2}$ M, $[H_2O_2]_0=0,92$ M, $[H_2SO_4]_0=2,5\cdot10^{-2}$ M, $[MnSO_4]_0=6,5\cdot10^{-3}$ M, $[KIO_3]_0=6,75\cdot10^{-2}$ M. A Falc-type magnetic stirrer ensured the forceful stirring of the reacting mixture. The solutions of studied compounds [ascorbic acid (Reanal, p.a), tartaric acid (2,3-dihydroxy-succinic acid, used as neutral sodium salt, Shering Kahlbaum, p.a), pyrogallol (1,2,3-trihydroxy-benzene, Laboratorium Chemiczne Gallol, p.a), salicylic acid (2-hydroxy-benzoic acid,

used as sodium salt, Reactivul, p.a)] were added with a micropipette (Labsystems Finnpipette) every time after the minimum of the third oscillation. In some cases we added 1,0 ml 1,0 w/w% starch (Reactivul, p.a) solution in the initial BR-mixture in order to visualize the variation of concentration of iodine, one of the intermediates of the reaction. Every measurement was performed at least three times. The reaction was monitored potentiometrically, employing a bright platinum and double-junction saturated calomel electrode. The potential difference between these electrodes was registered by a computer equipped with National Instruments® Data Acquisition Card. The sampling frequency of data acquisition was set to 5 s^{-1}. For data processing Origin® 6.0 program was used. The average and the standard deviation of the inhibition times were calculated. Inhibition times were plotted against the concentration of compounds, the equation of the straight lines was determined using a weighted linear regression [20].

ACKNOWLEDGMENTS

The author acknowledges the scholarship awarded by the PROFIL Group for the Cluj-Szeged Student Exchange Program to the University of Szeged, Hungary, Faculty of Natural Sciences.

REFERENCES

1. T. S. Briggs, W. C. Rauscher, *J. Chem. Ed*., **1973**, *50*, 469.
2. D. O. Cooke, *Inorg. Chim. Acta*, **1979**, *37*, 259.
3. S. D. Furrow, R. M. Noyes, *J. Am. Chem. Soc*, **1982**, *104*, 38.
4. S. D. Furrow, R. M. Noyes, *J. Am. Chem. Soc*, **1982**, *104*, 43.
5. S. D. Furrow, R. M. Noyes, *J. Am. Chem. Soc*, **1982**, *104*, 45.
6. P. De Kepper, I. R. Epstein, *J. Am. Chem. Soc*, **1982**, *104*, 49.
7. S.D.Furrow, *J. Phys. Chem.*, **1995**, *99*, 11131.
8. S. D. Furrow, R. Cervellati, G. Amadori, *J. Phys. Chem. A,* **2002**, *106*, 5841.
9. R. Cervellati, N. Crespi-Perrelino, S.D. Furrow, A. Minghetti, *Helv. Chim. Acta*, **2000**, *83*, 3179.
10. R. Cervellati, K. Höner, S. D. Furrow, C. Neddens, S. Costa, *Helv. Chim. Acta*, **2001**, *84*, 3533.
11. R. Cervellati, K. Höner, S. D. Furrow, F. Mazzanati, S. Costa, *Helv. Chim. Acta*, **2004**, *87*, 133.
12. D. Huang, B. Ou, R. L. Prior, *J. Agric. Food Chem.*, **2005**, **53**, 1841.
13. B. Halliwell, Chapter I in E. Cadenas, L. Packer (eds.), Handbook of Antioxidants, Oxidative Stress and Disease, Vol. 8, 2nd Edition, CRC Press, **2001**.

14. R. Moreau, W-J Zhang, T. M. Hagen, Chapter VII in E. Cadenas, L. Packer (eds.), Handbook of Antioxidants, Oxidative Stress and Disease, Vol. 8, 2nd Edition, CRC Press, **2001**.
15. S.D. Furrow, K. Höner, R. Cervellati, *Helv. Chim. Acta*, **2004**, *87*, 735.
16. B. Baderschneider, D. Luthria, L. Waterhouse, P. Winterhalter, *Vitis,* **1999**, *38*, 127
17. I. A. Pontos, Diploma Thesis, Babeş-Bolyai University, Faculty of Chemistry and Chemical Engineering, **1999**.
18. M. Wittmann, P. Stirling, J. Bódiss, *J. Chem. Phys. Lett.*, **1987**, *141*, 241.
19. E. Szabó, Diploma Thesis, Babeş-Bolyai University, Faculty of Chemistry and Chemical Engineering, **2000**.
20. Harvey, D., Modern Analytical Chemistry, Mc Graw Hill, **2000**, 104.

STUDIA UNIVERSITATIS BABEŞ-BOLYAI, CHEMIA, LIV, 4, 2009

PHYSICO-CHEMICAL CHARACTERIZATION OF 8YSZ NANOPARTICLES BY MODIFIED SOL-GEL METHOD

C. SUCIU[a,b], A. VIK[a], F. GOGA[b], E. DOROLTI[c], R. TETEAN[c], A.C. HOFFMANN[d]

ABSTRACT. 8 mol% Yttria Stabilized Zirconia (8YSZ) powders have been obtained by the modified sol-gel method using sucrose and pectin as organic precursors. The influence of the amounts of both sucrose and pectin were studied experimentally over a range of calcination temperatures. The obtained gels were investigated by Thermogravimetric/Differential Thermal Analysis (TG/DTA) to identify physico-chemical processes that take place during the process and to establish an optimal calcination temperature diagram. The final powders were investigated by X-ray diffraction (XRD) and Transmission Electron Microscopy (TEM) to evaluate the phase composition, the microstructure and morphology. Crystallite size and particle size of the final powders were determined using Scherrer formula and nitrogen adsorption with the Brunauer–Emmett–Teller (BET) isotherm. The results confirm that the particle properties, size and crystallite size, are strongly dependent on the calcination temperature. On the other hand, the particle properties are rather—but not completely—insensitive to (and therefore the process rather "forgiving" for) variations in the amounts of sucrose or pectin used.

Keywords: YSZ, yttria stabilized zirconia, nanoparticles, sol-gel processing, calcination temperature, organic precursors, sucrose, pectin

INTRODUCTION

The sol-gel method is emerging as a low-cost, flexible method for creating nanoparticles, and is also a promising method for creating thin layers of a controlled porosity [1], although much still remains to be known about the influence of the processing parameters on the final product. The method has been used to synthesize nano-sized particles of various materials, such as NiO, TiO_2, ZrO_2, YSZ (yttria-doped zirconia), La_2O_3, CeO_2, $BaFe_{12}O_{19}$ etc., useful for their mechanical, magnetic, ion conducting or optical properties.

[a] *CMR-PROTOTECH AS, NO-5892 Bergen, Norway, crina@prototech.no*
[b] *Universitatea Babeş-Bolyai, Facultatea de Chimie şi Inginerie Chimică, Str. Arany Janos, Nr. 11, RO-400028 Cluj-Napoca, Romania*
[c] *Universitatea Babeş-Bolyai, Faculatea de Fizică, Str. Kogălniceanu, Nr. 1, RO-400084 Cluj-Napoca, Romania*
[d] *University of Bergen, Institute of Physics and Technology, Allegaten 55, 5007 Bergen, Norway*

In what follows we mention some recent studies aimed at determining the effect of processing parameters on the properties of particles synthesized by sol-gel methods utilizing organic precursors, which are subsequently burnt off in a calcination step.

Most authors found a significant influence of the temperature used in the calcination step on the particles size. Increasing the calcination temperature leads to the formation of larger particles as measured by nitrogen adsorption and by TEM, for instance for YSZ particles [2,3]. Wang et al. [4] looked particularly closely at this issue, and found by TEM analysis that the size of La_2O_3 particles increased not only with temperature, but also with the duration of calcination.

A higher calcination temperature also leads to a higher quality of crystallization. In general, higher calcination temperatures give rise to higher and sharper peaks in XRD profiles. Zhang et al. [2] found this for YSZ, as did Laberty-Robert et al. [3]. The latter workers found diffraction peaks characteristic of a tetragonal crystal structure for calcination temperatures below 600^0C, and only a cubic structure above that temperature; they used 8% of Y_2O_3 dopant. Wang et al. [4] found some chemical transformations at lower calcination temperatures, and did not obtain the pattern characteristic for La_2O_3 until 750^0C, with the XRD diffraction pattern becoming much clearer with sharper peaks at 850^0C. Lian et al. [5] prepared a mixture of NiO and doped CeO_2 particles for use in anodes in SOFCs. They also found that the particles are sintering further after their autocombustion manufacturing process. Related to the higher and sharper XRD peaks is the fact that the Scherrer formula indicates larger crystallites for higher calcination temperatures for various types of particles and manufacturing processes [2,5,6]. Jung et al. [7] found that the photoluminescence intensity of their titania particles was enhanced and that the peak position in the photoluminescence spectrum moved to smaller wavelengths, as the calcination temperature was raised. This was all attributed to a progressively more ordered crystalline structure.

Widoniak et al. [8] carried out a special study in this respect. They produced larger TiO_2 and ZrO_2 particles by aggregation of nanoparticles. These particles were sometimes made porous by the judicious addition of different types of salts and polymers to the reaction mixtures. They found crystallite sizes much smaller than their particle sizes, and also much higher specific areas (up to 300 m^3/g) than the particle size would indicate.

Laberty-Robert et al. [9] studied the influence of the precursor ratios for Pechini synthesis of YSZ particles. They did not find a strong variation in the particle properties when varying the ratios citric acid/ethylene glycol or citric acid/transition metal, although they did find large differences in the viscosity of the gels. They attempted to control the particle size by adding surfactant to the reaction mixture to obtain a colloidal suspension, and found decreasing particle size with increasing surfactant concentration. For their strongly agglomerated particles, the BET surface was less than expected from the particle size, as determined by electron microscopy.

Many investigations [2,4,5,6,8] also include thermal analyses of the polymeric gel as it is being heated in a controlled temperature calcination process. In general, it is possible to recognize endothermic processes corresponding to dewatering and exothermic processes corresponding to combustion of organic material. Also exothermic processes corresponding to solid solutions or crystallographic changes can also be observed.

The objective of this work was to use the new modified sol-gel method, with sucrose and pectin as organic precursors, in order to obtain 8YSZ nanoparticles. The effect of the mass ratio between sucrose and pectin on the obtained powders was investigated at a larger domain compared with our previously work [10]. The obtained powders were calcinated at different temperatures and different thermal treatments (see below) to study the influence of the calcination process.

RESULTS AND DISCUSSION

The TA analysis for the A set (Figure 1) revealed an endothermic process at 200^{0}C (for A1) and 180^{0}C (for A4), visible on the DTA curve with a slight mass loss due to water elimination, followed by a large exothermic process visible extended up to 940^{0}C. Oxidation of the organic compound and formation of cubic zirconia stabilized with yttria take place in this large temperature interval and they may overlap.

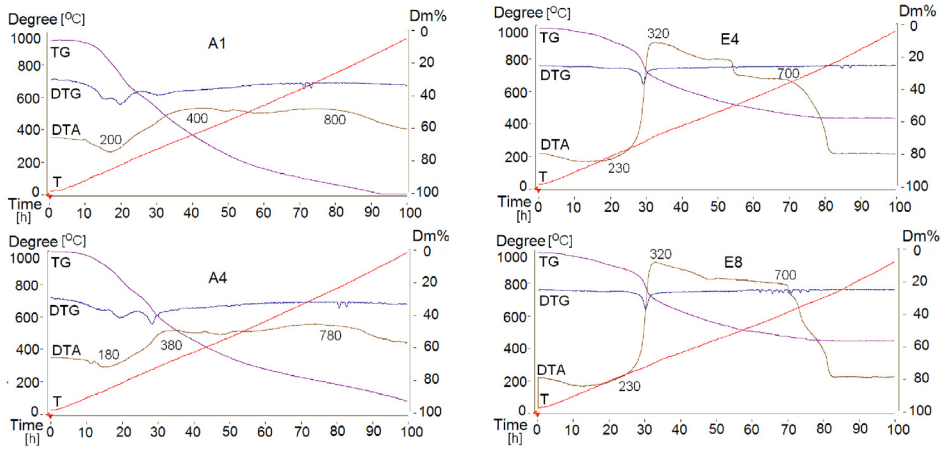

Figure 1. The thermal analysis of the dried gels.

These processes are distinguishable on the DTA curve through the two maxima at 400^{0}C and 780^{0}C (for A1) and at 380^{0}C and 800^{0}C (for A4), respectively. Loss of mass takes place along the whole temperature range from 100 to 940^{0}C, due to the elimination of water vapor and gaseous reaction products, and goes up to 98%.

Turning now to the E set shown in Figure 1, an exothermic peak of high intensity can be observed on the DTA curve. This starts at 230^{0}C and continues up to 840^{0}C. The curves present a maximum at 320^{0}C which corresponds to the oxidation of the organic components followed by a second maximum at around 700^{0}C due to the formation of cubic zirconia. A slight mass loss can be noticed under 200^{0}C on the TG curve due to water elimination. The rate of this process was very low so that no endothermic peak can be distinguished on the DTA curve. The mass loss increased between 230 and 700^{0}C. Overall, a 58% mass loss was determined.

Comparing the two sample sets the following remarks can be made:

– the exothermic effect corresponding to the oxidation of the organic compound was much more intense for the E set, due to the larger amount of organic compound present;

– the total mass variation was higher for the A set (98%) compared to the E set (58%), likely due to the higher water retention in the A set. Also, the gas elimination was slower along the whole temperature interval;

– the strong endothermic process in the A samples under 200^{0}C shows that more residual water was present in these samples. Thus the procedure of obtaining the A set yielded gels which retained water and gasses more strongly, and their elimination was more difficult and required higher temperatures;

– the exothermic effect corresponding to the formation of cubic zirconia was much more intense for the E set and ended at 840^{0}C. In the A set this process was much less intense, and persisted up to higher temperatures (940^{0}C). This shows that the crystallization process into cubic zirconia had a lower rate for the A set.

The obtained BET values of the specific surface area (S), the pore volumes (V_P) and the BJH pore diameter (r_p) for all the samples, at different sintered temperatures, are shown in the Figure 2.

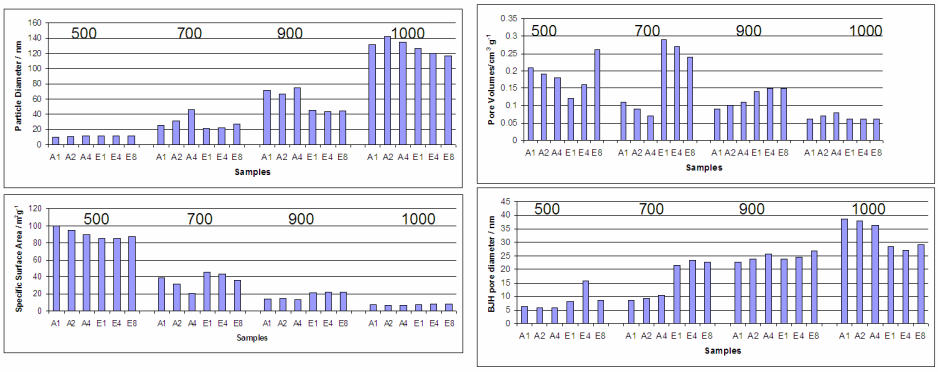

Figure 2. Specific surface area, pore volumes, BJH pore diameter and nanoparticles diameter at different temperatures.

Assuming that the particles are round and the theoretical density (ρ) of 8mol% YSZ is 6100 kg/m^3 [12], the equivalent grain size (D) corresponding to the obtained specific surface areas (S) were calculated following equation: $D=6/(\rho \cdot S)$.

Specific surface area decreased with the increasing of the calcination temperature. For example, the samples calcined at 500^0C have the highest specific surface area. However, upon calcination at 1000^0C, the specific surface area of the samples is reduced. This seems to be mostly due to the reduction in bulk porosity of the compound. On the other hand it is somewhat insensitive to the amount - and the proportions - of the organic precursors used. The highest specific area of 99.9 m^2/g was obtained at 500^0C and the values decreased with increasing temperature down to 6.9 m^2/g at 1000^0C.

The mean particle diameter decreased by increasing the temperature and by decreasing specific surface area. The values of the mean particle sizes vary from ~10 nm (500^0C) to ~150 nm (1000^0C). In the same way, the BJH pore diameters increased by increasing the temperature showing the presence of mesopores (smaller that 40 nm) even for the samples calcined at high temperatures.

Specific pore volume is calculated as the sum of volumes of all pores in one gram of adsorbent. We have to emphasise that for our samples, only internal volume inside the adsorbent particles was counted. At low calcination temperatures (500-700^0C), the obtained powders exhibit an increased pore volume, while, as the calcination temperatures increase (900-1000^0C), the pore volume decreased. This is mainly due to the longer thermal process, which allows the particles to grow in dimension and the pores to close.

The XRD data from all the samples show the presence of only one single phase, solid solution of ZrO_2 with Y_2O_3. The pattern no. 49-1468 corresponds to Yttrium Zirconium Oxide - $Y_{0.15}Zr_{0.85}O_{1.93}$–$92ZrO_28Y_2O_3$. The presences of other phases were not observed. Based on the phases identified in the XRD patterns, it can be concluded that a homogeneous solid solution of ZrO_2 with Y_2O_3, necessary to form cubic zirconia, was formed (Figure 3). The XRD of the mixtures treated at low temperature (500^0C) show a significant difference between the E and the A sets due to the mass ratio of sucrose:pectin used in the experiments. The spectra of the E set, obtained with a smaller amount of pectin, are sharper with relatively less noise, due to a better crystallization. At higher temperatures (700-1000^0C) the differences between the shapes of the peaks are less noticeable.

The FWHM and the 2θ values of the first four peaks were used to calculate the crystallite sizes of the obtained powders at different temperatures using the Scherrer formula [13]. In Figure 4 the mean crystallite size for all samples at each temperature in the studied interval are shown. The mean crystallite sizes varied between ~6 and 37 nm showing that the method is effective to synthesize nanosized powders.

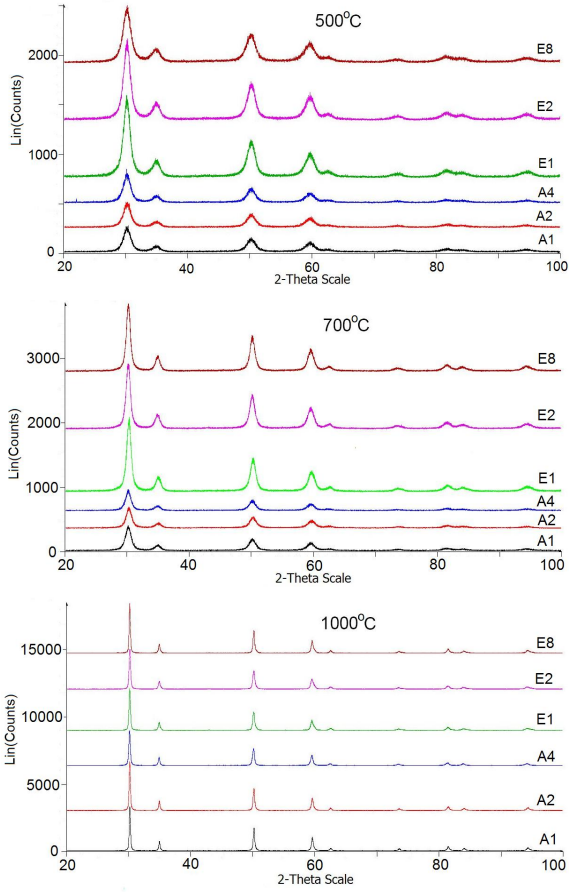

Figure 3. The X-ray diffraction spectra size of the samples calcined at 500, 700, and 1000^{0}C.

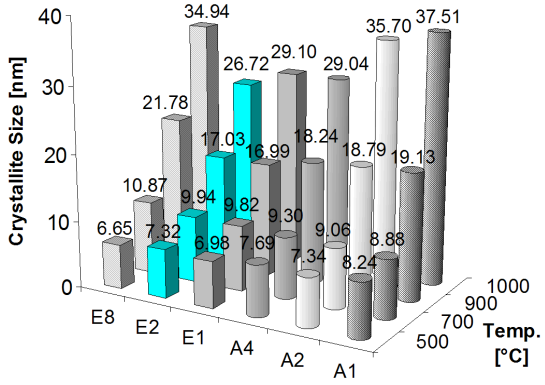

Figure 4. The mean crystallite size of the samples determined by XRD.

A comparison of particle size evaluated from XRD analysis and specific surface area measurements shows that the particles are less agglomerated at low temperatures. The mean particles and agglomerates sizes increase by increasing the calcination temperature. In addition, it can be seen that the specific surface area of the calcined powders regularly decreases when the calcination temperature goes up and the crystallite size of the powders increases. This strengthens the tendency of the particles to form a dense structure in the agglomerate and hence the specific surface area decreases. The calcination temperature and the duration of calcination affect both crystallite size and specific surface area of the powders. The results are comparable with the results obtained by other researchers [2,3,4,9]. Also, the calculated mean crystallites size is smaller than the calculated mean particles size, which is similar to the results obtained by Widoniak et al. [8].

The TEM images confirm the presence in powders of the agglomerates at high temperatures. At 500^{0}C the nanoparticles are relatively regular, rounded shapes, less agglomerated with a narrow size distribution (Figure 6).

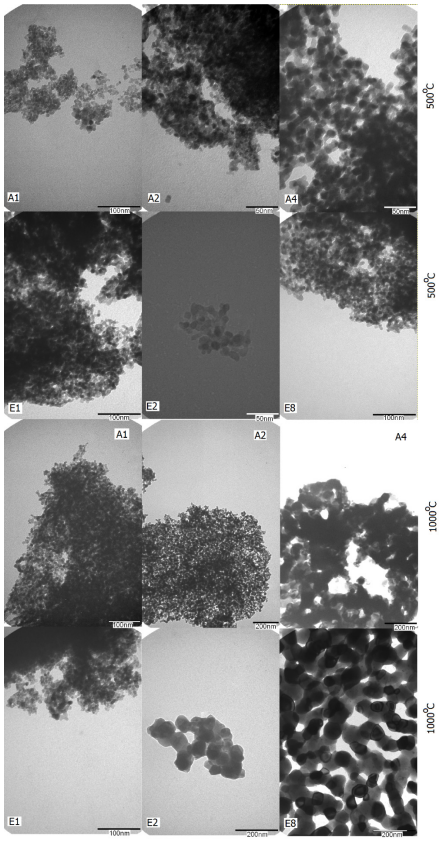

Figure 5. TEM images for the samples calcined at 500 and 1000^{0}C.

The mean particle size of the samples calcined at 500^0C is between 9 and 14 nm. The powder calcined at 1000^0C showed a partial sintering of the primary crystallites. This result is also observed during the synthesis of YSZ by a combustion process [14] or by a modified Pechini method [15], while the particle size measured for the samples calcined at 1000^0C is between 10 and 60 nm.

As it can be observed from the XRD measurements, the obtained crystallite sizes (6 nm at 500^0C and 37nm at 1000^0C, respectively) are smaller than the mean particle size obtained from the specific surface area measurements (10 nm at 500^0C and 150 nm at 1000^0C). The obtained mean particle sizes from the TEM micrographs (10 nm at 500^0C and 60 nm at 1000^0C, respectively) are more close to the crystallite sizes determined from the XRD. Similar results were found in [8], where the crystallites sizes are much smaller than the particles size and also much higher specific areas than the particle sizes due to the nanoparticles aggregation.

CONCLUSIONS

The influence of the process parameters on the properties of nanoparticles produced with a new sol-gel process using sucrose and pectin in place of conventional organic precursors has been investigated. Compared with the conventional sol-gel method, this method also allows the production of 8mol% YSZ powders at a relatively low temperature with good stoichiometric control, high quality of the produced nanoparticles and high degree of crystallization. The obtained powders using different mass ratio of sucrose and pectin and different calcination temperatures are comparable with the powders obtained through other sol-gel methods using different organic precursors. Comparisons can be made from different points of view, e.g. behavior under calcination; crystallite and particle size; specific surface areas and total pore volume.

High specific surface areas, up to ~100 m^2/g, were obtained by the modified sol-gel method and the calculated particle sizes correspond to 10 nm. The specific surface area is inversely proportional to particle diameter. Pore volumes, specific surface area, mean pore diameter and BJH pore diameter are correlated to each other.

The E set, was found to yield cubic yttria stabilized zirconia with a larger crystallite size as indicated by less noise and smaller peak width at low temperatures (500^0C). The calcination temperature was responsible for the higher crystallization quality observable from the XRD measurement (higher and sharper peaks). C. Laberty-Robert et al. [3] obtained tetragonal 8YSZ at temperatures below 600^0C and they also concluded that the calcination temperature influence the crystallization degree of the powders.

The estimated particle size showed a slightly decreasing trend with the decrease in the sucrose/pectin mass ratio concentration though the preparation condition was identical for all the samples. C. Laberty-Robert et al. [9] found

also that the organic precursor ratio (citric acid and ethylene glycol) and the ratio between the citric acid and metal ions does not influence much the particle sizes of the final powders. Additional studies to investigate the viscosity of the gels are required. The possibility of controlling the particle sizes by adding different surfactants to the initial solutions to obtain a colloidal suspension might also be worth of investigating.

EXPERIMENTAL SECTION

Preparation techniques

$ZrCl_4$ (Sigma-Aldrich, technical purity) and $Y(NO_3)_3 \cdot 6H_2O$ (Sigma-Aldrich, 99.9% purity) were used as raw materials at the molar ratios required to obtain 8YSZ (ZrO_2 doped with 8 mol% Y_2O_3). Two sets of samples labeled A and E, containing the sucrose/pectin mass ratios shown in Table 1 were used in order to study the effect of the amounts and proportions of the organic precursors on the process and the product particles.

Table 1. Sucrose/Pectin mass ratio used in experiments.

	A1	A2	A4	E1	E2	E8
Sucrose	100	100	100	100	100	100
Pectin	2	4	8	0.25	0.5	0.75

The flow chart for the synthesis of the 8YSZ compound powders is shown in Scheme 1. Aqueous solutions of the two salts were stirred on a warming plate at 90–100^{0}C in order to mix the solution uniformly. The sucrose/pectin solution was added gradually into the aqueous solutions under stirring until transparent colloidal suspensions were obtained. The transparent sol continuously transformed into wet gel and then into dried gel under heating. Finally, the obtained gels were calcined at different temperatures: 500, 700 and 1000^{0}C to form white 8 mol% YSZ compound nanoparticles. Each gel sample was calcined, in air, at a heating rate of 100^{0}C/h. The calcination temperature diagram, was designed in accordance with the results of the TG/TDA experiments discussed above The plateaus were as follows:

– 500◦C: 1 hr at 200^{0}C, 2 hrs at 400^{0}C and 6 hrs at 500^{0}C
– 700◦C: 1 hr at 200^{0}C, 2 hrs at 400^{0}C and 4 hrs at 700^{0}C
– 900◦C: 1 hr at 200^{0}C, 2 hrs at 400^{0}C, 3 hrs at 600^{0}C and 3 hrs at 900^{0}C
– 1000◦C: 1 hr at 200^{0}C, 2 hrs at 400^{0}C, 3 hrs at 600^{0}C and 2 hrs at 1000^{0}C.

This mechanism, and the role played by sucrose and pectin in the formation of YSZ powders, is discussed in more detail in reference [10]. The addition of sucrose and pectin to the solution of the metal cations forms a polymer matrix in which the Zr^{4+} and Y^{3+} cations are distributed through the polymeric network structure. Sucrose, which is always in excess, acts as a strong chelating

agent and as a pattern material. The sucrose solution contains NO^{3-} ions, which helps to hydrolyze the sucrose molecule into glucose and fructose, and afterwards oxidized to gluconic acid (GA) or polyhydroxyl acid. GA contains carboxilyc acid groups and hydroxyl groups which can participate in the complexation of metal ions and may form branched polymer with pectin. Pectin chains form long layers and sucrose molecules may bind between this layers. In the present process, metallic ions are bound by the sucrose molecule and the resulting complex molecule is trapped between pectin layers. During calcination this polymeric metal ion complex is decomposed into CO_2 and H_2O and a large amount of heat is generated preventing agglomeration by ensuring that the mixture remains porous.

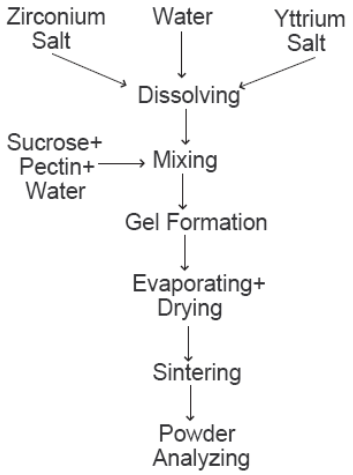

Scheme 1. Flow chart for 8YSZ preparation technique.

Analysis techniques

Thermo-gravimetry and differential thermal analysis (TG/DTA) curves were recoreded with a thermal analyzer Derivatograph Q 1500 (MOM Hungary) up to 1000^0C, in air, at a heating rate of 10^0C/min, using Al_2O_3 as reference. Apart from giving information about the physical and chemical processes taking place during calcination, the TA analyses were used for determining the optimal calcination temperature scheme (the levels and durations of the temperature plateaus described above) to allow the processes, such as dewatering, zirconia formation and solid solution formation to go to completion before proceeding with raising the temperature.

The BET specific surface area SBET and pore volume (V_P) distribution were measured by nitrogen physisorbtion using an Gemini 2380 analyzer from Micromeritics Co.Ltd. The pore size distribution was calculated from the

adsorbtion branch of the isotherms, based on the BJH method. The BJH pore diameter (r_p) was calculated as $4V_p/S_{BJH}$ [11]. All the final powders were degassed at 200^0C for 3h under vacuum before analysis.

X-ray diffraction patterns were generated using a Brucker D-8 Advance X-ray diffractometer with CuKα1 radiation in the 2θ range of 20-100 Å. The crystallite sizes were calculated from the XRD spectra using the Scherrer formula $D = \lambda/(\beta \cos\theta)$, where D is the crystallite size, λ is the wavelength (0.15406 nm), β is the Full Width at Half Maximum (FWHM) and θ is the diffraction angle.

The morphologies of the powders were examined by TEM (transmission electron microscopy) using a JEOL-JEM-1011 transmission microscope. From the samples dispersed in water under stirring, one drop was taken and deposited on a copper grid (Agar G2400C, 400 Square Mesh, copper 3.05mm). The grids were previously covered with an organic layer of Formvar powder (Agar Scientific LTD, Essex) dissolved in chloroform followed by carbon deposition process under vacuum (Agar Turbo carbon coater, Model 208C) and a glow discharge.

ACKNOWLEDGMENTS

This work was funded by the NFR (Norwegian Research Council) and Prototech A.S., Bergen, Norway made laboratory facilities available. Also, the authors are acknowledging the Laboratory for Electron Microscopy, University of Bergen, Norway for helping with all the micrographs.

REFERENCES

1. C.J. Brinker, G.W. Scherer, Sol-gel science: the physics and chemistry of sol-gel processing, Academic Press, New York, **1990**.
2. Y. Zhang, A. Li, Z. Yan, G.Xy, C. Liao, C. Yan, *Journal of Solid State Chemistry*, **2003**, *171*, 434.
3. C. Laberty-Robert, F. Ansart, C. Deloget, M. Gaudon, A. Rousset, *Materials Research Bulletin,* **2001**, *36*, 2083.
4. X. Wang, M. Wang, H. Song, B. Ding, *Materials Letters*, **2006**, *60*, *2261.*
5. J.S. Lian, X.Y. Zhang, H.P. Zhang, Z.H. Zhang, J. Zhang, *Materials Letters* **2004**, *58*, 1183.
6. A. Mali, A. Ataie, *Ceramics International,* **2004**, *30,* 1979.
7. K.Y. Jung, S. B. Park, M. Anpo, *Journal of Photochemistry and Photobiology A: Chemistry,* **2005**, *170,* 247.
8. J. Widoniak, S. Eiden-Assmann, G. Maret, C*olloids and Surfaces A: Physicochem. Eng. Aspects,* **2005**, *270–271,* 329.

9. C. Laberty-Robert, F. Ansart, S. Castillo, G. Richard, *Solid State Sciences,* **2002**, *4*, 1053.
10. C. Suciu, A.C. Hoffmann, A. Vik, F. Goga, *Chemical Engineering Journal,* **2008***,138*, 608.
11. E.P. Barrett, L.G. Joyner, P.H. Halenda, *Journal of the American Chemical Society,* **1951**, *73*, 373.
12. M. El-sayed Ali, Omar A. Abdelal, Ahmed A. Hassan, *Solid State Ionics*, **2007**, *178*, 1463.
13. H.M. Rietveld, *Journal of Applied Crystallography*, **1969**, *2*, 65.
14. K.R. Venkatachari, D. Huang, S.P. Ostrander, W.A. Sculze, G.C. Stangle, *Journal of Materials Research*, **1995**, *10*, 748.
15. C.L. Robert, F. Ansart, C. Deloget, M. Gaudon, A. Rousset, *Ceramics International,* **2003**, *29*, 151.

STUDIA UNIVERSITATIS BABEŞ-BOLYAI, CHEMIA, LIV, 4, 2009

USE AQUEOUS PEG-INORGANIC SALT TWO-PHASE SYSTEMS FOR Bi(III) EXTRACTION IN THE PRESENCE OF INORGANIC EXTRACTANTS

LAURA BULGARIU[a] AND DUMITRU BULGARIU[b, c]

ABSTRACT. The Bi(III) extraction behaviour was studied in aqueous polyethylene glycol (PEG) – $(NH_4)_2SO_4$ two-phase system, using inorganic anions (I^-, Br^-, Cl^- and SCN^-), as extractants. The aqueous two-phase systems were prepared using aqueous solutions of phase-forming components (PEG and $(NH_4)_2SO_4$) in water or in 1N H_2SO_4. The experimental results show that more adequate for Bi(III) extraction is the aqueous two-phase systems, where the aqueous solutions of phase-forming components are prepared in 1N H_2SO_4. Under these conditions, the addition of inorganic extractants determined the partitioning of Bi(III) into PEG-rich phase, easy observable at extractants concentration higher than 0.06 mol/dm^3. The efficiency of extractants follows the order: $I^- >> Br^- > Cl^- >> SCN^-$. Using the Bi(III) distribution coefficients calculated as a function of inorganic extractants concentration, the extracted species were assumed.

Keywords: aqueous PEG-based two-phase system, Bi(III) extraction, inorganic extractants

INTRODUCTION

Various conventional liquid-liquid extraction methods have been proposed for the recovery of bismuth ions, through years [1]. Its utilization at the manufacture of semiconductors, alloys and metallurgical additives, etc., are few cases where the solvent extraction can be used in order to solve environmental problems [2]. Several solvent extractions systems are mentioned for the extraction of bismuth as neutral complexes or ion-pairs, using different organic extractants [3-5]. But, the utilization of conventional extraction methods requires large volumes of organic solvents, which may cause environmental pollution, and thus are not appreciated.

[a] *Universitatea Tehnică "Gheorghe Asachi" din Iaşi, Facultatea de Inginerie Chimică şi Protecția Mediului, Bd-ul D. Mangeron, Nr. 71A, RO-700050 Iaşi, România, lbulg@ch.tuiasi.ro*

[b] *Universitatea "Al. I. Cuza" din Iaşi, Facultatea de Geografie şi Geologie, Bd-ul Carol I, Nr. 20 A, RO-700506 Iaşi, România, dbulgariu@yahoo.com*

[c] *Academia Română, Filiala din Iaşi, Colectivul de Geografie, Bd-ul Carol I, Nr. 18, RO-700506, Iaşi, România*

In recent years, the aqueous PEG-based two-phase systems have been suggested for several applications in metal ion recovery, particularly those formed by polyethylene glycol (PEG) and inorganic salts, as an alternative to the conventional extraction systems. These systems are formed by mixing an aqueous solution of PEG with an aqueous solution of certain inorganic salt (for example: $(NH_4)_2SO_4$, Na_2SO_4, K_2HPO_4, etc.) [6-8] and are composed by two immiscible phases, a superior one – rich in PEG, which has the role of organic phases from conventional extraction systems, and an inferior one – rich in inorganic salt. One of the main advantages of these systems is that the metal species partitioning occurs between two aqueous phases, which is an evident environmental benefit. In addition, the aqueous PEG- inorganic salt two-phase systems permit the utilization of cheaper inorganic anions (such as halide and pseudo-halide ions) as extractants, for the efficient extraction of several soft metal ions. For example, Cu(II), Co(II), Zn(II) and Fe(III) are extracted in presence of SCN^- ions at high acidity of salt stock solution [9-11]. Also, iodide ions can be successfully used for the quantitative extraction of Cd(II) and Hg(II) [12-15].

All these metal ions forms in presence of halide and pseudo-halide ions, anionic complexes and their extraction efficiency is mainly determined both by the properties of chemical species formed in extraction system (stability, hydration degree, electric charge), and by the characteristics of aqueous two-phase systems (nature and concentration of inorganic salt, molecular mass and concentration of PEG, acidity of phase-forming component solutions) [16, 17].

Starting from these observations, we believe that such aqueous PEG-inorganic salt two-phase systems can be used for efficient extraction of Bi(III) in presence of inorganic anions, as extractants. In the case of Bi(III), the stability of its chemical species with inorganic anions, such as I^-, Br^-, Cl^- and SCN^-, increases from SCN^- to I^-, and increase with the increasing of the inorganic anions number from molecule, following the order: $BiX^{2+} < BiX_2^+ < BiX_3 < BiX_4^- < BiX_5^{2-} < BiX_6^{3-}$ [18]. Under these conditions, at high acidity of phase-forming components solutions, a quantitative extraction of Bi(III) is expected to be obtained, and the extraction species should have a maximum number of inorganic anions (most probable 6) associated to metal ion.

In this study we have investigated the extraction behaviour of Bi(III) in aqueous PEG(1500) – $(NH_4)_2SO_4$, in order to establish the optimum experimental conditions for its efficient extraction. The experimental parameters considered in this study have been: initial concentration of metal ions, the type and concentration of inorganic extractants (I^-, Br^-, Cl^- and SCN^-) and the acidity of phase-forming components solutions. The aqueous two-phase systems were prepared using aqueous solutions of PEG and $(NH_4)_2SO_4$ in water and in 1 N H_2SO_4. The differences between these two ways of aqueous two-phase systems preparation have been evidenced using IR spectra of solidified PEG-rich phases. The extracted species were assumed on the basis of experimental distribution coefficients calculated in function of inorganic extractants concentration.

RESULTS AND DISCUSSION

The optimum conditions for Bi(III) extraction were established by varying several experimental parameters, such as: the pH of phase-forming components stock solutions, Bi(III) initial concentration, type and concentration of inorganic extractants.

In the study of Bi(III) extraction in aqueous PEG(1500) – $(NH_4)_2SO_4$ two-phase system, a first experimental parameter which should considered is the acidity of phase-forming components stock solutions. According with the distribution diagram of bismuth species [19], in aqueous solutions the free Bi^{3+} ions are present only in 0 – 0.8 pH range. Over this value the predominant species are BiO^+, which are more stable [18], but have a lower reactivity towards halide and pseudo-halide extractants, in comparison with Bi^{3+} ions.

On the basis of these observations, the influence of salt stock solution acidity on bismuth extraction in presence of 0.10 mol/dm^3 iodide extractants, have been studied in 0.20 – 3.50 pH range. The experimental results (Figure 1) indicate that the extraction efficiency increase with the increasing of salt stock solution acidity, but the maximum value of extraction percent is not higher than 50 %, even the salt stock solution pH is close to 0.

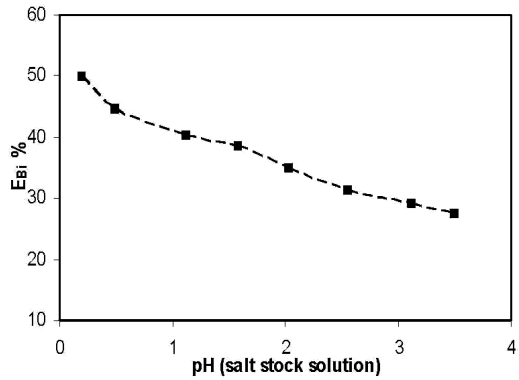

Figure 1. E_{Bi}% vs. salt stock solution pH. (Bi_i = 62.75 μg/cm^3, $[I^-]_{add}$ = 0.10 mol/dm^3; temperature = 24 °C).

This is due to the fact that the 40% (w/w) PEG aqueous stock solution has a higher pH value (6.2), and from this reason at interface, the apparition of a yellow precipitate can be observed, and the extraction process is stopped.

For to eliminated this inconvenient, both PEG and $(NH_4)_2SO_4$ stock solutions have been prepared using 1N H_2SO_4, instead of water. Under these conditions, in extraction systems bismuth is predominant as Bi^{3+} in both phases, and in presence of 0.10 mol I^-/dm^3, the obtained value of extraction percent is 99.65%. Thus, the extraction process could be considered a quantitative one, and this system was used for further Bi(III) extraction experiments.

But, the utilization of phase-forming components prepared in 1N H_2SO_4 instead of water, will change the characteristics of obtained aqueous two-phase system. For to underline the differences between the aqueous two-phase systems prepared using water and 1N H_2SO_4, the IR spectra of polymer-rich phases have been recorded.

In Figures 2 and 3 are presented the IR spectra obtained for solidified 40% (w/w) PEG(1500) solution (PEG) and blank PEG-rich phases (M), in water and 1N H_2SO_4.

It can be observed that the most significant changes are in the spectral region where appears the O–H stretching for water molecules hydrogen bonded by polymer chains [20, 21].

Thus, in the case of PEG solution in water, the large and splitter band from 3550-3238 cm^{-1} from PEG 1 spectra (Figure 2) is more attenuated in the spectra of blank PEG-rich phase (M 1) and moved to low wave number (3296 cm^{-1}). This is due to the fact that at the contact of PEG solution in water and salt stock solution with high acidity (in this case $(NH_4)_2SO_4$ solution with pH= 0.5), the dehydration of polymer chains occurs and the obtained PEG-rich phases are more hydrophobic [21]. This characteristic, plays an important role in extraction process of metal ions with inorganic extractants, and can be directly correlated with the number of extractants from extracted species molecules [10, 12, 14].

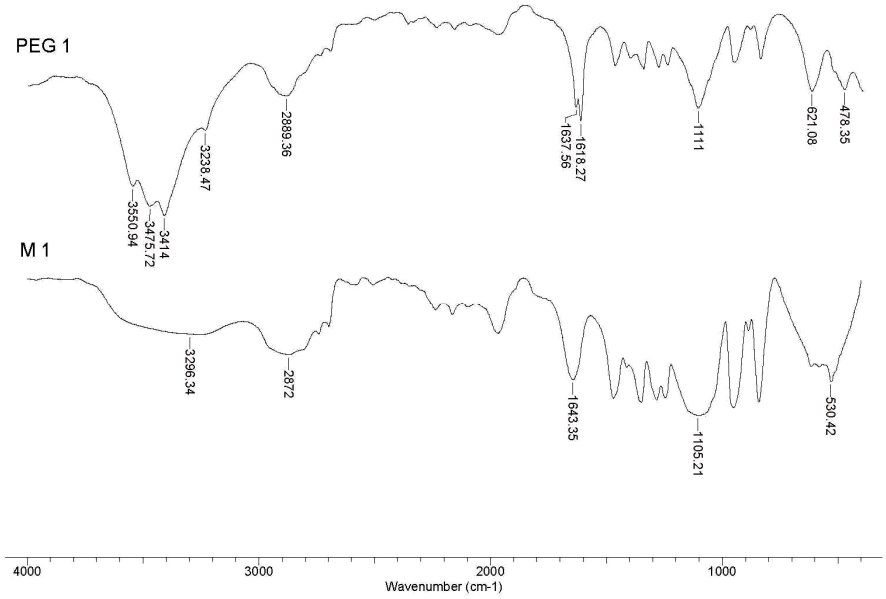

Figure 2. The IR spectra of solidified 40% (w/w) polyethylene glycol solution (PEG 1) and blank phase (M 1), in water.

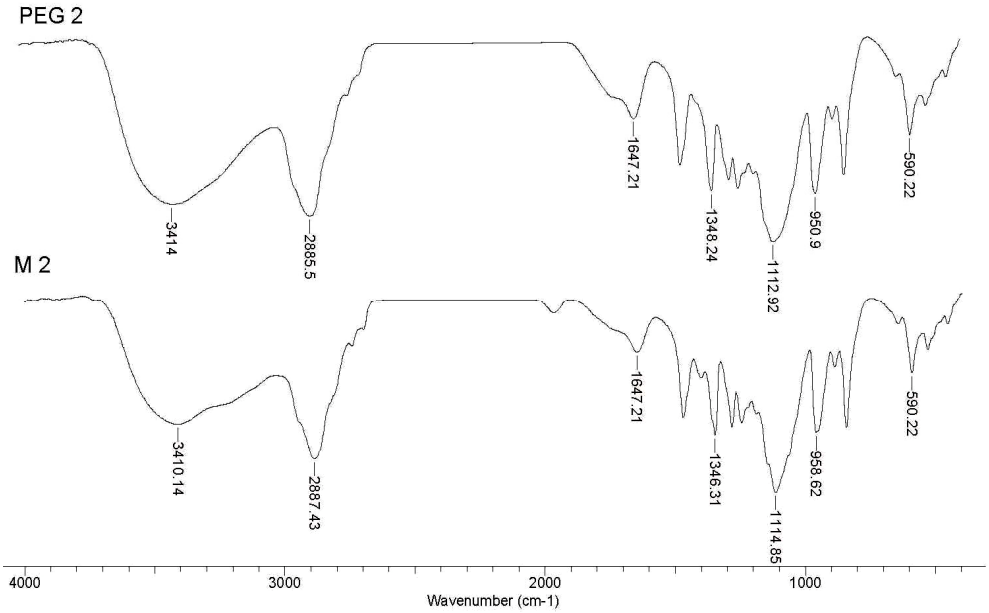

Figure 3. The IR spectra of solidified 40% (w/w) polyethylene glycol solution (PEG 2) and blank phase (M 2), in 1N H_2SO_4.

In case of PEG solution prepared in 1N H_2SO_4 (Figure 3), the maximum absorption band of water molecules is situated at 3414 cm^{-1} in solidified PEG solution (PEG 2) and remains almost unchanged after the formation of aqueous two-phase system (M 2). Thus, by using PEG solution prepared in 1N H_2SO_4, the dehydration degree of polymer chains is not significant changed after aqueous two-phase system formation, and the obtained PEG-rich phases have a lower hydrophobicity. In these conditions, is expected that in the extracted species molecules, the number of extractants associated to metal ion to be lower than maximum (6 in case of Bi(III)).

The influence of Bi(III) initial concentration was studied in the metal concentration range between 21 and 74 $\mu g/cm^3$. At it can seen from Figure 4, the Bi(III) concentration extracted into PEG-rich phase at constant concentration of iodide extractant (0.10 mol/dm^3) in considered aqueous two-phase system, increase with the increasing of initial concentration of metal ion.

On the basis of this observation and considering the limits of spectrophotometrically method used for Bi(III) analysis, in further distribution studies, an initial concentration of 62.75 $\mu g/dm^3$ was selected.

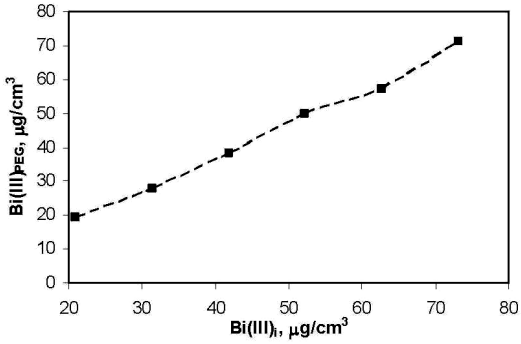

Figure 4. The influence of initial metal ion concentration on bismuth extraction in presence of iodide extractants, in considered aqueous two-phase system. ($[I^-]_{add}$ = 0.10 mol/dm^3; temperature = 24 °C).

The Bi(III) extraction behaviour was also investigated in function of type and concentration of inorganic extractants (I^-, Br^-, Cl^- and SCN^-) added in aqueous two-phase system. Comparatively, the variation of extraction parameters (D_{Bi} and E_{Bi} %) in function of NH_4X concentration added in extraction system are given in Figures 5a and 5b. An increasing of Bi(III) extraction into PEG-rich phase with increasing of inorganic extractants concentration was observed, for all cases. The values of extraction parameters follow the order: I^- >> Br^- > Cl^- >> SCN^-, which is in agreement with the results presented in other studies from literature [22, 23]. As it can seen from Figures 5a and 5b, the Bi(III) extraction parameters have higher values for I^- than Br^-, those for Br^- increase at lower concentrations that for Cl^-, and all of them are higher than the values of extraction parameters obtained in the case of SCN^-. This order could be explained by the increasing of bismuth extracted species stability from SCN^- to I^- [18]. The softness and most polarizable iodide ions have the smallest hydration Gibbs energy (ΔGhydr. = - 220 kJ mol^{-1}) [24] and form stronger complexes with bismuth, which are easy extracted into PEG-rich phase.

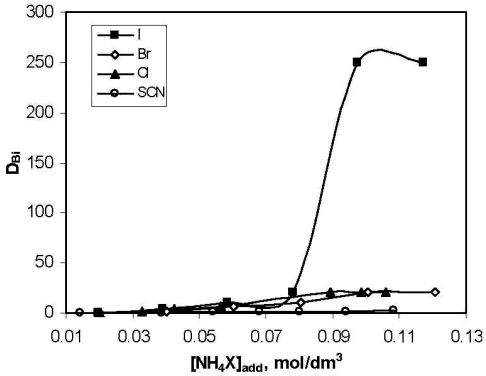

Figure 5a. The variation of Bi(III) distribution coefficient in function of extractants concentration. (Bi_i = 62.75 μg/cm^3, temperature = 24 °C).

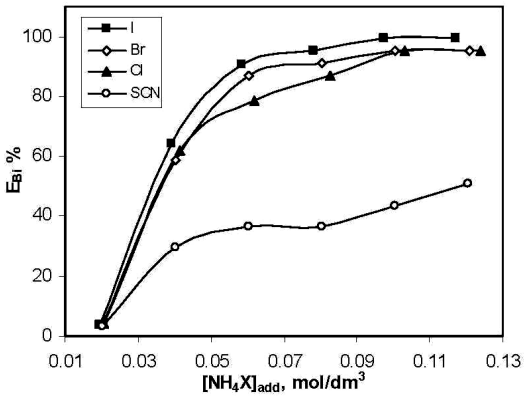

Figure 5b. The variation of Bi(III) extraction percent in function of extractants concentration. (Bi_i = 62.75 μg/cm^3, temperature = 24 °C).

The nature of the extracted species was deduced from log-log plots of distribution coefficients (D_{Bi}) versus the inorganic extractants concentrations in PEG-rich phases (in mentioned experimental conditions). The obtained dependences gave a straight line (Figure 6) with slopes 4 for halide extractants and 2 for SCN^- system, respectively. This indicate that in considered aqueous two-phase system in presence of halide extractants, Bi(III) is extracted predominant as anionic complexes (BiX_4^-), while in case of SCN^- extractant, the main extracted species have a molar ratio Bi : SCN^- = 1 : 2.

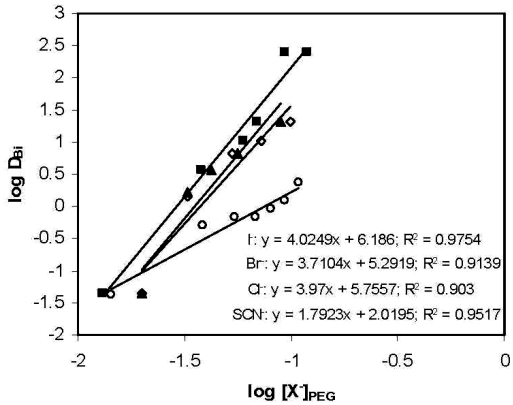

Figure 6. The log D_{Bi} against log $[X^-]_{PEG}$ dependences (Bi_i = 62.75 μg/cm^3, temperature = 24 °C).

The extraction of BiX_4^- species in case of halide extractants (instead of BiX_6^{3-}, which are more stable [18]), is mainly determined by the relative high water content of PEG-rich phases of this aqueous two-phase system (see

Figure 3). Because the hydrophobicity of these phases is lower, the formation of BiX_6^{3-} species (with a too lower hydration degree), is not necessary. In case of SCN^- extractant, the probable extraction of a mixed $Bi(SCN)_2NO_3$ species is a consequence of the appropriate stability of thiocyanate and nitrate bismuth species. This leads to the situation that during the extraction process, the exchange of NO_3^- ions with SCN^- ions, to be mainly determined by kinetics factors.

On the basis of obtained experimental results, the bismuth extraction process in presence of inorganic extractants (I^-, Br^-, Cl^- and SCN^-), in considered aqueous two-phase system can be schematic represented as in Figure 7.

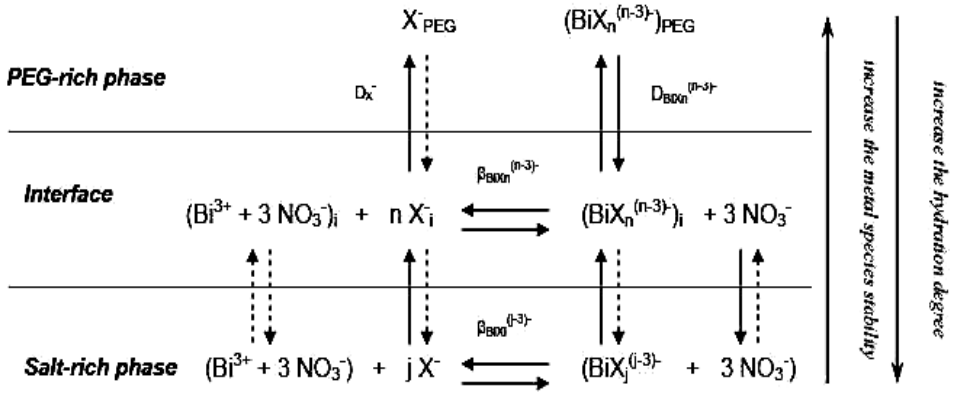

Figure 7. The schematic representation of the main elementary processes involved in Bi(III) extraction in presence of inorganic extractants, in the considered aqueous two-phase system.

According with this representation, the extraction process occurs step by step, until the hydration degree of metal ion become lowered enough (due to its complexation with extractants), and when this state is reached the metal species are immediately transferred into PEG-rich phase. After extractants addition, even in salt-rich phase, intermediary species $BiX_j(NO_3)_{3-j}$ (j = 1, 2 or 3) are probable formed, which are more stable than $Bi(NO_3)_3$, but have a hydration degree large enough for to maintain these species at the interface of this phase. At interface, these species will interact with other extractants, and in consequence the hydration degree of metal species will decrease. When, the metal species have a hydration degree compatible with those of PEG-rich phase, the partition of these occurs immediately.

The compatibility between metal species and PEG-rich phase hydration degree is a necessary condition, but not a sufficient one. According with the experimental results, an efficient extraction is obtained only when the metal ion react with inorganic extractants and form species with high stability. Thus, when in extraction system are formed a stable metallic species, these will

cross the interface with salt-rich phase, and will be efficient partitioned into PEG-rich phase (case of Bi(III) extraction in presence of halide extractants: I^-, Br^-, Cl^-). When, the formed metallic species formed in extraction system have a lower stability, the extraction process to occur until an "equilibrium state" is attained, depends on the hydrophobicity of the two aqueous phases (case of Bi(III) extraction in presence of SCN^- extractants).

CONCLUSIONS

The Bi(III) extraction behaviour in aqueous PEG(1500)–$(NH_4)_2SO_4$ two-phase system was investigated as a function of several experimental parameters: acidity of stock solutions of phase-forming components, initial concentration of Bi(III) in extraction system, type and concentration of inorganic extractants (I^-, Br^-, Cl^- and SCN^-).

The aqueous two-phase systems were prepared using aqueous solutions of phase-forming components in water and in 1N H_2SO_4. The experimental results have indicate that a quantitative extraction of Bi(III) is obtained only when both PEG and $(NH_4)_2SO_4$ stock solutions are prepared in 1N H_2SO_4, and such systems were chosen for the extraction experiments.

The addition of inorganic extractants determined an increasing of Bi(III) partition into PEG-rich phase, due to the formation of bismuth halide complexes, stable and with lower hydration degree. Under these conditions, for a given initial concentration of Bi(III) in extraction system (62.75 $\mu g/dm^3$), the extraction efficiency increase with the increasing of inorganic extractants concentration, and follow the order: $I^- >> Br^- > Cl^- >> SCN^-$. The nature of extracted species was assumed using the experimental distribution coefficients. The obtained results have indicate that in considered aqueous two-phase system in presence of halide extractants, Bi(III) is extracted predominant as BiX_4^-, while in case of SCN^- extractant, the main extracted species have a molar ratio Bi : SCN^- = 1 : 2.

On the basis of experimental results it can say that the Bi(III) extraction in presence of inorganic extractants (I^-, Br^-, Cl^- and SCN^-) occurs step by step, until the hydration degree of metal ion decrease enough (due to his complexation with extractants), and when this state is reach, the metal species are transferred into PEG-rich phase. Even the compatibility between metal species and PEG-rich phase hydration degree is a necessary condition this is not a sufficient one. An efficient extraction is obtained only when the metal species formed between Bi(III) and extractants, have a high stability.

EXPERIMENTAL SECTION

$(NH_4)_2SO_4$ (from Reactivul Bucharest) and NH_4X (X^- = I^-, Br^-, Cl^- and SCN^-) purchased from Aldrich, were analytical reagent degree and used without further purifications. Polyethylene glycol (PEG) with molecular mass

1500 (from Aldrich) was used as received. All aqueous solutions were prepared using double distilled water, obtained from a commercial distillation system.

Stock solutions of 40% (w/w) PEG(1500) were prepared by dissolving of an appropriate mass of solid polyethylene glycol in double distilled water or H_2SO_4 (Reactivul Bucharest) of known concentration. The 40% (w/w) of $(NH_4)_2SO_4$ stock solution was obtained similarly. The solution of ~ 2000 μg Bi(III)/cm^3 (10^{-2} mol/dm^3) was prepared by bismuth nitrate (from Fluka) dissolving in 20 cm^3 of HNO_3 concentrated solution (Reactivul Bucharest) and dilution to volume with double distilled water. After preparation, the exact concentration of Bi(III) was determined by standardization [25]. The solutions of inorganic extractants, containing 1 mol/dm^3 NH_4X (X^- = I^-, Br^-, Cl^- and SCN^-) were obtained by dilution of a known mass of inorganic salt to the volume with appropriate $(NH_4)_2SO_4$ stock solution. This approach provide a sever decreasing of salt forming-phase concentration after the addition of extractants.

For each experiment an aqueous two-phase system was prepared by mixing equal volumes (5 cm^3) of PEG(1500) and $(NH_4)_2SO_4$ stock solutions with different pH (measured with a Radelkis pH/ion-meter OK-281 equipped with a combined glass electrode), in a glass centrifuge tube. The systems were pre-equilibrated by centrifugation for 2 min at 2000 rpm. A 0.1 ÷ 0.5 cm^3 of Bi(III) stock solution and (0.1 ÷ 0.12) cm^3 of 1 mol/dm^3 NH_4X (X^- = I^-, Br^-, Cl^- and SCN^-) were added. The systems were again centrifuged 10 min at 2000 rpm. The centrifugation time was experimentally determined to be sufficient for these systems to reach equilibrium. Before analysis, the phases were separated using Pasteur pipettes and placed in separated tubes. 1.0 cm^3 from each phase were measured for spectrophotometrically Bi(III) analysis with KI (Digital S 104 D Spectrophotometer, 1 cm glass cell, λ= 460 nm, against a blank solution) [26]. Each Bi(III) concentration was determined in duplicate using a prepared calibration graph, and the extraction parameters (distribution coefficient (D_{Bi}) and the extraction percent (E_{Bi} %)) were calculated according to their definitions. The inorganic extractants concentration in PEG-rich phase was determined by conductometric titration with $AgNO_3$, using a Radelkis OK-109 conductometer.

For the IR experiments 1.0 ÷ 1.5 cm^3 from PEG stock solutions and blank PEG-rich phases separated from extraction systems (before the addition of metal ion and extractants), were measured and placed on the glass slides (chemical inert). The samples were solidified at room temperature (24 ± 0.5 °C). The IR spectra have been recorded using a FTIR Bio-Rad Spectrometer, in a 400 – 4000 cm^{-1} spectral domain with a resolution of 4 cm^{-1}, by KBr pellet technique.

ACKNOWLEDGMENTS

The authors would like to acknowledge the financial support from Romanian Ministry of Education and Research (Project PN II no. 51045/07).

REFERENCES

1. H. Reinhardt, *Proceedings of International Conference on Hazardous Waste*, **1998**, Cairo, Egypt, 12-16 December.
2. A.Y. Ku, J. M. Schoenung, *Toxicity, Availability and Extraction of the Metals*, **2002**, UC SMART Workshop UCLA, U.S.A, September 5.
3. S.H. Gaikwad, S.V. Mahamuri, M.A. Anuse, *Indian Journal of Chemistry and Technology,* **2005**, *12(3)*, 365.
4. T.S. Hannel, E.O. Out, M.P. Jensen, *Solvent Extraction and Ion Exchange*, **2007**, *25(2)*, 241.
5. Y. Moriya, M. Sugai, S. Nakata, N. Ogawa, *Analytical Science*, **2001**, *17(2)*, 297.
6. L. Li, C.Y. He, S.H. Li, F. Liu, S. Su, X.X. Kong, N. Li, K.A. Li, *Chinese Journal of Chemistry*, **2004**, *22*, 1313.
7. K.P. Ananthapadmanabhan, E.D. Goddar, *Langmuir*, **1987**, *3*, 25.
8. M. Shibukawa, K. Matsuura, Y. Shinozuka, S. Mizuni, K. Oguma, *Analytical Science*, **2000**, *16*, 1039.
9. M. Shibukawa, N. Nakayama, T. Ayashi, D. Shibuya, Y. Endo, S. Kawamura, *Analytica Chimica Acta*, **2001**, *427*, 293.
10. L. Bulgariu, D. Bulgariu, *Buletinul Institutului Politehnic Iaşi*, **2007**, *tom LIII (LVII)*, 21.
11. L. Bulgariu, D. Bulgariu, *Buletinul Institutului Politehnic Iaşi*, **2008**, *tom LIV (LVIII)*, 7.
12. L. Bulgariu, I. Sârghie, *Analele Stiințifice ale Universității "Al. I. Cuza" Iaşi*, s. Chemistry, **2005**, *tom XIII*, 27.
13. L. Bulgariu, D. Bulgariu, *Journal of the Serbian Chemical Society*, **2008**, *73(3)*, 341.
14. L. Bulgariu, D. Bulgariu, *Central European Journal of Chemistry*, **2006**, *4(2)*, 256.
15. R.D. Rogers, S.T. Griffin, *Journal of Chromatography B*, **1998**, *711*, 277.
16. R.D. Rogers, A.H. Bond, C.B. Bauer, *Separation Science and Technology*, **1993**, *28(5)*, 1091.
17. R.D. Rogers, A.H. Bond, C.B. Bauer, J. Zhang, S.T. Griffin, *Journal of Chromatography B*, **1996**, *680*, 221.
18. J. Lurie, "Handbook of Analytical Chemistry", Mir Publishers, Moscow, **1975**, chapter 4.
19. Bismuth distribution diagram calculated using EpH-web, accessed at 15 February 2008: http://www.crct.pdymtl.ca/ephweb.php.
20. H. Kitako, K. Ichikawa, M. Ide, M. Fukuda, W. Mizuno, *Langmuir*, **2001**, *17(6)*, 1889.
21. L. Bulgariu, D. Bulgariu, I. Sarghie, Th. Malutan, *Central European Journal of Chemistry*, **2007**, *5(1)*, 291.
22. T.A. Graber, B.A. Andrews, J.A. Asenjo, *Journal of Chromatography B*, **2000**, *743*, 57.
23. R.D. Rogers, A.H. Bond, C.B. Bauer, *Solvent Extraction in Process Industry*, **1993**, *3*, 1641.
24. Y. Marcus, *Journal of Chemical Society Faraday Trans*, **1991**, *87(18)*, 2995.
25. J. A. Dean, "Analytical Chemistry Handbook", McGrow-Hill Inc., New York, **1995**, chapter 3.
26. D.Bilba, L. Bulgariu, "Spectrometric methods of analysis" (in Romanian), Performantica, Iaşi, **2005**, chapter 5.

STUDIA UNIVERSITATIS BABEŞ-BOLYAI, CHEMIA, LIV, 4, 2009

DESFERAL EFFECT ON HUMAN ERYTHROCYTE MEMBRANE. AN ATOMIC FORCE MICROSCOPY ANALYSIS

MARIA TOMOAIA-COTISEL[a], DANIELA-VASILICA POP-TOADER[a], ULPIU VLAD ZDRENGHEA[b], GHEORGHE TOMOAIA[c], OSSI HOROVITZ[a] AND AURORA MOCANU[a]

ABSTRACT. The surface topography of erythrocyte membrane was imaged with the atomic force microscope (AFM), operating in tapping mode, and the effect of desferal (deferoxamine mesylate: DFO) at various concentrations on the cell membrane was investigated. The normal (control) human erythrocytes, without DFO, showed a clear concave form. After the incubation of fresh blood with increasing DFO concentrations, from 5 $x10^{-7}$ M to 5 x 10^{-3} M, a progressive increase in both concave depth and surface roughness of erythrocytes were observed. Further, the AFM images indicated that the particles (granules) of the cell surface nanostructure increased with the increasing DFO concentrations. This increase of surface granules is due to the aggregation of lipid nanoparticles and lipid domain formation, induced by DFO. The data are in substantial agreement with our previously published results obtained on lipid membrane models in the presence of DFO. Besides domain formation, the pore formation within human erythrocyte membrane was observed in the presence of desferal.

The DFO effect on lipid membranes might be also associated with the modification of both the conformation and the aggregation of membrane proteins, probably leading to an increased permeability of cell membrane.

Keywords: desferal, domain formation; porous membrane structure; erythrocyte membrane; AFM

INTRODUCTION

The molecular mechanism of the drug interaction with cells and the involvement of interfacial phenomena at the cell membrane are still not well understood, in spite of numerous investigations [1-12]. As a first step, the drugs action presumes that the drug molecules modify the lipid membrane structure [6-12] and thus, they may change the biological membrane properties [5, 9-12].

[a] *Babes-Bolyai University, Faculty of Chemistry and Chemical Engineering, Physical Chemistry Department, 11 Arany J. Str., 400028 Cluj-Napoca, Romania*

[b] *Iuliu Hatieganu University of Medicine and Pharmacy, Psychiatry Department, 43 Babes V. Str., 400012 Cluj-Napoca, Romania*

[c] *Iuliu Hatieganu University of Medicine and Pharmacy, Orthopaedics and Traumatology Department, 47 Mosoiu T. Str., 400132 Cluj-Napoca, Romania. E-mail: mcotisel@chem.ubbcluj.ro*

The objective of the present work is to analyze the effect of a drug, such as desferal, on the structural and topographical characteristics of erythrocyte membrane using atomic force microscopy (AFM). Recently, AFM was used to image the surface of membrane models [13-16] and of cell membranes [17-19]. AFM observations of erythrocyte membranes were used to characterize the membrane structure [20-24] and the AFM images revealed the effect of different organic and inorganic compounds on cellular membrane [25, 26].

Desferal (DFO) or desferrioxamine mesylate is *N*-[5-[3-[(5-aminopentyl)-hydroxycarbamoyl] propionamido] pentyl] -3- [[5-(*N*-hydroxyacetamido)-pentyl] carbamoyl] propionohydroxamic acid monomethanesulfonate (scheme 1). It is a transition metal chelator derived from ferrioxamine B, a sideramine isolated in 1960 from *Streptomyces pilosus*. Since it forms a very stable complex with iron(III), DFO is used for clinically removal of excess iron from blood and tissue [27] and consequently, for the treatment of acute iron poisoning and iron-overload anemia, such as thalassaemia major [28], as well as aluminium poisoning associated with chronic renal dialysis [29].

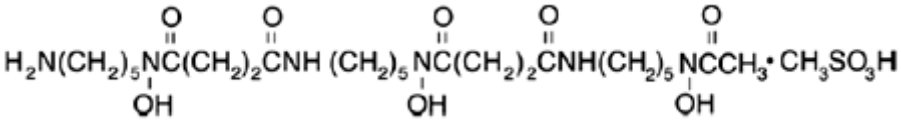

Scheme 1

We have previously investigated the acid and basic properties of desferal [30], and have made a spectroscopic study of this compound and its Fe(III) complex [31, 32]. Since desferal is supposed to act on erythrocyte membrane, we have previously investigated its effects on lipid membrane models, such as lipid monolayers, and determined the domain formation within lipid membrane layers as a function of drug concentration [12].

RESULTS AND DISCUSSION

For this work, we have chosen fresh human blood which offers stable erythrocytes. Erythrocytes samples without or treated with desferal (DFO) are investigated by AFM at room temperature in air.

The erythrocyte cell morphology

AFM images obtained for the whole cell surface morphology of control samples is presented in Figures 1, at two scanned areas of 10 μm x 10 μm and 0.5 μm x 0.5 μm. The AFM images of control samples show that erythrocytes present a concave donut shape with average lateral size.

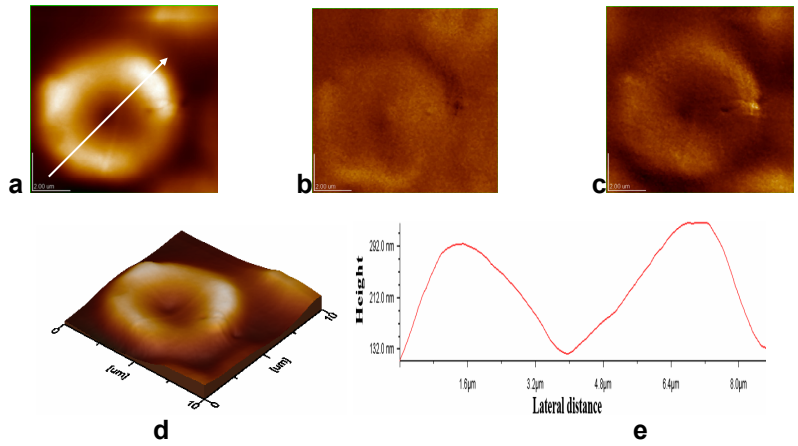

Figure 1A. AFM images of erythrocyte membrane surface, control sample: a) 2D – topography; b) phase image; c) amplitude image; d) 3D-topography; e) profile of the cross section along the arrow in image (a). Scanned area: 10 μm x 10 μm.

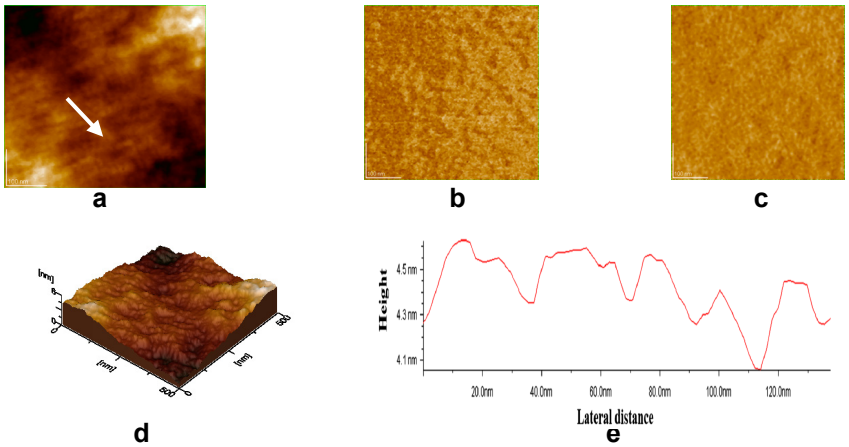

Figure 1B. AFM images of erythrocyte membrane surface, control sample: a) 2D – topography; b) phase image; c) amplitude image; d) 3D-topography; e) profile of the cross section along the arrow in image (a). Scanned area: 0.5 μm x 0.5 μm.

About 8 μm in diameter and nearly 0.14 μm in depth of concave shape (Figure 1A, Table 1). The nanostructure of normal human erythrocytes is featured by closely packed granules or particles with diameter of about 22 nm and almost uniformly distributed (Figure 1B, Table 1).

The granules probably correspond to membrane lipids well packed into the lipid part of the membrane surface in substantial agreement with lipid nanostructure found in monolayer membrane model [16]. These particles might also correspond to membrane protein protruding from the cell surface, mentioned as a probability [20].

The erythrocyte cell morphology in presence of low desferal concentration

Figures 2 and 3 show AFM images of erythrocytes treated with low desferal concentration for two different scanned areas. After mixing of fresh blood with desferal solution the desferal concentration became 5 x 10^{-7} M. The whole surface of erythrocytes is mainly characterized by the same cell shape (Figure 2) as for control sample without DFO (Figure 1A).

The membrane nanostructure in the presence of a low desferal concentration (Figure 3) is only a little different than for control (Figure 1B). The surface roughness, given by root mean square (RMS), is also very similar for these situations at the same scanned area (Table 1).

The erythrocyte cell morphology in presence of medium desferal concentration

The erythrocyte surface morphology is illustrated in Figs 4 and 5, for two different scanned areas, at medium desferal concentration of 5 x 10^{-5} M. AFM images indicate both the cell shape (Figure 4) and membrane surface nanostructures (Figure 5) are perturbed by the presence of desferal at medium concentration.

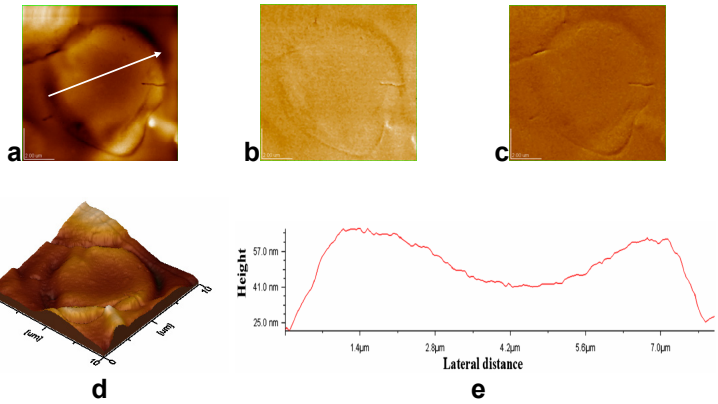

Figure 2. AFM images of erythrocyte membrane surface in the presence of DFO 5 x 10^{-7} M. a) 2D – topography; b) phase image; c) amplitude image; d) 3D-topography; e) profile of the cross section along the arrow in image (a). Scanned area: 10 µm x 10 µm.

Figure 4 presents the AFM images of an erythrocyte at a scanned area of 10 µm x 10 µm. It is clear that the concave form is again preserved as for control sample (Fig 1A), but the concave depth is much higher, to about 340 nm (Figs 4, e). The lateral size of the cell is about 8 or 8.5 µm in diameter.

It is to be noted that in Figure 4, around the cell some NaCl fragments are evidenced, probably formed during the drying process of samples. These small NaCl deposits will not affect the AFM analysis.

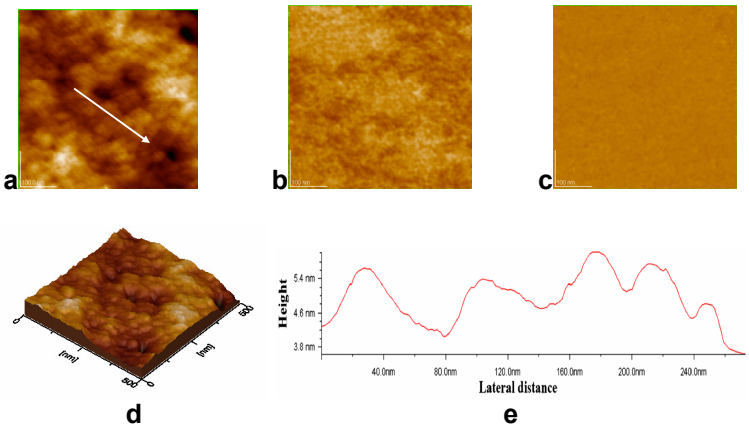

Figure 3. AFM images of erythrocyte membrane surface in the presence of DFO 5 x 10^{-7} M as shown in Figure 2. a) 2D – topography; b) phase image; c) amplitude image; d) 3D-topography; e) profile of the cross section along the arrow in image (a). Scanned area: 0.5 µm x 0.5 µm.

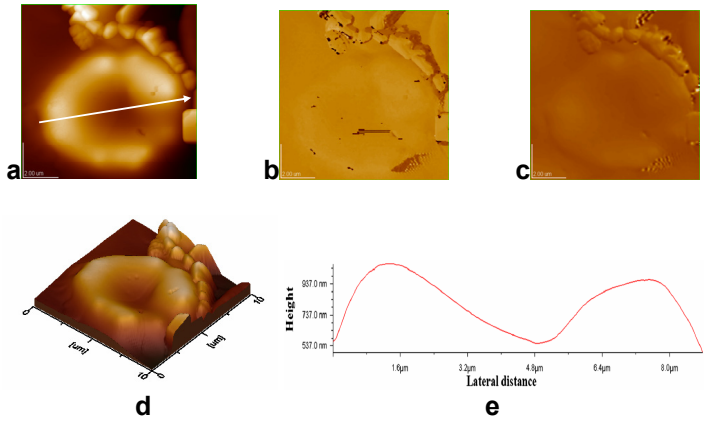

Figure 4. AFM images of erythrocyte membrane surface in the presence of DFO 5 x 10^{-5} M. a) 2D – topography; b) phase image; c) amplitude image; d) 3D-topography; e) profile of the cross section along the arrow in image (a). Scanned area: 10 µm x 10 µm. NaCl crystals were formed during the drying period of the erythrocyte cells on glass surface.

The membrane nanostructure in the presence a medium desferal concentration (Figure 5) is rather different than for control (Figure 1B) or for erythrocytes in presence of low desferal concentration (Figure 3).

The domain formation induced by desferal is well illustrated in Figure 5, particularly in panels b and c. In addition, in Figure 5b it is to be observed a clear tendency to pore formation for this desferal concentration.

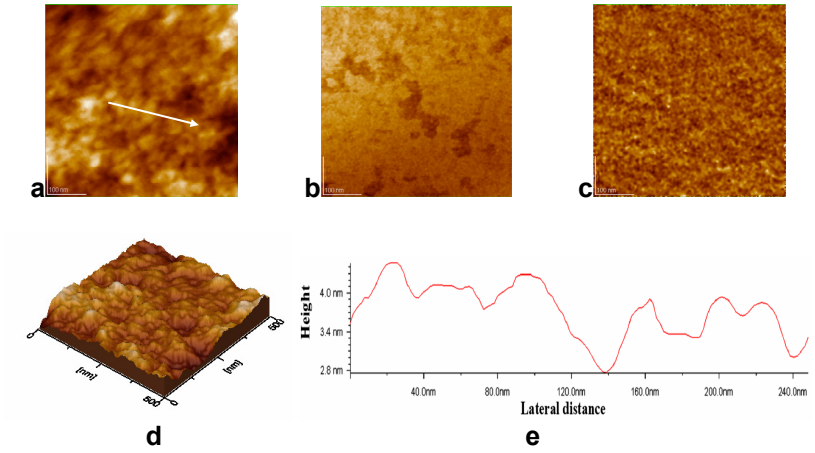

Figure 5. AFM images of erythrocyte membrane surface in the presence of DFO 5 x 10^{-5} M, as shown in Figure 4. a) 2D – topography; b) phase image; c) amplitude image; d) 3D-topography; e) profile of the cross section along the arrow in image (a). Scanned area: 0.5 μm x 0.5 μm.

However, it is to be observed that the membrane nanostructure is relatively uniformed (Figure 5, c and e) and the surface roughness is rather small (Table 1). The granules or surface particles are from about 30 nm to 50 nm (Figure 5 e, and Table 1). From these data, we can suggest a stabilizing effect of desferal on erythrocytes membrane which can be related with the desferal action on sickle cells deformability [33].

The erythrocyte cell morphology in presence of high desferal concentration

The erythrocyte surface morphology is illustrated in Figs 6-10, for four different scanned areas, at high desferal concentration of 5 x 10^{-3} M. AFM images indicate a remarkable change in both cell shape (Figs 6 and 7) and in membrane surface nanostructures (Figs 8-10).

Figure 6 presents the AFM images of several erythrocytes at a scanned area of 15 μm x 15 μm. It is clear that the three cells are somewhat separated from each other, but the cell concave form disappears.

In Figure 7, the AFM images are shown on a single cell (scanned area: 10 μm x 10 μm). Again they show that an erythrocyte is not of concave form, and it is completely different than the control sample (Figure 1A) or than erythrocytes at low (Figure 2) or medium desferal concentration (Figure 4). In other words the concave donut form can no more be identified. This situation can be correlated with a strong interaction of desferal with the cell membrane, leading to the deterioration of the membrane (Figure 6a and Figure 7a).

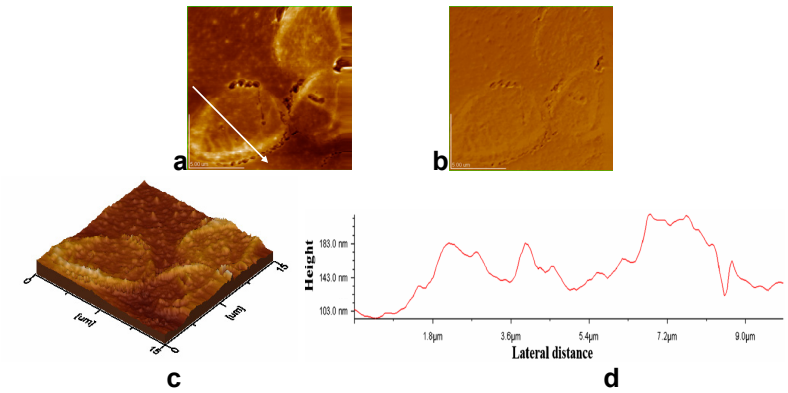

Figure 6. AFM images of erythrocyte membrane surface in the presence of DFO 5 x 10^{-3} M, zone 1. a) 2D – topography; b) amplitude image; c) 3D-topography; d) profile of the cross section along the arrow in image (a). Scanned area: 15 µm x 15 µm.

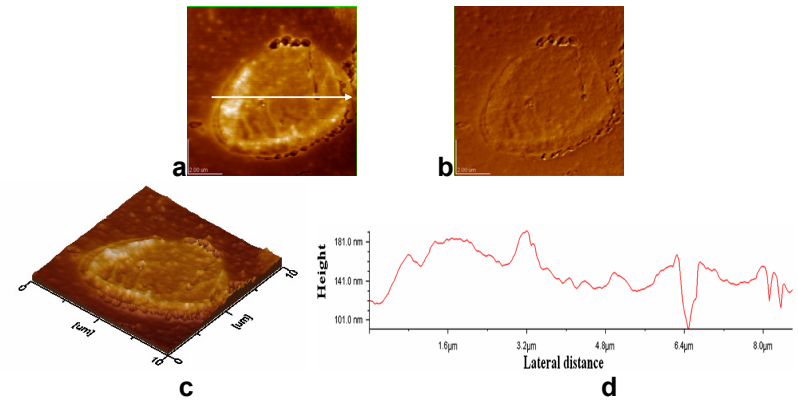

Figure 7. AFM images of erythrocyte membrane surface in the presence of 5 x 10^{-3} M desferal as described in Figure 6. a) 2D – topography; b) amplitude image; c) 3D-topography; d) profile of the cross section along the arrow in image (a). Scanned area: 10 µm x 10 µm.

The membrane nanostructure in the presence of high desferal concentration (Figs. 8 -10) is also much different as that for control sample (Figure 1B) or for erythrocytes in presence of low (Figure 3) or medium desferal concentration (Figure 5).

At this high desferal concentration (5 x 10^{-3} M) the further surface aggregation developed into a long array of aggregated particles and big elongated shaped pores (Figs. 9 and 10). The surface roughness is higher and the granules aggregates are very large (Table 1).

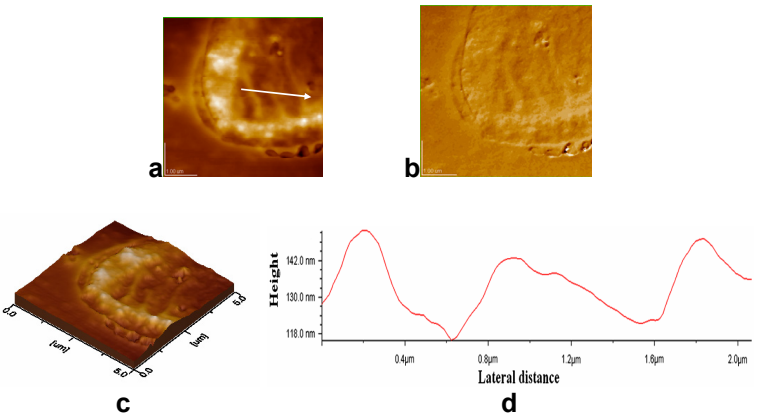

Figure 8. AFM images of erythrocyte membrane surface in the presence of DFO 5 x 10^{-3} M. a) 2D – topography; b) amplitude image; c) 3D-topography; d) profile of the cross section along the arrow in image (a). Scanned area: 5 μm x 5 μm.

Thus, desferal binds to human erythrocyte membranes and induces domain and pore formation on erythrocyte membranes. The domain and pore structures mediated by high desferal concentrations might be responsible for both enhanced surface aggregation of erythrocyte membrane and even perforation.

At low concentration, desferal can only induce the domain structure formation. With a higher DFO concentration, such as 5×10^{-3} M, the further aggregation developed into large pores.

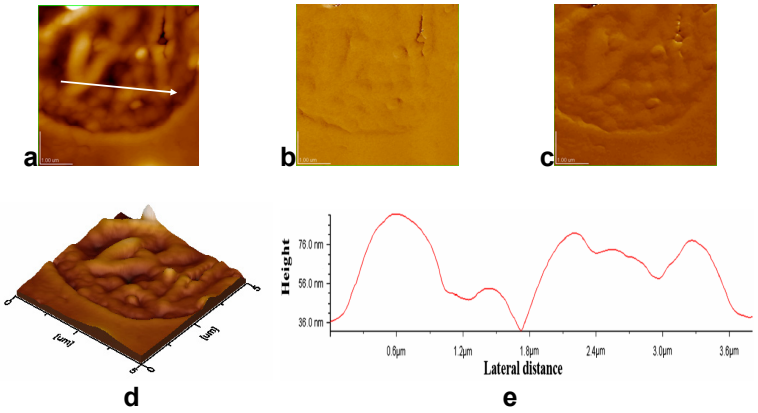

Figure 9. AFM images of erythrocyte surface in the presence of DFO 5 x 10^{-3} M, zone 2. a) 2D – topography; b) phase image; c) amplitude image; d) 3D-topography; e) profile along the arrow in image (a). Scanned area: 5 μm x 5 μm.

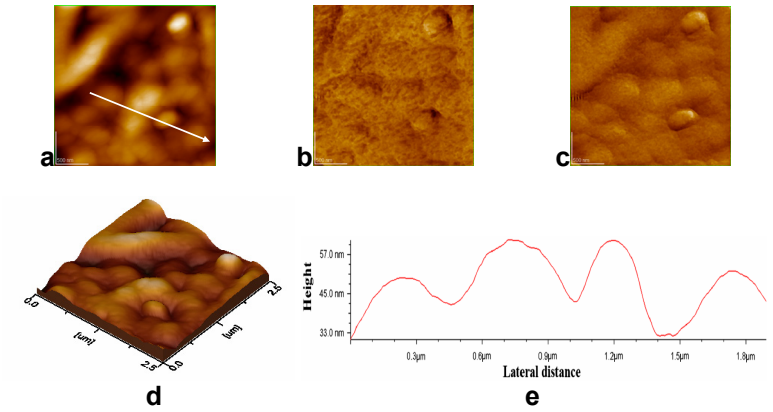

Figure 10. AFM images of erythrocyte membrane surface in the presence of DFO 5 x 10^{-3} M, zone 2. a) 2D – topography; b) phase image; c) amplitude image; d) 3D-topography; e) profile of the cross section along the arrow in image (a). Scanned area: 2.5 µm x 2.5 µm.

The erythrocyte membrane is a mosaic formed from a lipid bilayer with intrinsic and extrinsic proteins. DFO and other drugs may influence the interaction among lipids and proteins and bring changes in the membrane surface structure.

Table 1. Erythrocytes size, concave depth, granules diameter, RMS on scanned areas and on cross profile through the erythrocyte membrane, for fresh blood diluted with 0.15 M NaCl aqueous solution in the 1:1, (v:v), volume ratio, for various desferal (DFO) concentrations.

DFO conc., (M)	Fig.	Scanned areas, (µm x µm)	Cell size (µm)	Concave depth (nm)	Granules (nm)	RMS on scanned areas (nm)	RMS on cross profile (nm)
0	-	10 x 10	8.0	135	-	147	99
	-	0.5 x 0.5	-	-	24	1	0.2
	1A	10 x 10	8.4	140	-	150	101
	1B	0.5 x 0.5	-	-	22	1	0.2
5 x 10^{-7}	2	10 x 10	7.7	180	-	170	102
	3	0.5 x 0.5	-	-	30	2	0.6
5 x 10^{-5}	-	10 x 10	8	300	-	265	161
	-	0.5 x 0.5	-	-	55	3	2
	4	10 x 10	8.5	340	-	274	147
	5	0.5 x 0.5	-	-	50	1	1
5 x 10^{-3}	6	15 x 15	-	-	680	32	32
	7	10 x 10	-	-	600	33	20
	8	5 x 5	-	-	400	25	10
	9	5 x 5	-	-	400	18	16
	10	2.5 x 2.5	-	-	230	14	8

The mechanism of domain and pore formation leading to membrane perforation, provoked by high DFO concentration, could be discussed on the basis of specific interactions among DFO and lipids.

We suggest that the lipid and DFO interactions can lead to the aggregation of membrane lipids and to the coexistence of different lipid and protein phases in the erythrocyte membrane resulting from desferal membrane binding. Of course, the possibility of direct interaction of membrane proteins and desferal can not be eliminated.

The DFO might also alter the interaction of extrinsic proteins with lipid bilayer membrane, again as an effect of the drug binding to the human erythrocytes membranes.

At the same time, desferal molecules penetrated into the lipid membrane can influence the intrinsic membrane proteins and the membrane skeleton.

There might also be a drug distribution into the lipid layers, leading to an increased stability at low DFO concentrations or to a slightly decreased stability of the membrane for medium DFO concentration or even the damage of the erythrocyte membrane at very high DFO concentrations. Domain and pore formation are probably connected to an enhanced permeability of cells in presence of DFO at high concentrations.

Therefore we intend to extend our investigation on erythrocytes in the presence of higher desferal concentrations for a better understanding of desferal effects and potential implications in medical treatment.

CONCLUSIONS

The examination of AFM images on human erythrocytes in the absence and the presence of desferal at different DFO concentrations throw some light on the effect of desferal on cell membranes.

At low DFO concentrations, both the morphology of erythrocyte cells and their membrane nanostructures reveal no a significant difference in comparison with the situation of control sample, erythrocytes without DFO.

At intermediate DFO concentrations, the analysis of AFM images showed that the binding of desferal to erythrocyte membranes led to nanostructured domain formation but at the higher DFO concentration even the pore formation was evidenced.

The domain and pore structures mediated by desferal increased high concentrations might be responsible for both enhanced surface aggregation and the perforation of erythrocyte membrane.

The mechanism of domain and pore formation or the perforation process induced by desferal at its highest concentration used can be discussed on the basis of specific interactions among desferal and the membrane lipids.

These molecular interactions can lead to the aggregation of membrane lipids and to the coexistence of different lipids and proteins phases in erythrocyte membrane resulted from desferal membrane binding.

The possibility of direct interaction of membrane proteins and desferal can also contribute to the erythrocyte membrane changes in the presence of desferal.

EXPERIMENTAL SECTION

Desferal (DFO) of high purity was purchased from Ciba-Geigy, Basle, Switzerland. The DFO concentrations range in aqueous solutions, containing 0.15 M NaCl, was from 5×10^{-7} M to 5×10^{-3} M.

Fresh human blood was used in all experiments. To avoid osmotic pressure modifications, and consequently the swelling of human blood cells, all used aqueous solutions with or without drugs contained 0.15 M NaCl.

Human blood was diluted with 0.15 M NaCl aqueous solution in the 1:1 volume ratio, resulting in the control dispersion. The human blood was also treated with DFO solutions, containing 0.15 M NaCl, in the same 1:1 volume ratio as the control dispersion. The fresh blood was incubated with or without DFO, at room temperature, about 22 ^{o}C, for 30 min.

Then, 10 µL of control and DFO treated blood dispersions were each deposited on optically polished glass plate surface. The residual dispersion was removed with a piece of filter paper placed at the edge of deposited area and the samples were dried in the environmental air conditions.

During the drying process, the control and DFO treated blood samples were covered with a bicker to avoid durst. The dried control samples and DFO treated blood samples were imaged by atomic force microscope, AFM, JEOL 4210.

Atomic force microscopy is a surface imaging technique with a nanometer-scale resolution [13-18]. The cantilevers with a resonance frequency of 250 – 350 kHz were used. Triplicate samples were prepared from each blood sample and at least four separate areas were imaged for every independent sample.

Through this investigation, AFM images were obtained at several drug concentrations in order to examine the effect of desferal on the surface morphology of erythrocytes membrane.

ACKNOWLEDGMENTS

We are grateful for financial support from PN 2, grant no. 41-050.

REFERENCES

1. H. Tsuchiya, M. Mizogami, T. Ueno, K. Takakura, *Inflammopharmacol*., **2007**, *15*, 164.
2. T. Hata, H. Matsuki, S. Kaneshina, *Colloids and Surfaces B*, **2000**, *18*, 41.
3. Z. Leonenko, E. Finot, D. Cramb, *Biochimica et Biophysica Acta,* **2006**, *1758*, 487.

4. H. Matsuki, S. Kaneshina, H. Kamaya, I. Ueda, *Journal of Physical Chemistry B,* **1998**, *102*, 3295.
5. Z. V. Leonenko, D. T. Cramb, *Canadian Journal of Chemistry,* **2004**, *82*, 1128.
6. M. Tomoaia-Cotisel, E. Chifu, A. Mocanu, J. Zsakó, M. Salajan, P.T. Frangopol, *Revue Roumaine de Biochimie,* **1988**, *25* (3), 227.
7. M. Tomoaia-Cotisel, I.W. Levin, *Journal of Physical Chemistry B,* **1997**, *101,* 8477.
8. P. T. Frangopol, D. Mihailescu, *Colloids and Surfaces B,* **2001**, *22*, 3.
9. M. Tomoaia-Cotisel, *Progress in Colloid and Polymer Science*, **1990**, *83,* 155.
10. M. Tomoaia-Cotisel, D. A. Cadenhead, *Langmuir,* **1991**, *7,* 964.
11. B. Asgharian, D. A. Cadenhead, M. Tomoaia-Cotisel, *Langmuir,* **1993**, *9,* 228.
12. M. Tomoaia-Cotisel, A. Mocanu, Gh. Tomoaia, I. Zsako, T. Yupsanis, *Journal of Colloid and Surface Chemistry,* **2001**, *4* (1), 5.
13. M. Tomoaia-Cotisel, "Convergence of Micro-Nano-Biotechnologies, Series in Micro and Nanoengineering", Vol. *9,* Edts. M. Zaharescu, E. Burzo, L. Dumitru, I. Kleps, D. Dascalu, Rom. Academy Press, Bucharest, **2006**, pp. 147-161.
14. K. Hoda, Y. Ikeda, H. Kawasaki, K. Yamada, R. Higuchi, O. Shibata, *Colloids and Surfaces B*, **2006**, *52,* 57.
15. Gh. Tomoaia, M.Tomoaia-Cotisel, A. Mocanu, O. Horovitz, L.-D. Bobos, M. Crisan, I. Petean, *Journal of Optolectronics and Advanced Materials*, **2008**, *10* (4), 961.
16. P. T. Frangopol, D. A. Cadenhead, M. Tomoaia-Cotisel, A. Mocanu, *Studia Universitatis Babes-Bolyai, Chemia*, **2009**, *54* (1), 23.
17. P. C. Zhang, C. Bai, Y. M. Huang, *Scanning Microscopy*, **1995**, *9,* 981.
18. H. J. Butt, E. K. Wolff, S. A. C. Gould, *Journal of Structural Biology,* **1990**, *105*, 54.
19. Y. Cheng, M. Z. Liu, C. I. Bai, *Biochimica et Biophysica Acta,* **1999**, *1421*, 249.
20. X. Y. Zhang, F. H. Chen, P. H. Wei, J. Z. Ni, *Chinese Chem. Letters,* **2006**, *17*, 1105.
21. M. Takeuchi, H. Miyamoto, Y. Sako, H. Komizu, A. Kusumi, *Biophysical Journal*, **1998**, *74*, 2171.
22. S. Yamashina, O. Katsumata. *Journal of Electron Microscopy*, **2000**, *49*, 445.
23. A.H. Swihart, J.M. Mikrut. J.B. Ketterson, R.C. Macdonald, *Journal of Microscopy*, **2001**, *204*, 212.
24. M.S. Ho, F.J. Kuo, Y.S. Lee, *Applied Physics Letters*, **2007**, *91*, 023901.
25. Y. Cheng, M. Liu, R. Li, C. Wang, C. Bai, K. Wang, *Biochimica et Biophysica Acta – Biomembranes,* **1999**, *1421* (2), 249.
26. Y. Cheng, M. Liu, Y. Li, R. Li, C. Bai, K. Wang, *Chinese Science Bulletin*, **2000**, *45*, 426.
27. H. Keberle, *Annals of the New York Academy of Sciences*, **1964**, *119*, 758.
28. W. Banner Jr., T.G. Tong, *Pediatric Clinics of North America*, **1986**, *33,* 393.
29. J.P. Day, P. Ackrill, *Therapeutic Drug Monitoring*, **1993**, *15,* 598.
30. J. Zsako, M. Tomoaia-Cotisel, I. Albu, A. Mocanu, A. Aldea, *Revue Roumaine de Chimie*, **2002**, *47*, 869.
31. O. Cozar, N. Leopold, C. Jelic, L. David, V. Chis, M. Tomoaia-Cotisel, A. Mocanu, R. Grecu, *Studia Universitatis Babes-Bolyai, Physica,* **2004**, *49* (3), 115.
32. O. Cozar, N. Leopold, C. Jelic, V. Chis, L. David, A. Mocanu, and M. Tomoaia-Cotisel, *Journal of Molecular Structure*, **2006**, *788*, 1.
33. M. R. Clark, N. Mohandas, S. B. Shohet, *Journal of Clinical Investigation*, **1980**, *65*, 189.

STUDIA UNIVERSITATIS BABEŞ-BOLYAI, CHEMIA, LIV, 4, 2009

OMEGA POLYNOMIAL IN CUBE MED_MED_AII CRYSTAL-LIKE NETWORK

MIRCEA V. DIUDEA[a*], ALI IRANMANESH[b]

ABSTRACT. Omega polynomial $\Omega(G,x)$ is defined on opposite edge strips *ops* which are quasi orthogonal cuts *qoc* in a graph *G*=*G*(*V*,*E*), with the meaning the transitivity relation is not necessarily obeyed. The first and second derivatives, in *x*=1, of Omega polynomial provide the Cluj-Ilmenau *CI* index. The polynomial provides an appropriate topological description of infinite crystal-like networks. Close formulas for the number of atoms, Omega polynomial and *CI* index are derived for a lattice designed by using operations on maps/networks.

Keywords: graphene, CorSu network, Omega polynomial.

INTRODUCTION

The rigorous architecture of crystal networks attracted the interest of scientists in a broad area, from crystallographers, to chemists and mathematicians [1-9]. The studies on classification were followed by studies on the usefulness, in chemical reactions or in physical devices, and more recently by applied mathematical studies, in an effort to give new, more appropriate characterization of the world of crystals. Thus, recent articles in crystallography promoted the idea of topological description and classification of crystal structures [1-6]. They present data on real but also hypothetical lattices designed by computer.

Counting polynomials have been introduced, in the Mathematical Chemistry literature, by Hosoya [10,11]: *Z*(*G*,*X*) counts independent edge sets while *H*(*G*,*X*) (initially called Wiener and later Hosoya [12,13]) refers to distances in the graph. Hosoya also proposed the sextet polynomial [14-17] for counting the resonant rings in a benzenoid molecule. More about polynomials the reader can find in ref [18].

Some distance-related properties can be expressed in polynomial form, with coefficients calculable from the layer and shell matrices [19-22].

[a] *Faculty of Chemistry and Chemical Engineering, "Babes-Bolyai" University, 400028 Cluj, Romania; diudea@gmail.com*
[b] *Tarbiat Modares University, Tehran, I.R. Iran*
* This paper is dedicated to Professor Padmakar Khadikar, University of Indore, India, for his bright contributions in the field of Chemical Graph Theory.

These matrices are built up according to the vertex distance partitions of a graph, as provided by the TOPOCLUJ software package [23]. The most important, in this respect, is the evaluation of the coefficients of Hosoya $H(G,X)$ polynomial from the layer of counting LC matrix.

The present work describes the design and topology (in terms of Omega polynomial) of a crystal-like lattice, derived from the cube by applying map/net operations. The article is organized as follows: The second section illustrates the construction of the lattice while the third section provides definitions of Omega polynomial and *CI* derived index, and derives close formulas for their calculation in this network. Conclusions and references will close the article.

DESIGN OF NETWORK

A map *M* is a combinatorial representation of a (closed) surface. Some geometrical-topological transformations, called operations on maps, are used to relate parents and transformed associate graphs of fullerenes (in general, nanostructures). In this respect, operations such as: dualization *Du*, medial *Me*, truncation *Tr*, polygonal P_r capping or Snub Sn, are well known [24-28]. Our original software CageVersatile (CVNET), enables such operations and proved to be a useful tool [29].

Medial *Med* is an operation which can be achieved by putting a new vertex in the middle of each original edge and next by joining two such vertices if the parent edges spanned an angle. The *Med* transform is always a 4-valent graph, as can be seen in Figure 1. The medial operation rotates parent *s*-gonal faces by π/s. Points in the medial map represent original edges.

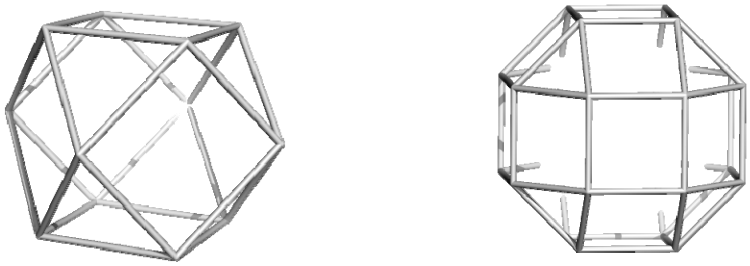

Figure 1. Transforms of the cube by Med (left) and Med(Med) (right) operations.

The objects in the above figure can be used as repeat units in building infinite networks. Figure 2 illustrates the crystal-like network built up by identifying the square faces of the *Med*(*Med*(*C*)) unit, in the three directions of coordinates. The same lattice can be obtained by performing the double medial *Med_Med_all* operation on all the hard rings which form the square 3D network [30].

Any lattice has its co-lattice, thus we focused on the *Med_Med_all* transform and assign it to be the main lattice (Figure 2, left column). Consequently, its co-lattice is that which includes the interstices and borders of the main net (Figure 2, right column).

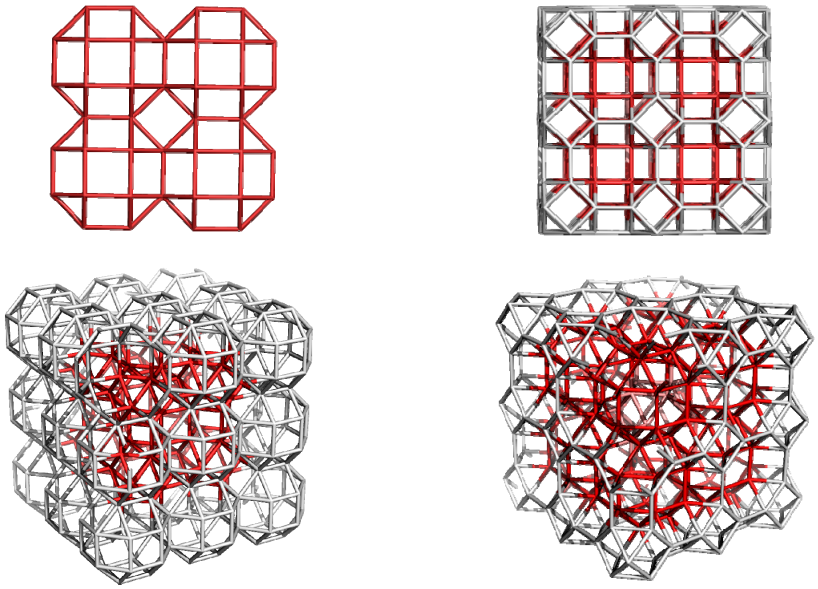

Figure 2. Lattice (333; *v*=432; left) and co-lattice (222; v=324; right) designed by Med(Med(C))_all operation, in plane projection (top) and 3D (bottom)

OMEGA POLYNOMIAL IN MED_MED_All CRYSTAL NETWORK

Let *G*(*V*,*E*) be a connected bipartite graph, with the vertex set *V*(*G*) and edge set *E*(*G*). Two edges *e* = (*x*,*y*) and *f* = (*u*,*v*) of *G* are called *codistant* (briefly: *e co f*) if

$$d(x,v) = d(x,u) + 1 = d(y,v) + 1 = d(y,u) \tag{1}$$

Let $C(e) := \{f \in E(G);\ f\ co\ e\}$ denote the set of edges in *G*, codistant to the edge $e \in E(G)$. If relation *co* is an equivalence relation, then *G* is called a *co-graph*. The set *C*(*e*) is called an *orthogonal cut (oc* for short*)* of *G*, with respect to edge *e*. If *G* is a *co-graph* then its orthogonal cuts $C_1, C_2, ..., C_k$ form a partition of *E*(*G*): $E(G) = C_1 \cup C_2 \cup ... \cup C_k,\ C_i \cap C_j = \varnothing, i \neq j$. Observe *co* is a Θ relation, (*Djoković-Winkler* [31-33]).

We say that edges *e* and *f* of a plane graph *G* are in relation *opposite, e op f,* if they are opposite edges of an inner face of *G*. Note that the relation *co* is defined in the whole graph while *op* is defined only in faces. Using the

relation *op* we can partition the edge set of *G* into *opposite* edge *strips, ops.* An *ops* is a quasi-orthogonal cut *qoc*, since *ops* is not transitive.

Let *G* be a connected graph and $s_1, s_2, ..., s_k$ be the *ops* strips of *G*. Then the *ops* strips form a partition of *E(G)*. The length of ops is taken as maximum. It depends on the size of the maximum fold face/ring F_{max}/R_{max} considered, so that any result on Omega polynomial will have this specification.

Denote by *m*(*G*,*s*) the number of *ops* of length *s* and define the Omega polynomial as [34-36]:

$$\Omega(G,x) = \sum_s m(G,s) \cdot x^s \tag{2}$$

Its first derivative (in *x*=1) equals the number of edges in the graph:

$$\Omega'(G,1) = \sum_s m(G,s) \cdot s = e = \left|E(G)\right| \tag{3}$$

On Omega polynomial, the Cluj-Ilmenau index [37], *CI*=*CI*(*G*), was defined:

$$CI(G) = \left\{ [\Omega'(G,1)]^2 - [\Omega'(G,1) + \Omega''(G,1)] \right\} \tag{4}$$

Within this paper, the main results (see Table) refer to $R_{max}(4)$. If faces instead rings are considered, the polynomial complicates both in much more terms and their structural interpretation. Other rings tested were $R_{max}(6)$ and $R_{max}(8)$. In the first case, the inclusion of hexagons consisting the cubeoctahedral units of the co-lattice brings complications in that the number of structural units, clearly envisaged in case of $R_{max}(4)$ (see below), will be lowered in the expense of longer, but more obscure *ops*. In the last case, there is a single strip and the polynomial is written as: $\Omega(G,x) = 1 \times x^s$. Consequently, the index $CI(G) = s^2 - (s + s(s-1)) = s^2 - s^2 = 0$. In this case, the strip is a "Hamiltonian strip" and its length gives just the total number of edges in *G*.

Resuming to our case $R_{max}(4)$, the Omega polynomial has only three terms (see Table). The term at *s*=2 refers to the squares visited from directions where odd rings are limiting the strip length. The term at *s*=4 counts the cubes filling the space (i.e., the interstices) left free from lattice (cube double medial) and co-lattice (cube single medial) main objects, visited from two isolated directions. Finally, the term at maximum exponent counts the main domains of the 3D structure, visited from the coordinate axe directions. We consider that this description is the most informative with respect to the infinite triple periodic crystal-like network herein studied.

The data on the co-lattice are similar to those for the main lattice (in fact is the same structure), the differences reflecting the different borders (as topology and number of atoms) of the cube domain taken into account. Formulas for counting the *CI* values (examples are given) and the number of atoms lying in the two delimitations of the structure are also included in the table.

Table. Formulas for Omega polynomial in *MedMed_all* transform of the Cube (*k*,*k*,*k*) net.

	Formulas
1	$\Omega(x) = a_2 x^2 + a_4 x^4 + a_{\max} x^{e_{\max}}$
2	$\Omega(MedMed\_all(C), x) = 12k(2k-1)x^2 + 6k(k-1)^2 x^4 + 3kx^{4k(k+1)}$
	$\Omega'(MedMed\_all(C), 1) = 12k^2(3k+1)$
	$\Omega''(MedMed\_all(C), 1) = 12k(4k^4 + 8k^3 + 9k^2 - 9k + 4)$
	$CI(MedMed\_all(C)) = 48k(27k^5 + 17k^4 + k^3 - 3k^2 + 2k - 1)$
3	Examples: (2,2,2): $72x^2+12x^4+6x^{24}$; *CI* = 108960 (4,4,4): $336x^2+216x^4+12x^{80}$; *CI* = 6148416 (7,7,7): $1092x^2+1512x^4+21x^{224}$: *CI* = 166257840
4	$\Omega(co-net, x) = 12(k+1)^2 x^2 + 6k(k+1)^2 x^4 + 3kx^{4(k+1)^2}$
	$\Omega'(co-net, 1) = 12(3k+2)(k+1)^2$
	$\Omega''(co-net, 1) = 12(k+1)^2(4k^3 + 8k^2 + 9k + 2)$
	$CI(co-net) = 48(k+1)^2(27k^4 + 89k^3 + 109k^2 + 57k + 11)$
5	Examples: (2,2,2): $108x^2+108x^4+6x^{36}$; *CI* = 736560 (3,3,3): $192x^2+288x^4+9x^{64}$; *CI* = 4418304 (4,4,4): $300x^2+600x^4+12x^{100}$; *CI* = 17509200
6	$v(MedMed\_all(C)) = 12k^2(k+1)$
	$v(co-net) = 12(k+1)^3$

Data were calculated by the original software Nano-Studio [38], developed at TOPO Group Cluj, Romania.

CONCLUSIONS

Omega polynomial $\Omega(G,x)$, defined on opposite edge strips *ops* which are quasi orthogonal cuts *qoc* in a graph, was aimed to be a simple tool in description of the topology of polyhedral molecules and crystal networks. Indeed, the first and second derivatives, in *x*=1, of Omega polynomial provide the Cluj-Ilmenau *CI* index but also an appropriate topological description of the mentioned structures. Close formulas for the Omega polynomial, *CI* index and the number of atoms, are derived for a lattice designed by using operations on maps/networks.

ACKNOWLEDGEMENTS

The article is supported by the Romanian Grant ID_506/2009.

REFERENCES

1. L. Carlucci, G. Ciani and D. Proserpio, *Coord. Chem. Rev*., **2003**, *246*, 247-289.
2. L. Carlucci, G. Ciani and D. Proserpio, *Cryst. Eng. Comm*., **2003**, *5*, 269-279.
3. V.A. Blatov, L. Carlucci, G. Ciani and D. Proserpio, *Cryst. Eng. Comm*., **2004**, *6*, 377-395.
4. I.A. Baburin, V. A. Blatov, L. Carlucci, G. Ciani and D. Proserpio, *J. Solid State Chem*., **2005**, *178*, 2452-2474.
5. O. Delgado-Friedrichs and M. O'Keeffe, *J. Solid State Chem*., **2005**, *178*, 2480-2485.
6. V.A. Blatov, O. Delgado-Friedrichs, M. O'Keeffe, and D. Proserpio, *Acta Cryst.,* **2007**, *A63*, 418-425.
7. M.V. Diudea and A. Ilić, *MATCH Commun. Math. Chem. Comput*., **2009** (submitted).
8. M.V. Diudea and A. Ilić, *MATCH Carpath. J. Math*., **2009** (submitted).
9. M.V. Diudea, A. E. Vizitiu and S. Chiger, *MATCH, Commun. Math. Chem. Comput*., **2009** (submitted).
10. H. Hosoya, *Bull. Chem. Soc. Japan*, **1971**, *44*, 2332-2339.
11. H. Hosoya, *Discrete Appl. Math*., **1988**, *19*, 239-257.
12. E. V. Konstantinova and M. V. Diudea, *Croat. Chem. Acta,* **2000**, *73*, 383-403.
13. I. Gutman, S. Klavžar, M. Petkovšek, and P. Žigert, *MATCH Commun. Math. Chem.*, **2001**, *43*, 49-66.
14. H. Hosoya and T. Yamaguchi, *Tetrahedron Lett*., **1975**, 4659-4662.
15. N. Ohkami and H. Hosoya, *Theoret. Chim. Acta*, **1983**, *64*, 153-170.
16. N. Ohkami, A. Motoyama, T. Yamaguchi, and H. Hosoya, *Tetrahedron*, **1981**, *37*, 1113-1122.
17. H. Hosoya, *Topics Curr. Chem*., **1990**, *153*, 255-272.
18. M.V. Diudea, I. Gutman, and L. Jäntschi, *Molecular Topology*, Nova, N. Y., **2002**.
19. M.V. Diudea, *J. Chem. Inf. Comput. Sci.*, **1994**, *34*, 1064-1071.
20. M.V. Diudea, *MATCH Commun. Math. Comput. Chem*., **2002**, *45*, 109-122.
21. M.V. Diudea and O. Ursu, *Indian J. Chem*., 42*A*, **2003**, 1283-1294.
22. M.V. Diudea, M. S. Florescu and P. V. Khadikar, *Molecular Topology and Its Applications*, EFICON, Bucharest, **2006**.
23. O. Ursu and M.V. Diudea, *TOPOCLUJ*, Babes-Bolyai University, Cluj, **2005**.
24. M.V. Diudea, P.E. John, A. Graovac, M. Primorac, and T. Pisanski, *Croat. Chem. Acta*, **2003**, *76*, 153-159.
25. M.V. Diudea, *Forma (Tokyo)*, **2004**, *19*, 131-163.

26. M.V. Diudea, M. Ştefu, P.E. John, and A. Graovac, *Croat. Chem. Acta*, **2006**, *79*, 355-362.
27. M. Ştefu, M.V. Diudea, and P. E. John, *Studia Univ. Babes-Bolyai*, **2005**, *50*, 165-174.
28. M.V. Diudea, *J. Chem. Inf. Model.,* **2005**, *45,* 1002-1009.
29. M. Stefu, M.V. Diudea, CageVersatile CVNET, Babes-Bolyai University, Cluj, **2007**.
30. M.V. Diudea and Cs. L. Nagy, *MATCH Commun. Math. Comput. Chem.*, **2008**, *60*, 835-844.
31. D.Ž. Djoković, *J. Combin. Theory Ser. B*, **1973**, *14*, 263-267.
32. P.M. Winkler, *Discrete Appl. Math*., **1984**, *8*, 209-212.
33. S. Klavžar, *MATCH Commun. Math. Comput. Chem.*, **2008**, *59*, 217-222.
34. M.V. Diudea, *Carpath. J. Math*., **2006**, *22*, 43-47.
35. M.V. Diudea, S. Cigher and P.E. John, Omega and Related Counting Polynomials, *MATCH Commun. Math. Comput. Chem.*, **2008**, *60*, 237-250.
36. M.V. Diudea, S. Cigher, A.E. Vizitiu, M.S. Florescu, and P.E. John, *J. Math. Chem.*, **2009**, *45*, 316-329.
37. P.E. John, A.E. Vizitiu, S. Cigher and M.V. Diudea, CI Index in Tubular Nanostructures, *MATCH Commun. Math. Comput. Chem.*, **2007**, *57* (2), 479-484.
38. Cs.L. Nagy and M.V. Diudea, *Nano-Studio software*, "Babes-Bolyai" Univ., **2009**.

STUDIA UNIVERSITATIS BABEŞ-BOLYAI, CHEMIA, LIV, 4, 2009

COMPETING ELECTROCHEMICAL AND CHEMICAL DISSOLUTION OF ALUMINUM IN PHOTOPOLYMERIZED ACRYLIC HYDROGELS

JEREMY P. WILBURN[a], CHARLIE DURHAM[b], MADALINA CIOBANU[a], ADRIAN PATRUT[c], DANIEL A. LOWY[d]*

ABSTRACT. Dissolution of aluminum in acrylic hydrogels was studied in printed ultra-thin galvanic cells, in open circuit potential, when only chemical corrosion occurred, and in the presence of external current flow, when the aluminium anode was electrochemically dissolved. By the appropriate design of the Al/hydrogel interface we were able to control the rate of electrochemical dissolution, a process driven by the applied voltage (upon short-circuiting the galvanic cell), and to avoid spontaneous chemical dissolution (and thus, maximizing the shelf life of devices in the absence of current flow). Aluminum anodes (thickness of 30-90 nm) were used in conjunction with a graphite or MnO_2 cathode. Photopolymerized acrylic gels with incorporated inorganic or quaternary ammonium salts served as the supporting electrolyte. The appearance of the first localized chemical damage of the surface defined the shelf life of the cell, and typically was on the order of days. The choice of anion and cation incorporated in the hydrogel affected both the electrochemical and chemical dissolution of aluminum.

Keywords: aluminum dissolution, aluminum anode, acrylic hydrogel, ultra thin galvanic cell, electrochemistry of aluminum.

INTRODUCTION

Over the past decade the organic electrochemistry of aluminum, an intermediately reactive metal, has developed dynamically [1-15]. Studies on the anodic behavior of Al in organic solutions with different electrolytic salts [1-9] and in ionic liquids [10, 11], respectively, were triggered by the use of Al as current collector in Li^+-ion batteries and the need for attenuating the corrosion of Al in such galvanic cells. By contrast, Yu et al. [2] and Licht et al. [12-14] studied galvanic cells equipped with Al anodes, attempting to increase the electrochemical activity of Al in organic media. Given that Al is electrochemically

[a] *Vanderbilt University, Department of Chemistry, Nashville, TN 37235, U.S.A.*
[b] *The University of Memphis, Tennessee, Department of Chemistry, Memphis, TN 38111, U.S.A.*
[c] *Babes-Bolyai University, Faculty of Chemistry and Chemical Engineering, 11 Arany Janos, RO-400028 Cluj-Napoca, Romania*
[d] *Davia, Inc., Woodbridge, VA 22191, U.S.A.; daniellowy@davia.biz*

passive in most organic electrolytes, specific solution phase activators (e.g., dissolved Hg, In, Ga, Sn, or Bi salts) are required [12]. Other research addressed Al corrosion in non-aqueous and mixed aqueous-organic media [15].

In this paper we investigate the behavior of Al in hydrogel media. We report data on the chemical and electrochemical dissolution of Al in ultrathin galvanic cells, in which the supporting electrolyte is either an inorganic or a quaternary ammonium salt, incorporated in a gel type polymer. Gels are obtained by photopolymerizing mixtures with one or two acrylic-type monomers, with water present in the system (hydrogels). We examine the dissolution rate of Al, when an external short is applied to the galvanic cell, and we are able to prevent (or minimize) the dissolution of Al in the open circuit mode. To the best of the authors' knowledge this is the first account on the electrochemical behavior of aluminum in a hydrogel system.

Presence of the thin, highly adherent native aluminum oxide layer prevents Al dissolution in many environments [16]. Chemical dissolution of Al is noticed when microscopic perforations of the natural protective oxide layer allow for the localized damage of the metal surface. For our purposes, the first localized dissolution of Al defines the *shelf life* of the cell; in the examined systems it typically is on the order of days. Electrochemical dissolution, as opposed to chemical dissolution, occurs only upon short-circuiting the galvanic cell; this causes the perforation of the protective oxide layer, and, hence, the flow of an external current.

Ellipsometry performed on 30-90 nm Al films revealed a variable thickness of the natural oxide layer over the surface, in the range of 1.8-24.8 nm, values in agreement with the average thickness of the oxide film reported in the literature [17].

Several components of the gel electrolyte in contact with the Al surface affect the rate of its electrochemical and chemical dissolution: the identity of the anion and cation present in the gel, the degree of cross-linking, the polymerization time, and the storage conditions. Therefore, we discuss these effects in detail.

RESULTS AND DISCUSSION

Choice of the supporting electrolyte

For the proper selection of the supporting electrolyte we considered: (i) the solubility of the salt in one particular photopolymerizable mixture (inorganic salts were incorporated in the hydrogels), (ii) total ionic strength in the hydrogel (the higher the ionic strength, the better the electrochemical activity); and (iii) reactivity of the anion (Cl^- ions attacked Al, while phosphates and tetraborate protected the metal) [18]. As revealed by gravimetric data (Table 1), the identity of the anion in the hydrogel affected significantly the rate of both the electrochemical and chemical dissolution of aluminum.

In the halide series (each at the same concentration) we found that: I^- inhibited the polymerization (as irradiation likely generated free iodine atoms) [19]; with F^- both chemical and electrochemical dissolutions proceeded very slowly (i.e., galvanic cells with F^- had extended shelf life, and the electrochemical dissolution rate was approximately the same as the chemical dissolution rate); with Cl^- present in the gel, the lifetime of galvanic cell decreased five fold as compared to Br^-; surprisingly, the electrochemical dissolution with Br^- was just slightly slower than with Cl^- (less by only 20%). Chloride ion is the main environmental factor, which accelerates pit initiation [20], which accounts for the much greater chemical dissolution rate in the presence of Cl^-.

Table 1: Effect of anions and cations present in the hydrogel on the dissolution rate of Al (data recorded in the two-electrode ultrathin system)

Salt Concentration	Investigated Ion	Electrochemical Dissolution Rate [$\mu g\ cm^{-2}\ s^{-1}$]	Chemical Dissolution Rate [$\mu g\ cm^{-2}\ s^{-1}$]
Potassium halides (0.88 *M*)	F^-	3.10×10^{-2}	3.10×10^{-2}
	Cl^-	27.9	1.57×10^{-2}
	Br^-	23.2	3.36×10^{-3}
	I^-	Interfered with the polymerization	
Other potassium salts (0.44 *M*)	NO_3^-, ClO_3^-, SO_4^{2-}, $H_2PO_4^-$, HPO_4^{-2}, PO_4^{3-}, $B_4O_7^{2-}$	$5 \times 10^{-5} - 2 \times 10^{-3}$	$< 10^{-5}$
Chlorides (0.48 *M*	Li^+, Na^+, K^+, Rb^+, Cs^+	17.6 ± 2.4	$(1.42 \pm 0.04) \times 10^{-2}$

Polyatomic anions, such as NO_3^-, ClO_4^-, HPO_4^{2-}, $H_2PO_4^-$, PO_4^{3-}, and $B_4O_7^{2-}$ were virtually inert; they did not sustain either chemical or electrochemical dissolution (in each experiment the cation was K^+). Current density, recorded upon short-circuiting the ultrathin galvanic cells, corresponds to the electrochemical dissolution rate of Al. Current delivered by the system over time, with various anions in the hydrogel, is displayed in Figure 1a. Nitrate was the least active, yielding maximum current values of less than 10 μA, which lasted just for a few seconds, the current decaying fast after ca. 10 s. While HPO_4^{2-} and PO_4^{3-} showed 7-9 fold greater initial currents than NO_3^-, they were still unable to sustain a constant current, which would correspond to a uniform dissolution rate of Al. Hence, polyatomic anions are not useful in the supporting electrolyte (despite the corrosion inhibiting properties of several of them, which would defer chemical dissolution of Al). When fast electrochemical dissolution is desired, Br^- exhibits the most favorable properties (Table 1): its electrochemical activity is close to that of Cl^- (only 17% less), and in the meanwhile it allows for an extended shelf life of the device (4.7 times longer than in the presence of Cl^-).

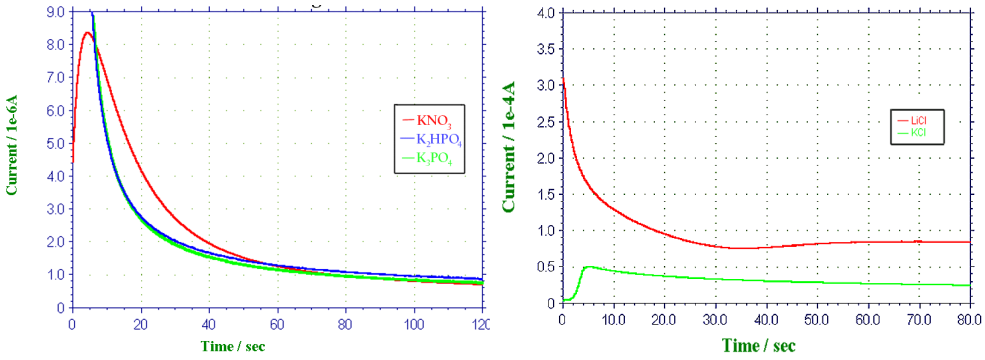

Figure 1. (**a**) Effect of anions on the electrochemical dissolution of Al in acrylic acid/ acrylonitrile copolymers: comparison of NO_3^-, HPO_4^{2-}, and PO_4^{3-}; (**b**) Cation effect on the electrochemical dissolution of Al: comparison of Li^+ (top curve) and K^+ (bottom curve). All experiments were performed with ultra thin galvanic cells (displayed schematically in Figure 3).

When comparing cations immediately after short-circuiting the device, Li^+ showed greater electrochemical dissolution rate than K^+ (Figure 1b), while Na^+ was approximately 40% less active (not shown). Over the long term (200 h) the average dissolution rate became identical for Li^+ and K^+: 102 ng h^{-1}. With CsCl incorporated in the hydrogel, an initial current of 60 μA was recorded over 300 s (a value intermediate between Li^+ and K^+), and then it dropped fast to 10 μA, within 100 s to (graph not shown). Multivalent cations were not useful, as they affected the texture of the hydrogel. Slow chemical dissolution is desirable; therefore, from the cations in Table 1, K^+ is the best choice. However, when fast electrochemical dissolution is attempted, Li^+ salts are the most efficient.

From these studies, best cations were K^+ (for slow electrochemical dissolution) and Li^+ (for fast electrochemical dissolution). When combined with bromide (the most convenient anion), they provided the best salts for being used in hydrogels.

In order to determine the optimal concentration of the supporting electrolyte, we tested the activity of hydrogels, which contained increasing salt concentrations. Electrochemical dissolution rate of Al increased with increasing KCl or KBr content up to 5.5-6.4 wt.%, and then it diminished, probably due to ion pairing. Ion pairs are poor charge carriers, as they do not possess a net charge and stay solvated. Therefore, the conductivity of the hydrogels decreased, and the corrosion current depleted. At high salt concentrations (9.3-11.6 wt.%) charged triplets were formed, and the current increased, again. Unlike ion pairs, triple ions do possess a net charge, and can act as charge carriers. Similar behavior of electrolytes is known in solvents with low dielectric constant [21]. Hence 5.5-6.0 wt.% represents the optimal concentration of the salt in the hydrogel.

These studies on ion effects revealed that while the chemical dissolution rate primarily depends on the adsorption of active anions and the destruction of the natural protective Al_2O_3 layer [22], the electrochemical dissolution is affected by the radius and mobility of the anions. Consequently, the viscosity of the hydrogel and thickness of the hydrogel layer influence to a considerable extent the electrochemical process. In most cases, it has proven an extremely difficult task to identify a system in which electrochemical dissolution can be driven efficiently, while keeping an extended shelf life of the battery via inhibiting spontaneous chemical dissolution.

Selection of monomers and setting the pH of the hydrogel

When keeping the supporting electrolyte concentration constant in the polymer (6.0 wt. %), the corrosion of Al matrices was 10 fold faster in poly(acryloyloxyethyl trimethylammonium chloride), which contains bound charged groups, as compared to acrylic acid/acrylonitrile copolymers, which becomes an ionic conductor via adding a salt to the gel. The looser texture and higher water content of the former hydrogel may allow for an easier migration of the ions, securing by this a better conductivity of the polymer matrix. As a general rule, the recorded current density decreased with decreasing water content of the hydrogel, its lowest value of 5 μA cm^{-2} being observed in the absence of water. We addressed the effect of water content on the polymer matrix in an earlier paper [23].

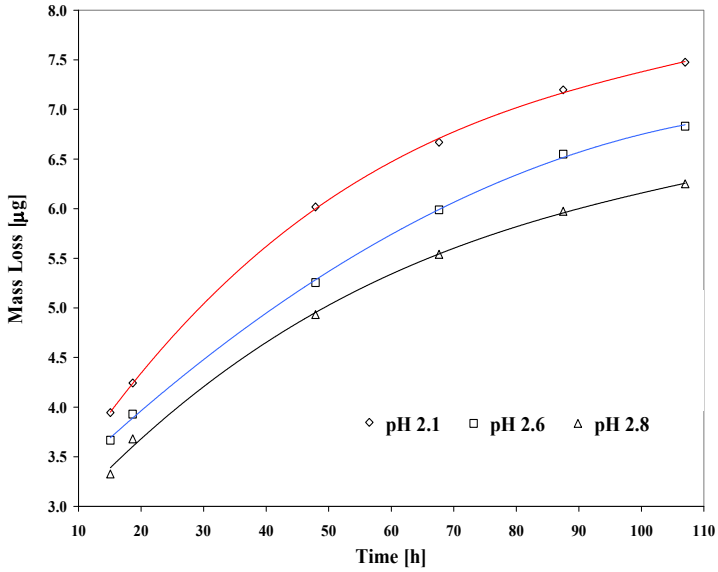

Figure 2. Electrochemical dissolution (mass loss) of Al over time at acidic pH values: bottom line – pH 2.1, middle line – pH 2.6, top line – pH 2.8.

Mass loss of Al over time in contact with hydrogels of decreasing pH value is shown in Figure 2. As the hydrogel becomes more acidic, the system is moved away from the passivity zone of Al (pH 4.0-8.6, according to the Pourbaix diagram [24]). Thus, the electrochemical activity of Al is enhanced and the corrosion rate increases; the average corrosion rate is 38.7 ng h^{-1} at pH 2.8, 40.1 ng h^{-1} at pH 2.6, and 48.6 ng h^{-1} at pH 2.1. Acidic pH values below pH 3.8 are favorable for fast electrochemical dissolution [24]. By setting the pH value we were able to fine-tune the rate of the dissolution process.

CONCLUSIONS

The use of supporting electrolytes incorporated in UV-cured acrylic-type gels allowed for a new approach toward the organic electrochemistry of aluminum. In addition to the chemical identities of the anion and cation, and the selection of the monomer, water content and the pH value of the hydrogel have proven critical to controlling the electrochemical activity of aluminum. Aluminum anodes were active in ultrathin galvanic cells with gel type electrolytes. Driving the electrochemical dissolution, while inhibiting or delaying spontaneous chemical dissolution appears to be an extremely demanding task.

EXPERIMENTAL SECTION

Materials. Gel-type electrolytes were prepared according to previously reported procedures [25, 26]. Typically, hydrogels contained 30-50 wt.% of water and an inorganic salt, such as alkali halides: LiCl, NaCl, RbCl, and CsCl (99+% each, Aldrich), and KCl (Spectro pure, SPEX Industries, Inc.). Several other salts were tested: Na^+ and K^+ chlorates, bromides, nitrates, sulfates, phosphates, hydrogenphosphates, and dihydrogenphosphates (all from Aldrich). For preventing the formation of Al/O_2 batteries, prior to polymerization the curable mixture was degassed with Ar for 15 min [23].

Electrochemical measurements. Electrochemical measurements were conducted with screen-printed ultra thin galvanic cells (Wisconsin Labels Associates, Peachtree City, GA), equipped with Al anode (surface area of 0.20-0.75 cm^2 and thickness of 30-90 nm). Ultrathin galvanic cells operate with Al anode and MnO_2 or graphite cathode; the hydrogel serving as the ionic conductor, is sandwiched between the electrodes (Figure 3). Model 660a Electrochemical Workstation (CH Instruments, Austin, TX) was utilized, measurements being performed under a Faraday cage, at 298.2 ± 0.1 K, thermostated with a Model RTE-210 thermostat (Neslab Instruments, Inc., Newington, NH).

Surface examination. The thickness of the natural protecting Al_2O_3 layer on the surface of Al thin films was determined by ellipsometry with a Model Compel ELC-10 ellipsometer (InomTech Products, Inc., West Hartford, CT), data processing being performed by means of the software supplied

by the manufacturer. Microscopic perforations of the natural protective oxide layer on Al were observed with a stereo magnifier (Bausch & Lomb, magnification 10) and a stereo microscope (Fisher Micromaster®, magnification 400). The thin cell design included a red-colored substrate beneath the thin Al layer to facilitate detection of localized perforations.

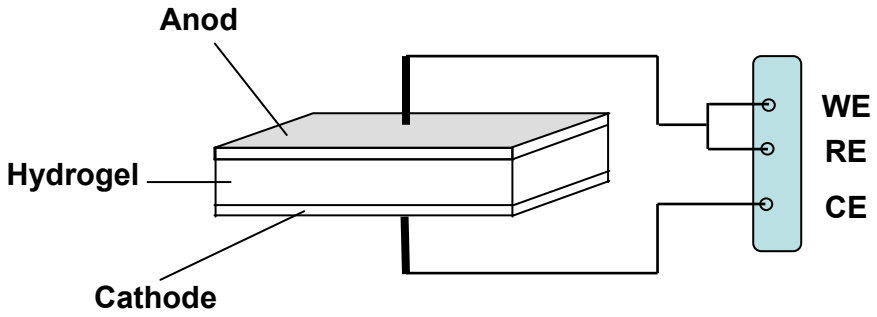

Figure 3. Schematics of the ultra thin galvanic cell setups used for testing of Al in hydrogel electrolytes (Anode: metallic Al; Cathode: graphite or MnO_2; Hydrogel: acrylic polymer; WE – working, RE – reference, and CE – counter electrodes)

Gravimetric method. Dissolution of Al was monitored by gravimetric method, i.e., the weight loss over time of the ultrathin galvanic cell.

ACKNOWLEDGEMENTS

Authors are grateful for support from Wisconsin Labels Associates (Peachtree City, GA), Translucent Technologies, LLC and The University of Memphis (both in Memphis, TN).

REFERENCES

1. J.B. Wang, J.M. Wang, H.B. Shao, X.T. Chang, L. Wang, J.Q. Zhang, C.N. Cao, *Materials and Corrosion – Werkstoffe und Korrosion*, **2009**, *60*, 269.
2. L. Yu, F.C. Liu, Z.W. Fu, *Electrochim. Acta*, **2009**, *54*, 2818.
3. A. Abouimrane, J. Ding, I.J. Davidson, *J. Power Sources*, **2009**, *189*, 693
4. J.B. Wang, J.M. Wang, H.B. Shao, J.Q. Zhang, C.N. Cao, *J. Appl. Electrochem.*, **2007**, *37*, 753.
5. T.C. Hyams, J. Go, T.M. Devine, *J. Electrochem. Soc.*, **2007**, *154*, C390.
6. X.Y. Zhang and T.M. Devine, *Electrochem. Soc.*, **2006**, *153*, B351.

7. X.Y. Zhang and T.M. Devine, *Electrochem. Soc*., **2006**, *153*, B375.
8. X.Y. Zhang, B. Winget, M. Doeff, J.W. Evans, T.M. Devine, *Electrochem. Soc*., **2005**, *152*, B454.
9. T. Kawamura, T. Tanaka, M. Egashira, I. Watanabe, S. Okada, J. Yamaki, *Electrochem. Solid State Lett.*, **2005**, *8*, A459.
10. X.C. Peng, L. Yang, Z.X. Zhang, K. Tachibana, Y. Yang, S.Y. Zhao, *Elchim. Acta*, **2008**, 53, 4764.
11. C.X. Peng, L. Yang, Z.X. Zhang, K.H. Tachibana, Y. Yang, *J. Power Sources*, **2007**, *173*, 510.
12. G. Levitin, C. Yarnitzky and S. Licht, *Electrochem. Solid State Lett.*, **2002**, *5*, A163.
13. S. Licht, G. Levitin, R. Tel-Vered, C. Yarnitzky, *Electrochem. Comm*., **2000**, *2*, 329.
14. S. Licht, R. Tel-Vered, G. Levitin, C. Yarnitzky, *Electrochem. Soc*., **2000**, *147*, 496.
15. L.R.B. Holzle, D.S. Azambuja, C.M.S. Piatnicki, G.E. Englert, *Mater. Chem. Phys*., **2005**, *91*, 375.
16. S.K. Toh, D.G. McCulloch, J. Du Plessis, P.J.K. Paterson, A.E. Hughes, D. Jamieson, B. Rout, J.M. Long, A. Stonham, *Surface Rev. Lett*., **2003**, *10*, 365.
17. E. McCafferty, Surface Hydroxyls: the Outermost Layer of the Passive Film, in: R.G. Kelly, G.S. Frankel, P.M. Natishan, R.C. Newman (Eds.), *Electrochemical Society Proceedings*, Vol. 98-17, 1998, pp. 42-55.
18. D.A. Lowy and J.P. Wilburn, 'Electrochemistry of Aluminum in Organic Hydrogel Systems,' 219th ACS Meeting, San Francisco, CA, March 26-30, 2000, Paper #382231.
19. J.P. Wilburn, M. Ciobanu, N.I. Buss, D.R. Franceschetti, D.A. Lowy, *Anal. Chim. Acta*, **2004**, *511*, 83.
20. J.W. Braithwaite, A. Gonzales, G. Nagasubramanian, S.J. Lucero, D.E. Peebles, J.A. Ohlhausen, W.R. Cieslak, *J. Electrochem. Soc*., **1999**, *146*, 448.
21. J.O'M. Bockris, A.K.N. Reddy, *Modern Electrochemistry*, Plenum Press, New York, 1999.
22. M.Z.A. Munshi, R. Gopalienger, B.B. Owens, *Solid State Ionics*, **1988**, *27*, 259.
23. J.P. Wilburn, M. Ciobanu, D.A. Lowy, *J. Appl. Electrochem.*, **2004**, *34*, 729.
24. R.J. Small, M.L. Peterson, A. Robles, D. Kempa, J. Knittel, *Micro*, **1998**, *16*, 61.
25. M. Ciobanu, J.P. Wilburn, N.I. Buss, P. Ditavong, D.A. Lowy, *Electroanalysis*, **2002**, *14*, 989.
26. M. Ciobanu, J.P. Wilburn, D.A. Lowy, *Electroanalysis*, **2004**, *16*, 1351.

STUDIA UNIVERSITATIS BABEŞ-BOLYAI, CHEMIA, LIV, 4, 2009

GAS CHROMATOGRAPHY-MASS SPECTROMETRY METHOD FOR DETERMINATION OF MONOTERPENE AND SESQUITERPENE EMISSIONS FROM STRESSED PLANTS

LUCIAN COPOLOVICI[a], ASTRID KÄNNASTE, ÜLO NIINEMETS

ABSTRACT. Emissions of biogenic volatile organic compounds (BVOCs) play important roles in plant biology and atmospheric chemistry at a wide range of spatial and temporal scales. This article describes a headspace method coupled with gas chromatography – mass spectrometry (GC-MS) for the detection of volatile terpenes (monoterpenes and sesquiterpenes) and other related compounds emitted from plants, especially under stress conditions. A protocol is developed for simultaneous detection and quantification of isoprene, and mono- and sesquiterpenes from plant emissions.

Keywords: BVOC emission, Mass spectrometry, Monoterpenes, Plant stress, Sesquiterpenes

INTRODUCTION

Plants emit more than 30000 chemically different volatile organic compounds (BVOC). The emissions of some of these compounds result from and serve as markers of activation of certain metabolic pathways in plants, end-products or intermediates of which are volatile [1]. Many of these volatiles also play important roles in plant communication with other plants and animals [2]. There are further constitutive emissions of several specific volatile compounds thought to be involved in plant non-specific defence to various abiotic and biotic stresses [1, 3]. Worldwide, it has been estimated that biogenic production of volatile organic compounds exceeds the anthropogenic production by an order of magnitude. Apart from the significance for plants, these emissions play important role in atmospheric chemistry and physics, in particular in formation of atmospheric pollutant ozone in the troposphere and formation of aerosols [4-7].

The volatile isoprenoids – isoprene (5 carbon atoms, C5) and volatile terpenes consisting of isoprene building blocks, monoterpenes (C10, MT) and sesquiterpenes (C15, SQT) – form a major part of plant-generated BVOC. Several widespread plant species are strong constitutive emitters of volatile isoprenoids, while volatile isoprenoid emissions can be induced by various environmental and biotic stimuli also in species not emitting these compounds constitutively [8, 9].

[a] *Institute of Agricultural and Environmental Sciences, Estonian University of Life Sciences, Kreutzwaldi 1, Tartu 51014, Estonia*

Plant volatile isoprenoid emissions consist of a complex blend of chemically heterogeneous compounds. Often more than 20 different MT [10, 11] are emitted by a single plant species. These compounds have widely differing chemical reactivity and ozone-forming potentials in the atmosphere [12]. A number of SQT and some oxygenated sesquiterpene alcohols, aldehydes, and ketone derivatives ($C_{15}H_{22}O$, $C_{15}H_{24}O$, $C_{15}H_{26}O$) have further been identified in studies on BVOC emissions from both natural [13-17] and agricultural vegetation [18, 19]. All volatile isoprenoids, isoprene, MT and SQT, are anticipated to importantly participate in secondary aerosol-forming processes and in chemical reactions in the lower troposphere [6, 16, 21-23], but SQT are generally more reactive than isoprene and MT. The atmospheric lifetimes of reactive SQT such as β-caryophyllene as determined by their rapid gas-phase reactions with ozone, and OH and NO_3 radicals have been estimated to be on the order of only a few minutes[11, 15], while the life-time of isoprene and most monoterpenes varies between 36 min during daytime in summer and a few hours during nighttime in winter [24].

A vast array of volatile terpenes (MT and SQT) is involved in the communication between plants and between plants and herbivores [9, 25-29]. Under stress, the emissions of volatile isoprenoids may be amplified in constitutive emitters and be induced also in species not emitting these compounds constitutively [8, 9], modifying the plant communication with other organisms. For instance, emission of *de novo* synthesized compounds such as methylsalicylate, farnesenes, (*E*)-*β*-ocimene, linalool, *etc*, which serve as signals of the induced defence reactions in stressed plants, is often observed in plants not emitting isoprenoids in non-stressed conditions [30, 31]. Plant-insect relationships can also be altered by increased emissions of other stress compounds that occur simultaneously with enhanced isoprenoid emissions, e.g. emissions of green leaf volatiles (GLV, volatile aldehydes formed via the lipoxygenase pathway) occur in stressed plants as the result of the destruction of free fatty acids in lipoxygenase pathway [31, 32]. Apart from plant communication, volatile isoprenoid emissions are also thought to increase the plant tolerance to a variety of biotic and abiotic stresses [3 for a review].

Simultaneous measurement of the wide spectrum of plant volatiles with different physico-chemical characteristics constitutes an analytical challenge. Preconcentration of BVOCs on cartridges filled with solid adsorbents followed by thermal desorption and GC analysis has become a well-accepted analysis technique in a wide range of applications [14, 33, 34]. Additionally, other methods based on the sampling of headspace into stainless steel canisters followed by cryo-focusing and analysis by gas chromatography equipped with the flame ionization detector (GC-FID) analysis [35], or the technique for rapid collection of volatiles by solid-phase micro-extraction (SPME) coupled with GC-MS have been used [36-38]. The techniques described in the literature are generally for compounds in the range of volatility of C5–C10. In contrast, the

applicability of adsorbent sampling/thermal desorption for semi-volatile BVOC has received much less attention and application (see [39, 40] for review). The most commonly used adsorbents include diverse carbon adsorbents (active carbon, graphitized carbon, and carbon molecular sieves) and also synthetic polymeric adsorbents (Tenax, Chromosorb, etc.) [39, 41].

The goal of this study was to develop a quantitative method for simultaneous determination of mono- and sesquiterpenes in air samples from plants exposed to different biotic and abiotic stresses. The developed method is based on preconcentration of BVOCs on solid absorbents coupled with GC-MS analysis, and is optimized for quantitative determination of plant volatiles with widely varying physico-chemical properties.

RESULTS AND DISCUSSION

Combinations of adsorbents in a single adsorbent cartridge (volatile trap) have been previously used to trap and analyze compounds over a wider range of volatility than can be achieved with a single adsorbent [42]. In preliminary experiments of our study, the type and the amount of absorbent, and the cleanup method of adsorbent cartridges were optimized. We finally used the combination of Carbotrap C, Carbopack C and Carbotrap X for the multibed cartridges. These chemically neutral carbon-based adsorbents permit trapping of unsaturated compounds (*e.g.* monoterpenes) without intervening chemical reactions in the ambient air that can for instance happen with organic polymer adsorbents such as Tenax TA in oxidative atmosphere [43].

Several GC parameters and oven temperature program were optimized to achieve excellent separation of main mono- and sesquiterpenes emitted from the stressed plants in a single GC column. Different temperature regimes, flow rates of carrier gas and columns with differing polarity were tested. Ions based on the following criteria were selected for compound detection: (i) molecular ions for compound detection (together with the fragment mass spectrum); (ii) fragment ions with high abundance, such as base peaks; (iii) target ions with selectivity minimizing the cross-interferences between different BVOC's. Based on these criteria, scanning tests of the standard solutions trapped in cartridge of each monoterpene and sesquiterpene were carried out to describe the scanning mass spectrum and retention time of various isoprenoids. One target ion and two qualitative ions (qualifiers) for each compound were selected (Table 1). Operative conditions (oven program, time and temperature of desorption etc) were fixed on the basis of optimization results. Overall, the retention times of terpene standards were relatively concentrated in two parts of the chromatogram: one part featuring most of the monoterpene peaks and the other most sesquiterpene peaks. Among the tested columns (DB-1, DB-2, ZB-5) a fused silica ZB-624 column proved to provide the best separation of common monoterpenes and sesquiterpenes present in the emission of stressed plants (Table 1).

Table 1. Chromatographic and mass spectral data obtained by the GC-MS methods for all the tested terpene standards and methylsalicylate

	Molecular mass (g mol^{-1})	Retention time (min.)	Target ion (m/z)	Qualifiers* (m/z)
α-Pinene	136	18.74	93	92, 91
β-Pinene	136	21.44	93	41, 69
α-Phellandrene	136	22.56	93	91, 77
Δ^3-Carene	136	22.88	93	91, 77
α-Terpinene	136	23.33	93	121, 91
(*E*)-β-Ocimene	136	23.72	93	92, 91
Limonene	136	23.94	68	67, 93
β-Phellandrene	136	24.39	93	91, 77
1,8-Cineole (Eucalyptol)	154	24.78	43	81, 71
γ-Terpinene	136	25.60	93	91, 77
α-Terpinolene	136	27.46	93	121, 136
4,8-Dimethyl-1,3,7-nonatriene	150	28.80	69	41, 81
Linalool	154	29.87	71	43, 81
α-Thujone	152	31.74	81	110, 41
β-Thujone	152	32.47	110	81, 41
Methylsalicylate	204	37.73	120	92, 152
Bornyl acetate	204	42.67	95	43, 93
(*Z*)-β-Farnesene	204	49.51	69	41, 93
α-Cedrene	204	50.38	119	93, 105
(*E*)-β-Caryophyllene	204	51.08	41	69, 93
α-Humulene	204	53.25	93	80, 41, 121
(*E*,*E*)-α-Farnesene	204	53.83	93	41, 69
Nerolidol	204	56.33	69	41, 43

* The qualifier ion (or SRM transition) is often an isotope peak or a higher mass product ion as opposed to the second most abundant ion in the spectra.

Terpene quantification was based on the total ion current monitored by the GC-MS system calibrated with terpene standards.

The GC-MS response for all monoterpenes and sesquiterpenes was linear in the concentration range assayed ($3\cdot10^{-9}$-$1\cdot10^{-7}$ mol/L). Relevant data from the calibration plots are summarized in Table 2. It is apparent that the linear calibration ranges and the slopes (analytical sensitivity) of the calibration

graphs are similar for all the mono and sesquiterpenes investigated. The detection limits of the method were estimated as three times of standard deviation of the response (10 determinations) to a blank sample. The values found ranged between 0.1 and 4.7 nmol mL^{-1}, depending on the terpene. The average relative standard deviation was 0.2% for ten samples.

Table 2. Features of calibration plots for the determination of different terpenes

	Slope* (area mol^{-1} L^{-1})	Relative standard deviation of the slope (%)	Correlation coefficient	Detection limit (nmol mL^{-1})
α-Pinene	$6.76 \cdot 10^{16}$	1.0	0.995	1.6
β-Pinene	$5.87 \cdot 10^{16}$	0.9	0.992	1.8
α-Phellandrene	$3.90 \cdot 10^{16}$	5.1	0.994	2.7
Δ^3-Carene	$5.05 \cdot 10^{16}$	5.0	0.995	2.1
α-Terpinene	$4.71 \cdot 10^{16}$	3.1	0.995	2.3
(*E*)-β-Ocimene	$2.28 \cdot 10^{16}$	4.8	0.991	4.7
Limonene	$7.42 \cdot 10^{16}$	5.8	0.993	1.4
β-Phellandrene	$5.19 \cdot 10^{16}$	5.2	0.997	2.1
1,8-Cineole (Eucalyptol)	$7.52 \cdot 10^{16}$	6.1	0.994	1.4
γ-Terpinene	$4.71 \cdot 10^{16}$	6.0	0.995	2.3
α-Terpinolene	$7.72 \cdot 10^{16}$	4.9	0.998	1.4
4,8-Dimethyl-1,3,7-nonatriene	$3.29 \cdot 10^{16}$	4.9	0.992	3.3
Linalool	$7.51 \cdot 10^{16}$	3.5	0.991	1.4
α-Thujone	$3.24 \cdot 10^{16}$	2.2	0.990	3.3
β-Thujone	$2.06 \cdot 10^{16}$	6.1	0.991	5.2
Methylsalicylate	$5.94 \cdot 10^{19}$	1.2	0.993	0.1
Bornyl acetate	$9.93 \cdot 10^{17}$	1.1	0.994	0.1
(*Z*)-β-Farnesene	$2.90 \cdot 10^{16}$	5.2	0.992	2.9
α-Cedrene	$2.03 \cdot 10^{17}$	2.3	0.994	0.4
(*E*)-β-Caryophyllene	$1.39 \cdot 10^{17}$	3.2	0.996	0.6
α-Humulene	$1.23 \cdot 10^{17}$	4.5	0.997	0.7
(*E*,*E*)-α-Farnesene	$2.45 \cdot 10^{16}$	2.4	0.991	3.4
Nerolidol	$2.77 \cdot 10^{17}$	5.6	0.993	0.3

* Based on three calibration curves y = slope x, y: peak-area ratio, x: terpene concentration (mol/L).

In chemistry, the emission rate is defined as the amount of given substance released to the air per unit of time. In plants, the emission rate is normalized with leaf area or leaf dry mass. In the literature, area-based plant emissions are commonly expressed in nmol m^{-2} s^{-1}, while for mass-basis ng g dw^{-1} h^{-1} is often employed [44]. We recommend always to use SI units and express the compound emission in molar units.

Our GC-MS method was applied for quantification of a vast array of mono- and sesquiterpenes released from differently stressed plants. Figure 1 shows chromatograms of sunflower (*Helianthus annuus* L.) leaf emissions under controlled conditions (chamber temperature of 25 °C) (A) and after 5 min. temperature stress at 51 ^{O}C (B) measured 1 min. after application of the heat pulse. This pilot experiment demonstrates that cold stress significantly enhances the emissions of monoterpenes in *Helianthus annuus L.* (Figure 2).

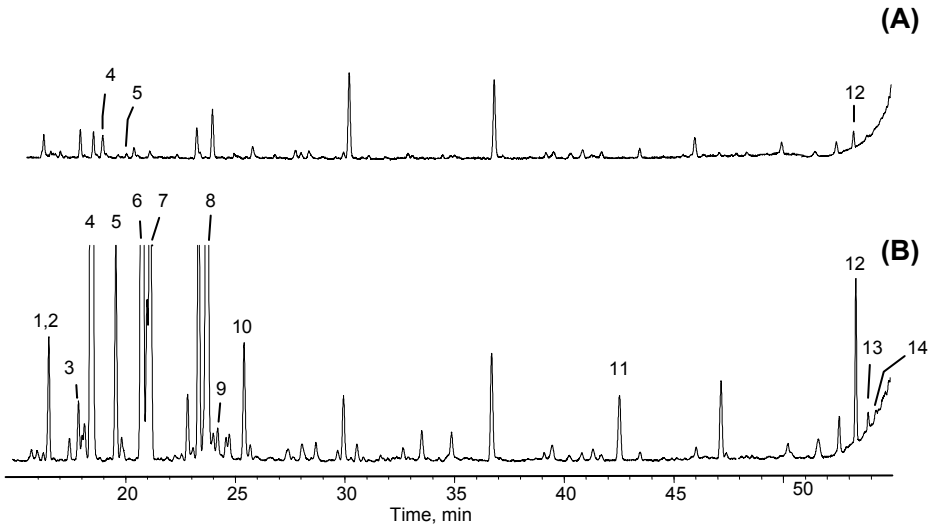

Figure 1. Chromatograms of sunflower (*Helianthus annuus* L.) leaf emissions. A: control plant; B: plant measured 1 min. after application of a 5 min. heat pulse of at 51 ^{o}C. Identified compounds – 1,2: (3*Z*)-hexenol co-eluted with (2*E*)-hexenal; 3: *α*-thujene; 4: *α*-pinene; 5: camphene; 6: sabinene; 7: *β*-pinene; 8: limonene; 9: *β* -phellandrene; 10: γ-terpinene; 11: bornyl acetate; 12: geranyl acetone; 13: (*E*,*E*)-*α*-farnesene; 14: germacrene D.

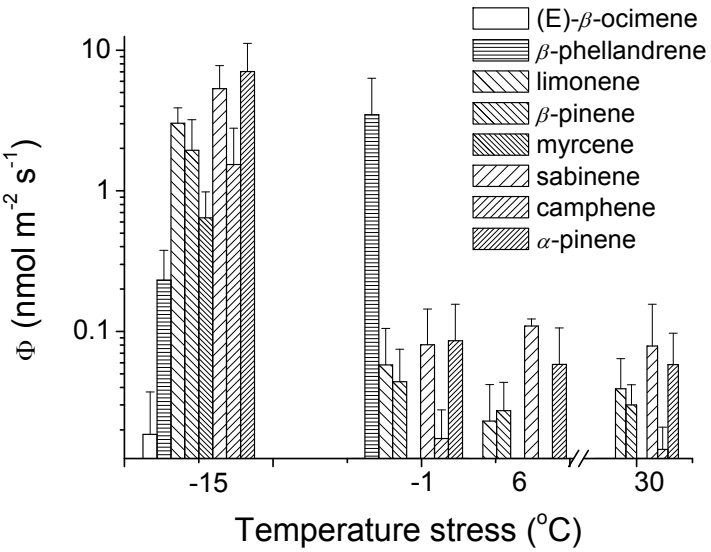

Figure 2. The emission rates (Φ) of monoterpenes from sunflower (*Helianthus annuus* L.) leaves measured after 1 min. exposure to 5 min. pulses of cold stress. *N* = 3 for all treatments.

Analogous results were obtained with tomato (*Lycopersicum esculentum* Mill.) plants under heat and cold stress (Figure 3).

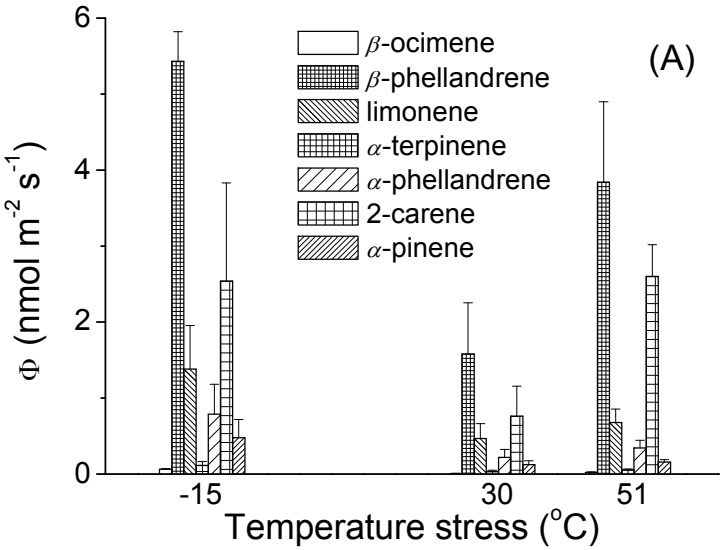

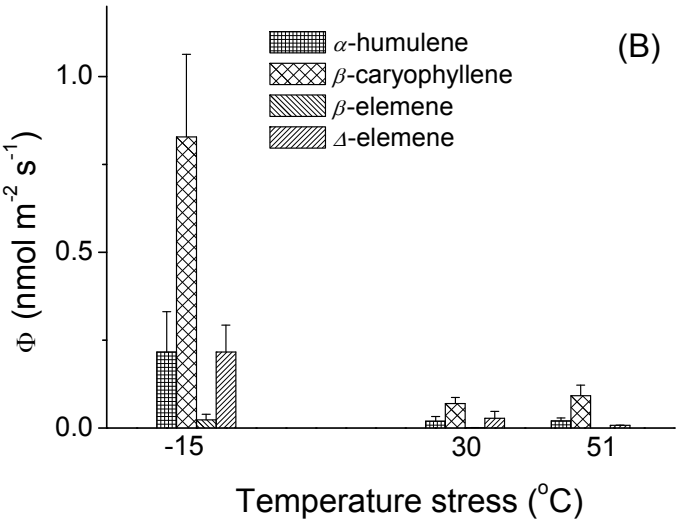

Figure 3. The emission rates (Φ) of monoterpenes (A) and sesquiterpenes (B) from tomato (*Lycopersicum esculentum* Mill.) leaves measured after 1 min. exposure to 5 min. pulses of heat and cold stress. *N* = 3 for all treatments.

CONCLUSIONS

The major drawback with current plant stress studies is that with very few exceptions [8] plant stress responses, including emissions, are not quantitatively assessed. Our method permits to obtain quantitative relationships between signal strength and plant response, and thus, to develop quantitative plant stress models. These models are needed to predict plant responses to environmental stress and simulate plant volatile compound emissions under different environmental conditions.

EXPERIMENTAL SECTION

All chemicals were purchased from Sigma-Aldrich, (St. Louis, MO, USA, GC purity) with exception of 4,8-dimethyl-1,3,7-nonatriene (DMNT) which was synthesized from commercial citral using methyltriphenylphosphonium bromide and butyl lithium at Kuopio University, Kuopio, Finland [45].

All plants used in measurements were grown from seeds. Plants were grown in 1 L clay pots filled with commercially-available potting soil and were watered daily. The gas exchange measurements were performed using a custom-built gas-exchange system described in detail in Rasulov et. al. [46]. Shortly, the flow-through plant chamber of 1.2 L was made of two glass layers. Water with set temperature was circulated between the outer and

inner glass layers to control the chamber temperature. All tubing in the system was made of stainless steel or Teflon. Flow rate through the system was maintained at 1.4 L min^{-1}. Light was provided by four perpendicularly positioned 50 W halogen lamps, and light intensity could be regulated between 0-1000 $\mu mol\ m^{-2}\ s^{-1}$ by changing the lamp voltage. In these experiments the light intensity was kept at 650 $\mu mol\ m^{-2}\ s^{-1}$.

Volatiles from the chamber exhaust air were adsorbed at a flow rate of 200 ml min^{-1} for 20 min. (altogether 4L air) onto multibed stainless steel cartridges (10.5 cm length, 3 cm inner diameter, Supelco, Bellefonte, USA) filled with Carbotrap C 20/40 mesh (0.2 g), Carbopack C 40/60 mesh (0.1 g) and Carbotrap X 20/40 mesh (0.1 g) adsorbents (Supelco, Bellefonte, USA). Before the collection of volatiles, the traps were cleaned by the passage of a stream of ultrapure helium at a flow rate of 200 ml min^{-1} and at temperature of 250 °C for 2 hours. Sampling of plant volatiles was done at room temperature of 25 °C. Background air samples were collected from the empty chamber before and after the measurements. Adsorbent cartridges were analyzed with a combined Shimadzu TD20 automated cartridge desorber and Shimadzu QP2010 plus GC MS instrument (Shimadzu Corporation, Kyoto, Japan). The following TD20-parameters were used: He purge flow 40 ml min^{-1}, primary desorption temperature 250 °C, primary desorption time 6 min, second stage trap temperature during primary desorption: −20°C, second stage trap desorption temperature 280°C, hold time 6 min. Adsorbent cartridges were backflushed with high purity He during thermal desorption. A Zebron ZB-624 fused silica capillary column (0.32 mm i.d.×60 m, 1.8 µm film thickness, Phenomenex, USA) was employed for the volatile separation using the following GC oven program: 40 °C for 1 min, 9 °C min^{-1} to 120 °C, 2 °C min^{-1} to 190 °C, 20 °C min^{-1} to 250 °C, 250 °C for 5 min. The GC carrier gas was He (99.9999%, Elmer Messer Gaas AS, Tallinn, Estonia) with 1.48 ml min^{-1}. Shimadzu QP2010 Plus mass spectrometer was operated in the electron impact mode. The transfer line temperature was set at 240 °C and ion-source temperature at 150 °C. The absolute amounts of terpenes were calculated based on an external standard consisting of known amounts of mono and sesquiterpenes. The compounds were identified by comparing the mass spectrum of an individual compound to the spectra of compounds in external standard and in the NIST Library.

ACKNOWLEDGMENTS

The authors are grateful for the financial support from the Estonian Ministry of Science and Education (grant SF1090065s07) and the Estonian Science Foundation (grant 7645, post-doctoral grants JD101 and MJD8-2/T9094PKPK). Special thanks are due to Prof. Dr. J. Holopainen (Kuopio University, Kuopio, Finland) for their generous supply of 4,8-dimethyl-1,3,7-nonatriene (DMNT).

REFERENCES

1. S.M. Owen, J. Peñuelas, *Trends in Plant Science*, **2005**, *10*, 420.
2. E. Pichersky, J. Gershenzon, *Current Opinion in Plant Biology*, **2002**, *5*, 237.
3. C.E. Vickers, J. Gershenzon, M.T. Lerdau, F. Loreto, *Nature Chemical Biology*, **2009**, *5*, 283.
4. W. Chameides, R. Lindsay, J. Richardson, C. Kiang, *Science*, **1988**, *241*, 1473.
5. K.E. Huff Hartz, T. Rosenørn, S.R. Ferchak, T.M. Raymond, M. Bilde, N.M. Donahue, S.N. Pandis, *Journal of Geophysical Research - Atmospheres*, **2005**, *110*, D14208.
6. T.M. VanReken, N.L. Ng, R.C. Flagan, J.H. Seinfeld, *Journal of Geophysical Research-Atmospheres*, **2005**, *110*.
7. F. Fehsenfeld, J. Calvert, R. Fall, P. Goldan, A.B. Guenther, C.N. Hewitt, B. Lamb, S. Liu, M. Trainer, H. Westberg, P. Zimmerman, *Global Biogeochemical Cycles*, **1992**, *6*, 389.
8. J. Beauchamp, A. Wisthaler, A. Hansel, E. Kleist, M. Miebach, U. Niinemets, U. Schurr, J. Wildt, *Plant Cell and Environment*, **2005**, *28*, 1334.
9. F. Brilli, P. Ciccioli, M. Frattoni, M. Prestininzi, A.F. Spanedda, F. Loreto, *Plant Cell and Environment*, **2009**, *32*, 542.
10. U. Niinemets, M. Reichstein, *Global Biogeochemical Cycles*, **2002**, *16*.
11. N. Theis, M. Lerdau, *International Journal of Plant Sciences*, **2003**, *164*, S93.
12. A. Arneth, R.K. Monson, G. Schurgers, U. Niinemets, P.I. Palmer, *Atmospheric Chemistry and Physics*, **2008**, *8*, 4605.
13. B. Bonn, A. Hirsikko, H. Hakola, T. Kurten, L. Laakso, M. Boy, M. Dal Maso, J. M. Makela, M. Kulmala, *Atmospheric Chemistry and Physics*, **2007**, *7*, 2893.
14. D. Helmig, J. Ortega, T. Duhl, D. Tanner, A. Guenther, P. Harley, C. Wiedinmyer, J. Milford, T. Sakulyanontvittaya, *Environmental Science & Technology*, **2007**, *41*, 1545.
15. N.C. Bouvier-Brown, R. Holzinger, K. Palitzsch, A.H. Goldstein, *Atmospheric Environment*, **2009**, *43*, 389.
16. T. Sakulyanontvittaya, T. Duhl, C. Wiedinmyer, D. Helmig, S. Matsunaga, M. Potosnak, J. Milford, A. Guenther, *Environmental Science & Technology*, **2008**, *42*, 1623.
17. T. R. Duhl, D. Helmig, A. Guenther, *Biogeosciences*, **2008**, *5*, 761.
18. R.J. Bartelt, D. T. Wicklow, *Journal of Agricultural and Food Chemistry*, **1999**, *47*, 2447.
19. P. Ciccioli, E. Brancaleoni, M. Frattoni, V. Di Palo, R. Valentini, G. Tirone, G. Seufert, N. Bertin, U. Hansen, O. Csiky, R. Lenz, M. Sharma, *Journal of Geophysical Research-Atmospheres*, **1999**, *104*, 8077.
20. A. Guenther, C.N. Hewitt, D. Erickson, R. Fall, C. Geron, T. Graedel, P. Harley, L. Klinger, M. Lerdau, W.A. McKay, T. Pierce, B. Scholes, R. Steinbrecher, R. Tallamraju, J. Taylor, P. Zimmerman, *Journal of Geophysical Research*, **1995**, *100*, 8873.

21. M. Claeys, B. Graham, G. Vas, W. Wang, R. Vermeylen, V. Pashynska, J. Cafmeyer, P. Guyon, M. O. Andreae, P. Artaxo, W. Maenhaut, *Science*, **2004**, *303*, 1173.
22. T. Sakulyanontvittaya, A. Guenther, D. Helmig, J. Milford, C. Wiedinmyer, *Environmental Science & Technology*, **2008**, *42*, 8784.
23. W. Vizuete, V. Junquera, D. . Allen, *Aerosol Science and Technology*, **2004**, *38*, 167.
24. E. Liakakou, M. Vrekoussis, B. Bonsang, C. Donousis, M. Kanakidou, N. Mihalopoulos, *Atmospheric Environment*, **2007**, *41*, 1002.
25. J.D. Blande, K. Turunen, J.K. Holopainen, *Environmental Pollution*, **2009**, *157*, 174.
26. R. M. C. Jansen, J. W. Hofstee, J. Wildt, F. W. A. Verstappen, H. J. Bouwmeester, M. A. Posthumus, E. J. van Henten, *Annals of Applied Biology*, **2009**, *154*, 441.
27. R.W. Jost, A.V. Rice, D.W. Langor, Y. Boluk, *Journal of Wood Chemistry and Technology*, **2008**, *28*, 37.
28. U. Niinemets, F. Loreto, M. Reichstein, *Trends in Plant Science*, **2004**, *9*, 180.
29. J. Penuelas, J. Llusia, *Trends in Plant Science*, **2003**, *8*, 105.
30. A.B. Johne, B. Weissbecker, S. Schutz, *Journal of Chemical Ecology*, **2006**, *32*, 2303.
31. L. Chen, H. Y. Fadamiro, *Bulletin of Entomological Research*, **2007**, *97*, 515.
32. J.C. Dickens, R.F. Billings, T.L. Payne, *Experientia*, **1992**, *48*, 523.
33. D. Helmig, F. Bocquet, J. Pollmann, T. Revermann, *Atmospheric Environment*, **2004**, *38*, 557.
34. D. Tholl, W. Boland, A. Hansel, F. Loreto, U. S. R. Rose, J.P. Schnitzler, *Plant Journal*, **2006**, *45*, 540.
35. S. Pressley, B. Lamb, H. Westberg, A. Guenther, J. Chen, E. Allwine, *Atmospheric Environment*, **2004**, *38*, 3089.
36. S. Vichi, J.M. Guadayol, J. Caixach, E. Lopez-Tamames, S. Buxaderas, *Journal of Chromatography A*, **2006**, *1125*, 117.
37. N. Yassaa, J. Williams, *Journal of Chromatography A*, **2007**, *1141*, 138.
38. A. Kannaste, N. Vongvanich, A.K. Borg-Karlson, *Arthropod-Plant Interactions*, **2008**, *2*, 31.
39. J. Ortega, D. Helmig, *Chemosphere*, **2008**, *72*, 343.
40. J. Ortega, D. Helmig, R.W. Daly, D.M. Tanner, A.B. Guenther, J.D. Herrick, *Chemosphere*, **2008**, *72*, 365.
41. W. Kornacki, P. Fastyn, T. Gierczak, I. Gawlowski, J. Niedzielski, *Chromatographia*, **2006**, *63*, 67.
42. P. Ciccioli, A. Cecinato, E. Brancaleoni, M. Frattoni, A. Liberti, *Hrc-Journal of High Resolution Chromatography*, **1992**, *15*, 75.
43. A. Calogirou, B.R. Larsen, C. Brussol, M. Duane, D. Kotzias, *Analytical Chemistry*, **1996**, *68*, 1499.
44. J. Kesselmeier, M. Staudt, *Journal of Atmospheric Chemistry*, **1999**, *33*, 23.
45. M.A. Ibrahim, A. Stewart-Jones, J. Pulkkinen, G.M. Poppy, J.K. Holopainen, *Plant Biology*, **2008**, *10*, 97.
46. B. Rasulov, L. Copolovici, A. Laisk, U. Niinemets, *Plant Physiology*, **2009**, *149*, 1609.

STUDIA UNIVERSITATIS BABEŞ-BOLYAI, CHEMIA, LIV, 4, 2009

USING THE TOPOLOGICAL INDEX ZEP IN QSPR STUDIES OF ALCOHOLS

ZOIȚA MĂRIOARA BERINDE[a]

ABSTRACT The paper is devoted to the modelling of a class of molecular compounds containing heteroatoms (alcohols) by means of the concept of weighted electronic distance and the corresponding connectivity matrix CEP. A topological index derived from this matrix, the ZEP topological index, is then correlated with the boiling point (BP) and the water solubility (log(1/S)) of alcohols, using simple and multiple linear regression analysis. In order to improve the simple models we also calculated a novel parameter, H_d, derived from the usual topological distances between the vertices of the graph. The obtained results indicate the combination of ZEP and H_d indices as a promise in the QSPR analysis of complex compounds.

Keywords: weighted electronic distance; CEP connectivity matrix; ZEP topological index; parameter $H_{d,}$ linear regression analysis.

INTRODUCTION

A chemical compound can be represented by using the concept of molecular graph *G*. A molecular graph can itself be represented by several topological matrices [1-4]. The most used matrices are the adjacency matrix, *A*=*A*(*G*), and the distance matrix, *D*=*D*(*G*). The mathematical modelling of chemical structures by using descriptors derived from the molecular graphs, by means of topological matrices, has grown rapidly in the last decade [5-7]. Among these descriptors, the topological indices have been widely used in QSPR (Quantitative Structure-Property Relationship) and QSAR (Quantitative Structure–Activity Relationship) analysis. Both adjacency and distance matrices, in their original form [2-4], are appropriate for modelling chemical compounds with no multiple bonds or heteroatoms. When structurally different molecules, such as isobutane, isobutene, 2-propanol, 2-cloropropane, 2-aminopropane, are under study, difficulties appear in amending the classical topological matrices to account for there structural differences. The question how to represent the multiple bonds and/or heteroatoms, gained more than one answer.

[a] *Department of Chemistry and Biology, North University of Baia Mare, Romania, e-mail: zoitaberinde@ubm.ro; zoita_berinde@yahoo.com*

A first approach to represent heteroatoms and multiple bonds has been proposed by Kier and Hall [8], and also by Barysz and collaborators [9]. Basak and collaborators [10] have treated the presence of heteroatoms by applying the information theory. The method proposed by Balaban [11], considers the electronegativities, the atomic number and the number of the group in Mendeleev's short form of the periodic chart. The same problem has been also tackled successfully by Randić [12], and Estrada [13].

In the present paper we shall treat the presence of heteroatoms, especially those in the alcohols class, by means of the weighted electronic distance (w.e.d.), a new local invariant considered by the author in [14]. By replacing the usual topological distances from the adjacency matrix, by the values of the weighted electronic distances, we obtain a new connectivity matrix, CEP, used for the construction of some topological indices [14-16]. Such a topological index is the ZEP index, which is correlated in this paper to the boiling point (BP) and the water solubility (log(1/S) for aliphatic alcohols.

The weighted electronic connectivity matrix and topologic ZEP index

For a molecule having N atoms, whose graphs is G = (V(G), E(G)), the weighted electronic connectivity matrix, CEP(G), is a square N x N matrix given by:

$$CEP\,(G)=\left\{[CEP]_{i,j};\quad i,j\in V(G)\right\} \tag{1}$$

where its entries $[CEP]_{i,j}$ are defined as follows:

$$CEP_{ij}=d.e.p.(i,j),\ if\ i\neq j \text{ and } (i,j)\in E(G) \text{ and } CEP_{ij}=0 \text{ otherwise} \tag{2}$$

and:

- d.e.p. (i, j) denotes the weighted electronic distance between the atoms (vertices) i and j;
- V(G) is the set of all vertices (atoms) of the moleular graph G;
- E(G) is the set of all edges (bonds) of the graph G;

The weighted electronic distance, w.e.d. was recently defined in [14] by the formula:

$$w.e.d.(i,j)=\frac{1}{b_r}\cdot\frac{Z_i^{'}+Z_j^{'}}{v_i\cdot v_j} \tag{3}$$

where

- b_r is the bond weight (or bond order) with values: 1 for single bond, 2 for double bond, 3 for triple bond like in Barysz et al. [9]

- ν_i denotes the degree of vertex i (that is, the number of bonds of the atom i to other atoms),

- $Z_i^{`}$ denotes the formal degree of vertex i, it is defined by:

$$Z_i^{`} = Z_i \cdot \nu_i \tag{4}$$

- Z_i being the order of the atom i (that is, the number of all electrons in the atom i).

Similar formulas which use the atomic number and the multiplicity order of bonds have been considered in an other context by Barysz and collaborators [9], where it is detected only the presence of multiple bonds and heteroatoms, but their model is not able to reproduce the information related to the neighborhood of bonds, as in the case of weighted electronic connectivity.

The formal degree $Z_i^{`}$ of the vertex i is in fact a local invariant on vertex (LOVI), which replaces the classical degree of the vertex, while the weighted electronic distance, w.e.d. (i,j) represents a local invariant on edge (LOEI).

Having in view that for oxigen we have $Z = 8$, it results that its formal degrees will be $Z'_O = 8$ for alcohols. The carbon atom in the structure of an alcohol may have the formal degree Z'_j equal to 6, 12, 18 or 24, respectively. These aspects are illustrated in Figure 1, on the molecular graphs of 1-propanol (G.1), 2-propanol (G.2) and 2-methyl-2-propanol (G.3).

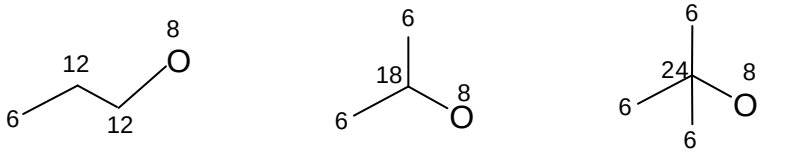

G.1 { Z' } G.2 { Z' } G.3 { Z'}

Figure 1. The graphs G.1, G.2 , G.3 and formal degrees (Z')

By replacing (4) in (3) and taking into account that $b_r = 1$, because the oxigen atom establishes only simple bonds in the class of alcohols, we obtain

$$w.e.d.(i, j) = \frac{Z_i}{\nu_j} + \frac{Z_j}{\nu_i} \cdot \tag{5}$$

The weighted electronic distances computed by means of equation (5) for the covalent bonds carbon–carbon and oxigen–carbon represent local edge invariants (LOEI).

On the edges of each graph in Figure 2 are written the w.e.d., computed by (5).

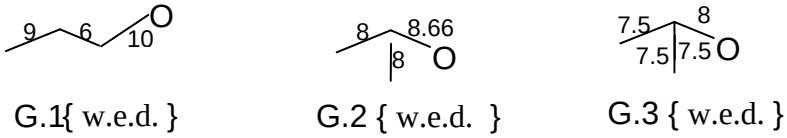

G.1{ w.e.d. } G.2 { w.e.d. } G.3 { w.e.d. }

Figure 2. The graphs G.1, G.2, G.3 and w.e.d.

Figure 3 shows the CEP matrix for 2-propanol whose graph, G.2, is depicted in the same figure, with the values of w.e.d. computed by formula (5).

SEP_i

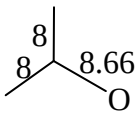

G.2

$$CEP(G.2) = \begin{bmatrix} 0 & 8 & 0 & 0 & 8 \\ 8 & 0 & 8 & 8.66 & 24.66 \\ 0 & 8 & 0 & 0 & 8 \\ 0 & 8.66 & 0 & 0 & 8.66 \end{bmatrix}$$

Figure 3. The CEP matrix for 2-propanol

The sum of all entries on the i-th row in CEP(G.2) is denoted by SEP_i (and is written at the matrix right hand side):

$$SEP_i = \sum_{j=1}^{N} [CEP]_{ij}; \; i=1, N \tag{6}$$

The electronic connectivity matrix can function as a basis for the construction of several new topological indices. The simplest index is given by the sum of root square of SEP_i:

$$ZEP = \sum_{i=1}^{N} (SEP_i)^{1/2} \tag{7}$$

The calculation technique of ZEP index is illustrated in Figure 4 for the hydrogen-suppressed graph G.2 of 2-propanol

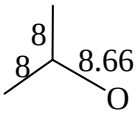

$$ZEP(G.2) = 2 \cdot 8^{\frac{1}{2}} + 24.66^{\frac{1}{2}} + 8.66^{\frac{1}{2}} = 13.565$$

G.2

Figure 4. The calculation technique of ZEP index for the hydrogen-suppressed graph of 2-propanol

A novel parameter H_d

We propose now a novel parameter, denoted by H_d, which is calculated as the arithmetic mean of the distances from the heteroatom to the other atoms, using the usual topological distance between two vertices.

The parameter H_d is hence defined by the formula:

$$H_d = \frac{1}{n}\sum_{i=1}^{n} d_i \qquad (8)$$

where:

- n represents the number of carbon atoms in the molecular graph;
- d_i represents the distance between the heteroatom and the atom *i.*

The calculation technique of parameter H_d is illustrated in Figure 5 for the hydrogen-suppressed graph G.4 of 2-butanol

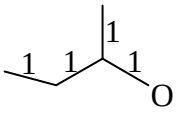

$$H_d = \frac{1}{4}(3+2+2+1) = 2$$

G. 4

Figure 5. The calculation technique of parameter H_d for the hydrogen-suppressed graph of 2-propanol (G.4)

ZEP and H_d could be used together in order to improve the QSPR models for several representative physical properties on several data sets of alcohols by using two-variable linear regression analysis.

RESULTS AND DISCUSSIONS

Correlations to normal boiling points (BP) of 132 alcohols

As a starting point, we consider a data set of 132 alcohols to develop the structure-boiling point model. The observed BP values for the normal boiling points at normal pressure are listed in Table 1 and were taken from [17].

Values of ZEP and H_d index were calculated for the same set of 132 alcohols and are presented in Table 1, too. A boiling point model is then generated using the ZEP index and H_d parameter.

The simple linear regression equation and its statistical parameters for a monovariable correlation with ZEP are shown below:

$$BP = 11.619 + 5.11\ ZEP;\ r = 0.960;\ s = 11.126;\ F = 1517;\ N = 132; \quad (9)$$

were: r-represents the correlation coefficient, s- the standard deviation and F is the Fischer ratio.

For the same 132 alcohols the simple linear regression with the ZEP index leads to a poorer correlation (r = 0.960 and s= 11.126 ^{0}C), comparable with the simple model obtained by Lu et al.[17] (r = 0.9665 and s= 9.797^{0}C). Obviously, a single ZEP index cannot give a simple and accurate correlation. It is important to stress that the statistical parameters of the QSPR equations could be improved by using multidimensional correlations involving also other topological descriptors. In this work we propose a combined use of the ZEP index and parameter H_d. The regression equation and its statistical parameters found to describe boiling points of the 132 alcohols considered are depicted below:

$$BP = 17.843 + 3.593\ ZEP + 12.391 H_d;$$
$$r = 0.985;\ s = 6.794;\ F = 2143;\ N = 132 \quad (10)$$

Statistics indicate that equation (10) is a good model for calculating BP. Values of BP predicted by this equation are also shown in Table 1.

The statistical parameters of the model given by Eq. (10) can be compared to several results that have been reported elsewhere. The model found by Yang et al. [18] using the extended adjacency matrix EA∑ and EAmax indices gave r = 0.9837 and s = 6.35 for only 37 alcohols, while our model is applied to 132 alcohols, but the molecular connectivity ^1X and $^1X^v$ indices provided a slightly superior model to those using EA∑ and EAmax indices. Analogously, a multiple linear model constructed by Yao et al. [19] using X_{m1}, X_{m2}, and X_{m3} indices gave r = 0.987 and s = 7.4988 for the same series of 37 alcohols, while our model gave r = 0.985 and s = 6.794 for the richer series of 132 alcohols. Galvez et al. [20] reported that the three-parameter model using N (the number of the vertices) and two charge indices G_1 and J_2 gave r = 0.979 and s = 3.63 for 29 alcohols. Recently, Ren [21] developed a model by using AI and Xu indices and gave r = 0.9957 and s = 3.576 but only for the same restricted data.

Table 1. The index ZEP, parameter H_d and the experimental and calculated boiling points for 132 alcohols using Equation (10)

No.	Compound	ZEP	H_d.	BP (^{0}C)	
				Exp.	Calc.
1	1-propanol	14.035	2	97.1	93.1
2	2-propanol	13.565	1.667	82.4	87.2
3	1-butanol	17.499	2.5	117.6	111.7
4	2-methyl-1-propanol	17.274	2.25	107.9	107.8
5	2-butanol	17.166	2	99.5	104.3
6	2-methyl-2-propanol	16.566	1.75	82.4	99
7	1-pentanol	20.963	3	137.5	130.3
8	3-methyl-1-butanol	20.718	2.8	131	127
9	2-pentanol	20.614	2.4	119.3	121.6
10	2-methyl-1-butanol	20.847	2.6	128	125
11	3-pentanol	20.745	2.2	116.2	119.6
12	3-methyl-2-butanol	20.445	2.2	112.9	118.6
13	2,2-dimethyl-1-propanol	20.382	2.4	113.1	120.8
14	2-methyl-2-butanol	20.223	2	102.3	115.3
15	1-hexanol	24.427	3.5	157	149
16	4-methyl-1-pentanol	24.182	3.333	151.9	146
17	2-hexanol	24.078	2.833	140	139.5
18	3-methyl-1-pentanol	24.291	3.8	153	152.2
19	2-methyl-1-pentanol	24.295	3	148	142.3
20	3-hexanol	24.193	2.5	135	135.7
21	2-ethyl-1-butanol	24.391	2.833	146.5	140.6
22	4-methyl-2-pentanol	23.826	2.667	132	136.5
23	3,3-dimethyl-1-butanol	23.814	2.833	143	138.5
24	2,3-dimethyl-1-butanol	24.115	3	144.5	141.7
25	2-methyl-2-pentanol	23.663	2.333	121.5	131.8
26	3-methyl-2-pentanol	24.009	2.5	134.3	135.1
27	2-methyl-3-pentanol	24.015	2.333	129.5	133
28	2,2-dimethyl-1-butanol	23.979	2.667	136.5	137
29	3-methyl-3-pentanol	23.865	2.167	123	130.4
30	3,3-dimethyl-2-butanol	23.576	2.333	120.4	131.5
31	2,3-dimethyl-2-butanol	23.526	2.167	118.4	129.2
32	1-heptanol	27.891	4	176.4	167.6
33	5-methyl-1-hexanol	27.646	3.85	170	164.9
34	2-heptanol	27.543	3.286	160.4	157.5
35	4-methyl-1-hexanol	27.755	3.714	173.3	163.6
36	2-methyl-1-hexanol	27.760	3.428	164	160.1
37	3-heptanol	27.657	2.857	157	152.6
38	3-methyl-1-hexanol	27.739	3.571	169	161.8
39	4-heptanol	27.641	2.714	156	150.8
40	5-methyl-2-hexanol	27.551	3.143	151	155.8
41	2-methyl-3-hexanol	27.463	2.571	145.5	148.4
42	2-methyl-2-hexanol	27.127	2.714	143	148.9
43	2,4-dimethyl-1-pentanol	27.508	3.285	159	157.4
44	5-methyl-3-hexanol	27.405	2.714	148	149.9
45	3-methyl-3-hexanol	27.304	2.428	143	146

No.	Compound	ZEP	H_d.	BP (^{0}C)	
				Exp.	Calc.
46	2,4-dimethyl-2-pentanol	26.871	2.571	133.1	146.2
47	2,4-dimethyl-3-pentanol	27.282	2.428	140	146
48	3-ethyl-3-pentanol	27.487	2.286	142	144.9
49	2,3-dimethyl-2-pentanol	27.085	2.428	139.7	145.2
50	2,3-dimethyl-3-pentanol	27.161	2.286	139	143.8
51	3-methyl-2-hexanol	27.457	2.857	151	151.9
52	6-methyl-1-heptanol	31.110	4.375	188.6	183.8
53	2-octanol	31.007	3.75	180	175.7
54	3-octanol	31.122	3.25	175	169.9
55	4-methyl-1-heptanol	31.204	4.125	188	181.1
56	4-octanol	31.106	3	176.3	166.8
57	2-ethyl-1-hexanol	31.303	3.5	184.6	173.7
58	2-methyl-2-heptanol	30.591	3.125	156	166.5
59	2,5-dimethyl-1-hexanol	30.979	3.75	179.5	175.6
60	5-methyl-2-heptanol	30.871	3.5	172	172.1
61	6-methyl-3-heptanol	30.877	3.125	174	167.5
62	3.5-dimethyl-1-hexanol	30.952	3.875	182.5	177.1
63	3-methyl-2-heptanol	30.922	3.25	166.1	169.2
64	2-methyl-3-heptanol	31.155	2.875	167.5	165.4
65	2-methyl-4-heptanol	30.854	2.875	164	164.3
66	5-methyl-3-heptanol	30.979	3	172	166.3
67	3-methyl-3-heptanol	30.768	2.75	163	162.5
68	4-methyl-3-heptanol	31.028	2.875	170	165
69	3-methyl-4-heptanol	31.028	2.75	162	163.4
70	3,4-dimethyl-2-hexanol	30.838	3	165.5	165.8
71	4-methyl-4-heptanol	30.743	2.625	161	160.8
72	3-ethyl-3-hexanol	30.927	2.5	160.5	159.9
73	2,3-dimethyl-2-hexanol	30.533	2.75	160	161.6
74	3,5-dimethyl-3-hexanol	30.512	2.625	158	160
75	2,3-dimethyl-3-hexanol	30.600	2.5	158.1	158.8
76	2-methyl-3-ethyl-2-pentanol	30.611	2.625	156	160.4
77	2,4,4-trimethyl-2-pentanol	29.961	2.75	147.5	159.6
78	2,2,4-trimethyl-3-pentanol	30.407	2.5	150.5	158.1
79	2,2-dimethyl-3-hexanol	30.589	2.625	156	160.3
80	2,5-dimethyl-3-hexanol	30.675	2.75	157.5	162.1
81	4,4-dimethyl-3-hexanol	30.774	2.625	160.4	160.9
82	6-methyl-2-heptanol	30.762	3.625	174	173.3
83	3-methyl-1-heptanol	31.204	4	186	179.5
84	2-methyl-3-ethyl-3-pentanol	30.777	2.375	158	157.9
85	2,3,4-trimethyl-3-pentanol	30.456	2.375	156.5	156.7
86	7-methyl-1-octanol	34.574	4.889	206	202.6
87	2-nonanol	34.471	4.222	198.5	194
88	3-nonanol	34.586	3.667	195	187.5
89	4-nonanol	34.569	3.333	192.5	183.3
90	5-nonanol	34.569	3.222	193	182
91	2-methyl-2-octanol	34.055	3.555	178	184.3
92	2,6-dimethyl-2-heptanol	33.810	3.444	173	182

No.	Compound	ZEP	H_d.	BP (^{0}C)	
				Exp.	Calc.
93	2,6-dimethyl-3-heptanol	33.987	2.75	175	174
94	2,6-dimethyl-4-heptanol	34.065	3	174.5	177.4
95	3,6-dimethyl-3-heptanol	30.675	3	173	165.2
96	3,5-dimethyl-4-heptanol	34.410	2.778	171	175.9
97	2,3-dimethyl-3-heptanol	34.065	2.777	173	174.6
98	2,4-dimethyl-4-heptanol	33.952	2.777	171	174.2
99	2,4,4-trimethyl-3-hexanol	34.039	2.667	170	173.2
100	3,4,4-trimethyl-3-hexanol	33.932	2.555	165.5	171.4
101	4-methyl-4-octanol	35.075	2.889	180	179.7
102	4-ethyl-4-heptanol	34.366	2.667	182	174.4
103	2-methyl-2-octanol	34.055	3.555	178	184.3
104	8-methyl-1-nonanol	38.039	5.4	219.9	221.4
105	2-methyl-3-ethyl-3-heptanol	34.006	2.8	177.5	174.7
106	2-methyl-3-ethyl-1-heptanol	38.124	4	193	204.4
107	5-methyl-3-ethyl-3-heptanol	34.709	2.9	172	178.5
108	2-decanol	37.935	4.7	211	212.4
109	4-decanol	38.034	3.7	210.5	200.3
110	3,7-dimethyl-1-octanol	37.887	4.8	212.5	213.4
111	2,7-dimethyl-3-octanol	37.611	3.5	193.5	196.3
112	2,6-dimethyl-4-octanol	34.696	3.2	195	182.2
113	2,3-dimethyl-3-octanol	38.816	3.1	189	195.7
114	5-methyl-5-nonanol	37.672	3.1	202	191.6
115	4-methyl-1-nonanol	38.132	5	216	216.8
116	2-methyl-3-nonanol	37.856	3.6	200	198.5
117	2,2,5,5-tetramethyl-3-hexanol	33.952	2.9	170	175.8
118	4-propyl-4-heptanol	33.932	2.8	191	174.5
119	2,4,6-trimethyl-4-heptanol	37.160	2.9	181	187.3
120	3-ethyl-3-octanol	37.855	3.1	199	192.3
121	3-ethyl-2-methyl-3-heptanol	37.681	2.8	193	187.9
122	1-undecanol	41.748	6	245	242.2
123	2-undecanol	41.399	5.182	228	230.8
124	3-undecanol	41.514	4.545	229	223.3
125	5-undecanol	41.498	3.818	229	214.3
126	6-undecanol	41.498	3.727	228	213.1
127	1-dodecanol	45.212	6.5	261.9	260.8
128	2-dodecanol	42.035	5.667	246	239.1
129	1-tridecanol	48.676	7	276	279.5
130	1-tetradecanol	52.140	7.5	289	298.1
131	1-pentadecanol	55.604	8	304.9	316.8
132	1-hexadecanol	59.068	8.5	312	335.4

Correlations to water solubility (log(1/S)) of 60 alcohols

Aqueous solubility, S, of liquids and solids is defined as the concentration (moles per liter) of solute in the aqueous phase, at equilibrium whih a pure solute phase. This property of organic compounds is very important and widely

applied in many research areas, such as pharmaceutical chemistry, biological chemistry or environmental science.

We consider in our study a data set of 60 alcohols [17] to develop the structure-water solubility model. The experimental water solubility as log (1/S), for these alcohols, are listed in Table 2.

The simple linear correlation found is illustrated by the following equation and statistical parameters:

$$\log 1/S = -3.218 + 0.167\ ZEP;\ r = 0.972;\ s = 0.248;\ F = 992;\ N = 60; \quad (11)$$

A better water solubility point model was generated by using a two variable linear model constructed with the index ZEP and parameter H_d and is expressed by equation (12):

$$\log 1/S = -3.196 + 0.129\ ZEP + 0.337H_d;$$
$$r = 0.988;\ s = 0.164;\ F = 1175;\ N = 60; \quad (12)$$

Values of log (1/S) predicted by equation (12) are also shown in Table 2.

Table 2. Experimental and calculated log (1/S) for 60 alcohols

No	Compound	Log (1/S)		No	Compound	Log (1/S)	
		Exp.	Calc.			Exp.	Calc
1	etanol	-1.10	-1.33	31	3-heptanol	1.44	1.33
2	1-propanol	-0.62	-0.71	32	4-heptanol	1.40	1.28
3	1-butanol	-0.03	-0.10	33	5-methyl-2-hexanol	1.38	1.42
4	2-methyl-1-propanol	-0.10	-0.21	34	2-methyl-3-hexanol	1.32	1.21
5	2-butanol	-0.47	-0.31	35	2-methyl-2-hexanol	1.07	1.22
6	1-pentanol	0.59	0.52	36	2,4-dimethyl-1-pentanol	1.60	1.46
7	3-methyl-1-butanol	0.51	0.42	37	3-methyl-3-hexanol	0.98	1.14
8	2-pentanol	0.28	0.27	38	2,4-dimethyl-2-pentanol	0.93	1.14
9	2-methyl-1-butanol	0.46	0.37	39	2,4-dimethyl-3-pentanol	1.22	1.14
10	3-pentanol	0.21	0.22	40	2,3-dimethyl-2-pentanol	0.87	1.12
11	3-methyl-2-butanol	0.18	0.18	41	2,3-dimethyl-3-pentanol	0.84	1.08
12	2-methyl-2-butanol	-0.15	0.09	42	1-octanol	2.35	2.37
13	1-hexanol	1.21	1.13	43	2-octanol	2.09	2.07
14	4-methyl-1-pentanol	1.14	1.05	44	2-ethyl-1-hexanol	2.11	2.02
15	2-hexanol	0.87	0.86	45	2-methyl-2-heptanol	1.72	1.80
16	2-methyl-1-pentanol	1.11	0.95	46	3-methyl-3-heptanol	1.60	1.70
17	3-hexanol	0.80	0.77	47	1-nonanol	3.01	2.98
18	2-ethyl-1-butanol	1.01	0.91	48	7-methyl-1-octanol	2.49	2.91
19	4-methyl-2-pentanol	0.79	0.78	49	2-nonanol	2.74	2.67
20	3,3-dimethyl-1-butanol	0.50	0.83	50	3-nonanol	2.66	2.50
21	2,3-dimethyl-1-butanol	0.37	0.93	51	4-nonanol	2.59	2.39
22	2-methyl-2-pentanol	0.49	0.64	52	5-nonanol	2.49	2.35
23	3-methyl-2-pentanol	0.71	0.74	53	2,6-dimethyl-4-heptanol	2.16	2.21
24	2-methyl-3-pentanol	0.70	0.69	54	3,5-dimethyl-4-heptanol	2.51	2.18
25	2,2-dimethyl-1-butanol	0.91	0.80	55	1-decanol	3.63	3.60
26	3-methyl-3-pentanol	0.36	0.61	56	1-dodecanol	4.67	4.83
27	3,3-dimethyl-2-butanol	0.61	0.63	57	2,2-dimethyl-3-pentanol	1.15	1.12
28	2,3-dimethyl-2-butanol	0.37	0.57	58	2,2-dimethyl-1-pentanol	1.52	1.36
29	1-heptanol	1.81	1.75	59	4,4-dimethyl-1-pentanol	1.55	1.53
30	2-heptanol	1.55	1.46	60	2,2-diethyl-1-pentanol	2.42	2.36

The two-variable regression model (12) is slightly better than the two-variable regression model based on the combined use of Lu index and DAI (-OH) indices [17], which produces an model with r = 0.984 and s = 0.1807, while our model has r = 0.988 and s = 0.164. Actually, our two-variable regression model (12) is slightly better even than the three-variable regression model based on the combined use of Lu, DAI (-OH) and DAI (CH_3-) [18], which produces a model with r = 0.9876 and s = 0.1604.

CONCLUSIONS

According to the results previously presented, we conclude that the topological index ZEP based on the concept of weighted electronic distance and weighted electronic matrix CEP of the molecular graph can accurately describe the molecular structures involving heteroatoms, in this case the presence of oxigen.

The w.e.d. has the merit that it is able to differentiate not only the covalent bonds carbon-oxigen from the ones of carbon–carbon, but is also able to discriminate the covalent bonds of oxigen to a primary carbon from that to secondary or tertiary carbons. To our best knowledge, no other models have similar discrimination power for the covalent bonds with regard to their structural neighbourhood.

Two variable linear regression using ZEP and $\mathbf{H_d}$ can provide high-quality QSPR models for the two studied properties of alcohols: boiling point and water solubility.

REFERENCES

1. M. Randić, W.L. Woodworth, A. Graovac*, Int. J. Quantum. Chem*., **1983**, *24*, 435-452
2. A.T. Balaban*, Rev. Chim*., **1988**, *39*, Nr. 12, 1026-1031
3. M. Diudea, O. Ivanciuc*, Topologie moleculară*, Comprex, Cluj-Napoca, **1995**
4. M. Randić*, J. Math. Chem*., **1991**, *7*, 155-168
5. Z. Mihalić, S. Nikolić, N. Trinajstić*, Inf. Comput. Sci*., **1992**, *32*, 28-37
6. O. Ivanciuc, *Rev. Roum. Chim*., **2000**, *45*, 1037-1054
7. M. Randić, P.J. Hansen, P.C. Jurs*, J. Chem. Inf. Comput. Sci*., **1988**, *28*, 60-68
8. L.B. Kier, L.H. Hall*, Molecular Connectivity in Structure-Activity Analysis*, John Wiley & Sons, New York, **1986**
9. M. Barysz, G. Jashari, R.S. Lall, V.K. Srivastaya, N. Trinajstić*,* in "*Chemical Applications of Graph Theory and Topology*", King, R.B. (Ed), Elsevier, Amsterdam, **1983**, 222-230

10. S.C. Basak, V.R. Magnuson, G.J. Nieni, R.R. Regal, G.D. Veith**,** *Math. Modelling*, **1987**, *8*, 300-305
11. A.T. Balaban, *J. Chem*. *Inf. Comput. Sci*., **1985**, *25*, 334-343
12. M. Randić, *Chemometrics Intel. Lab. Syst*., **1991**, *10*, 213-227
13. E. Estrada, *J. Chem. Inf. Comput. Sci*., **1995**, *35*, 701-707
14. Z. Berinde, *Applications of molecular topology in the study of physico-chemical properties of organic compounds (in Romanian),* Cub Press 22, Baia Mare, **2001**
15. Z. Berinde, Rev. Chim. (Bucureşti), **2001**, *52*, No. 12, 788-792
16. Z. Berinde, Revue Roumaine de Chimie, **2006**, *51*, No. 11, 1131-1135
17. Lu, C. Guo, W., Wang, Y. and Yin, C., J. Mol. Model, **2006**, *12,* 749-756
18. YQ Yang, L. Xu, CY Hu, *J. Chem. Inf. Comput. Sci*., **1994**, *34*, 1140-1145
19. YY Yao, L. Xu, YQ Yang, YS Yuan, *J. Chem. Inf. Comput. Sci*., **1993**, *33*, 590-594
20. J. Gavez, R. Garcia, MT. Salabert, R. Soler, *J. Chem. Inf. Comput. Sci*., **1994**, *34*, 520-525
21. B. Ren, *J. Chem. Inf. Comput. Sci*., **2002**, *42*, 858-868